Author:
Down, Colin J

Title:
Quantification of the glycocalyx in the study of pre-eclampsia

Quantification of the Glycocalyx in the Study of Pre-eclampsia

Dr Colin James Down

A dissertation submitted to the University of Bristol in accordance with the requirements for award of the degree of Doctor of Philosophy in the Faculty of Health Sciences.

February 2023

Word Count 37,180

Abstract

Introduction: Pre-eclampsia is a multisystem disorder of pregnancy characterised by widespread endothelial dysfunction. The glycocalyx is present at the luminal surface of endothelial cells and at the maternal-fetal interface of the placenta. It has important roles in maintaining normal endothelial function and may be shed in disease, including pre-eclampsia. The aim of this project was to develop reliable methodologies of imaging and quantifying the glycocalyx of the maternal endothelium and placenta, to test if glycocalyx shedding is a feature of pre-eclampsia.

Methods: A prospective cohort study enrolled pregnant women with pre-eclampsia and normotensive controls. The maternal sublingual glycocalyx was measured using sidestream darkfield (SDF) imaging with GlycoCheck™. Placental tissue was collected following delivery and processed for both light and electron microscopy. Methodologies were developed to image and quantify the glycocalyx at the maternal-fetal interface using confocal and transmission electron microscopy (TEM).

Results: An increase in the sublingual perfused boundary region (PBR) was detected using GlycoCheck™ in women with early-onset pre-eclampsia (<34 weeks' gestation), compared to women with normotensive pregnancy. No difference was observed in women with late-onset disease (≥34 weeks' gestation).

A trend was observed towards a reduction in the depth of the glycocalyx of the syncytiotrophoblast in women with early-onset pre-eclampsia, but this did not reach statistical significance. The trend could not be replicated in an independent cohort.

Conclusion: Disruption of the maternal endothelial glycocalyx is a feature of early-onset pre-eclampsia, but not late onset disease. Further work is required to determine the role the placental glycocalyx in pre-eclampsia.

For my wife Lindsay,

for your love, patience and understanding

and

Aoife and Esther

who can’t wait to read Daddy’s really boring book!

ACKNOWLEDGEMENTS

I would like to thank Dr Victoria Bills for her support and guidance with every aspect of this project. Your advice and encouragement have been invaluable and allowed me to develop as both an obstetrician and a researcher.

To Prof. Simon Satchell and Dr Becky Foster, for accepting an obstetrician into your renal endothelial group and teaching me what it means to be a clinical academic. Your support, direction and reassurance have helped me develop skills in critical thinking and a desire to understand why. I think I've learnt a little about the kidney too!

To Dr Chris Neal for your unwavering support, assistance with experimental design and instruction in how to become an electron microscopist. I hope I've imparted a new love for the placenta.

To Dr Charley Heffer, Dr Hui Liew and Dr Laura Skinner. Your countless hours in patient enrolment, lectin staining, image analysis (and support when it all went wrong) will be always appreciated. Also, to Dr Matthew Butler and all the Bristol Renal and Endothelial Research Group, for accepting me as one of your own, sharing your expertise and teaching me how to be a scientist.

I would like to recognise the staff of the Wolfson Bioimaging Facility for their help and support in this project. The excellent facilities and advice have made this project possible. I would particularly like to mention Dr Stephen Cross who developed the automated macro.

To Dr Hiten Mistry and Dr Lesia Kurlak at the University of Nottingham Salt in Pregnancy Study (SAPS) Biobank, for their kind collaboration and allowing me access to their extensive biobank of placental samples.

I am incredibly grateful for the financial support of the David Telling Charitable Trust, without which this project would not have been possible.

Finally, I would like to thank Mat and Lucy Britton of the Capella Foundation for the purchase of the GlycoCheck™ device. After your own experience of pregnancy

complications, your devotion to fundraising to enable pioneering medical research in obstetrics is inspirational. I hope this thesis is testament to what all your hard work is helping to achieve.

PUBLICATIONS ARISING

CONTRIBUTIONS TO JOURNAL ARTICLES

- Crompton, M., Ferguson, J., Ramnath, R., Onions, K., Ogier, A., Gamez, M., **Down, C.,** Skinner, L., Wong, K., Dixon, L., Sutak, J., Harper, S., Pontrelli, P., Gesualdo, L., Heerspink, H., Toto, R., Welsh, G., Foster, R., Satchell, S., Butler, M. Mineralocorticoid receptor antagonism in diabetes reduces albuminuria by preserving the glomerular endothelial glycocalyx. JCI Insight. 2023 Feb 7:e154164. (In press preview available)
- Butler, M., **Down, C.**, Foster, R., Satchell, S. The Pathological Relevance of Increased Endothelial Glycocalyx Permeability. Am J Pathol. 2020 Apr;190(4):742-751. (Appendix 1).
- Fabre-Gray, A., **Down ,C.**, Neal, C., Foster, R., Satchell, S., Bills, V. Imaging the placental glycocalyx with transmission electron microscopy. Placenta. 2018 Dec 15;74:59-61. (Appendix 2).

PRESENTATIONS

- **Down, C.,** Liew, H., Heffer, C., Skinner, L., Neal, C., Foster, R., Satchell, S., Bills, V. Changes in the sublingual and placental glycocalyx in pre-eclampsia. Oral Presentation (virtual) at UK Proteoglycan Meeting, UK. 2021.
- **Down, C.,** Neal, C., Foster, R., Satchell, S., Bills, V. Imaging the Placental Glycocalyx. Oral presentation (virtual) at Bristol Heart Institute Annual Conference, Bristol, UK. 2020.
- **Down, C.,** Foster, R., Satchell, S., Bills, V. Quantifying the Placental Glycocalyx with Lectin Histochemistry. Oral presentation at RCOG Annual Academic Meeting (Blair Bell Research Society), London, UK. 2020.
- **Down, C.,** Neal, C., Foster, R., Satchell, S., Bills, V. Quantifying the Placental Endothelial & Syncytiotrophoblast Glycocalyx with Lectin Histochemistry. Poster and oral presentation at European International Society for the Study of Hypertension in Pregnancy (EuroISSHP) Conference, Lund, Sweden. 2019.
- **Down, C.,** Neal, C., Fabre-Gray, A., Foster, R, Satchell, S., Bills, V. Imaging the placental glycocalyx. Poster presentation at Congress of the International Society for the Study of Hypertension in Pregnancy (ISSHP), Amsterdam, The Netherlands. 2018.
- **Down, C.,** Neal, C., Fabre-Gray, A., Foster, R., Satchell, S., Bills, V. Imaging the placental glycocalyx with transmission electron microscopy. Oral presentation at British Microcirculation Society Conference, Nottingham, UK. 2018.

PRIZES

- First Prize, for best oral presentation – Bristol Heart Institute Annual Conference, Bristol, UK. 2020.
- Second Prize, for best oral presentation – Royal College of Obstetricians & Gynaecologists (RCOG) Annual Academic Meeting (Blair Bell Research Society), London, UK. 2020.

- Second Prize, for best poster and oral presentation – European International Society for the Study of Hypertension in Pregnancy (EuroISSHP) Conference, Lund, Sweden. 2019.

COVID-19 IMPACT STATEMENT

Enrolment in the clinical arms of this study was severely impacted by the COVID-19 pandemic. I received a suspension of studies for 20 weeks during the height of the first wave of the pandemic as I returned to full time clinical training.

On resumption of my studies, several adaptions to the protocol were made to ensure the continued compliance with University and NHS regulations regarding patient research during the pandemic. This further delayed enrolment and ultimately affected the total number of participants included.

Funding for my clinical role as a Clinical Research Fellow, which I was conducting alongside my PhD studies, could not be extended to the full 20 weeks of my suspension leaving a 3-month shortfall prior to returning to clinical training. Most of my write-up has therefore taken place alongside my full-time role as a clinical trainee in obstetrics and gynaecology. An extension for submission of this thesis was requested and approved on this basis.

Author's declaration

I declare that the work in this dissertation was carried out in accordance with the requirements of the University's *Regulations and Code of Practice for Research Degree Programmes* and that it has not been submitted for any other academic award. Except where indicated by specific reference in the text, the work is the candidate's own work. Work done in collaboration with, or with the assistance of, others, is indicated as such. Any views expressed in the dissertation are those of the author.

SIGNED: ..... DATE:.....

TABLE OF CONTENTS

List of Figures

List of Tables

ABBREVIATIONS

Abbreviation	Expansion
AB	Alcian Blue
ACOG	American College of Obstetricians and Gynecologists
AF-488	Alexa Fluor 488
AFS	Automatic Freeze Substitution
AFLP	Acute fatty liver of pregnancy
ALT	Alanine transferase
BDMA	N-benzyldimethylamine
BM	Basement membrane
BMI	Body mass index
BP	Blood pressure
BSA	Bovine serum albumin
BSA	Bovine serum albumin
CAP	Capillary
CI	Confidence interval
ConA	Concanavalin A
COVID-19	Coronavirus disease 2019
CS	Chondroitin sulphate
DAPI	4’6-diamidino-2-phenylindole
DDSA	Dodecenyl succinic anhydride
DIC	Disseminated intravascular coagulopathy
EC	Endothelial cell
ECM	Extracellular matrix
Eng / sEng	Endoglin / soluble endoglin
eNOS	Endothelial nitric oxide synthase
FGR	Fetal growth restriction
FITC	Fluorescein isothiocyanate
GA	Glutaraldehyde
GAGs	Glycosaminoglycans
GlcA	Glucuronic acid
GlcNAc	N-acetyl-d-glucosamine
GPI	Glycosylphosphatidylinositol
HA	Hyaluronic acid / hyaluronan
HAS	Hyaluronan synthases
Hb	Haemoglobin
HELLP	Haemolysis, elevated liver enzymes and low platelets
HIP	Heparan-sulphate interacting protein
HRA	Health Regulatory Authority
HS	Heparan sulphate
HTA	Human Tissue Act 2004
HUS	Haemolytic uraemic syndrome
HVCS	Handheld Video Capillaroscopy System
HYAL1/2	Hyaluronidase 1 and 2
ICC	Intraclass correlation coefficient
IL-1	Interleukin 1
IQR	Interquartile range
ISOM	International Society for Obstetric Medicine
ISSHP	International Society for the Study of Hypertension in Pregnancy
IUGR	Intrauterine growth restriction

IVS	Intervillous space
K2EDTA	Dipotassium ethylenediaminetetraacetic acid
LaDy	Lanthanum and dysprosium
LED	Light emitting diodes
LEL	Lycopersicon esculentum
LMWH	Low-molecular weight heparin
LPS	Lipopolysaccharide
MAL II	Maackia amurensis II
MAP	Mean arterial blood pressure
MMP	Metalloproteinase
mRNA	Messenger ribonucleic acid
MTA	Material transfer agreement
MVHS	Microvascular Health Score
NA	Not applicable
NICE	National Institute for Health and Care Excellence
NO	Nitric oxide
NRES	National Research Ethics Service
P-P	Peak-to-peak
PBR	Perfused boundary region
PBS	Phosphate buffered saline
PCR	Protein to creatine ratio
PE	Pre-eclampsia
PFA	Paraformaldehyde
PGI2	Prostanoid prostacyclin
PI3K	Phosphatidylinositol-3 kinase
PKC	Protein kinase C
PLCγ	Phospholipase C gamma
PLGF	Placental growth factor
PMT	Photomultiplier tubes
PPE	Personal protective equipment
PRES	Posterior reviersible leukoencephalopathy
QD	Quantum dot
R18	Octadecyl rhodamine B chloride
RBC	Red blood cell
ROUT	Robust regression and outlier removal
RR	Ruthenium red
SA-ßGal	Senescence-associated beta galactosidase
SD	Standard deviation
SDF	Sidestream dark field
SEM	Standard error of the mean
sFlt-1	Soluble fms-like tyrosine kinase 1
SLE	Systemic lupus erythematosus
SNR	Signal-to-noise ratio
STB	Syncytiotrophoblast
TEM	Transmission electron microscopy
TFPI	Tissue factor pathway inhibitor
TGF-ß1	Transforming growth factor - ß1
TNFα	Tissue necrosis factor alpha
TTP	Thrombotic thrombocytopenic purpura
UEA I	Ulex europaeus I
UHBW	University Hospitals Bristol and Weston NHS Foundation Trust

UK	United Kingdom of Great Britain and Northern Ireland
UV	Ultraviolet
VEGF	Vascular endothelial growth factor
VEGFR-	Vascular endothelial growth factor receptor
VSM	Vasculo-syncytial membrane
WGA	Wheat germ agglutinin

1. INTRODUCTION

1.1 PREAMBLE

Our understanding of pre-eclampsia as a multi-system syndrome characterised by endothelial dysfunction, has been a paradigm shift in how we consider and study the disease. This thesis will explore the link between the placental origins of pre-eclampsia and describe how placentally released factors interact and activate the maternal endothelium. Particular focus will be on how different pre-eclampsia phenotypes develop and converge along a common pathway of endothelial activation and dysfunction.

I will present the glycocalyx, the carbohydrate rich surface layer present at both the placental syncytiotrophoblast and maternal endothelium and make the argument for its important role in maintaining endothelial health. I propose that disruption of the endothelial and placental glycocalyx are important pathophysiological features of pre-eclampsia.

This thesis will look to explore the difficulties in measuring the glycocalyx and present novel methodologies for quantifying and comparing glycocalyx in both normal and pre-eclamptic pregnancy. Pilot data will be presented demonstrating the feasibility of these approaches in clinical studies.

1.2 PRE-ECLAMPSIA

> *In pregnancy, the onset of drowsy headaches with heaviness is bad; such cases are perhaps liable to some sort of fits at the same time.*
>
> Coan Prognosis, XXXI, No. 523, c. 400 BCE [1]

1.2.1 A BRIEF HISTORY OF PRE-ECLAMPSIA

The ancient Greeks provide some of the first recorded evidence of an understanding of the seriousness of the condition we today recognise as eclampsia, and its premonitory condition, pre-eclampsia [2]. The *Coacae Praenotiones*, a collection of statements about disease prognosis, is perhaps the earliest confirmed description [3].

There was little further characterisation of the condition until the eighteenth and nineteenth centuries when eclampsia was accepted as a distinct entity from epilepsy [2]. Robert Johns, in 1843 went on to define a number of precursory symptoms, that if recognised, could predict women likely to suffer with eclampsia [4]. These include oedema (especially of the hands, arms, and face), headaches, visual disturbance, and stomach pains. Women are still routinely requested to monitor and report the development of these symptoms in the surveillance of pre-eclampsia today [5, 6].

John Lever, also in 1843, reported the association of proteinuria in patients with eclampsia [7]. Importantly, this was observed to rapidly resolve after delivery, differentiating it from Bright's disease (acute glomerulonephritis). Hypertension in eclampsia, although long suspected, was not definitively described until the late nineteenth century with the advent of reliable sphygmomanometry [8]. Until relatively recently, the most widely accepted definition of pre-eclampsia was characterised as the onset of these key measurable signs of *de novo* hypertension and proteinuria, occurring in the second half of pregnancy [9].

The historical context of how our understanding of pre-eclampsia has evolved is an important consideration in guiding how we approach future research into the condition.

It is now recognised that hypertension and proteinuria represent measurable endpoints for a much wider underlying disease process. They were selected serendipitously in the

nineteenth century because they could be easily measured, and not because they represent the most important pathophysiological process. Neither is able to adequately predict severe adverse maternal or perinatal outcomes [10].

A much broader definition of pre-eclampsia is now accepted, as a multi-system disorder, characterised by widespread endothelial dysfunction [11, 12]. There is a large degree of heterogeneity in its presentation and its subsequent maternal and fetal effects [13]. Several authors have suggested distinct phenotypes of the disease that may or may not share a common pathological process, yet converge to the common endpoint of endothelial dysfunction and the many symptoms we associate with the condition [14].

To this end, it is perhaps better to think of pre-eclampsia as a syndrome; a constellation of signs and symptoms, that when occur together, identify a group of women at increased risk of adverse pregnancy outcome [15]. Importantly, this does not infer a single causative pathophysiology, but it does recognise the common endpoint of endothelial dysfunction. With this understanding, research has started to move away from the concept of a singular cure for pre-eclampsia and is instead focussed on trying to understand the pathophysiological distinctions in different disease subgroups, which may prove superior in identifying preventative or therapeutic targets [14].

1.2.2 Epidemiology

Globally, hypertensive disorders of pregnancy are the second biggest direct cause of maternal mortality, representing 14% of maternal deaths, more than 60,000 women annually [16]. Maternal mortality affects low and middle-income countries disproportionately, where access to timely expert antenatal and delivery care may not be available [17].

In the UK, pre-eclampsia effects around 6% of pregnancies [18]. With advances in recognition and management, the risk of dying from pre-eclampsia is now less than one per million in the UK, with some experts suggesting that nearly all pre-eclampsia deaths could be preventable with expert care [19].

With delivery being the only definitive treatment for pre-eclampsia, perinatal morbidity and mortality remain a significant challenge. In the UK between 8 and 10% of all preterm deliveries are to women with pre-eclampsia [18]. It is estimated that around 1,000 babies

per year are either stillborn or die in the neonatal period as a result of complications of maternal pre-eclampsia [20, 21]. Iatrogenic prematurity is a significant contributor to this statistic [22].

Aside from the human cost, pre-eclampsia also represents a significant economic burden to healthcare systems and wider society. A study in the United States calculated a total expenditure of $2.18 billion within the first 12 months of delivery for the year 2012 [23]. This comprised $1.03 billion for maternal care, and $1.15 billion for neonatal and infant care. The cost was disproportionately borne by infants that delivered extremely preterm [23].

1.2.3 Clinical Features and Classification

Pre-eclampsia is variable in its presentation which can range from a complete absence of symptoms to severe end-organ compromise. All of the observed features of pre-eclampsia are a consequence of endothelial dysfunction, although the pattern, degree and severity of end-organ involvement is highly variable [24].

The majority of accepted definitions of pre-eclampsia still require the onset of *de novo* hypertension after 20 weeks' gestation as a mandatory feature for diagnosis [5, 12, 25]. Hypertension is defined as a systolic blood pressure (BP) ≥ 140 mmHg, or a diastolic BP ≥ 90 mmHg on at least two occasions, measured more than four hours apart. [12].

Proteinuria is no longer a mandatory feature of pre-eclampsia; however, it is still a common finding, occurring in up to 75 % of cases [26]. Clinically significant proteinuria is defined as a protein to creatinine ratio (PCR) ≥ 30 mg/mmol on a spot urine sample, or a total urinary protein ≥ 300 mg on a 24-hour urine collection, in the absence of another cause [5, 12].

Other commonly affected systems, along with their suggested mechanism are summarised in Table 1.

Organ / Body System	Clinical Signs / Symptoms	Pathology	Mechanism
Cardiovascular	Blood pressure ≥140/90 mmHg Peripheral oedema	Hypertension	Increased endothelin-1 and superoxide. Decreased nitric oxide. Increased sensitivity to angiotensin II. Impaired renal-pressure natriuresis and increased total peripheral vascular resistance [27]
Renal	Proteinuria Rise is serum creatinine ≥97 µmol/L Hyperuricemia Oliguria / anuria	Glomerular endotheliosis Acute kidney injury Renal failure	Reduced ultrafiltration coefficient [28] Decreased renal plasma flow, renal vasoconstriction and ischaemic injury [29]
Respiratory	Dyspnoea and orthopnoea Hypoxia	Pulmonary oedema Acute respiratory distress syndrome	Elevated pulmonary pressure, reduced plasma oncotic pressure and capillary leak [30] Iatrogenic fluid overload [31] Heart failure
Central Nervous System	Headache Altered mental state / loss of consciousness Visual disturbance Hyperreflexia / clonus Seizure	Central nervous system irritability Transient ischaemic attack (TIA) Stroke Eclampsia Posterior reversible leukoencephalopathy syndrome (PRES)	Vasospasm of cerebral and retinal vasculature Cerebral oedema Vascular responses to severe hypertension Ischaemia / haemorrhage [32]
Hepatic / Gastrointestinal	Right upper quadrant / epigastric pain Jaundice Maternal collapse Elevated liver transaminases Abnormal clotting	Hepatic failure Hepatic rupture / haemorrhage Pancreatitis	Hepatic endothelial injury, fibrin deposition and ischaemia. Can lead to intra-hepatic bleeding, capsular tears and hepatic rupture [33]
Haematological	Haemorrhage (antenatal or postpartum) Abruption Abnormal clotting Thrombocytopaenia	Thrombocytopaenia Disseminated intravascular coagulopathy (DIC)	Increased platelet activation and consumption due to endothelial dysfunction. Microthrombi [34]
Uteroplacental	Reduced growth velocity Abnormal arterial Doppler studies Abruption Stillbirth	Intrauterine growth restriction (IUGR) Utero placental insufficiency	Decreased utero-placental blood flow [35] Placental microthrombi and infarction secondary to hypoxia and oxidative stress [36]

Table 1 – The Clinical Features of Pre-eclampsia by Organ System

Historically there has been little consensus on the precise definition of pre-eclampsia, which has created difficulties in comparing research outputs. To remedy this an international committee of experts was formed by the International Society for the Study of Hypertension in Pregnancy (ISSHP), with the primary aim of producing guidance on how hypertensive disorders of pregnancy should be classified and diagnosed. The most recent statement from 2018 defines pre-eclampsia in the following way [12]:

- Hypertension accompanied by *one or more* of the following new-onset conditions at or after 20 weeks' gestation:
    1) Proteinuria
    2) Other maternal end organ dysfunction, including;
        a. Acute kidney injury (creatinine ≥ 90 μmol/L)
        b. Elevated liver transaminases
        c. Neurological complications (eclampsia, altered mental state, blindness, stroke, clonus, severe headache, persistent visual scotoma)
        d. Haematological complications (platelet count < 150 x 10^9/L, DIC, haemolysis)
    3) Uteroplacental dysfunction (IUGR, abnormal umbilical artery Doppler waveform, stillbirth)

This definition has the largest international acceptance including recognition by the International Society for Obstetric Medicine (ISOM) [12] and the National Institute for Health and Care Excellence (NICE) [5]. The American College of Obstetricians and Gynecologists (ACOG) definition is similar, except for the exclusion of uteroplacental dysfunction, and the specific inclusion of pulmonary oedema as a recognised diagnostic marker of maternal end-organ dysfunction [25].

1.2.4 Pre-eclampsia With Severe Features

The terms "mild" and "severe" pre-eclampsia are discouraged in general clinical use, as seemingly mild disease can rapidly progress with potentially life-threatening complications [12].

It is important, however, to recognise features of pre-eclampsia that convey an increased risk of maternal or fetal adverse outcome, in order to identify women who may benefit

from additional therapeutics or care (e.g., magnesium sulphate or access to maternal and neonatal high dependency care). In the context of research, there is also a question as to whether women who develop severe features represent a distinct subgroup of pre-eclampsia patients.

Severe hypertension is diagnosed when systolic BP ≥ 160 mmHg, or diastolic BP ≥ 110 mmHg [5, 12, 25]. It is associated with worse maternal outcomes including stroke [37]. Severe hypertension should be managed emergently, and when refractory to maximal antihypertensive therapy, is an indication for delivery.

Signs and symptoms attributable to end-organ dysfunction should be considered as severe features if unresponsive to adequate treatment. These include recurring severe headaches, visual disturbance (scotoma, floaters), epigastric or right-upper quadrant pain, oliguria and persistent nausea and vomiting [5, 12].

ACOG recognises biochemical and haematological derangement including liver transaminases twice the upper limit of the normal range, thrombocytopenia with platelets < 100 x 10^9/L and a serum creatinine that has doubled or is elevated > 1.1 mg/dl (> 90 µmol/L) as cut-off values for severe disease [25]. NICE and ISSHP highlight progressive deterioration in these parameters without defining specific severe thresholds [5, 12].

There is debate regarding the relative importance of the quantity of proteinuria in identifying severe disease, but generally it is not considered predictive of adverse outcome unless in the nephrotic range [38, 39].

ISSHP and NICE include fetal assessment in their definitions of severe pre-eclampsia with fetal growth restriction or abnormal umbilical artery Dopplers highlighted [5, 12].

HELLP syndrome occurs when **h**aemolysis, **e**levated **l**iver enzymes and thrombocytopaenia (**l**ow **p**latelets) occur in combination during pregnancy. It has an incidence of 0.2 – 0.8 % of pregnancies and is generally considered a severe manifestation of pre-eclampsia. It is strongly associated with an increase in maternal morbidity and mortality [40, 41].

1.2.5 Early- and Late-Onset Pre-eclampsia

Pre-eclampsia categorised by gestation is widely acknowledged, with important clinical and pathophysiological distinctions between the two sub-types [42]. There is, however, only partial consensus on the definition of what constitutes early- and late-onset disease.

In a survey of ISSHP experts, 73% of respondents considered a diagnosis of pre-eclampsia at < 34 weeks to be early-onset [43]. Others have argued that the exact gestation of disease onset is difficult to determine, and gestation of delivery is a more reliable measure [14]. Preterm delivery thresholds of both 37 weeks and 34 weeks have been cited in the literature as definitions of early-onset pre-eclampsia.

In an international comparative study, the rate of early-onset pre-eclampsia was between 0.3 % and 0.7 % of pregnancies, accounting for around 10 – 30 % of all pre-eclampsia cases [44]. Early-onset pre-eclampsia is associated with more severe disease, with higher rates of maternal and perinatal morbidity and mortality [45]. Uteroplacental dysfunction, fetal growth restriction and placental pathology are much more common with early disease [46, 47].

Late-onset pre-eclampsia is less commonly associated with the fetal effects of the condition, with birthweights similar to those of babies born to normotensive mothers [48]. Although often associated with less severe disease, late-onset pre-eclampsia is not a benign condition; around 56% of incidences of eclampsia occur in women who are > 37 weeks' gestation [49]. Many of the severe features of late-onset pre-eclampsia are likely moderated by the practice of inducing labour in women with pre-eclampsia after 37 weeks' gestation, which is consistent with its shorter duration compared to early-onset disease [50].

The different placental origins of early- and late-onset pre-eclampsia will be discussed later in this thesis.

1.2.6 Related Conditions and Atypical Presentations

Pre-eclampsia represents one of several conditions grouped as "hypertensive disorders of pregnancy".

Gestational hypertension occurs when *de novo* hypertension develops after 20 weeks' gestation, without proteinuria or other end-organ dysfunction that would suggest a diagnosis of pre-eclampsia [12]. In this sense, a diagnosis can only be definitively made retrospectively, in the absence of these features after the completion of pregnancy.

Gestational hypertension is common, affecting around 6 % of pregnancies [51]. Debate exists as to whether it represents a truly independent condition or is a milder phenotype of pre-eclampsia. There is large degree of overlap in the risk factors for both conditions and progression to pre-eclampsia is common; between 25 – 46 % [52, 53].

Chronic or pre-existing hypertension can sometimes be first diagnosed during pregnancy. It is usually identified in the first or second trimester, or when gestational hypertension fails to resolve in the postnatal period [12]. Chronic hypertension is an important risk factor for pre-eclampsia, with around 25% of women developing superimposed disease [54]. The diagnosis of superimposed pre-eclampsia can be challenging, particularly in women who have concurrent renal disease and proteinuria [55].

Atypical presentations of pre-eclampsia that occur before 20 weeks' gestation or > 48 hours postpartum are acknowledged. The former is most commonly associated with hydatidiform molar pregnancies [56]. Other atypical presentations, including pre-eclampsia without overt hypertension are also recognised, as is observed in up to 20 % of cases of HELLP syndrome [57].

There are several conditions that can present in pregnancy that may mimic the multi-system features of pre-eclampsia. These include acute fatty liver of pregnancy (AFLP), thrombotic thrombocytopenic purpura (TTP), haemolytic uraemic syndrome (HUS) and systemic lupus erythematosus (SLE) [51].

1.2.7 Risk Factors for the Development of Pre-eclampsia

Women should be screened in early pregnancy for the presence of risk factors which increase the likelihood of the development of pre-eclampsia and other hypertensive disorders of pregnancy [5, 6]. NICE divide these risks into 'high' and 'moderate' categories. Women with one 'high', or two 'moderate' risks should be offered closer monitoring and antiplatelet therapy [5]. Several large meta-analyses have determined the relative risk of different factors in the development of pre-eclampsia. These are displayed in Table 2

Risk Factor	Unadjusted Relative Risk (95% CI)	Reference
Previous pre-eclampsia	8.4 (7.1 – 9.9)	[58]
Chronic kidney disease	1.8 (1.5 – 2.1)	[58]
Autoimmune (SLE / antiphospholipid antibody syndrome)	SLE: 2.5 (1.0 – 6.3) APS 2.8 (1.8 – 4.3)	[58]
Type 1 or type 2 diabetes	3.7 (3.1 – 4.3)	[58]
Chronic Hypertension	5.1 (4.0 – 6.5)	[58]
Nulliparity	2.1 (1.9 – 2.4)	[58]
Maternal age ≥ 40	1.5 (1.2 – 2.0)	[58]
Pregnancy interval > 10 years	1.3 (1.1 – 1.5)	[59]
Body mass index (BMI) ≥ 35 kg/m^2	2.1 (2.6 – 2.9)	[60]
Family history of pre-eclampsia	2.9 (1.7 – 4.9)	[60]
Multi-fetal pregnancy (twins or higher order multiple)	2.9 (2.6 – 3.1)	[58]

Table 2 – Risk Factors for the Development of Hypertensive Disorders of Pregnancy

Shaded rows are risks categorised by NICE as 'high' versus unshaded 'moderate'. One high risk factor or two or more moderate risk factors should prompt pre-eclampsia prophylaxis with antiplatelet therapy (aspirin).

1.3 The Placental Origins of Pre-eclampsia

> *"There can be no doubt that pregnancy is the cause of eclampsia and that the poison is, at any rate, in its ultimate origin to be traced to the child or to the placenta. That it is not the child is proved by its occurring in cases of hydatid mole, where there is no foetus. This leads inevitably to the conclusion that the direct or indirect source of the poison resides in the chorionic elements".*
>
> James Young, 1914 [61]

1.3.1 Embryological Development of the Placenta

The placenta forms from trophoblasts, which is the first cell line to differentiate in human embryonic development, around five days following fertilisation. The development marks the transition from the morula to the blastocyst, which is characterised by a layer of mononuclear trophoblasts, surrounding a fluid filled cavity (blastocoel) and the inner-cell mass.

Implantation begins from day six, when the trophoblasts adjacent to the inner-cell mass connect with the uterine endometrium (Figure 1). The cells at the contact point fuse with their neighbouring trophoblasts, forming the first multinucleated syncytiotrophoblasts; a process that continues, so that by day eleven the blastocyst is surrounded by a syncytium [62].

Fluid filled spaces (lacunae) begin to appear in the syncytiotrophoblasts at the site of implantation from day eight following fertilisation. The lacunae continue to enlarge and coalesce, until three major zones of the primitive placenta become evident [62]. A layer of chorionic trophoblasts adjacent to the embryo, which will form the chorionic plate; the lacunar zone of syncytiotrophoblasts which will form the villous trees and intervillous space; and a layer of cells contacting the endometrium forming the basal plate [63].

A layer of mononuclear trophoblasts, now termed cytotrophoblasts, persists between the syncytium and the inner cell mass. From day twelve, these cells start to invade and then breach the layers of the placenta forming extravillous trophoblasts. Migrating in columns,

these cells further differentiate into interstitial trophoblasts that invade the decidua and anchor the placenta, and endovascular trophoblasts that migrate to the maternal spiral arteries and are involved in vascular remodelling [64, 65].

The formation of the villous system is the final part of placental embryological development. From approximately day thirteen, proliferation within the syncytial trabeculations of the lacunar zone, lead to a development of a cytotrophoblast core. The villi start elongating and branching and whilst made solely of trophoblasts are termed primary villi [62].

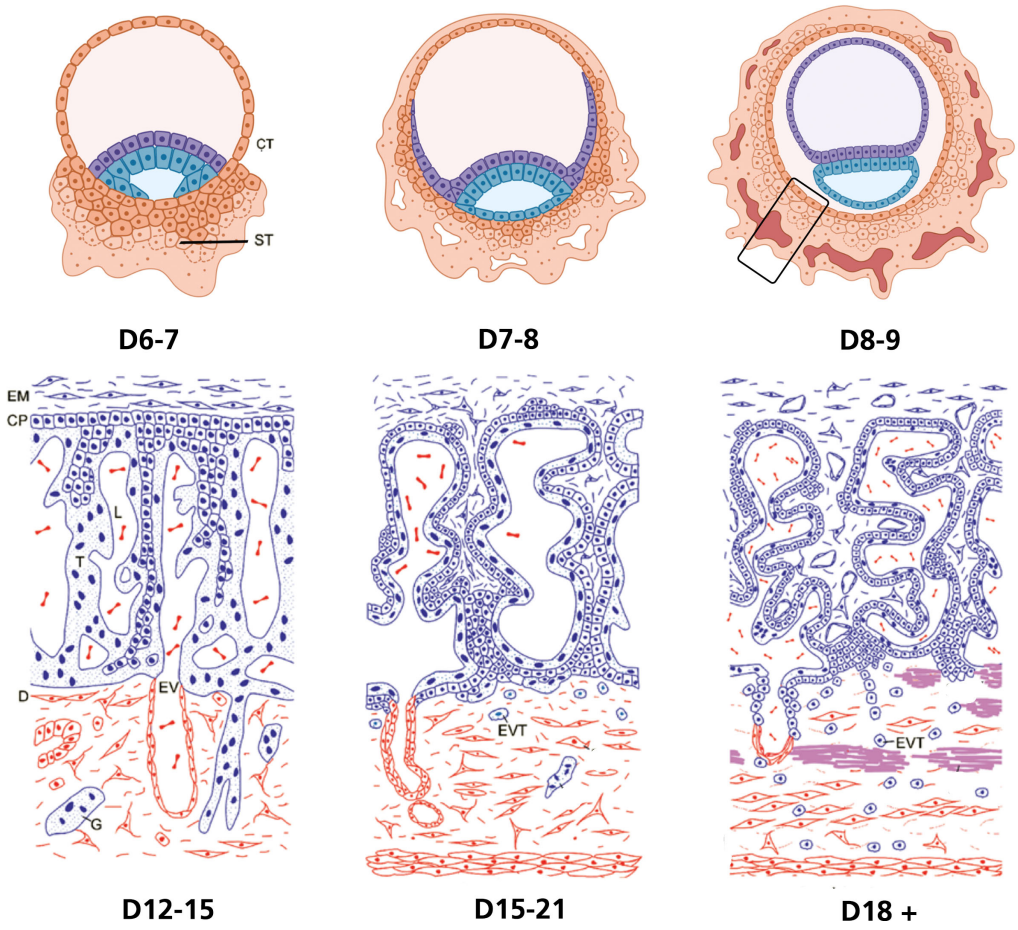

Figure 1 – Placental Development and Embryogenesis
At day 6-7 the blastocyst contacts the endometrium and form the first syncytiotrophoblasts, which will by day 11 surround the blastocyst. Day 8-9 represents the start of the lacunar phase as fluid filled spaces appear in the syncytium. By day 12 the first primary villi are formed, which progress to secondary and tertiary villi from day 15 and 18 respectively. CT: cytotrophoblast, SB: syncytiotrophoblast, D: decidua, EV: endometrial vessel, EVT: extravillous trophoblast, EM: extraembryonic mesoderm, CP: chorionic plate., G: giant cell Adapted from Pathology of the Human Placenta, Benirschke et al. (2006). Created with BioRender.com

Cells from the embryonic mesoderm start to penetrate the primary villi from around day fifteen, marking the transition to the secondary villous stage [62]. Haemangioblastic progenitors contained within this villous core of mesoderm, differentiate into endothelial and placental blood cells, with the first tertiary villi containing early fetal capillaries evident from around day twenty-one [62]. This pattern of villous development continues throughout pregnancy, but with the accumulation of tertiary villi as the placenta grows the relative number of primary and secondary villi present in advanced gestations is very low [66].

1.3.2 Spiral Artery Remodelling

Remodelling of the endometrial spiral arteries is an important step in the adaptation of the maternal uterine vasculature to pregnancy. It begins in the first few weeks of gestation and is largely complete by the mid-second trimester [67].

Outside of pregnancy the uterine spiral arteries are comprised of an endothelial layer, surrounded by extracellular matrix (ECM) proteins and a layer of vascular smooth muscle cells. They can be described as low-flow and high-resistance vessels. Remodelling takes place in several stages, with the result of altering the characteristics of the spiral arteries creating the high-flow, low resistance vessels that are required to support the growing fetus [68].

The first stage of spiral artery remodelling occurs independently of trophoblasts. Dilation, disorganisation and fibrinoid changes of the vascular smooth muscle and ECM is observed very early after implantation and is thought to be driven by decidual natural killer cells and macrophages [69, 70]. The arrival of interstitial trophoblasts that invade the perivascular tissues and stroma marks the start of the second stage and results in further disruption and damage to the smooth muscle layer of the vessel [71].

Endovascular trophoblasts are then able to migrate through to the lumen of the spiral arteries and initially form trophoblastic plugs [72]. These plugs have the effect of obstructing the flow of maternal blood into the intervillous space and creates an environment of feto-placental hypoxia, which is maintained until the end of the first trimester [72]. This low oxygen tension is important for trophoblastic function and differentiation and their role in vessel remodelling [73, 74].

There are several mechanisms by which the endovascular trophoblasts are implicated in the changes which occur in spiral arteries. Trophoblasts appear to induce apoptosis of vascular cells, including endothelial cells, followed by trophoblast phagocytotic clearance [75, 76]. Extra-villous trophoblastic production of proteases including metalloproteinase (MMP) -2, and -9 are important in the breakdown and remodelling of ECM proteins [77].

The result is the destruction and replacement of the endothelial layer of the artery, with endovascular trophoblasts. These are embedded into a fibrinoid layer that has replaced the vascular smooth muscle cells. The effect is vessel dilation, a loss of elasticity and a loss of vasomotor control [71]. Over the course of the pregnancy, the vessel will eventually re-endothelialise and develop subintimal cushions that may help repair the vessels postnatally [64, 78].

The trophoblastic plugs begin to lyse around eight weeks gestation, a process that starts peripherally and progresses centripetally. This allows the perfusion of maternal blood into the intervillous space and an increase in oxygen tension [79, 80]. The process continues over several weeks and can be demonstrated by Doppler ultrasound, displaying a steady decline in vascular resistance and progressive intervillous space perfusion up to twenty weeks [63, 81].

1.3.3 Normal Placental Anatomy

At term the placenta is a discoid organ, approximately 22cm in diameter with a thickness of 2.5cm and weight of 470g [62]. The fetal surface comprises the chorionic plate which is in turn covered by the amnion. The umbilical cord typically attaches centrally and is comprised of two arteries delivering deoxygenated blood from the fetus, and one vein delivering oxygenated blood from the placenta [82]. The umbilical vessels are continuous with the chorionic vessels which run prominently on the fetal surface (Figure 2), which in turn supply the villous trees.

The maternal surface of the delivered placenta consists of the basal plate, which is further divided by several grooves corresponding to between ten and forty individual cotyledons or lobes. Each cotyledon contains between one and four villous trees that arise from the chorionic plate (Figure 2) [62, 83].

The functional part of the placenta is the villous system. In the term placenta, several subtypes of villi can be identified. Stem villi are large structures that connect to the chorionic plate and provide structural support to the whole villous network. They are characterised by large feeding arteries and veins, arranged in a dense stroma with very few capillaries [62].

Mature intermediate villi arise from the peripheral aspects of stem villi. They are generally long slender projections, containing a stroma with small peripheral vessels and capillaries. Vessels occupy up to 50% of the villous when in cross section [62].

Terminal villi are grape like structures and the final branches of the villous system. They arise from mature intermediate villi and are small (30-80 µm in diameter) with a high degree of capillarisation (greater than 50% of the villous in cross section) [62, 84]. They are the primary functional site of maternal-fetal exchange which takes place at the vasculo-syncytial membrane. The capillaries in terminal villi often dilate into sinusoids and are separated from the syncytiotrophoblast by a thin joint basement membrane. The large surface area of terminal villi means they account for about 50% of the total villous system [84].

The ultrastructure of the terminal villous further highlights its important role in diffusional exchange. The syncytiotrophoblast is covered in a micro-villous brush border, increasing

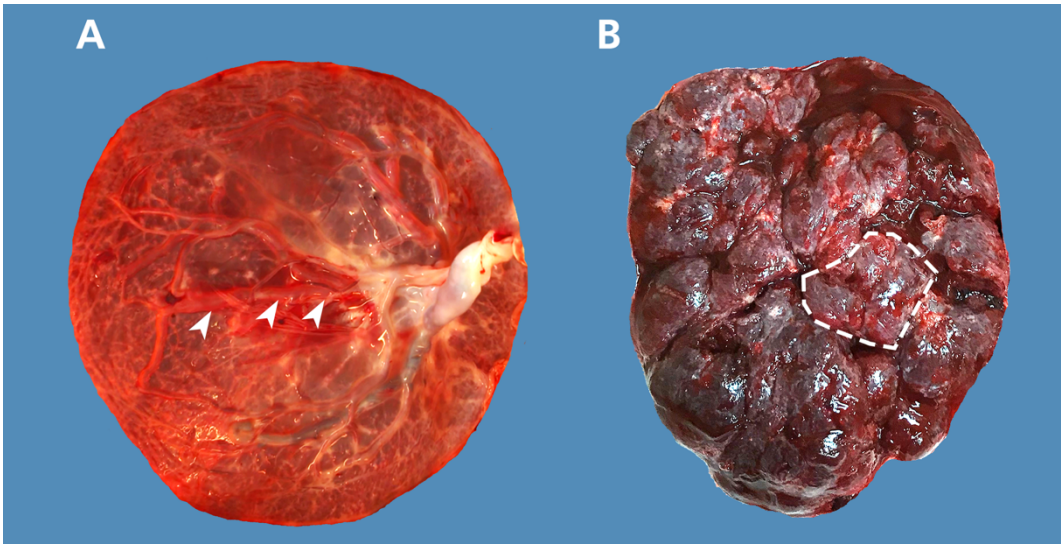

Figure 2 – Placental Surface Anatomy
The fetal (**A**) and maternal (**B**) surfaces of the term normal placenta. The cord insertion is slightly eccentric in this example. The chorionic vessels are evident over the fetal surface (arrows). A single cotyledon has been shown on the maternal surface. The average placenta will have between 10 and 40 cotyledons.

the available cellular surface area [85]. The microscopic features of the terminal villous are demonstrated in Figure 3

1.3.4 Abnormal Placentation - The Two-Stage Model

The link between poor placentation and the development of pre-eclampsia has been known for over 50 years, with particular focus on the abnormal remodelling of the uterine spiral arteries [86].

A failure in the process of extra-villous trophoblasts to sufficiently invade the spiral arteries leads to shallow remodelling, which in turn leads to a state of utero-placental dysfunction [64, 68]. This forms the basis of the original two-stage model of pre-eclampsia suggested by Redman in 1991. A failure in the process of spiral artery remodelling and placentation occurring in the first trimester represents stage one. The long term consequence of this, is an oxidatively stressed placenta, triggering the release of factors into the maternal circulation and stage 2, the maternal syndrome of pre-eclampsia, presenting in the second and third trimesters [87].

Over time the two-stage model has been further developed and refined. The early focus on the role of extra-villous trophoblasts in remodelling has been expanded to include other mechanisms which also contribute to the first trimester failure of placentation. Specifically, the pre-conceptional function of the endometrium, the trophoblast independent phase of remodelling and the premature unplugging of the spiral arteries [88, 89].

The mechanism of placental injury resulting from inadequate spiral artery remodelling has also been clarified. Historically poor placentation was assumed to lead to a state of chronic placental hypoxia, which in turn tiggered a placental response [24]. More recent work has demonstrated that the flow volume of maternal blood into the intervillous space is actually relatively unaffected [90]. Instead, poorly remodelled spiral arteries lead to a more pulsatile and high-pressured flow, which leads to ischaemic-reperfusion injury and oxidative stress [89, 90]. The result is the release of inflammatory factors which target the maternal endothelium and lead to the syndrome of pre-eclampsia [24].

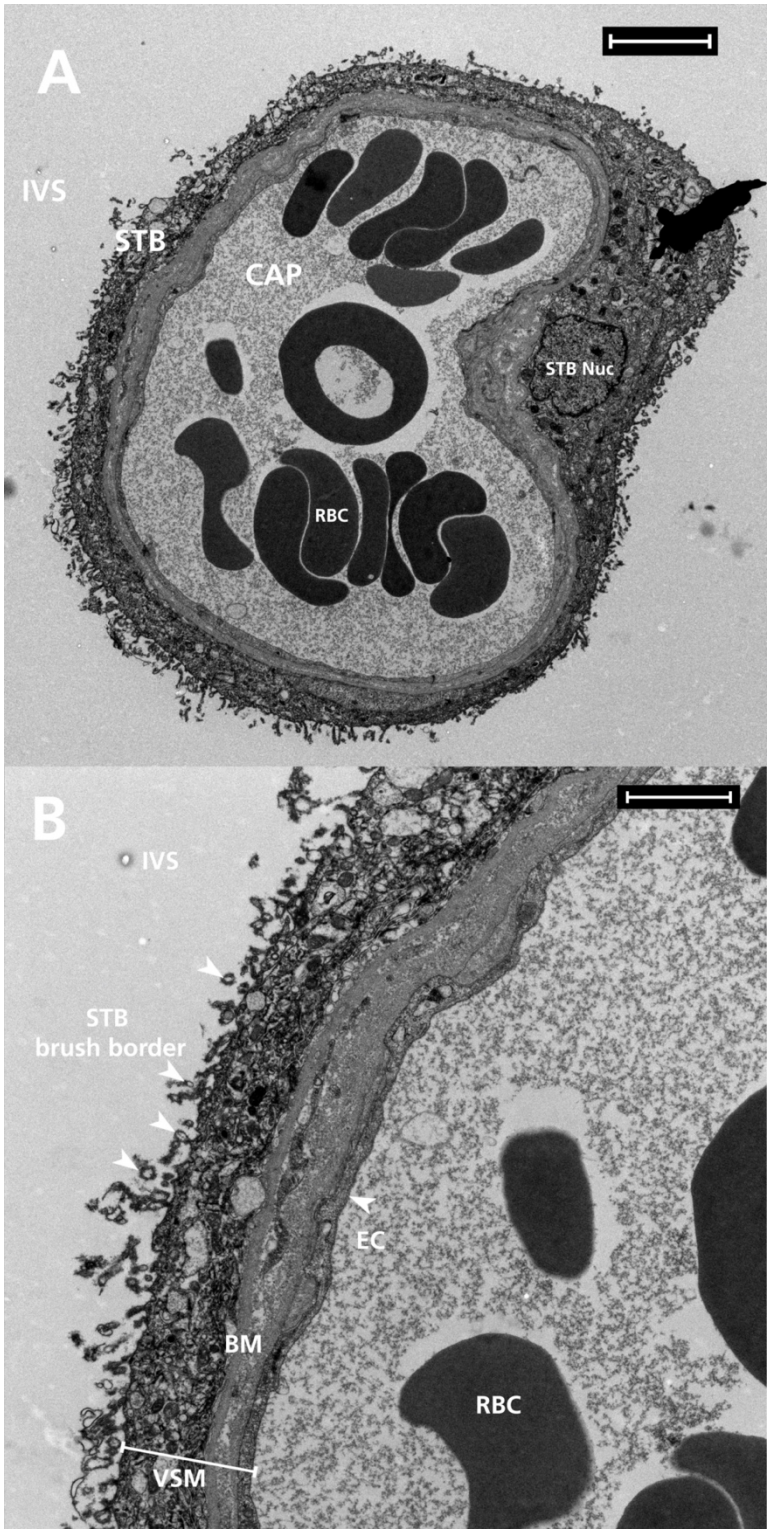

Figure 3 – Ultrastructure of the Terminal Villus

A. An electron micrograph of a cross section of a terminal villus. The capillary (CAP) has formed a sinusoid occupying nearly the whole cross section. Fetal red blood cells (RBC) can be seen within. In life, the intervillous space (IVS) would be perfused with maternal red blood cells. B. At higher magnification the syncytiotrophoblast (STB) micro-villi brush border (arrows) can be seen. The vasculo-syncytial membrane (VSM) consists of the endothelial cell (EC), a joint basement membrane (BM) and the syncytiotrophoblast, approximately two microns in this example. Scale marker A is equal to 5 µm and B 2 µm.

The main difficulty with the original two-stage model, is that inadequate spiral artery remodelling is neither specific nor a universal feature of pre-eclampsia [91]. In one meta-analysis the incidence of villous and vascular histopathological placental lesions was 42% in the pre-eclamptic population, highlighting most placentae from women with pre-eclampsia are histologically normal [92]. Similarly, histological evidence of malplacentation can be commonly observed in women with pregnancy complications other than pre-eclampsia (e.g. fetal growth restriction) [93], and in 9% of placentae from apparently normal pregnancies [92]. Placental pathology and fetal growth restriction is a much more common feature of early-onset pre-eclampsia than late-onset disease [46, 47].

The current evidence makes it clear that abnormal placentation cannot be the definitive cause of pre-eclampsia, but instead represents one of the pathways which can lead to a specific phenotype of the condition; specifically, early-onset disease.

1.3.5 Syncytiotrophoblast Stress

The two-stage model had to adapt and expand to give a unified explanation of the placental origin of the many different phenotypes of pre-eclampsia. A key development in this process was the identification of syncytiotrophoblast stress as a potential common convergent pathway in pre-eclampsia pathogenesis [14].

Senescence describes the process of cellular aging and is characterised by the irreversible arrest of cellular proliferation [94, 95]. Progressive shortening of telomeres is one of the key driving forces, causing the exposure and damage of underlying DNA, starting the pathway towards senescence [96]. Environmental stressors, and particularly oxidative stress, mitochondrial stress, and endoplasmic reticulum stress, have been demonstrated to accelerate this process [97, 98].

Syncytiotrophoblasts demonstrate one of the key features of senescence as soon as they are created; their fusion into a singular layer mandates the arrest of the cell cycle and therefore their ability to proliferate [14]. As the placenta ages there is increasing expression of cellular markers of senescence, including p16, p21 and senescence-associated beta galactosidase (SA-ßGal) and progressive telomere shortening [95]. Senescence can be considered physiological; the placenta has a lifespan and ages as it approaches term [95].

In instances where the progress towards senescence is accelerated, syncytiotrophoblasts can start a process of decompensation. This is characterised by the production of pro-inflammatory cytokines and antiangiogenic factors, which can be released into the maternal circulation to deleterious effect [99].

Syncytial knots are an example of the effects of syncytiotrophoblast senescence and can be easily visualised by microscopy making them helpful in explaining this concept. They are characterised by aggregates of nuclei that occur as outgrowths at the trophoblastic surface [100]. They can be induced *in vitro* by exposing trophoblasts to a hypoxic environment demonstrating that oxidative stress is important in their formation [101]. They are commonly observed in early-onset pre-eclampsia and in other conditions where maternal hypoxia exists [101].

Importantly, syncytial knots are also present in increasing numbers with advanced gestation in uncomplicated pregnancy (Figure 4); their presence has been considered physiological [100]. An alternative interpretation, however, would be that this is evidence of an underlying progression towards syncytial stress, even in seemingly normal pregnancy. Pre-eclampsia, or other placenta related adverse pregnancy outcomes occur when this process is accelerated towards decompensation and may explain the increase incidence of these conditions with post maturity [14, 100].

Redman et al. refer to the late decline in placental function towards term as the “twilight placenta” [14]. The mature placenta is characterised by increasing hypoxia and subsequent acceleration towards senescence which would eventually lead to decompensation of the syncytiotrophoblast. Mathematical modelling suggests that if delivery (spontaneous or iatrogenic) were not to intervene, all pregnancies would eventually succumb to the effects of syncytiotrophoblast stress, with the development of pre-eclampsia or one of the other associated complications [102].

This is an important consideration for pre-eclampsia research which often utilises comparisons of disease against control subjects with seemingly uncomplicated pregnancies. These ‘normal’ pregnancies may instead represent a pre-disease state with the outcome moderated by delivery prior to the onset of a clinically detectable syndrome [14].

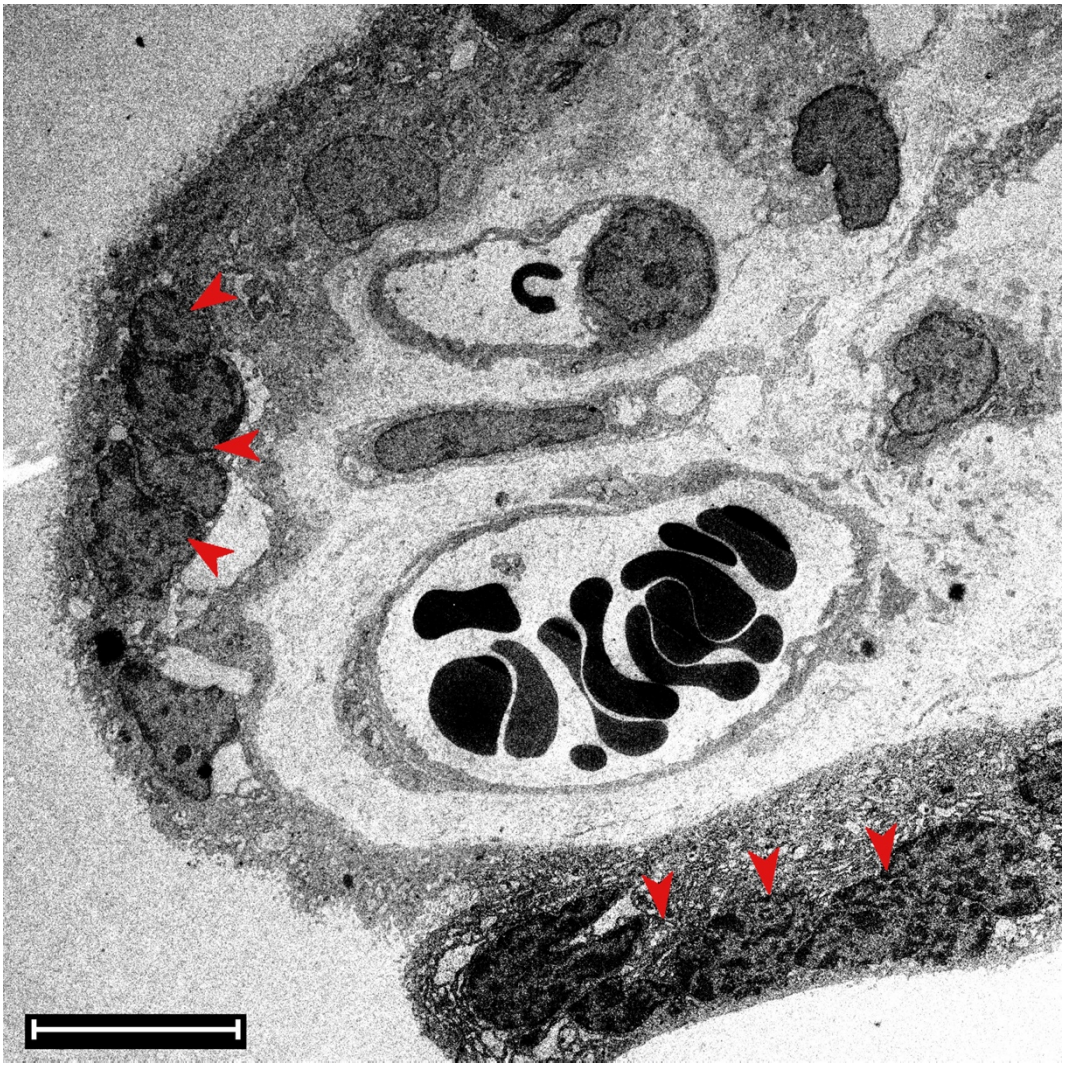

Figure 4 – Syncytial Knots
Evidence of syncytial knots (red arrows) in a term uncomplicated pregnancy. They are characterised by clusters of transcriptionally inactive syncytiotrophoblast nuclei. Syncytial knots are a feature of placental malperfusion and are commonly seen in early onset pre-eclampsia but are also seen in increasing frequency in the aging normal placenta. Their presence provides evidence of syncytial stress in apparently healthy pregnancy. Scale marker is 10 µm.

1.3.6 The Revised Two-Stage Model of Pre-Eclampsia

A revised version of the two-stage model was suggested in 2019, focussing on the role of syncytial stress as the key convergent mechanism defining stage one, Figure 5 [103].

Two distinct mechanistic pathways were described. The first is familiar from the original model. Poor placentation in the first trimester, developing over a period of many months and characterised by a failure of spiral artery remodelling leading to placental oxidative stress and importantly syncytial stress [103]. This pathway is typically associated with early-

onset pre-eclampsia, with the failure of placentation over an extended period, accounting for the strong association with fetal growth restriction [103].

The second pathway occurs on a background of normal placentation, but with an intrinsic placental problem developing over weeks, typically in the latter stages of pregnancy. Redman et al. attributes this process to villous congestion [91]. There is an increased demand of the placenta by the growing fetus, but this is limited by the finite space of the uterus [91]. Terminal villi are compressed with an increased packing density, resulting in restricted perfusion of the intervillous space and a relative hypoxia [104]. The result is the same as in the first pathway; syncytial stress and accelerated senescence, triggering an equivalent maternal response.

The scenario described in the second pathway more typically leads to the development of late-onset or term pre-eclampsia, which, due to its much shorter disease course is less likely to be associated with fetal growth restriction [103]. It also explains the association of

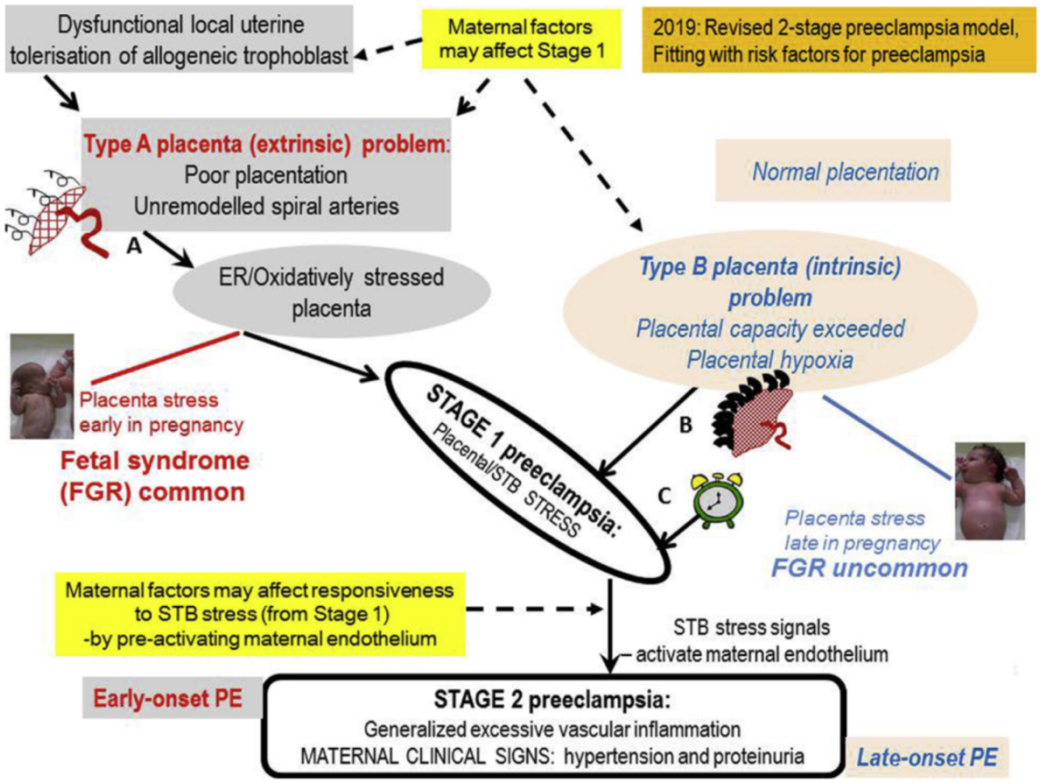

Figure 5 – The 2019 Revised Two-Stage Model of Pre-eclampsia
Two main mechanisms of placental dysfunction. Type A through the effects of poor placentation in the first trimester and Type B through relative placental hypoxia through villous compression. Both culminate in syncytial stress and represent stage 1. The effect of syncytial stress is activation of the maternal endothelium, leading to dysfunction and vascular inflammation. Figure from Staff (2019).

increasing pre-eclampsia rates in conditions which have larger placentas such as in multiple pregnancy [105, 106].

The model recognises that not all cases of pre-eclampsia will comfortably fit into these two mechanistic pathways, nor are the pathways necessarily fully described or understood [91]. A mixed picture with a combination of suboptimal placentation and an accelerated trend towards senescence for other reasons is possible [103]. Similarly rarer causes of pre-eclampsia with defined mechanistic pathways such as can occur following parvovirus infection can also be incorporated into the model. The key feature is the convergence of all these processes at syncytial stress [14].

The second stage of the revised two-stage model is largely unchanged and represents the maternal consequences of syncytial stress mediated through vascular inflammation and endothelial dysfunction. It is at this level that we propose the glycocalyx is important in mediating the endothelial response and will be discussed in detail later.

1.3.7 Maternal Factors

The revised model highlights the importance of the pre-existing maternal condition at all stages of both the development of syncytial stress and the subsequent maternal response to it. Staff et al. used a worked example of maternal obesity, a recognised risk factor for pre-eclampsia to explain this [89, 103].

Obesity is known to cause chronic inflammation, which in turn can affect maternal endometrial function and therefore play a role in the dysfunctional remodelling of the spiral arteries [107]. Obesity is also associated with fetal macrosomia and large placentas which, as previously described, may contribute to villous congestion [108]. Thirdly obesity causes an elevated level of vascular inflammation, thus causing pre-activation of the maternal endothelium, making it more susceptible to the effects of the proinflammatory factors released by the placenta [109].

The example of obesity highlights the complexity of the interplay of the pre-existing maternal condition with multiple different, but interconnected pathways. Through effects of placentation and villous congestion hastening syncytiotrophoblast stress, through to the maternal response to the stressed syncytium. Most recognised pre-eclampsia risk factors can be incorporated into the model in this way [103].

Although the prevailing opinion is that pre-eclampsia remains a primary placental condition, it is worth acknowledging that this is not universally accepted. Thilaganathan et al. argue that pre-eclampsia is instead a manifestation of cardiovascular disease, and the failure of the maternal cardiovascular system to adequately adapt to pregnancy. The placental manifestations are secondary to this [110, 111].

Evidence for this interpretation comes from the many shared risk factors for pre-eclampsia and cardiovascular disease, along with research demonstrating cardiovascular and angiogenic dysfunction prior to the onset of pre-eclampsia [112]. Similarly, the increased risk towards cardiovascular disease in later life, suggest an underlying disease process that is revealed by the cardiovascular strain of pregnancy, in a similar way to gestational diabetes [113]. It is clear that the interplay between pre-existing maternal cardiovascular dysfunction and its placental effects is going to be an important area of ongoing research.

1.4 ENDOTHELIAL DYSFUNCTION IN PRE-ECLAMPSIA

> *"We propose that poorly perfused placental tissue releases a factor(s) into the systemic circulation that injures endothelial cells. The changes initiated by endothelial cell injury set in motion a dysfunctional cascade of coagulation, vasoconstriction, and intravascular fluid redistribution that results in the clinical syndrome of preeclampsia".*
>
> Roberts et al, 1989 [11]

1.4.1 ANGIOGENIC IMBALANCE

The recognition of the endothelium as the primary disease target in pre-eclampsia was an important advancement in our understanding. It changed the focus away from just hypertension, towards our current understanding of widespread endothelial dysfunction and vascular inflammation.

Roberts et al. in 1989 highlighted the endothelial effects of the condition, ranging from the characteristic renal finding of glomerular endotheliosis to the circulating biomarkers that are hallmark of endothelial damage [11]. Increased concentrations of generalised markers of endothelial dysfunction, including fibronectin, factor VIII antigen and thrombomodulin are all recognised [114, 115]. It is now accepted that all the clinical signs and symptoms of pre-eclampsia can be attributed to dysfunction of the endothelium.

Evidence for a circulating factor or factors as the cause of pre-eclampsia, came from experimental models demonstrating dysfunction in isolated endothelial cells when exposed to pre-eclamptic serum. It was theorised that the placenta was the likely source and formed the basis of the original two-stage model previously discussed [11, 87].

Throughout the 1990s there was renewed focus in trying to identify the link between the placenta and the dysfunction of the maternal endothelium. Maynard et al. in 2003 identified soluble fms-like tyrosine kinase 1 (sFlt-1) as a potential target [116]. In their seminal paper they demonstrated that expression of sFlt-1 is upregulated by the placenta in pre-eclampsia, with corresponding increases in circulating levels. Additionally, they were able to demonstrate that sFlt-1 administration to a pregnant rat model, induced the key

features of the condition; hypertension, proteinuria and glomerular endotheliosis [116]. The concept of pre-eclampsia occurring secondary to a placentally driven imbalance in angiogenesis was created.

1.4.2 THE VEGF SYSTEM

Vascular endothelial growth factor – A (VEGF) is an important regulator of angiogenesis and general endothelial health [117]. It belongs to a wider family of glycoproteins that includes placental growth factor (PLGF), VEGF-B, VEGF-C and VEGF-D which vary in their angiogenic potency and tissue targets [118].

VEGF family signalling in endothelial cells is mediated through two related receptor tyrosine kinases, VEGFR-1 (also know as Flt-1) and VEGFR-2 [119, 120]. VEGF binds to both VEGFR-1 and VEGFR-2, whereas PLGF only binds VEGFR-1 [121]. The majority of angiogenic effects of VEGF seem to be mediated through VEGFR-2 [122]. VEGFR-1 does not convey an effective mitogenic signal and may actually perform an inhibitory role by reducing the available VEGF for binding with VEGFR-2 [123]. There are, however, several non-mitotic effects of VEGFR-1 binding which include the release of growth factors, upregulation of MMP-9 and a role in the regulation of haematopoiesis [123, 124].

sFlt-1 is a naturally occurring soluble form of VEGFR-1 (it is otherwise known as sVEGFR-1). It is formed by an alternative VEGFR-1 gene splicing which lacks the transmembrane and cytoplasmic domains. It has an inhibitory role, by reducing VEGF and PLGF bioavailability for binding with endothelial VEGFR-1 and -2 [125, 126].

One of the primary effects of VEGF signalling is through the production of nitric oxide (NO) [127]. When VEFG binds with VEGFR-2 phosphorylation and dimerization causes intracellular signalling via the phosphatidylinositol-3 kinase (PI3K) / protein kinase B (also known as Akt) pathway [128]. The result is the activation of endothelial NO synthase (eNOS) which occurs both directly through PI3K/Akt activation and also through a calcium dependent pathway by activation of calmodulin [128]. NO promotes vascular permeability, endothelial cell survival and vasodilation by its effects on vascular smooth muscle. These conditions promote angiogenesis [127].

VEGF signalling also promotes vasodilation through the production of prostanoid prostacyclin (PGI_2) [129]. In this instance VEGFR-2 autophosphorylation triggers signalling

via the phospholipase C gamma (PLCγ)/protein kinase C (PKC) pathway, which activates phospholipase A2 [129].

VEFG has also been demonstrated to be important in many pathological conditions, including tumour angiogenesis [127]. This has led to the pharmacological development of several VEGF signalling pathway inhibitors. The clinical use of these agents gives clear evidence as to the effects of an imbalance in systemic VEGF functioning. Common side-effects include hypertension, proteinuria, renal dysfunction, vascular events, and cardiomyopathy [127], which are clearly all complications common to pre-eclampsia.

1.4.3 VEGF, PLGF AND SFLT-1 IN PRE-ECLAMPSIA

VEGF, PLGF and sFlt-1 are all expressed by the syncytiotrophoblast, and the balance of these factors appears critical to normal placental morphogenesis [130]. The fact that the placenta produces both angiogenic factors (VEFG and PLGF) and their natural antagonist (sFlt-1) is a strong argument to suggest a placental mechanism of regulating placental angiogenesis [130].

PLGF levels are low in non-pregnant women but rise steadily throughout pregnancy peaking at between 29 to 32 weeks before then gradually declining [131]. VEGF by comparison remains low throughout pregnancy [131]. Although PLGF has only a tenth of the affinity for VEGFR-1 when compared to VEGF, its concentration in pregnancy is 40 times higher and highlights its relative importance in angiogenesis during gestation [132].

sFLT-1 levels remain consistent and low throughout normal pregnancy but start to rise gradually from between 33 to 36 weeks until delivery [131].

As previously described circulating levels of sFlt-1 are elevated in women with pre-eclampsia [116], and they begin to rise before the onset of the clinical syndrome [133]. The excess of placentally produced sFlt-1 seems to drive the angiogenic imbalance, as evidenced by a reduction in free (unbound) PLGF and VEGF, but unchanged values when the total concentrations are measured [134].

The trigger for the upregulation of sFLT-1 by syncytiotrophoblasts is not fully understood but may be driven by placental hypoxia. *In vitro* studies demonstrate that cytotrophoblasts upregulate expression of sFlt-1 in response to low oxygen conditions [135]. Similarly,

syncytial knots, which as previously described are marker of syncytiotrophoblast senescence, show a strong localised expression of sFlt-1 [136].

Changes in angiogenic markers have been used to aid in the prediction and diagnosis of pre-eclampsia. In the UK, PLGF testing is now routinely used as a diagnostic adjunct in women presenting with features that are suggestive of pre-term pre-eclampsia [5]. This recommendation was made after a large step-wedged cluster-randomised controlled trial (the PARROT study), demonstrated that PLGF testing led to a significant reduction in the time from presentation to clinical confirmation of pre-eclampsia, with a corresponding fall in maternal adverse outcomes [137].

Redman et al. suggest that syncytiotrophoblast production of sFlt-1 should be considered a biomarker of syncytial stress [14]. The increase in sFlt-1 and reduction in PLGF after 32 weeks in normal pregnancy is further evidence of the gradual increase in syncytial stress with advancing gestation and the concept of syncytial senescence [14]. Although both early- and late-onset pre-eclampsia are associated with changes in the sFLT-1 and PLGF, the relative differences are more pronounced in early-onset disease, which would also be consistent with this hypothesis [138].

1.4.4 Soluble Endoglin

Endoglin (Eng), also known as CD105, is a cell surface co-receptor for transforming growth factor - ß1 (TGF-ß1) which is highly expressed by both endothelial cells and syncytiotrophoblasts [139]. Like VEGF, TGF- ß1 signalling leads to the production of NO, through calcium / calmodulin regulated eNOS activation [140].

A soluble form of Eng (sEng) has been demonstrated to be released from syncytiotrophoblasts, with increased concentrations found in the sera of women with pre-eclampsia [140]. sEng is potently antiangiogenic through its competitive inhibition of TGF-ß1 signalling [140].

The effects of sEng appear to be synergistic and potentiate the antiangiogenic effects of sFlt-1. Patients with especially severe complications of pre-eclampsia have been found to have significantly elevated levels of sEng [141].

1.4.5 End-Organ Effects of Angiogenic Imbalance

The angiogenic imbalance triggered by the pre-eclamptic placenta is an important mechanism in the development of the end organ dysfunction observed in the syndrome.

Many of the target organs effected by pre-eclampsia are characterised by fenestrated endothelium [132]. The induction of endothelial fenestrae is a process which is regulated by the effects of VEGF [142]. In the glomerulus, a reduction in VEGF expression has been shown to result in a loss of endothelial fenestrations, endothelial swelling, and occlusion of capillary lumens, all histological features which describe glomerular endotheliosis, the pathognomonic renal lesion associated with pre-eclampsia [28].

sFlt-1 and sEng mediated reduction in NO and vasodilatory prostacyclins appear to be a key contributory pathway in the development of hypertension in pre-eclampsia. NO is known to be an important regulator of blood pressure through its vasodilating and antiproliferative effects on smooth muscle cells [143]. A reduction in NO and other vasoactive molecules results in vasoconstriction and increased peripheral vascular resistance and suppression of the renin-angiotensin-aldosterone system [144]. Deprivation of VEGF by over-expression of sFlt-1 in a pregnant rat model has been shown to cause hypertension, which can be alleviated through administration of a VEGF isoform [145].

A summary of the end-organ targets and our current understanding of the mechanisms of organ specific endothelial dysfunction has been previously summarised in Table 1.

The protective role of the glycocalyx in maintaining endothelial health, is heavily influenced by VEGF [146-148]. Many of the mechanisms described above, resulting in endothelial activation and inflammation can be mediated by functions of the glycocalyx [149]. I will present data to suggest that the angiogenic imbalance created by the placenta in response to hypoxia, can have a direct effect on the endothelial glycocalyx and may represent one of the mechanistic features which links stage 1, syncytial stress, with stage 2, endothelial dysfunction.

1.5 THE GLYCOCALYX

> *"I deem it desirable to assign a single, general, inclusive term to this extracellular, sugary coating, wherever it may be found. The ancient Greeks had no word for sugar, but they had one for sweet – a taste which we often associate with sugars. I proposed last September ... that we choose to speak generally of this polysaccharide-rich coating of cells as the "glycocalyx". This word means "sweet husk".*
>
> H. Stanley Bennett, 1962 [150]

1.5.1 A SUGARY COATING

With improvements in electron microscopy in the mid twentieth century, it became clear than many different cells and tissue types demonstrate an extracellular layer rich in polysaccharides [150]. By virtue of its location, it was clear that this layer must exert an influence on the interaction between the cell and its external environment. In 1962 Bennett published work summarising the different cell types and tissues that had been shown to exhibit this sugary coating and suggested the term glycocalyx to encompass its description [150].

An extracellular layer on the luminal surface of endothelial cells was hypothesised and modelled for several years prior to its eventual discovery by Luft in 1966 [151]. Using transmission electron microscopy (TEM) in combination with ruthenium red staining, a fine endocapillary layer of glycocalyx was revealed [151].

Decades of research has demonstrated the endothelial glycocalyx to have many vital roles in the function of the endothelium, with increasing evidence that damage to this layer represents a key pathological pathway in several different disease processes, including pre-eclampsia [149].

1.5.2 STRUCTURE OF THE ENDOTHELIAL GLYCOCALYX

The current model of the endothelial glycocalyx is that of two layers [152]. The inner core forms the backbone and is comprised of membrane associated proteoglycans, glycolipids, and glycoproteins [153]. The structure is further stabilised by the binding of proteoglycans to several long polysaccharide chains of repeating disaccharide units called

glycosaminoglycans (GAGs) [154]. The most abundant GAGs within the endothelial glycocalyx are heparan sulphate (HS), chondroitin sulphate (CS) and hyaluronic acid (also known at hyaluronan) (HA) [153]. The nature of the bound GAGs and sialic acid residues of the glycoproteins give the glycocalyx an overall net negative charge [155].

The outer layer of the glycocalyx is comprised of loosely bound plasma soluble components which include plasma proteins, enzymes, growth factors and cytokines which are specifically organised and incorporated into the layer [155]. A schematic of the glycocalyx is presented in Figure 6.

1.5.2.1 Proteoglycans

Syndecans are a family of 4 transmembrane proteoglycans. They consist of an N-terminal ectodomain, a transmembrane domain, and a C-terminal cytoplasmic domain [156]. Post transcription, GAG chains covalently bind to the N-terminal sites. HS is the GAG most associated with syndecans, although syndcan-1 and -4 can also bind CS [156].

The expression pattern of syndecans is complex and varies by tissue [156]. Syndecan-1 is expressed in epithelial cells, plasma cells and importantly by placental syncytiotrophoblast [157, 158]. Syndecan-2 is primarily expressed by mesenchymal cells; syndecan-3 by neural tissue and developing musculoskeletal tissue; and syndecan-4 is abundant in many cell and tissue types [157]. Syndecan-1, -2, and -4 are expressed in the endothelial glycocalyx [155].

Glypican-1 is the other core proteoglycan abundant in the endothelial glycocalyx [155]. As with the syndecans, it binds HS at three or four binding sites [159]. It is bound through a glycosylphosphatidylinositol (GPI) anchor to caveolae in the cell membrane, a type of lipid raft, which are important for vesicular transport and cell signalling [160].

1.5.2.2 Glycosaminoglycans

Heparan sulphate is the most abundant GAG in the endothelial glycocalyx, accounting for up to 90% [161]. It consists of between 50 and 150 repeating disaccharide units of β1–4-linked D-glucuronic acid (GlcA) and α1–4-linked *N*-acetyl-D-glucosamine (GlcNAc) with an average molecular weight of 30 kDa [162]. Heterogenicity in the structure is created through the variable sulphation pattern at the 2-O – position on the uronic acid, or 6-O and 3-O – positions on the glucosamine, which also results in the overall net negative charge [162].

Chondroitin sulphate similarly comprises around 100 repeating disaccharide repeat units, but of GlcA and GlcNAc with varying sulphation [163]. Both HS and CS form covalent bonds with proteoglycans.

The positioning of HS and CS allow direct interaction with many extracellular ligands, including growth factors, cytokines, chemokines, and enzymes, allowing the attached proteoglycans to act as co-receptors with several important physiological effects [157].

Hyaluronan, in contrast to HS and CS is not attached to a trans-membrane proteoglycan and is instead interacts with the cell through various hyaluronan binding surface proteins including CD44 [164]. Unlike HS and CS which are produced intracellularly and excreted, HA is manufactured at the cell membrane by hyaluronan synthases (HAS) [165]. It consists of β-1,3-N-acetyl glucosamine and β-1, 4-glucuronic acid disaccharide repeats. It is much

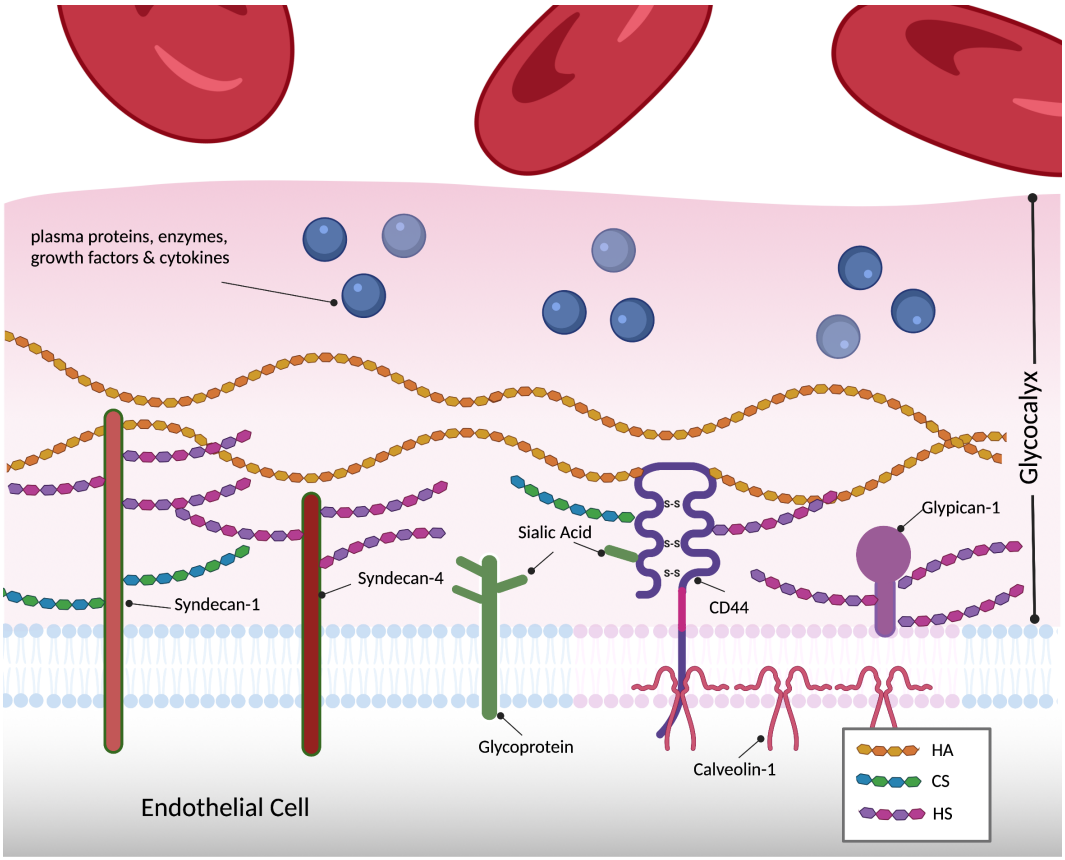

Figure 6 – Structure of the Endothelial Glycocalyx
A simplified schematic of the endothelial glycocalyx is represented. The main structure consists of proteoglycans (syndecans and glypican-1), glycoproteins and glycolipids. The glycosaminoglycans (GAG) heparan sulphate (HS) and chondroitin sulphate (CS) bind to proteoglycans and CD44. Hyaluronan (HA) is a long GAG and signals through CD44. The combination of the GAGs and sialic acid residues present on glycoproteins create a net negative charge. Adapted from Weinbaum et al (2007) and Dane et al (2015). Created with BioRender.com

larger than other GAGs with 2,000 – 25,000 repeats giving a molecular mass of 10^7 kDa [166]. HA is not sulphated, but instead gains its negative charge from the carboxyl groups of glucuronic acid [166].

HA is important to the structural integrity of the glycocalyx due its size and hydrodynamic characteristics. Repulsion between carboxyl groups creates an expanding porous meshwork trapping water inside [166]. Its interaction with CD44 induces signalling that is implicated in cellular aggregation, proliferation, migration, and angiogenesis [167].

1.5.2.3 Glycoproteins

Many endothelial cell surface proteins have short, branched oligosaccharides present and are thus termed glycoproteins. They are characterised by sialic acid caps, which add to the net negative charge of the glycocalyx. Important endothelial glycoproteins include selectins, integrins and immunoglobulins [155].

1.5.3 Endothelial Glycocalyx Function and physiology

1.5.3.1 Microvascular permeability

The endothelial glycocalyx is an important regulator of vascular permeability and therefore the balance between fluid filtration and absorption from the capillary [168]. The physical properties and structure of the glycocalyx have been shown to limit filtration of larger molecules like dextran and albumin [169, 170]. The net negative charge of the glycocalyx also contributes to its control of vascular permeability, favouring smaller anionic molecules [171]. Although difficult to study, it is now widely accepted that damage to the endothelial glycocalyx layer contributes to increased vascular permeability and may have an important pathogenic role in a number of different conditions [149].

1.5.3.2 Modulates adhesion of erythrocytes, inflammatory cells, and platelets

Interactions between circulating blood cells and the endothelium is moderated by the endothelial glycocalyx. Red blood cells, which have their own glycocalyx and a negatively charge are repelled by the endothelial glycocalyx, and encourage adequate laminar flow [172].

Leukocyte adhesion to the endothelial cell is also regulated by the presence of the glycocalyx. Neutrophil, monocyte and T cell migration and adhesion is regulated by the endothelial cell surface glycoproteins P-selectin and E-selectin [173]. In normal physiology

the structure and charge of the endothelial glycocalyx restricts access of leukocytes to these receptors. In conditions of systemic inflammation, cytokines including interleukin 1 (IL-1), tissue necrosis factor alpha (TNFα) and bacterial endotoxins including lipopolysaccharide (LPS) both upregulate the expression of E-selectin and cause damage to the glycocalyx, allowing access of leukocytes to the endothelial surface. The result is increased leukocyte adhesion and extravasation [173-175]. Platelet adhesion is regulated in a similar way [175]

Finally, the endothelial glycocalyx is the site of several factors involved in the clotting cascade, including the important anticoagulants heparin cofactor II, thrombomodulin, antithrombin III, and tissue factor pathway inhibitor (TFPI) [176].

1.5.3.3 Mechanosensor of shear stress

Shear stress is the force applied to a cell through the flow of a fluid across its surface; its value is proportional to the velocity of the fluid [177]. Several studies have identified that components of the glycocalyx are important sensors of vascular sheer stress and are able to respond to increased sheer forces by the release of NO initiating vessel dilation [178, 179]. Removal of HS from cultured endothelial cells by heparinase has been shown to disrupt this process [178].

1.5.4 Glycocalyx Shedding in Endothelial Disease

In normal physiology the glycocalyx is in a carefully balanced equilibrium of biosynthesis of new glycans and shear related removal of the existing components [180]. An increase in glycocalyx shedding has been demonstrated in many different conditions affecting the endothelium including diabetes [181], sepsis [182, 183], atherosclerosis [184], stroke [185], hypertension [186] and more recently pre-eclampsia [187].

The mechanism of glycocalyx shedding is regulated through several enzymes which can cleave specific components of the glycocalyx and are collectively termed ‘sheddases’.

Heparanase cleaves the carbohydrate chains of HS releasing fragments into the circulation. It is present in normal physiology but is upregulated in inflammatory conditions [188, 189]. HA can be cleaved by two hyaluronidase enzymes (HYAL1 and HYAL2) which have similarly been shown to be implicated in glycocalyx damage present in endothelial disease [190].

MMPs are a family of related enzymes, some of which have been demonstrated to have important roles in the maintenance of the glycocalyx. Several MMPs have been shown to cleave both syndecans-1 and syndecan-4 [191, 192].

1.5.5 The Placental Glycocalyx

The placenta has been demonstrated to have two distinct glycocalyx layers at both the maternal and fetal interface. The fetal glycocalyx, is present on the luminal surface of the placental vasculature and was first demonstrated using TEM by Leach et al through placental perfusion of Alcian Blue [193, 194].

The syncytiotrophoblast represents the maternal interface and has been shown to express in large quantities many of the proteoglycans and GAGs familiar with the endothelial glycocalyx including syndecans, glypican-1, HA and HS [195-197]. TEM imaging of this layer was demonstrated by Martin et al in the 1970s using ruthenium red [198] and later by Hofmann-Kiefer using lanthanum [196], although the images are not especially convincing.

There has been limited research into the function of the placental glycocalyx, but there is an assumption that it would share many of the purposes of those attributed to the endothelial glycocalyx [199]. The syncytiotrophoblast, as the placental interface with the maternal blood in many ways behaves like an endothelium.

Alteration of the placental expression of glycocalyx components has been implicated in several pregnancy conditions, including pre-eclampsia. Syndecan-1 is abundantly expressed at the syncytiotrophoblast in the term placenta, but has been shown to be reduced in pre-eclampsia compared to normotensive controls [200]. Similarly, glypican-1 mRNA and protein expression has also shown to be reduced in pre-eclampsia [201].

Large quantities of heparanase are expressed in the placenta. Heparanase is considered pro-inflammatory through its cleavage of HS triggering the release of angiogenic factors like VEFG from the glycocalyx. Heparan-sulphate interacting protein (HIP) is also abundant in the placenta and is a competitive antagonist of heparanase [202]. Expression of HIP is reduced in pre-eclampsia, thus favouring heparanase cleavage and shedding of HS [199, 203].

1.5.6 The Maternal Endothelial Glycocalyx in Pregnancy

Circulating levels of glycocalyx components have been demonstrated in the sera of both normal pregnancy and those complicated by pre-eclampsia.

Circulating syndecan-1 has been demonstrated to increase with gestation in uncomplicated pregnancy, with a 50-fold rise at term, that rapidly falls again following delivery [204, 205]. HA demonstrates a similar increase with advancing gestation, whereas HS levels appear constant throughout pregnancy [206].

Changes in circulating glycocalyx components have been described in pregnancies complicated by pre-eclampsia, although the interpretation is difficult due to conflicting data. Syndecan-1 for example, has been shown to be both increased in HELLP syndrome compared to normotensive controls [206], but either decreased [204, 205, 207] or unaffected in pregnancies with pre-eclampsia [187].

Difficulties in the interpretation of circulating biomarkers may reflect the heterogeneity in the pre-eclampsia phenotypes included for study, as well as methodological differences in the assay used for detection.

The interpretation of circulating glycocalyx biomarkers is further complicated as the source of many of the components is likely to be the placenta rather than the maternal endothelium. The rapid decline in syndecan-1 following delivery in both normal and pre-eclamptic pregnancy would lend to this theory.

Weissgerber et al addressed this in 2019 by using SDF imaging using the GlycoCheck™ device [187]. This study which reported during the preparation of this project and is to date, the largest study using GlycoCheck™ in pregnancy and pre-eclampsia. They demonstrated an increased PBR in early-onset pre-eclampsia compared to normotensive controls, but not in late-onset disease, highlighting maternal glycocalyx shedding as a feature of this specific pre-eclampsia subgroup.

1.6 QUANTIFYING THE GLYCOCALYX

> *"Now is the most beautiful moment to go into preeclampsia research. There have been so many advances in scientific knowledge over the past 10 years that are just waiting to be applied. Answers are going to come tumbling out over the next generation."*
>
> Prof Chris Redman, 2019 [208]

1.6.1 METHODS OF STUDYING THE GLYCOCALYX

The glycocalyx has proven incredibly difficult to study due to its dynamic and fragile nature *ex-vivo*. The thickness of the measured glycocalyx in the literature is highly variable and ranges from between 0.02 µm to up to 4.5 µm [151, 209]. This may partially be explained by genuine variations in the depth of the glycocalyx on different cell types and in different species, but more often is a result of variation in either fixation or the imaging techniques employed.

Reliable methodology for the imaging and most importantly, quantification of the glycocalyx at the maternal and placental surfaces are going to be important to the success of this project, in determining the role of the glycocalyx in the pathogenesis of pre-eclampsia. An appraisal of some of the commonly used techniques for visualising the glycocalyx are presented below.

1.6.1.1 Electron Microscopy

Due to its high polysaccharide content, the glycocalyx lacks an intrinsic electron density and does not react to the common post fixation stains used for transmission electron microscopy (TEM). Luft was the first to demonstrate that the addition of the cationic dye ruthenium red during fixation, was able to bind the anionic residues of the sulphated GAGs, and for the first time demonstrate the glycocalyx [151]. Others have since had success using several different cationic dyes including Alcian blue, lanthanum, dysprosium, ferritin, and L-lysine [210-213].

Perfusion fixation and delivery of the cation gives a more reliable estimation of the endothelial glycocalyx compared to immersion fixation [214]. This is perhaps due to the relative difficulty of the timely access of the fixative and cationic dye to reach the

endothelium and glycocalyx in immersion fixed samples. This feature makes it difficult to examine the glycocalyx of biopsy specimens using TEM [153].

Traditional tissue processing techniques for TEM have been proven to be detrimental to the *ex-vivo* structure of the glycocalyx. The process of chemical fixation followed by dehydration with solvents has been shown to disrupt the covalently bound GAGs causing the glycocalyx to collapse, grossly underestimating its size and appearance [215]. Several techniques have been employed to try and stabilise the structure with some good results with the use of Alcian Blue [210]. An alternate fixation technique using high pressure freezing followed by freeze substitution has been demonstrated by Ebong et al. demonstrating remarkable preservation of the layer compared to conventional chemical tissue fixation [215]. Others have demonstrated that this technique is still associated with substantial collapse and change in the glycocalyx structure [216].

1.6.1.2 Light / Florescence Microscopy

Light microscopy techniques have been utilised to demonstrate the endothelial glycocalyx, either using fluorescently labelled lectins, or antibodies to specific glycocalyx components.

Lectins are carbohydrate binding proteins with high affinity to specific sugar moieties including those found in the endothelial glycocalyx [217]. Several different lectins have been demonstrated to bind with components of the glycocalyx, although the pattern of binding is highly tissue and species specific.

Fluorescently labelled lectins have also been used in confocal microscopy, multiphoton and intravital microscopy techniques [217, 218].

1.6.1.3 Sidestream Darkfield Imaging

Intravital microscopy has been used for several years to demonstrate the endothelial glycocalyx *in-vivo*. It utilises sidestream dark field (SDF) imaging, which is a non-invasive technique of visualising haemoglobin within erythrocytes in real-time. The technology is incorporated into a video microscope, that contains concentrically placed green light emitting diodes (LED), which pulse in synchrony with the camera framerate. The LED emission wavelength of 540 nm corresponds to the absorption range of haemoglobin. The strobed illumination reduces blurring and other movement artefacts [219].

SDF imaging demonstrates an erythrocyte exclusion zone on the luminal surface of endothelial cells which is consistent with the presence of the glycocalyx. In various microvascular diseases where glycocalyx damage is present, erythrocytes can more deeply penetrate the glycocalyx towards the endothelium in an area called the perfused boundary region (PBR) (Figure 7) [220]. SDF imaging can measure the lateral movement of erythrocytes into the PBR in micrometres, providing an indirect measure of glycocalyx depth. An increased PBR is reflective of deeper penetration of erythrocytes towards the endothelium and a more damaged endothelial glycocalyx [220, 221].

1.6.1.4 Biomarkers of Glycocalyx Shedding

The shed components of the glycocalyx are released into the circulation and can be measured in serum and urine assays. Commonly assessed analytes include syndecans, HA and HS with evidence of alteration in the levels of shed glycocalyx components in several disease states [222-224].

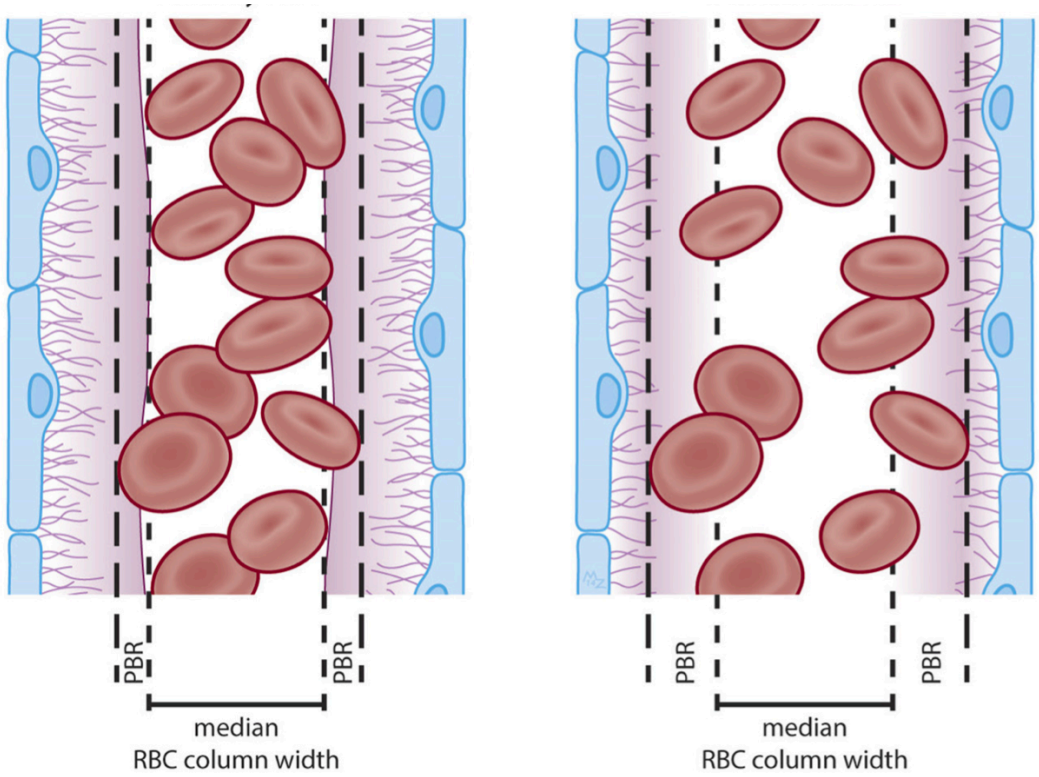

Figure 7 – The Perfused Boundary Region

The glycocalyx acts as a barrier and creates an erythrocyte exclusion zone at the luminal endothelium. In health there is limited lateral movement of erythrocytes and the depth of the perfused boundary region (PBR) is small (left image). In diseases of the microvasculature where there is glycocalyx is damaged, there is greater lateral movement of erythrocytes towards the endothelium and the PBR is increased (right image). Image adapted from Dane et al (2015)

1.7 Introduction Summary and Hypothesis

> *The eclamptic patient has certainly tested the ingenuity of physicians throughout the centuries as she has been blistered, bled, purged, packed, lavaged, irrigated, punctured, starved, sedated, anaesthetized, paralyzed, tranquilized, rendered hypotensive, drowned, been given diuretics, had mammectomy, been dehydrated, forcibly delivered and neglected.*
>
> Zuspan & Ward, 1964 [225]

Acknowledging how our understanding of the pathogenesis of pre-eclampsia has developed with time is important, as it explains the still prevailing clinical focus on the common key observable endpoints of hypertension and proteinuria.

Considering pre-eclampsia instead as a condition of generalised vascular inflammation and endothelial cell dysfunction is an important paradigm shift, that can explain the many varied presentations and organ systems involved. Importantly it has also changed our research focus. There is now acceptance that it is unlikely that a singular cure for this varied condition exists, which has allowed a renewed focus on identifying the mechanistic pathways driving different pre-eclampsia phenotypes.

Redman and Staff have presented a robust model, encompassing our understanding of the two-stage approach to the development of the condition. Stage one is characterised by placental hypoxia, which converges at syncytial stress, resulting in an angiogenic imbalance. Stage 2 describes the effects of this imbalance on the maternal endothelium and the development of the clinical syndrome. It is acknowledged that this occurs in the context of pre-existing maternal factors that can moderate both placental development and the maternal response.

The glycocalyx is the first barrier at the maternal fetal interface, with a significant presence at the syncytiotrophoblast. Combined with our increasing understanding of the important role of the glycocalyx to endothelial health and vascular permeability, it makes for an attractive research target in trying to discern the mechanisms which might link stage 1 and stage 2 of the pre-eclampsia model.

This project will look to determine if glycocalyx shedding at the placental and maternal endothelial glycocalyx is present in pregnancies complicated by pre-eclampsia. If present this would suggest an important mechanistic role for the glycocalyx in the activation and dysfunction of the endothelium in pre-eclampsia.

Due to its small size and fragile nature *ex vivo*, imaging and quantifying the depth of the glycocalyx has proven difficult. To answer my research question, I will look to develop and critically appraise novel research methodologies for quantifying the glycocalyx in the placenta and the maternal endothelium. Techniques used will include *in-vivo* assessment of the maternal sublingual glycocalyx using GlycoCheck™, and TEM and confocal microscopy techniques for demonstrating the placental glycocalyx.

HYPOTHESIS

The depth of the maternal endothelial and placental glycocalyx is reduced in pre-eclampsia, compared to normotensive pregnancy

2. METHODOLOGY

2.1 STUDY DESIGN

2.1.1 ETHICS AND REGULATORY APPROVAL

This research was assessed by the National Research Ethics Service (NRES) committee South West – Central Bristol in 2006 and received a favourable opinion (ref 06/Q2006/54) with the University of Bristol acting as sponsor.

In January 2015, a substantial amendment was submitted by Dr Victoria Bills (University Hospitals Bristol and Weston NHS Foundation Trust) including an updated protocol for the measurement of serum glycocalyx markers and the collection of tissue samples.

Due to a lapse in the necessary NHS permissions, I submitted a non-substantial amendment in January 2018 reconfirming Health Regulatory Authority (HRA) approval and University Hospitals Bristol and Weston NHS Foundation Trust (UHBW) as the study site. The study is registered with the UHBW research and innovation department and has local approval for recruitment (ref. OG/2006/2352).

I submitted a further substantial amendment in February 2019 with a change in the study protocol to include sublingual assessment of the glycocalyx using intravital microscopy.

Sponsorship for the study was temporarily paused in March 2020 due to the impact of the global pandemic of coronavirus disease 2019 (COVID-19). Alterations in the study protocol, particularly around the use of personal protective equipment (PPE) and the handling of biological specimens were approved and sponsorship restored in July 2020.

All biological specimens collected as part of this study are logged, stored and disposed of in accordance with the regulations of the Human Tissue Act 2004 (HTA).

2.1.2 Funding

Funding has been achieved through competitive grant application to the David Telling Charitable Trust. I was awarded £17,940 for the consumables and microscopy costs for the project.

I was also able to secure a charitable donation of £24,600 from the Capella Foundation, who kindly supported the purchase of the intravital microscopy equipment and software.

My time and salary were provided by UHBW through my employment as a clinical research fellow. Approximately 50% of my work schedule was dedicated to research.

2.1.3 Location and Timescale

St Michael's Hospital is part of UHBW and is a large tertiary unit in obstetrics and gynaecology. Specialist services include maternal and fetal medicine which attracts referrals from the South West of England and South Wales. It has a level 3 neonatal intensive care unit (NICU). In the year 2019-2020 there were 4,850 births recorded [226].

Participant enrolment began in August 2017 and continued until March 2021. Enrolment was temporarily paused between March 2020 and September 2020 due to COVID-19.

2.1.4 Participant Selection and Enrolment

A convenience sample of participants who were diagnosed with pre-eclampsia were approached for participation in the study. Pre-eclampsia was defined as per the ISSHP guidelines as *de novo* hypertension (systolic BP ≥ 140 mmHg or diastolic BP ≥ 90 mmHg) on two occasions four hours apart; and at least one of; proteinuria, other maternal end organ dysfunction (in the absence of another cause); or uteroplacental dysfunction [12]. Early-onset pre-eclampsia was defined as diagnosis of pre-eclampsia prior to 34 weeks', whereas late-onset pre-eclampsia was defined as diagnosis at or after 34 weeks' gestation.

Patients were enrolled opportunistically within the hospital from the labour ward, antenatal assessment unit and antenatal ward. A gestation and age matched group of normotensive controls were recruited from routine antenatal clinic appointments.

Participants were excluded if they were less than 18 years old, less than 20 weeks' gestation, had a multifetal gestation, or were in active labour.

Patients were initially approached and provided with verbal information about the study. A written patient information leaflet was provided (appendix 3), and sufficient time allowed to read the information and ask questions. Patients who agreed to participate signed a written consent form (appendix 4) which is stored in the study file, with copies for the patient and their medical record. Participants were assigned an anonymised study number.

2.1.5 Study Visit

I was able to conduct the majority of patient selection, enrolment and study visits myself, but am grateful for the assistance of Dr Hui Liew (University of Bristol, Bristol Renal) and Dr Charles Heffer (University of Bristol, Bristol Renal) who were able to support on occasions I was unavailable.

At enrolment, baseline characteristics, demographic and clinical data were recorded on a case report form (appendix 5). This included a record of laboratory test results (haematology, biochemistry, microbiology, radiology) that were performed as part of routine care in the preceding two weeks.

Blood pressure was recorded whilst sitting using a manual aneroid sphygmomanometer after a period of 5 minutes at rest in accordance with recognised protocols.

Samples of blood and urine were collected and processed as per section 2.2. Approval for the addition of sublingual intravital microscopy to the study visit was granted in February 2019; from this date, imaging of the sublingual glycocalyx was performed and analysed using the GlycoCheck^{TM} software. This procedure is described in section 2.3.

On admission to the central delivery suite in labour, the midwife caring for the patient would alert me by telephone. I would attend the delivery in order to collect samples from the placenta as outlined in section 2.4. Due to the unpredictable nature of labour and my limited capacity to attend every delivery, it was recognised that not all placentas could be collected.

Labour and delivery outcome data was collated postnatally and recorded on the case report form.

2.1.6 Pilot Study

A small number of participants were enrolled into the study who only donated placental tissue for the purposes of methodological development of the tissue fixation protocols.

These participants were selected opportunistically and were generally women undergoing elective caesarean section. They had uncomplicated pregnancies and were normotensive. Indications for caesarean section included maternal request, previous caesarean section and breech presentation.

Elective caesarean sections were chosen as they generally take place at fixed and predictable times, providing convenience when planning experiments. Delivery of the placenta at caesarean section is also generally quicker than vaginal birth; the stability of the glycocalyx after delivery was an important research question that I looked to consider.

2.1.7 Non-Pregnant Participants

A small number of male and non-pregnant female volunteers were selected for the purposes of operator training and inter- and intra-operator reliability assessments with the sublingual intravital microscopy, as described in section 2.3.3.

2.2 Collection, Processing and Storage of Blood & Urine

2.2.1 Blood

Blood was collected by peripheral venepuncture directly into 2 x 4ml BD Vacutainer® serum tubes with silica (clot activator) (Becton, Dickinson and Company, Franklin Lakes, USA, 368975), and 2 x 4ml BD Vacutainer® plastic whole blood tubes with spray coated dipotassium ethylenediaminetetraacetic acid (K_2EDTA) (Becton, Dickinson and Company, Franklin Lakes, USA, 367839).

Samples were kept at room temperature for between 60 – 120 minutes and then centrifuged using an MSE Centaur 2 centrifuge (Medical Scientific Equipment, Nuaillé, France), at 3000 rpm (1300 g) for 10 minutes, in accordance with the manufacturer's instructions [227].

The resulting serum and plasma were divided into 500 µL aliquots and stored at -20^{o}C. Within 30 days of collection, samples were transferred on dry ice to longer term storage at

-80°C. This timeframe allowed for the clinical convenience of processing samples locally, but addressed the lack of -80°C facilities within the clinical site, with no adverse effect on sample integrity [228].

Plasma and serum samples were not utilised as part of this project but have been stored for future analysis.

2.2.2 URINE

Participants were asked to provide a 'clean-catch' midstream urine specimen. This is achieved by cleaning the urethra with tap water and obtaining a urine specimen from the middle of the stream into a sterile container.

A dipstick analysis using a Combur^{7} Test® (Roche, Basel, Switzerland, 23001241) was performed. The test strip was briefly dipped into the urine and excess urine is then removed. After 60 seconds the reaction colour of the test strip is compared against the strip container. The presence of protein, erythrocytes, whole blood, leucocytes, nitrites and ketones were quantified, and the pH recorded.

Within 60 – 120 minutes of collection, the sample is divided into 500 µL aliquots and stored in the same way as serum and plasma samples. Urine samples are not utilised in this part of the project but have been stored for future analysis.

2.3 GLYCOCHECK™

2.3.1 GLYCOCHECK™ HARDWARE AND SOFTWARE

Intravital microscopy was achieved using the CapiScope Handheld Video Capillaroscopy System (HVCS) (KK Technology, Honiton, UK).

GlycoCheck™ (Microvascular Health Solutions, American Fork, USA) is a software package which automates the process of image acquisition and analysis of SDF videos of the sublingual microvasculature. It allows automated calculation of the PBR (as well as other vessel characteristics) in a reliable and reproducible way. When imaging, the software will automatically adjust to ensure optimal brightness / contrast and will alert the operator to ensure adequate focus and the absence of movement artefact and air bubbles.

During image acquisition all micro-vessels less than 30 µm thick within the frame are detected and highlighted. Once identified, the software places vascular segments that transect the vessel perpendicularly at 10 µm intervals. A sequence of 40 frames is recorded that typically demonstrate around 300 individual vascular segments. The operator then moves the camera to a different area in the sublingual microvasculature and the process repeats, until a total of more than 3000 vascular segments have been recorded [220]. Video acquisition can take up to five minutes, but more typically takes between 2 -3 minutes.

Prior to image analysis the software completes several quality checks to ensure the integrity of the data. This includes the measurement of the microvascular density and the erythrocyte filling percentage. Erythrocyte filling is determined by the number of vascular segments that have erythrocytes present during all 40 frames of the recording and is an index of perfusion [221].

For each of the validated vascular segments, radial intensity profiles are produced, which identify the dynamic lateral position of the erythrocytes to enable calculation of the maximum and median erythrocyte column width, which in turn can be used to calculate the PBR [220].

The software presents PBR and erythrocyte filling percentages grouped by vessel size. The 'headline' output is the median PBR in vessels in the range of 5-25 µm; but other subgroups of 5-9 µm, 10-19 µm and 10-25 µm are also reported. Users can access the raw measurement data and perform further analysis by individual vessel size if desired.

2.3.2 Protocol for Performing GlycoCheck™ Reading

The imaging protocol was developed from combining manufacturer recommendations, published protocols and personal experience with the device [229].

The manufacturer has determined a number of features that may interfere with the reliability of the recording and analysis. Specifically, participants are recommended to avoid strenuous exercise, the consumption of alcohol, eating in the four hours prior to the test and the consumption of caffeine on the day of the test [230]. Low-molecular weight heparin (LMWH) has been demonstrated to interact with the glycocalyx and could similarly affect the reliability of the results [231].

In a prospective study, where patients are recruited opportunistically it is not possible to control for all of the above variables. Generally, however, many women in pregnancy have a tendency to avoid caffeine and alcohol and are less likely to be performing strenuous exercise. Information was recorded on when the participant last ate, drank and consumed caffeine or alcohol in relation to the test and were asked about current medications including LMWH.

The GlycoCheck™ measurement was performed after a period of rest of at least five minutes. Participants were seated, usually on a couch, with their head supported by a pillow. A new disposable probe cover was placed over the CapiScope probe. Participants were advised to try to avoid moving their tongue during the examination, and to alert the operator if they were uncomfortable.

The probe is inserted under the tongue onto the oral mucosa and the focus adjusted until indicated acceptable by the GlycoCheck™. The software automatically starts recording and stops when the required number has been achieved. Care needs to be taken not to press too firmly which may occlude vessels. The procedure is completed three times in succession, with the mean of the three readings selected as the final reading.

Readings were only performed by persons who had suitable training on the device, specifically Dr Hui Liew, Dr Charles Heffer and I.

GlycoCheck™ data is regularly removed from the device and stored in a password protected back-up file until analysis.

2.3.3 Operator Training and Validation Study

Operator training was provided in the form of an online tutorial with Microvascular Health Solutions and in-person training by Dr Hui Liew who has extensive experience with the device from previous research.

Eleven male and non-pregnant female colleagues were enrolled for the purpose of operator training. Each participant had their PBR measured using GlycoCheck™ twice by myself and twice by Dr Liew. The readings were performed consecutively during one visit in accordance with the protocol outlined in section 2.3.2. The starting operator alternated between participants and alternated between readings to remove any potential bias.

Fifteen normotensive or pre-eclamptic patients enrolled to the main study also underwent readings by me and Dr Liew in the same fashion. The results of these two groups were combined to create twenty-six patients for the evaluation of inter- and intra-operator variability.

2.4 Placental Tissue Collection & Sampling

2.4.1 The Third Stage of Labour and Placental Sampling

After delivery of the infant and before the placenta separates, the cord is routinely left to pulsate for at least one minute, according to the wishes of the parents, the condition of the infant at birth and the absence of any birth complications which would prohibit it. This is termed 'delayed-cord-clamping'. After a designated period of time, separation of the placenta or when the cord stops pulsating, the cord is usually clamped and cut.

All women are recommended to have active management of the third stage of labour, which has been shown to reduce the incidence of post-partum haemorrhage. Active management involves the administration of a uterotonic drug as the infant delivers, followed by controlled traction of the umbilical cord once it has been clamped, to aid delivery of the placenta [232].

The time between delivery of the infant and delivery of the placenta is the length of the third stage of labour and is routinely recorded. This can vary from a few minutes to an hour in uncomplicated birth.

The process of placental tissue sampling has been standardised from guidelines adapted from Burton *et al* [233]. These standards have been adopted by many researchers and placental tissue biobanks. Collecting placental tissue using these methods reduces sampling bias and allows for comparison with placental tissue from other sources.

Immediately following delivery, the placenta is transferred to the laboratory and positioned with the basal plate uppermost. A sampling site is selected from an area which appears macroscopically normal near the middle of the placenta. The basal plate is carefully dissected and a 1 cm^3 biopsy is removed from the exposed area. This sample can be subsequently further divided for both electron and light microscopy as described in

section 2.5. For experiments involving perfusion of the placenta, the placenta was kept intact until the perfusion completed as per section 2.5.1.

2.5 Tissue Fixation

2.5.1 Chemical Immersion Fixation for Electron Microscopy

The placental biopsy for TEM was divided by sharp dissection using two razor blades, into approximately 1 -2 mm^3 specimens. Smaller tissue samples aid in the quality of the fixation of the sample and are preferred for TEM.

The tissue was fixed by immersion in 4 mls of freshly prepared 2.5% electron microscopy grade glutaraldehyde (Agar Scientific, Stansted, UK, AGR1012) in 0.1 M sodium cacodylate buffer, pH 7.4, which was made from sodium cacodylate (Agar Scientific, Stanstead, UK, AGR1104). Glutaraldehyde fixes tissue by forming crosslinks from its two aldehyde groups, to tissue proteins, nucleic acids and lipids. It is used in preference to formaldehyde as a better fixative for the cellular microstructure [234]. Glycocalyx was stained using 0.1% Alcian blue 8GX (Santa Cruz Biotechnology, Dallas, USA, 75881-23-1) and 75 mM L-lysine monohydrochloride (Sigma-Aldrich, St. Louis, USA, L5626) which was decided after an experiment comparing different cationic probes described in section 2.6.3.

Tissue was fixed for 24 – 36 hours at 4°C to allow for full penetration of the glutaraldehyde into the tissue specimen. The rate of fixation depends on factors including the size of the specimen, temperature and pH. Fixation performed at lower temperatures has been shown to prevent self-dissolution of the specimen, but in turn will require a longer fixation time. Fixation causes cell death, and the release of the cell lysosomal contents; this process lowers the pH of the solution which needs to be countered by adequate buffering [234, 235].

After fixation, the glutaraldehyde was removed and the tissue is washed four times in 0.1 M sodium cacodylate buffer, pH7.4 and then stored in buffer at 4°C until further processing.

2.5.2 Chemical Perfusion Fixation for Electron Microscopy

Placental perfusion was performed using a protocol adapted from Leach et al [193]. After collection, the whole placenta was placed in a fume hood with the fetal side uppermost

and the umbilical cord was trimmed to around 5 cm in length. A 4 mm nasogastric tube was sheathed onto a 21-gauge needle (Becton, Dickinson and Company, Franklin Lakes, USA, 305167), and an umbilical artery is cannulated. The nasogastric tube was advanced off the needle and into a placental vein.

The free end of the nasogastric tube was connected to a sealed unit which was custom built with the assistance of Dr Chris Neal (Wolfson Bioimaging Facility, University of Bristol) and is represented by the schematic in Figure 8. The perfusion apparatus contained both a flush and a separate fixative solution. The perfusion pressure was adjusted by inserting air into the system and measured with an aneroid sphygmometer. A perfusion pressure of 50 mmHg was selected to represent the normal physiological pressures in the placental circulation [193].

The placenta was first perfused with 250 mls of glucose free mammalian Ringer solution (pH 7.4, in mM: 132.10 NaCl, 4.41 KCl, 1.34 $MgCl_2$ 7(H_2O), 1.91 $CaCl_2$ 2(H_2O), 3.06 HEPES acid and 1.92 HEPES base) at 4^{o}C to flush fetal blood cells from the vessels.

Immediately after the flush, 500mls of fixative was perfused at the same pressure over five minutes. The fixative was composed of 1% glutaraldehyde, in glucose free mammalian Ringer with 0.1% Alcian blue.

Successful perfusion was determined by the development of a blue discolouration of the placenta, which would become firm to touch and the presence of returned flush and fixative in the umbilical vein. After the perfusion, the placenta was inverted, and a biopsy obtained as previously described in section 2.4. It was clear from observing the placenta that the perfusion was far from uniform. Samples were obtained from multiple points from tissue that appeared well stained with Alcian blue.

After sampling, the placental biopsies were further trimmed to 1 – 2 mm^3 and immersion fixed at 4^{o}C for 24 -36 hours in the fixative solution. After fixation, the glutaraldehyde was removed, and the tissue washed four times in 0.1 M sodium cacodylate buffer, pH 7.4 and stored at 4^{o}C before further processing.

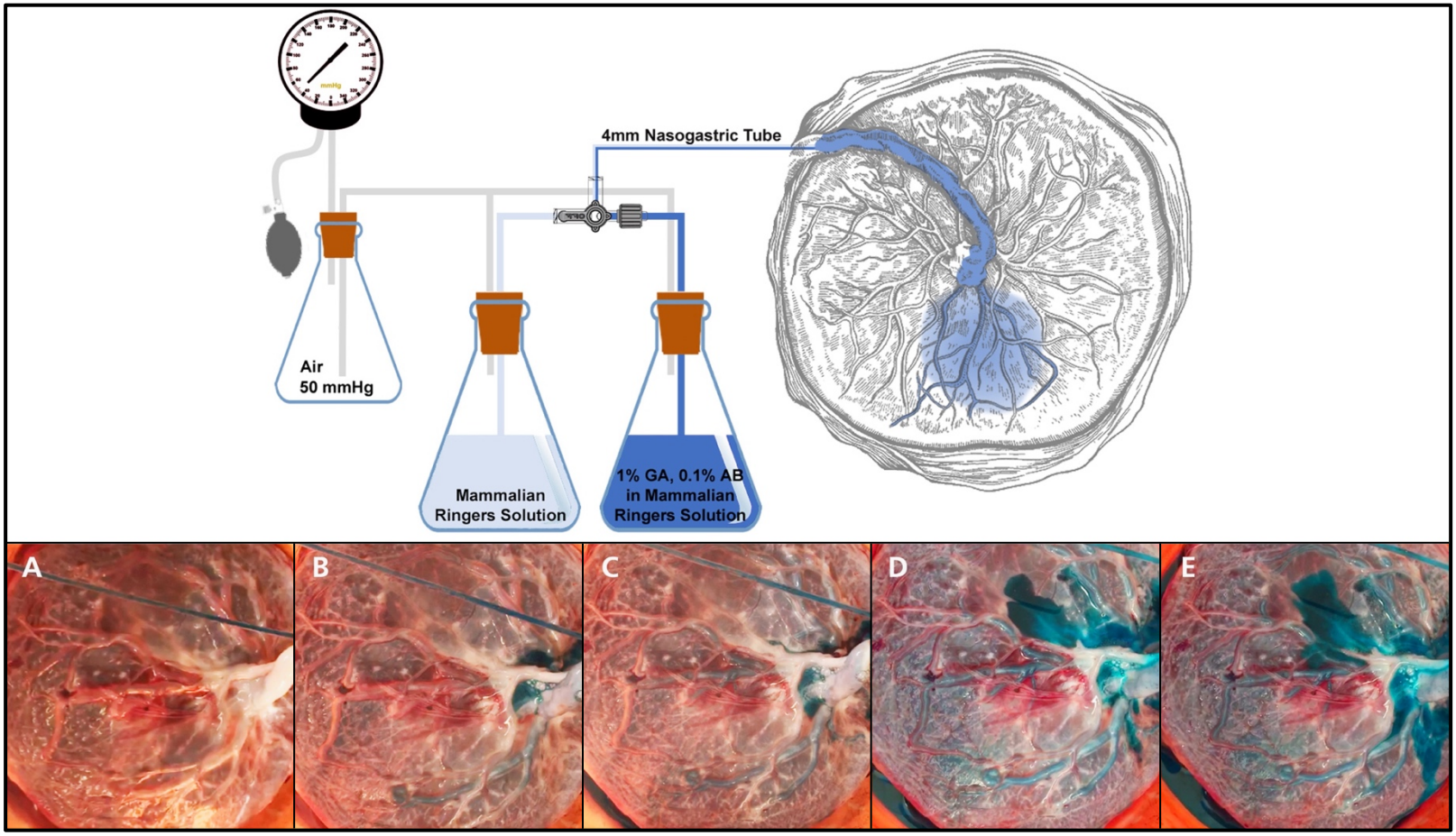

Figure 8 – Placental Perfusion Experimental Design

Placental perfusion was achieved with a custom-built perfusion apparatus which was assembled as displayed in the schematic. This allowed for a constant perfusion pressure of 50 mmHg of both flush and fixative. A successful perfusion is demonstrated in the time series of images (A-E) captured at 20 second intervals. Progressive staining with Alcian blue is seen confirming delivery of fixative.

2.5.3 High Pressure Rapid Freeze Fixation for TEM

Rapid freeze fixation was achieved using the Leica EM PACT2 (Leica Microsystems, Wetzlar, Germany) high-pressure freezing system and was achieved with the assistance of Dr Chris Neal. The device can vitrify tissue in less than 5 seconds. To allow timely fixation of the placental tissue after delivery, the machinery was temporarily transported to the laboratory in St Michael's Hospital for the duration of the experiments.

Placental tissue was collected using a 2mm biopsy gun from the same sampling sites described previously in 2.4. The specimens were transferred to a carrier and inserted into the high-pressure freezing system. An automated process rapidly impacts the tissue and carrier against a machine surface that is cooled to liquid nitrogen temperature. A graphical representation of the performance parameters is produced by the software confirming correct functioning of the freeze cycle.

The frozen tissue specimens and attached carrier were stored into liquid nitrogen until further processing.

2.5.4 Placental Chemical Immersion Fixation for Light Microscopy

After placental collection and biopsy, the tissue was further sharp dissected into 5 – 10 mm^3 pieces. Fixation was by immersion in 4% paraformaldehyde (PFA) in phosphate buffered saline (PBS) (bioWORLD, Ohio, USA, 730280), pH 7.4 at 4^oC for 24 – 48 hours. After fixation, the PFA was removed and the tissue was washed three times in PBS (pH 7.4, in mM: 137.0 NaCl, 27.0 KCl, 10.0 Na_2HPO_4, 1.8 KH_2PO_4), before storage in 70 % ethanol, prepared by dilution of absolute ethanol with distilled water.

2.6 Specific Fixation Experiments

2.6.1 Hyaluronidase Tissue Treatment

It is important to demonstrate that the placental glycocalyx can be disrupted and that the imaging protocols were validated to detect this. Hyaluronidase cleaves hyaluronan from the glycocalyx and has been used in several studies to produce structural and functional changes to the glycocalyx, including a reduction in glycocalyx thickness [190, 236-238].

Two placentas were used for this experiment with tissue fixed by both immersion and perfusion fixation with the protocol and assistance provided by Dr Matthew Butler (University of Bristol, Bristol Renal).

Tissue for immersion fixation was sampled as described in section 2.4. Prior to fixation, tissue was first immersed in hyaluronidase (Sigma-Aldrich, St. Louis, USA, H3506), 200 units/ml in glucose free mammalian Ringer's, pH 7.2, for five minutes on ice. Tissue was then briefly washed, and then immersion fixed with lysine and Alcian blue as described. For the perfusion experiment, the same concentration of hyaluronidase was added to the perfusion flush and perfused and fixed as per the protocol in 2.5.2.

2.6.2 Fixation Time Series

The stability of the glycocalyx after delivery of the placenta was investigated in a time-series study. This was an important experiment to guide protocol development, determining how quickly placental sampling needs to occur to maintain glycocalyx integrity.

Five placentas were collected from women undergoing elective caesarean section. The placenta was stored on the laboratory bench at room temperature to simulate the usual conditions of placental storage for disposal after birth. Placental samples were taken at set time intervals of 0-, 10-, 20-, 30-, 60- and 1440-minutes from delivery and immersion chemical fixed for both TEM and confocal microscopy as described in 2.5.1 and 2.5.4.

2.6.3 Comparison of Cationic Dyes

The glycocalyx lacks an intrinsic electron density, such that the addition of a cationic probe is required to label the anionic sugar residues and render it visible using electron microscopy [153].

A number of different cationic dyes were trialled during the development of the immersion fixation protocol to investigate if any were superior. Cationic probes used include 0.1 % Alcian blue 8GX, 0.1% ruthenium red (Sigma-Aldrich, St. Louis, USA, R2751), 0.3% lanthanum (III) nitrate hexahydrate (Sigma-Aldrich, St. Louis, USA, 203548) with 0.3% dysprosium (III) chloride hexahydrate (Sigma-Aldrich, St. Louis, USA, 289272) and 75 mM L-lysine monohydrochloride.

2.7 Post Fixation Tissue Processing for Electron Microscopy

2.7.1 Chemical Fixed Tissue

Post fixation processing of glutaraldehyde fixed placental tissue (both immersion and perfusion), was completed by me or Dr Chris Neal in the Wolfson Bioimaging Facility. In 2019 the Leica EM TP Automatic Tissue Processor (Lecia Microsystems, Wetzlar, Germany) was acquired. All processing after this date was automated, but in accordance with the original protocol.

The interval between tissue fixation and processing varied between 0 and 30 days. Samples were processed in batch where possible, providing a cost and time saving.

Fixed tissue was removed from its storage buffer and postfixed in 1% osmium tetroxide (Electron Microscopy Sciences, Hatfield, USA, 19110) in 0.1 M sodium cacodylate for one hour, on a low-speed rotating mixer. The sample was then washed three times in deionised water, before overnight incubation in 3% aqueous uranyl acetate (Electron Microscopy Sciences, Hatfield, USA, 22400). Osmium has the effect of stabilising tissues and improving the electron conductivity during imaging. Uranyl acetate acts as a negative stain, providing contrast [235].

Samples were further washed in deionised water, and then dehydrated in increasing concentrations of ethanol (50, 70, 90 and 100%). Dehydration is an important step in tissue processing for electron microscopy, which takes place in a vacuum. Residual water in a specimen would quickly evaporate, destroying the structure of the sample.

Samples were embedded and cured in the epoxy resin Araldite®. Araldite was prepared by mixing Araldite CY212 (Agar Scientific, Stanstead, UK, R1042), dodecenyl succinic anhydride (DDSA) (Agar Scientific, Stanstead, UK, R1053), N-benzyldimethylamine (BDMA) (Agar Scientific, Stanstead, UK, R1062B), and dibutyl phthalate (Agar Scientific, Stanstead, UK, R1071) in a ratio of 25 : 25 : 1 : 1.

Tissue was washed twice in propylene oxide (Agar Scientific, Stanstead, UK, R1080) before a 2-hour incubation in a 1:1 mix of propylene oxide and Araldite® resin. Propylene oxide was used as a transitional solvent between the dehydration and embedding steps, as it is

fully miscible with epoxy resins, whereas ethanol is not [239]. The resin was changed for fresh 100% Araldite® and has two further incubations of 3 hours and overnight.

Samples were transferred to rubber block moulds, labelled and filled with Araldite®. The blocks were cured in an oven at 60°C for 72 hours. Well cured blocks can be stored at room temperature for many years without significant deterioration.

2.7.2 High Pressure Rapid Freeze Fixed Tissue

Placental tissue fixed by high pressure freezing, was dehydrated and stained using freeze substitution in the Leica EM Automatic Freeze Substitution System (AFS) 2 (Lecia Microsystems, Wetzlar, Germany) and completed with the assistance of Dr Chris Neal.

The process involves the replacement of water in the tissue with an organic solvent, which also contains a fixative and a stain for the glycocalyx. The procedure is conducted at low temperatures, before gradually being warmed over a number of hours. This avoids the formation of damaging ice-crystals that would occur if the sample was to thaw prior to dehydration [215].

A solution of 95% anhydrous acetone and 5% methanol with 0.25% lanthanum nitrate, 0.25% dysprosium chloride, 0.5% osmium tetroxide and 0.05% uranyl acetate was prepared and cooled to -90°C within the chamber of the freeze substitution unit. The sample, still attached to its carrier, was then placed into the solution and the device sealed. The temperature was initially held at -90°C for 5 hours, followed by a graduated increase of 5°C per hour for 18 hours to 0°C, where it was held for a further 24 hours.

After freeze substitution, the samples were removed from the chamber and transferred to a fume hood. At room temperature, the sample was washed twice in acetone, and twice in propylene oxide. Embedding and curing in Araldite® epoxy resin was as previously described in 2.7.1.

2.7.3 Section Cutting and Mounting for Electron Microscopy

Ultrathin sections were produced from the resin tissue blocks. The majority of the sectioning was completed by Dr Chris Neal and Dr Sally Hobson (University of Bristol, Wolfson Bioimaging Facility), although I completed training in the technique.

Blocks were initially trimmed to the level of the tissue using a razor blade. Tissue fixed by freeze substitution still had the carriers attached. These were removed by immersing the trimmed block in alternating liquid nitrogen and hot water, allowing for the carrier to detach.

An ultramicrotome Leica EM UC7 (Leica Microsystems, Wetzlar, Germany) was first used with a glass knife to create 'thick' 1 µm sections, which were stained with toluidine blue and viewed under a benchtop light microscope to confirm an area of interest.

A 45° diamond knife (DiATOME, Hatfield, USA) is used to create 'thin' 70 nm sections. The water boat of the knife was carefully filled with distilled water, the block tightly secured in the holder and aligned to the cutting edge of the knife. Cut sections collect on the surface of the water and were lifted using a mounted eyelash and transferred onto pioloform coated copper grids (Electron Microscopy Sciences, Hatfield, USA, EMS2010-Cu) to air dry.

Grids were further post-stained with lead citrate (Electron Microscopy Sciences, Hatfield, USA, 17800) to enhance the heavy metal staining of the osmium and uranyl acetate improving contrast.

2.8 Post Fixation Tissue Processing and Staining for Light Microscopy

2.8.1 Wax Processing and Sectioning

Paraformaldehyde fixed placental tissue for light microscopy was processed and sectioned by Mrs Debbie Martin (University of Bristol, Histology Services Facility) and her team. An automated tissue processor first dehydrates the tissue in graded ethanol, before an organic solvent is applied, allowing for tissue infiltration with molten paraffin wax.

Wax blocks containing the embedded tissue were sectioned at 5 µm thickness, mounted on Superfrost Plus slides (Thermo Fisher Scientific, Waltham, USA, 12372098) and allowed to dry. Each slide typically had between 2 – 4 serial sections.

2.8.2 Lectin Histochemistry

Lectins are glycan binding proteins that have a high affinity to specific carbohydrate epitopes, including those of the glycocalyx. Lectin histochemistry has previously been used

in the placenta to demonstrate the pattern of sugar chain expression, but not in a way that quantified the depth of the glycocalyx in normal and complicated pregnancies [240-242].

I adapted and optimised a protocol that had been produced by the University of Bristol Endothelial Group and used successfully to stain the glycocalyx in other tissues / species.

PFA fixed placental tissue sections were dewaxed in Histo-Clear II (Agar Scientific, Stanstead, UK, AGR1353) for 15 minutes, before rehydration in graded ethanol (100, 90, 70%) for two minutes each.

After washing in PBS, pH 7.4, the sections were edged with a hydrophobic pen, ImmEdge Hydrophobic Barrier PAP Pen (Vector Laboratories, Burlingame, USA, H-4000) and blocked by incubation with filtered 1% bovine serum albumin (BSA) (Sigma-Aldrich, St. Louis, USA, A3059) in PBS with 0.1% Tween®-20 (Thermo Fisher Scientific, Waltham, USA, 1379), pH 7.4, for 30 minutes.

The majority of lectins utilised were biotinylated, it was therefore important to block endogenous biotin, biotin receptors and streptavidin binding sites. After washing in PBS – Tween, the sections were incubated for 15 minutes in streptavidin solution (Vector Laboratories, Burlingame, USA, SP-2002), followed by a brief rinse in PBS – Tween, and a further 15-minute incubation in biotin solution (Vector Laboratories, Burlingame, USA, SP-2002).

A panel of different lectins were trialled to confirm the specific pattern of lectin glycocalyx binding in the placenta, summarised in Table 3, with the specific carbohydrate binding site and concentration used. All lectins were procured from Vector Laboratories (Vector Laboratories, Burlingame, USA).

The working concentration of chosen lectin was freshly prepared in 1% BSA in PBS – 0.1% Tween, pH 6.8, and incubated at room temperature for 1 hour. After washing in PBS-Tween the tissue was further incubated with the fluorescent streptavidin conjugate, Alexa Fluor 488 (AF-488) Streptavidin (Thermo Fisher Scientific, Waltham, USA, S11223) at a working concentration of 1:500 in 1% BSA, PBS, 0.1% Tween, pH 6.8, for one hour at room temperature with light protection.

After washing, slides were co-stained with the nuclear stain 4'6-diamidino-2-phenylindole (DAPI) (ThermoFisher Scientific, Waltham, USA, 62248) diluted to 1:500 in PBS, followed by the membrane stain octadecyl rhodamine B chloride (R18) (Biotium, Fremont, USA, 60033) diluted to 1:1000 in PBS. Slides were mounted with VECTASHIELD Antifade Mounting Medium (Vector Laboratories, Burlingame, USA, H-1000-10) and coverslips applied.

2.8.3 PRECONJUGATED LECTINS

Concanavalin A (Con-A) lectin was purchased in a form preconjugated with fluorescein isothiocyanate (FITC) (Vector Laboratories, Burlingame, USA, Fl-1001). The biotin/streptavidin blocking steps and secondary incubation with AF-488 streptavidin was therefore not required.

Lectin	Source	Sugar Specificity	Working Concentration	Product Code
ConA Concanavalin A	Canavalia ensiformis (Jack Bean) seeds	αMan, αGlc	1:100	Fl-1001
LEL *Lycopersicon esculentum*	*Lycopersicon esculentum* (tomato) fruit	αFuc	1:100	B-1175
MAL II *Maackia amurensis II*	*Maackia amurensis* seeds	α-2,3 Sialic Acid	1:100	B-1265
UEA I *Ulex europaeus I*	*Ulex europaeus* (Furze Gorse) seeds	αFuc	1:100	B-1065
WGA Wheat Germ Agglutinin	*Triticum vulgaris* (wheat germ)	GlcNAc	1:200	B-1025

Table 3 – Panel of Lectins Used for Glycocalyx Staining.

The majority of lectins used were biotinylated and incubated with a streptavidin conjugated Alexa-Fluor for visualisation with confocal microscopy. Con-A lectin was preconjugated with FITC and therefore did not require this step.

2.9 IMAGING WITH ELECTRON MICROSCOPY

I completed all transmission electron microscopy imaging independently after a period of training using the Tecnai 12 – FEI BioTwin Spirit (Field Electron and Ion Company, Hillsboro, USA) transmission electron microscope (TEM).

Electron microscopes generate a particle beam of electrons inside a vacuum. They are focussed through several electromagnetic lenses towards the prepared tissue sample, and then down to a fluorescent screen and camera. An image is formed according to the relative electron density of the specimen. The major advantage of TEM over light microscopy is the enhanced magnification and resolution ability, due to the much smaller wavelength of the electron beam compared to light [243].

The sample, mounted on a copper grid, was carefully loaded into the specimen holder and inserted into the airlock of the microscope. A 'map' of the specimen was created using the track function at a low magnification and 3 regions selected at random. Images were obtained at low, medium and high-power magnifications (x 2,900, x 9,300 and x49,000), with at least 3 highest-power images of the syncytiotrophoblast brush border and the capillary endothelium from each of the 3 selected regions (Figure 9).

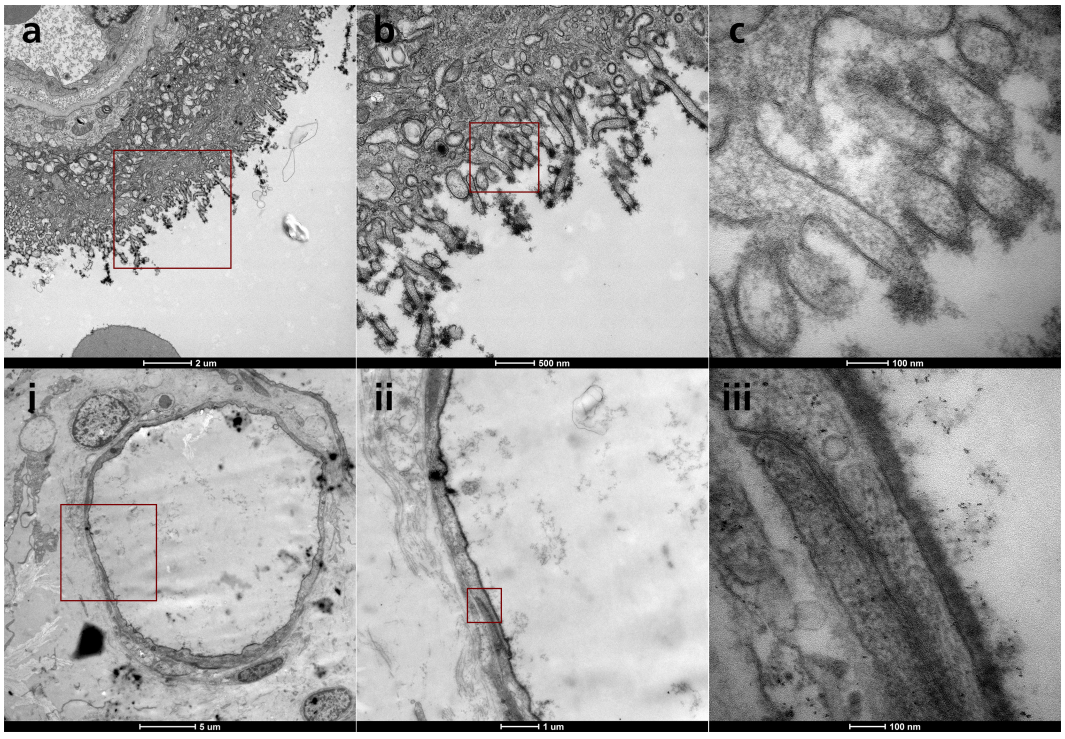

Figure 9 – Image Selection for Electron Microscopy
Three regions are selected, and low, medium and high-power images obtained of the syncytiotrophoblast microvilli (a-c) and capillary endothelium (i-iii). High magnification images are used for the quantification of the glycocalyx depth and coverage.

2.10 Imaging with Confocal Laser Scanning Microscopy

I completed all fluorescent microscopy imaging using the Leica SP5-AOBS confocal laser scanning microscope and attached Leica DMI 6000 inverted epifluorescence microscope (Leica Microsystems, Wetzlar, Germany) in the Wolfson Bioimaging Facility.

Confocal microscopy utilises lasers which can be focussed to a specific depth within a tissue sample. The pinhole within the microscope prevents the signal from out of focus areas from escaping and being detected. Z-stacks from serial planes within a specimen can be combined to create 3D rendered images of a tissue section. By using lasers of different wavelengths, combined with emission and excitation filters, a number of different fluorophores can be detected simultaneously [244].

Immersion lens oil was applied to the coverslip of the tissue sections and the slide loaded onto the microscope stage. Imaging was performed using a Leica HCX PL APO 63x lens (Leica Microsystems, Wetzlar, Germany) which has a numerical aperture of 1.4. A zoom factor of 1.59 was applied, with a digital aspect resolution of 2048 x 2048, producing a pixel resolution of 75.72 nm, which is at the limits of what is achievable with light microscopy [245]. A scan speed of 400 Hz, with a frame average of 4 was used.

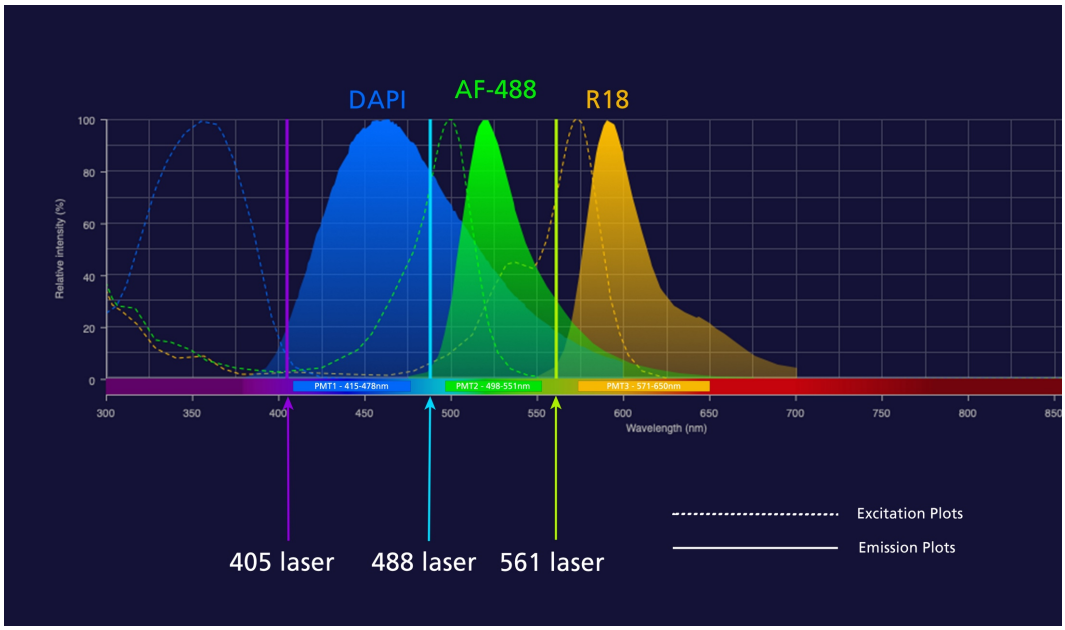

Figure 10 – Excitation and Emission Profiles of Fluorophores
The excitation (dashed line) and emission (solid, coloured plot) for DAPI, AF-488 and R18. As demonstrated, there is minimal cross emission in the excitation of the fluorophores by excitation with the 405, 488 and 561 nm lasers respectively. PMT emission detection ranges are set according to the peak emission profiles of the fluorophore.

The sequential scan setting was used between lines, with scans for each of the three fluorophores to be detected. Emitted fluorescence from the sample is detected by photomultiplier tubes (PMT) with the emission range determined for each scan. Scan 1: DAPI, 405 nm laser, PMT 415 – 478 nm; scan 2: AF-488, 488 nm laser, PMT 498 – 551; scan 3: R18, 561 nm laser, PMT 571 – 650. This is represented graphically in Figure 10.

A minimum of six randomly selected capillaries or regions of syncytiotrophoblast brush border were selected for imaging, to provide a representative sample of the tissue section. The selection of these regions / vessels was identified by the R18 staining to avoid potential operator bias that could have occurred if regions were selected by lectin staining.

2.11 Glycocalyx Quantification using Electron Microscopy

Glycocalyx depth and coverage were measured using the images obtained at high power (x 49,000) using the open-source software Fiji is Just ImageJ (Fiji) [246]. Each image was opened and a 0.1 µm grid with random offset overlaid. Assessments of depth and coverage were made if a grid line intercepted an area of phospholipid bilayer of either the capillary

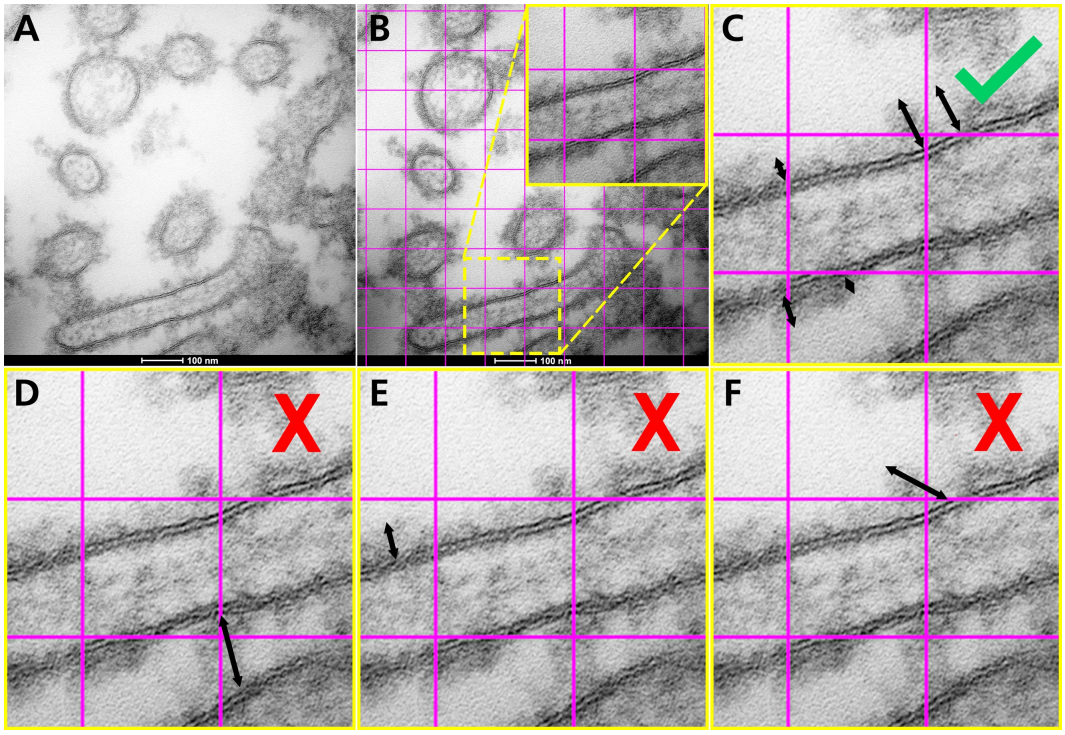

Figure 11 – Quantifying Glycocalyx Depth by Electron Microscopy
Raw images are opened in Fiji (A) and a 0.1 µm grid overlaid with random offset (B). Correct glycocalyx depth is measured perpendicular to the phospholipid bilayer at a gridline (C). Examples of incorrect measurements include overlapping glycocalyx between two microvilli with no clear separation (D), not measuring from a gridline intersection (E), no clear phospholipid bilayer (E) and not measuring perpendicular to the bilayer (F).

endothelium, or syncytiotrophoblast (Figure 11B). The recognition of the phospholipid bilayer is important to ensure the segment being measured is in complete cross-section. Oblique sections would have the effect of over or under-estimating the glycocalyx.

Glycocalyx depth was measured by drawing a line perpendicular from the phospholipid bilayer to the end point of the continuous glycocalyx (Figure 11C). Where no glycocalyx was present a depth of zero was recorded. On occasions where the glycocalyx between two microvilli of the syncytiotrophoblast over-lapped, the measurement was excluded (Figure 11D).

Around one hundred measurements of glycocalyx depth were obtained from the nine high power images and three placental regions for each placental specimen. The mean glycocalyx depth and standard deviation was calculated.

Glycocalyx coverage was calculated as a percentage of measurements where glycocalyx was present out of the total number of measurements taken. Glycocalyx was considered to be present if the depth was ≥ 10 nm, a convention used by others in our group using this technique. The following equation was used:

$$\%\ Glycocalyx\ Coverage = \frac{number\ of\ measurements\ \geq 10\ nm}{total\ number\ of\ measurements} \times 100$$

2.12 Glycocalyx Quantification Using Confocal Microscopy

2.12.1 Peak-to-Peak Measurements

Direct measurement of the glycocalyx with light microscopy is difficult, as the anatomical depth of this layer is close or even beyond the diffraction limit of light [153]. Although confocal microscopy improves resolution, the glycocalyx depth is still within a couple of pixels at maximum resolution.

Betteridge et al. tested a number of indirect methods of determining the depth of the glycocalyx using lectin histochemistry and reported that a peak-to-peak (P-P) measurement of glycocalyx depth was most reliable [217]. In this technique the cell membrane stained with a fluorescent label and the glycocalyx stained using a lectin conjugated with a fluorophore is imaged as previously described. In the analysis software a line of interest is drawn transecting and perpendicular to the glycocalyx and cell

membrane and the intensity profile is plotted for each fluorophore (Figure 12). The separation of the peak membrane and lectin stain from the intensity profiles can be measured and was demonstrated to correlate with the depth of the glycocalyx when measured by electron microscopy. I adapted this technique for use in both the quantification of the glycocalyx at the syncytiotrophoblast and placental endothelial cell.

2.12.2 Manual Peak-to-Peak Measurements

Placental capillary endothelial and syncytiotrophoblast glycocalyx were initially measured using a manual technique. All image analysis was performed using Fiji.

Capillaries were identified visually using the R18 (red) staining. This was to prevent operator bias in selecting capillaries which may have had favourable glycocalyx lectin staining. Only capillaries imaged in complete cross-section were included for analysis, as oblique sections may alter the perceived glycocalyx depth. Vessels were initially selected if they appeared circular. The shortest diameter was measured and divided by the longest diameter of the vessel with a value of 0.8 – 1.0 accepted as an arbitrary cut-off confirming a circular capillary transection.

A line of interest was placed transecting the capillary endothelium perpendicularly as previously described (Figure 12), and the process repeated to achieve ten measurements per vessel. The peak-to-peak measurement was calculated for each line of interest, and the mean calculated for each vessel. A minimum of five vessels from different regions

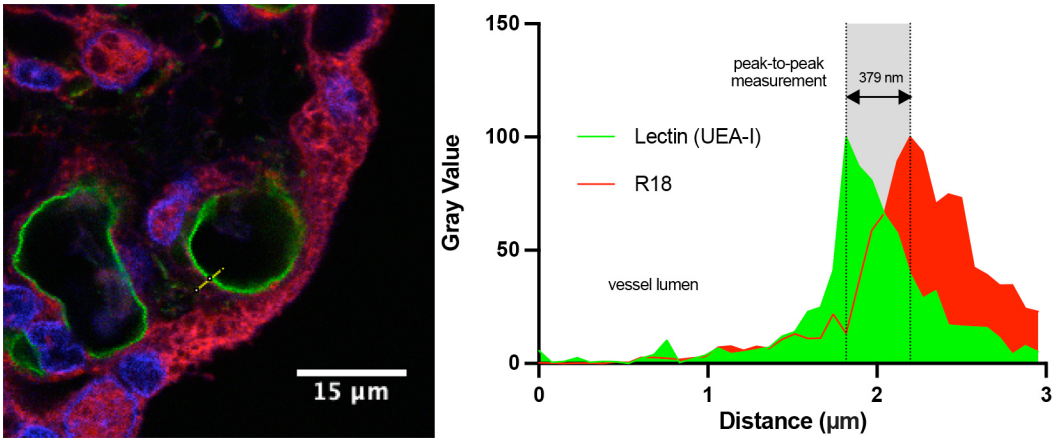

Figure 12 – Peak-to-Peak Glycocalyx Measurement
A line of interest is drawn transecting and perpendicular to the glycocalyx / endothelial cell wall. The peak intensity profiles of the R18 (red) and glycocalyx (green – in this example AF488 – biotinylated UEA-I lectin) are plotted. The separation of the two peaks is representative of the depth of the glycocalyx, in this example 379 nm.

within the sample were analysed, with the mean value of the vessels accepted as the specimen peak-to-peak measurement.

Syncytiotrophoblast glycocalyx peak-to-peak was measured in a similar way. A line of interest was drawn perpendicular to the glycocalyx and syncytiotrophoblast brush border. A minimum of ten peak-to-peak measurements per image were obtained and the mean calculated. The mean values from a minimum of five different regions of the specimen were calculated as the specimen peak-to-peak value.

2.12.3 Gaussian Correction

The pixel resolution is an important limitation when calculating the peak-to-peak value using the raw image data, with the majority of peak separation values falling between 0 and 6 pixels (approximately 0 – 450 nm). Measurements can only be expressed in multiples of whole pixels and do not account for situations where the true peak intensity lies between two pixels.

To correct for this situation, a gaussian curve is fitted to both the red and green plot intensity profiles, and the peak separation between the two gaussian fits accepted as the peak-to-peak measurement (Figure 13), a method also validated by Betteridge et al [217].

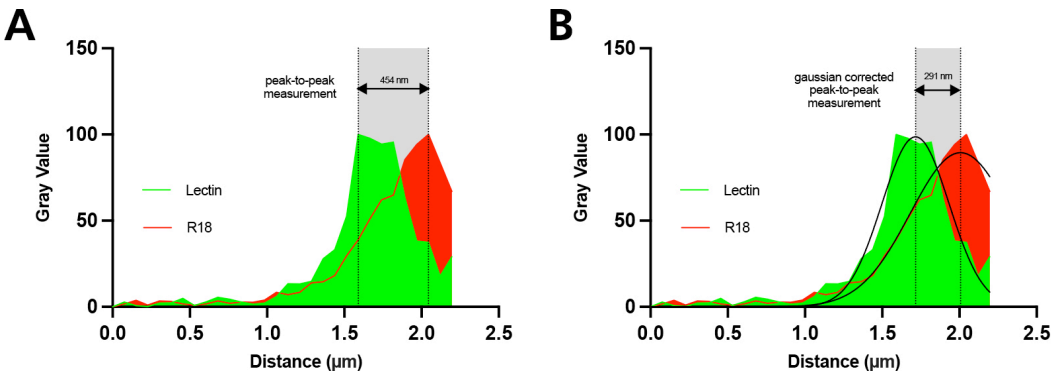

Figure 13 – Gaussian Correction

Graph A demonstrates the peak-to-peak of the placental capillary glycocalyx using raw data. This method does not account for situations where the 'true' peak lies between two pixels. The blunted top of the green peak is representative of this. Graph B demonstrates a gaussian fit applied to the same data, providing a mathematical estimation of the location of the true peak. In this example the peak separation is over 150 nm different.

2.12.4 AUTOMATED PEAK-TO-PEAK – CAPILLARY

The manual process of peak-to-peak analysis is time consuming and labour intensive. There are also inherent operator biases involved with the selection and placement of measurement lines that can only be partially adjusted for in the methodology. An automated process of peak-to-peak measurement was therefore considered advantageous when processing large volumes of data.

Image analysis can be automated in Fiji with the use of macros, which are a series of instructions that the software can automatically apply to images in a reproducible way. There were several key components I designed to be included in the macro as listed below:

1) The user measures the longest and shortest diameter of the vessel and confirms the ratio is between 0.8 – 1.0.
2) The user selects the vessel to be measured by placing the point tool in the approximate centre of the vessel.
3) The user inputs the shortest and longest diameter measurements in pixels. A radial region of interest is created by subtracting 15 pixels from the shortest measurement and adding 15 pixels to the longest measurement. This accounts for slight variations in the shape of the vessels.
4) 360 intensity plot profiles, taken at 1^{o} intervals for the circumference of the vessel are recorded on the red channel. A gaussian fit is added to each profile and the peak recorded.
5) The same measurements are recorded on the green channel.
6) The peak-to-peak separation of each raw measurement and gaussian corrected measurement is calculated.
7) The output table contains the 360 raw and gaussian peak-to-peak measurements and calculates the vessel median and interquartile range.

The code for the macro was produced by Dr Stephen Cross (University of Bristol, Wolfson Bioimaging Facility) (appendix 6).

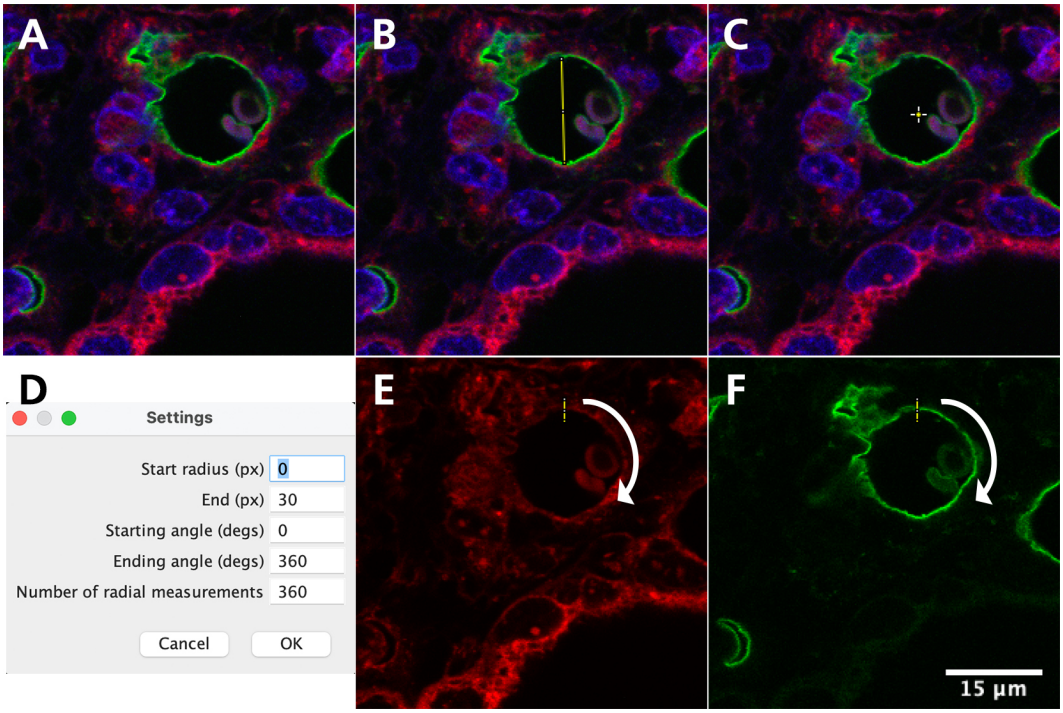

Figure 14 – Capillary Macro Peak-to-Peak Measurement
The user selects a suitable vessel in cross-section (A) and measures the shortest and longest diameters confirming a ratio of 0.8 – 1.0 (B). The approximate centre is marked (C) and the macro run. The user inputs the shortest (start) and longest (end) diameters in pixels and can customise the number of measurements to be taken (D). The radial line of interest is produced by subtracting 15 pixels from the shortest and adding 15 pixels to the longest diameter. 360 measurements are taken on the red (E) and green (F) channels, with the peak-to-peak and gaussian correction calculated for each.

2.12.5 Automated Peak-to Peak – Syncytiotrophoblast

A different approach was required for the automation of the peak-to-peak measurement at the syncytiotrophoblast. For this technique the software was required to identify the brush border independently and apply multiple regions of interest for peak-to-peak measurements.

Thresholding is a methodology used for reducing background noise and segmenting images. By applying an adjustment to the image contrast and applying a threshold function Fiji is able to more easily detect the edge of the syncytiotrophoblast and the intervillous space and draw an outline of the edge of the cell. A region of interest was plotted every tenth pixel perpendicular to the detected edge, across the glycocalyx of the syncytiotrophoblast. This would typically create several hundred measurement lines (Figure 15).

An intensity plot profile for the red and green channels were calculated for each region of interest and a gaussian fit overlaid. The actual and gaussian corrected peak-to-peak value was reported for each region of interest, with the median and interquartile range reported for each image. A minimum of five different placental regions per specimen were analysed, with the mean of the regions taken as the glycocalyx depth for the specimen. The macro code was written by Dr Stephen Cross (appendix 7).

Thresholding and edge detection was not always successful in Fiji. Images with poor contrast, large defects in the tissue, or clots / debris in the intervillous space were common reasons for the edge detection to fail (Figure 15). Each image was validated manually to ensure quality of the edging. Data was excluded if, on visual inspection, it appeared that less than 90% of the regions of interest corresponded to the syncytiotrophoblast glycocalyx.

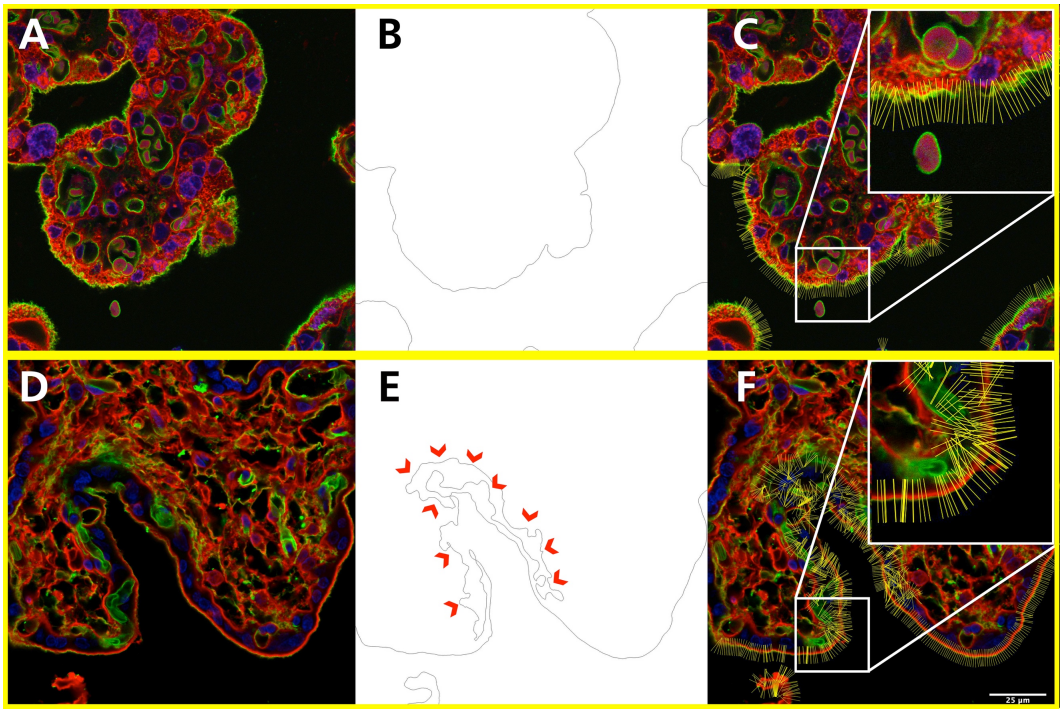

Figure 15 – Syncytiotrophoblast Macro Peak-to-Peak Measurement
Selected images are processed in Fiji. The macro applies a contrast adjustment and thresholding tool to allow automatic detection of the syncytiotrophoblast edge (B). Lines of interest are drawn every 10th pixel perpendicular to the edge profile (C). The peak intensity profile of the red and green channel is calculated and a gaussian correction applied. The median peak-to-peak value is reported per image. Occasionally the edging processing fails (E), the images are manually removed, and the data excluded.

2.12.6 Cleaning Data – Gaussian Fit Standard Deviation

The macro automation of the peak-to-peak measurement produces a large volume of data but cannot determine the quality of all measurements.

There were frequent examples where the peak intensity profile of either the red or green channel was not 'clean'. Double or mishappen peak profiles occur if a line of interest does not completely intersect the glycocalyx perpendicularly; if the vessel wall is irregular in shape; in instances where there is intraluminal or intervillous artefacts (erythrocytes); or if the staining is generally poor.

The standard deviation of the gaussian plot is one way of cleaning data to only include values where it is likely that a 'true' peak has been identified. Gaussian plots which have a large standard deviation were likely to represent intensity profiles that included anomalous data or double peaks. Plots with a very small standard deviation were likely to represent artefacts. After visual inspection of several different standard deviation plot profiles (Figure 16), an arbitrary cut-off of a standard deviation of the gaussian plot between 1.0 and 7.5 px was selected as representative of quality data. Peak-to-peak measurements from gaussian plots outside of this range were excluded from analysis.

2.12.7 Cleaning Data – Signal to Noise Ratio

The standard deviation of the gaussian fit is affected by the amplitude of the peak intensity profile. Low amplitude intensity profiles are more commonly associated with poor staining in that region, and although may demonstrate a standard deviation of between 1.0 and 7.5 px, may not represent 'true' peaks above the background noise (Figure 17).

Dr Michael Crompton (University of Bristol, Bristol Renal) demonstrated a technique to further clean the automatically generated data by expressing the amplitude as the signal-to-noise ratio (SNR).

$$SNR = \frac{Signal\ Amplitude}{Gaussian\ Plot\ Standard\ Deviation}$$

After reviewing several data outputs, an arbitrary cut-off for SNR of 15 was selected. Gaussian plots with an SNR of < 15 were more likely to be associated with poor quality data and inferior staining and were excluded from analysis.

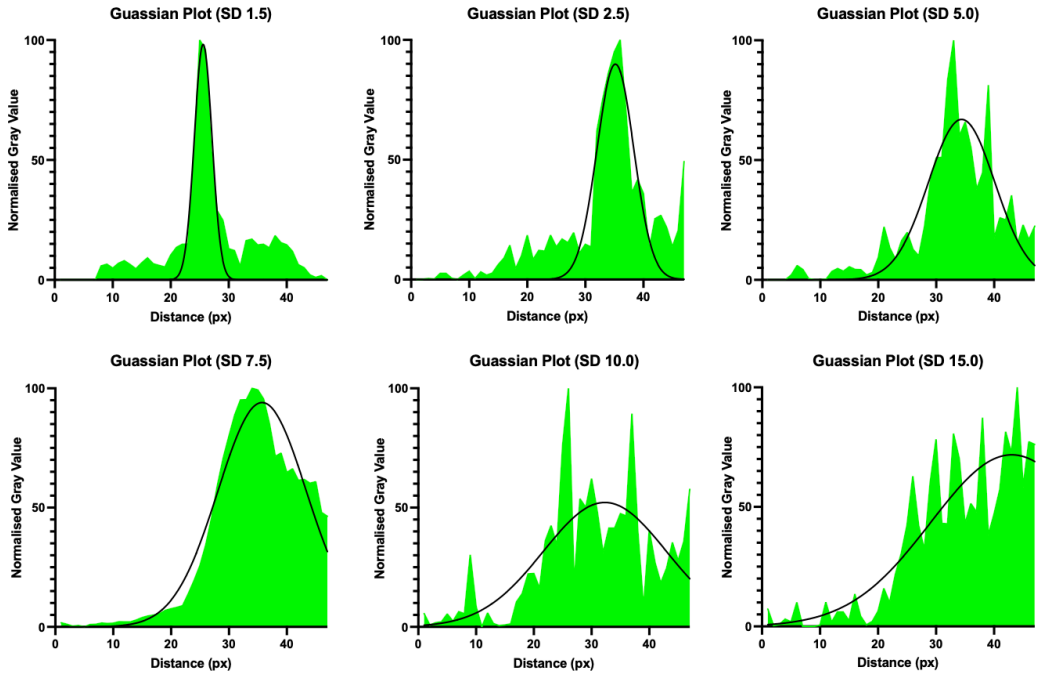

Figure 16 – Cleaning Automated Data by Gaussian Plot Standard Deviation

Representative examples of lectin intensity plot profiles with a gaussian plot overlaid. Where the standard deviation of the gaussian plot was <1.0 or >7.5 px the data was more likely to represent artefacts, tissue anomalies or poor staining. The software was automatically set to exclude data where the standard deviation of the gaussian plot fell outside of these arbitrarily set ranges.

Plot	Gaussian Plot (SD)	Gaussian Plot Peak Amplitude	SNR	
A	6.9	30.6	4.4	❌
B	6.6	101.0	15.3	✅
C	6.7	164.0	24.5	✅

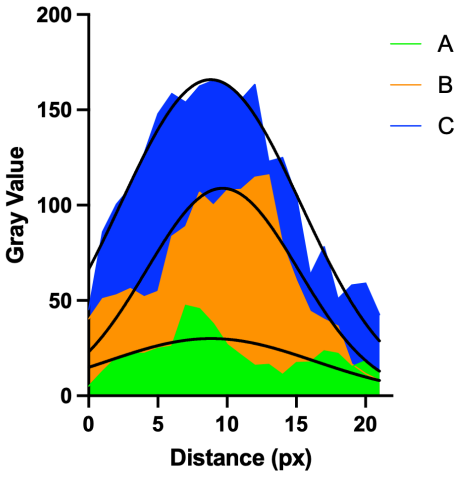

Figure 17 – Cleaning Automated Data by Signal-to-Noise Ratio

A graphical representation of three intensity profile plots overlain with a gaussian fit plot. All of the plots have a similar standard deviation (6.6 – 6.9 px) but different plot amplitudes. The signal-to-noise ratio (SNR) is calculated by dividing the amplitude by the standard deviation. A small SNR is more likely to be associated with poor quality data and peaks that are part of the background noise. A larger SNR is more likely associated with a true peak. An arbitrary cut-off value of > 15 was selected for data inclusion.

2.12.8 Automated Data Cleaning

The raw data produced by the Fiji macro for both the capillary and syncytiotrophoblast peak-to-peak measurements was copy and pasted into a dedicated Excel (Microsoft® Excel for Mac, v16.49, Microsoft Corporation, Redmond, USA) spreadsheet. A macro created in Excel automatically applied the thresholding for the gaussian fit standard deviation and SNR as previously described. The median and interquartile range of each image was automatically calculated, and the mean and standard deviation for each placental specimen presented.

The number of values remaining after cleaning of the data varied depending on the quality of the tissue and the amount of glycocalyx staining. Images were excluded if fewer than 10 individual peak-to-peak values were remaining after the data was cleaned.

2.12.9 Glycocalyx Coverage

A measure of glycocalyx coverage was also calculated in Excel. Glycocalyx was considered present if both a green and red peak were present that fit between the gaussian standard deviation and SNR thresholds previously described. The following equation was used:

$$Coverage\ (\%) = \frac{Number\ of\ included\ peak-to-peak\ measurements}{Total\ number\ of\ measurements}$$

It is recognised that this method will be confounded by the quality of the tissue staining and anomalies in the shape of the vessel or syncytiotrophoblast and is perhaps not directly comparable to the measure of coverage described using transmission electron microscopy. Nevertheless, the method does produce a value of the uniformity and degree of lectin (glycocalyx) staining in a vessel or at the syncytiotrophoblast brush border which we have ostensibly described as coverage.

2.13 Correlative Electron Microscopy and Confocal Microscopy

Correlative microscopy involves the imaging of the same tissue sample using both light and electron microscopy. I used this technique to demonstrate that the glycocalyx staining observed using lectin histochemistry corresponded to the expected location of the glycocalyx when observed with electron microscopy.

Quantum dots (QDs) are semiconductor nanocrystals which exhibit photoluminescence when excited by UV light, with the emission wavelength determined by the size of the QD [247]. They can be conjugated and used in fluorescence microscopy in place of other fluorophores. Importantly they are also electron dense and can be observed using electron microscopy.

Placental tissue sections were prepared and processed as per the standard lectin histochemistry protocol described in section 2.8.2. Sections were either incubated with biotinylated-UEA-I or WGA. Qdot™ 655 streptavidin conjugate (Thermo Fisher Scientific, Waltham, USA, Q10123MP) was used in place of the AF488. The Qdot™ streptavidin conjugate was first centrifuged at 5000g for three minutes in accordance with the manufacturer's instructions. A working concentration of 1:100 Qdot™ streptavidin conjugate was freshly prepared in 1% BSA in PBS – 0.1% Tween, pH 6.8 and the tissue incubated at room temperature for one hour.

Tissue sections were co-stained with R18 but not DAPI which shares a similar excitation as QDs and has a broad emission profile. Coverslips were applied to the sections as per previous.

Imaging with confocal microscopy was as described in section 2.10, with minor adjustments made to the laser configuration and PMT emission detection ranges for the different excitation and emission profile of the QDs. After imaging, the sections were soaked in PBS, pH 7.4 overnight and the coverslips removed.

Tissue processing for electron microscopy was completed by Dr Chris Neal. In brief, the sections were post-fixed with 1% glutaraldehyde in 0.1M phosphate buffer for 15 minutes, before staining with 1% osmium tetroxide and 3% uranyl acetate for 15 and 20 minutes respectively. The sections are then dehydrated through gradated ethanol washes, before embedding and curing in epoxy resin whilst still on the glass slide.

The glass slides are removed by repeated freezing in liquid nitrogen and thawing in boiling water. The expansion and contraction of the glass in these conditions is different from the resin allowing the glass to separate, leaving the embedded section in the resin.

Samples were cut and imaged by transmission electron microscopy as per the protocols previously described in sections 2.7.3 and 2.9.

2.14 Lectin Histochemistry in an Independent Cohort

To demonstrate the validity of the lectin histochemistry methodology and confirm reproducibility in an independent cohort, I made an application to access placental specimens from a biobank held by the University of Nottingham.

A material transfer agreement (MTA) was agreed with Dr Hiten Mistry (University of Nottingham) and Dr Lesia Kurlak (University of Nottingham). Sampling for the biobank typically took place within a few minutes of delivery of the placenta. Tissue was fixed in formalin for up to 2 weeks, before being processed into 70% ethanol and batch processed into wax. Samples were provided on slides, sectioned at 5 μm.

Lectin histochemistry and confocal imaging was performed as per the protocols described in section 2.8.2 and 2.10 respectively. Glycocalyx peak-to-peak measurements for the placental capillaries and syncytiotrophoblast were measured using the respective automated macros described in section 2.12. Imaging and analysis took place blinded.

Unblinding and anonymised demographic and clinical data was provided by Dr Hiten Mistry once image analysis was complete.

2.15 Statistics and Data Handling

Statistics and graphs have been produced in Prism v 9.1.2 for macOS (GraphPad Software, San Diego, USA) unless stated below.

Data was assessed for normality by visual inspection and the Shapiro-Wilk normality test. Descriptive statistics for normally distributed data were presented as the mean and standard deviation. For non-parametric data, the median and interquartile range is presented.

When comparing two groups for statistical significance an unpaired t-test was used for normally distributed data, and the Mann-Whitney test for non-parametric data. When more than two groups were analysed, an ordinary one-way ANOVA was used for normally distributed data. Individual comparisons between groups are achieved with the post hoc

Dunnett's multiple comparisons test, with single pooled variance. Nonparametric data with more than two groups was assessed with the Kruskal-Wallis test, with a post hoc Dunn's multiple comparisons test for individual group comparisons. Data is presented graphically with the mean value and standard error of the mean, or the median and interquartile range where applicable.

Correlation between two continuous variables is assessed using the Pearson correlation for normally distributed data and the Spearman correlation for nonparametric data. By convention the strength of the correlation is interpreted by the correlation coefficient (r) as either negligible (0 – ±0.09); weak (±0.10 – ±0.39); moderate (±0.40 – ±0.69), strong (±0.70 - ±0.89); or very strong (±0.90 - ±1.00) [248]. Correlation data is presented graphically with a line of best fit produced through simple linear regression and displayed with 95% confidence bands.

Inter and intra-operator variability was calculated using IBM SPSS Statistics for Mac v 27.0.1.0 (IBM, Armonk, USA) using the reliability analysis intraclass correlation coefficient (ICC). A two-way mixed effects model was used, with single measures and absolute agreement. By convention the ICC was interpreted as poor (<0.4); fair (0.40 – 0.59); good (0.60 – 0.74); or excellent (0.75 – 1.00) [249]. Bland-Altman plots of intra- and inter-rater reliability are presented with the bias and standard deviation shown.

Power-calculations for future work were computed using the open-source software G*Power v3.1.9.6 [250, 251]. By convention alpha was set at 0.05 with a power of 0.8 [250]. The effect size was calculated from the pilot data produced in this work.

Statistical significance was determined if the p value calculated was ≤ 0.05. P values are displayed on graphs as either; not significant (ns) = $P > 0.05$; * = $P \leq 0.05$; ** = $P \leq 0.01$; and *** = $P \leq 0.001$.

3. IMAGING THE SUBLINGUAL GLYCOCALYX

3.1 INTRODUCTION AND SPECIFIC AIMS

Intravital microscopy and sidestream darkfield imaging have been used to assess the general condition of the microvasculature for many years. GlycoCheck™, provides a novel way of interpreting the data obtained through this imaging technique to focus on the endothelial glycocalyx. As previously described, a software package interprets SDF images to determine the lateral motion of RBCs into the perfused boundary region (PBR). In conditions where the glycocalyx is shed, there is greater lateral movement of RBCs and the PBR is higher [220].

This technique is attractive as it provides an approach for measuring the depth of the glycocalyx *in-vivo* and allows for the possibility of repeating measurements in the same participant at different time points. It is minimally invasive, quick and it automates the processing of large volumes of data.

There is a growing number of publications which have demonstrated changes in the PBR in a variety of different conditions effecting the endothelium, including cerebral vascular disease [252], cardiovascular disease [253], sepsis [254], COVID-19 [255], diabetes [256] and pre-eclampsia [187].

The measurement of the glycocalyx using this technique is, however, indirect and some have questioned the reliability and reproducibility of the PBR measurements, especially within an individual participant [257].

In this chapter I look to determine the usability, reliability and reproducibility of the GlycoCheck™ device by completing a reliability analysis. I will then look to define changes in the PBR in pregnant women with and without pre-eclampsia.

3.2 Is the GlycoCheck™ Device Reliable and Reproducible?

3.2.1 Operator and Patient Experience

Prior to starting general enrolment of patients, it was important to determine the feasibility, usability and most importantly the reliability of the GlycoCheck™ device.

Although specific qualitative data were not collected, the general feedback from participants and operators demonstrated that the device was well tolerated and easy to use. All participants were able to complete a minimum of two consecutive readings for analysis.

Participant positioning was especially important during the examination. Initially in the feasibility study of non-pregnant participants we completed the examination with the participant sitting on a chair with their head unsupported. Movement artifact was common using this technique, with several failed measurements that were not able to complete within 5-minutes. This was much improved by completing the examination with the participant sitting on a couch, with their head supported by a pillow.

During training, it was clear that operator technique was important for the quality of the output data. Ensuring the correct amount of pressure is applied to the sublingual capillary bed was one of the most difficult proficiencies; too much pressure resulted in occlusion of capillaries with a direct effect on the data, whereas too little pressure resulted in poor image quality and difficulty in focussing the device.

Participant factors were also important and may affect the quality of the data. The key variable was on the ability of the participant to keep their tongue still during the examination. It seemed some people naturally found this easier than others.

The device was sufficiently portable to be used in a variety of locations. We used the device routinely in the labour ward, antenatal ward and in an antenatal clinic setting with relative ease.

3.2.2 Intra-Operator Reliability

Intra-rater reliability was assessed by taking two consecutive GlycoCheck™ readings by the same operator on the same participant. The reliability was fair (n=23, ICC=0.469, 95% CI

0.105 – 0.724) for Operator A and poor (n=16, ICC=0.199, 95% CI -0.288 – 0.602) for Operator B when assessing the PBR for vessels 5-25 µm.

The intra-rater reliability was also assessed across the other standard vessel size composites (5-9, 10-19 and 20-25 µm), which ranged between poor and good (Table 4). There was no discernible pattern regarding vessel size and reliability.

The experience of the operator did not seem to affect reliability; Operator A who had significantly less experience than Operator B, had a greater level of agreement in some composite vessel sizes.

These findings are consistent with other published work which have demonstrated a low level of agreement between two consecutive GlycoCheck™ readings [187, 258]. Reliability has been shown to improve, however, if the average of two (or more) consecutive measurements are used [187, 229, 259]. This reportedly accounts for spatial heterogeneity of the sublingual microvasculature [229].

	Operator A		Operator B	
Composite Vessel Size Category (µm)	ICC	Interpretation	ICC	Interpretation
5-25	0.46 (0.08 – 0.73)	Fair	0.20 (-0.29 – 0.60)	Poor
5-9	0.09 (-0.35-0.49)	Poor	0.51 (0.05-0.79)	Fair
10-19	0.72 (0.45-0.87)	Good	0.24 (-0.27-0.63)	Poor
20-25	-0.24 (-0.41 – 0.15)	Poor	-0.04 (-0.50 – 0.43)	Poor

Table 4 – Intra-Operator Reliability
The intra-operator reliability for two operators completing two consecutive GlycoCheck™ measurements on the same patient. The intraclass correlation coefficient was calculated using a two-way mixed model, single measures, absolute agreement. By convention the ICC was interpreted as poor (<0.4); fair (0.40 – 0.59); good (0.60 – 0.74); or excellent (0.75 – 1.00)

3.2.3 Inter-Operator Reliability

Inter-operator reliability was assessed by comparing GlycoCheck™ measurements taken by two operators on the same participant. Allowing for the findings of the intra-rater reliability study, two measurements were obtained by each operator, with the mean of the two values used for comparison.

There was no difference between the mean PBR for vessels 5-25 µm between the two operators: 2.19 (SD 0.21) vs 2.24 (SD 0.18), n = 15, p = 0.49. The ICC for this composite, however, was poor; 0.115 (95% CI -1.80 – 0.709).

The ICC value in the 5-25 µm composite, was skewed by larger vessels in the 20-25 µm range, ICC -0.73 (95% CI -4.37 – 0.43), as both the 5-9 µm and 10-19 µm composites were fair; ICC 0.46 (95% CI -0.74 – 0.822) and 0.53 (95% CI -0.47 – 0.844) respectively.

The inter-operator reliability is demonstrated graphically in a Bland-Altman plot (Figure 18), demonstrating the level of agreement between the two operators. There was no evidence of an operator bias between the estimated true value and the observed values, bias -0.05 µm (SD 0.27). These values are very consistent with other published inter-rater reliability data [229].

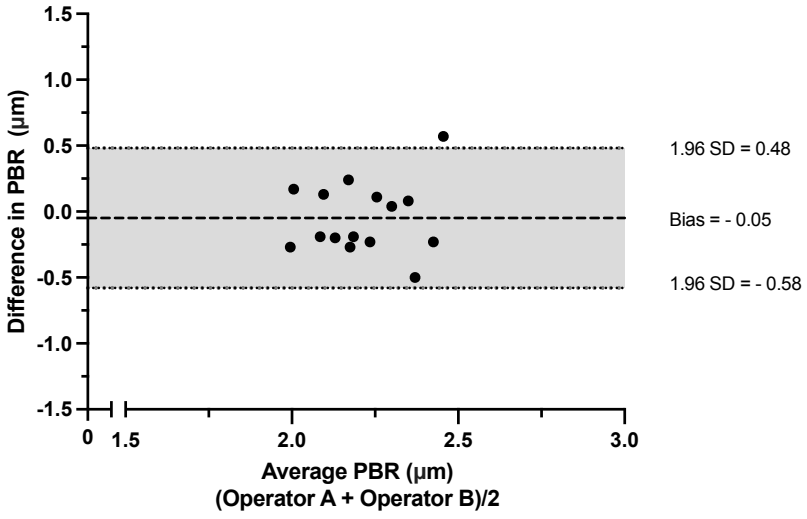

Figure 18 – Bland-Altman Plot of Inter-Rater Reliability
A visual representation demonstrating the limits of agreement between two operators. There was no evidence of operator bias (-0.05). The 1.96 standard deviation thresholds are displayed.

The data gained during the reliability study guided production of the GlycoCheck™ protocol used in the main study as outlined in section 2.3.2. For each participant a single operator would conduct between 2 and 3 consecutive GlycoCheckTM measurements, with the mean values used for comparison.

3.3 Participant Characteristics for the GlycoCheck™ study

Sixty-four participants were enrolled and had GlycoCheck™ measurements as part of the study. Forty were normotensive controls and 24 had a diagnosis of pre-eclampsia. The pre-eclampsia group was further subdivided into early- and late-onset groups, n = 7 and 17 respectively.

Demographic and outcome data was recorded for all participants. There was no difference in the age, parity, BMI, smoking status, and blood pressure at pregnancy booking across the groups. Most participants described their ethnic group as white (92%).

The control and pre-eclampsia groups were gestation matched, with no significant difference between the gestation at the time of the test; median 35+2 weeks (IQR 30+0 - 36+3) for the control group and 35+2 (IQR 29+6 – 38+5) for the pre-eclamptic group, p = 0.20. When the pre-eclamptic group was subdivided into early- and late-onset pre-eclampsia, as expected, there was a clear difference in the gestation at the time of the test, with median gestation of 28+2 weeks (IQR 25+5 - 28+6) in the early-onset pre-eclampsia group and 38+0 weeks (IQR 34+4 – 39+2) in the late onset group, p = <0.001.

As expected, the systolic, diastolic, and mean arterial blood pressure (MAP) was significantly higher in both the early- and late-onset pre-eclampsia groups compared to normotensive controls, p = <0.001. Most pre-eclampsia participants were medicated with at least one anti-hypertensive; 86% in the early-onset group and 88% in the late-onset group.

Both pre-eclampsia subgroups had significant proteinuria, quantified by mean urinary PCR of 160 mg/mmol (SD ± 169) and 100 mg/mmol (SD ± 69) in the early- and late-onset groups respectively. Normotensive controls did not routinely have urinary PCR quantified, but all had a negative result for protein on urine dipstick analysis.

Gestation at delivery similarly reflected the expected differences in the early- and late onset groups, with mean gestations of 40+1 weeks (SD 9 days) in the control group, 28+4 weeks (SD 12 days) in the early-onset group and 38+0 weeks (SD 14 days) in the late-onset group. The median latency period between recruitment and delivery was 38 days (IQR 26-71) in the control group; 3 days (IQR 0-7) in the early-onset group; and 1 day (IQR 1-4) in the late-onset group, highlighting the iatrogenic intervention of delivery in the treatment of pre-eclampsia.

There was no difference in mode of delivery and the sex of the infant. As expected, the birthweights of both the early-onset and late-onset groups were significantly smaller, compared to normotensive controls, reflective of the earlier gestation at delivery, $p = <0.001$. Interestingly, there was no significant difference in the birth centiles between the groups, $p = 0.14$, but the early-onset group did demonstrate a trend towards a smaller birth centile, mean 31st centile (±36) vs 54th centile (±26) in the normotensive group, highlighting the potential association of FGR in this sub-group.

The participant characteristics are further displayed in Table 5.

	Normotensive (n=40)	Early-Onset PE (n=7)	Late-Onset PE (n=17)	P Value
Booking Demographics				
Age, years	31 (± 5)	28 (± 5)	31 (± 7)	0.32
Primiparous, n (%)	25 (63)	5 (71)	14 (82)	0.33
Weight, kg, median (IQR)	65 (58-79)	72 (63-82)	75 (60-89)	0.33
BMI, kg/m^2, median (IQR)	23 (21-29)	26 (24-30)	29 (20-35)	0.13
Booking Systolic BP, mmHg, median (IQR)	106 (100-118)	112 (110-120)	120 (100-122)	0.25
Booking Diastolic BP, mmHg, median (IQR)	60 (60-70)	62 (60-75)	64 (60-72)	0.93
Smoker, n (%) yes	0 (0)	0 (0)	0 (0)	NA
Ethnicity, n (%) White	38 (95)	6 (86)	15 (88)	0.54
At GlycoCheck™ Measurement				
Gestation, weeks+days, median (IQR)	35+2 (30+1 - 36+3)	28+2 (25+5 - 28+6)*	38+0 (34+4 – 39+2)**	**<0.001**
Systolic BP, mmHg, median (IQR	110 (102-120)	136 (126-140)***	134 (126-144)***	**<0.001**
Diastolic BP, mmHg, median (IQR)	62 (60-70)	80 (80-85)**	85 (79-89)***	**<0.001**
MAP, mmHg, median IQR	80 (75-84)	99 (97-101)**	103 (93-105)***	**<0.001**
Urine PCR, mg/mmol	Not performed	160 (± 164)	100 (± 69)	NA
Hb, g/L	116 (± 9)	116 (± 8)	117 (± 14)	0.54
Antihypertensives, n (%), yes	0 (0)	6 (86)	15 (± 88)	**<0.001**
Delivery Outcomes				
Gestation, weeks+days	40+1 (± 9)	28+4 (± 12)***	38+0 (± 14)***	**<0.001**
Delivery, n (%) vaginal	23 (59)	5 (71)	10 (59)	0.79
Sex, n (%), male	14 (36)	4 (57)	7 (35)	0.53
Birth weight, kg	3.39 (± 0.36)	1.02 (± 0.51)***	2.91 (± 0.75)**	**<0.001**
Birth Centile, %	54 (± 26)	31 (± 36)	45 (± 36)	0.14
Apgar 1 minute, median (IQR)	9 (9-9)	5 (4-8)***	9 (6-9)	**<0.001**
Apgar 5 minutes, median (IQR)	10 (9-10)	6 (5-9)***	10 (8-10)	**<0.001**

Table 5 – Participant Demographics and Outcome Data

Results are displayed as mean (±SD) unless stated. Normally distributed continuous variables were compared by one-way ANOVA, with post hoc Dunnett's comparing individual groups to control. Non-parametric data was assessed by Kruskal-Wallis test, with post hoc Dunn's multiple comparisons. Categorical data was assessed by χ^2 test. BP is blood pressure, IQR is interquartile range, MAP is mean arterial pressure, NA is not applicable, and PE is pre-eclampsia. P values are displayed as * = ≤ 0.05; ** = ≤ 0.01; and *** = ≤ 0.001

3.4 PBR IN NORMOTENSIVE AND PRE-ECLAMPTIC PREGNANCY

When comparing women with pre-eclampsia to normotensive controls, there was no difference in the PBR in the 5-25 µm vessel composite; 2.28 µm (SD ± 0.13) vs 2.35 (SD ± 0.18), p = 0.10,Figure 19.

When pre-eclampsia sub-types were considered, a significant increase in PBR was identified in women with early-onset disease, compared to normotensive controls; 2.43 µm (SD ± 0.10) vs 2.29 µm (SD ± 0.13), adjusted p value = 0.046. There was, however, no difference in the PBR values of women with late-onset pre-eclampsia; 2.32 µm (SD ± 0.20), adjusted p value = 0.68,Figure 19.

This data provides evidence that there is increased glycocalyx shedding in women with early-onset pre-eclampsia but not in late-onset disease.

Interestingly, the two participants with the highest PBR readings in the late-onset pre-eclampsia group (highlighted in a red circle in Figure 19) were pre-term, both 34+3 weeks. By some definitions this would be considered 'early-onset' and lends further support that maternal glycocalyx damage is a more prominent feature of preterm disease.

The PBR was also compared for each of the standard GlycoCheck^{TM} output vessel size composites of 5-9, 10-19 and 20-25 µm. PBR was increased in early-onset pre-eclampsia compared to normotensive controls in vessels 5-9 µm, adjusted p value 0.006, but was no different in vessels 10-19 and 20-25 µm, adjusted p value, 0.10 and 0.15 respectively. There was no difference in any of the composite vessel sizes for late-onset pre-eclampsia when compared to normotensive controls.

The PBR for each individual vessel size was also calculated (Table 6). Significant increases in PBR were noted in early-onset pre-eclampsia compared to normotensive controls in vessels of 7, 8, 9, 14 and 17 µm. A significant increase in PBR was recorded in late-onset pre-eclampsia, but only in vessels of 21 µm.

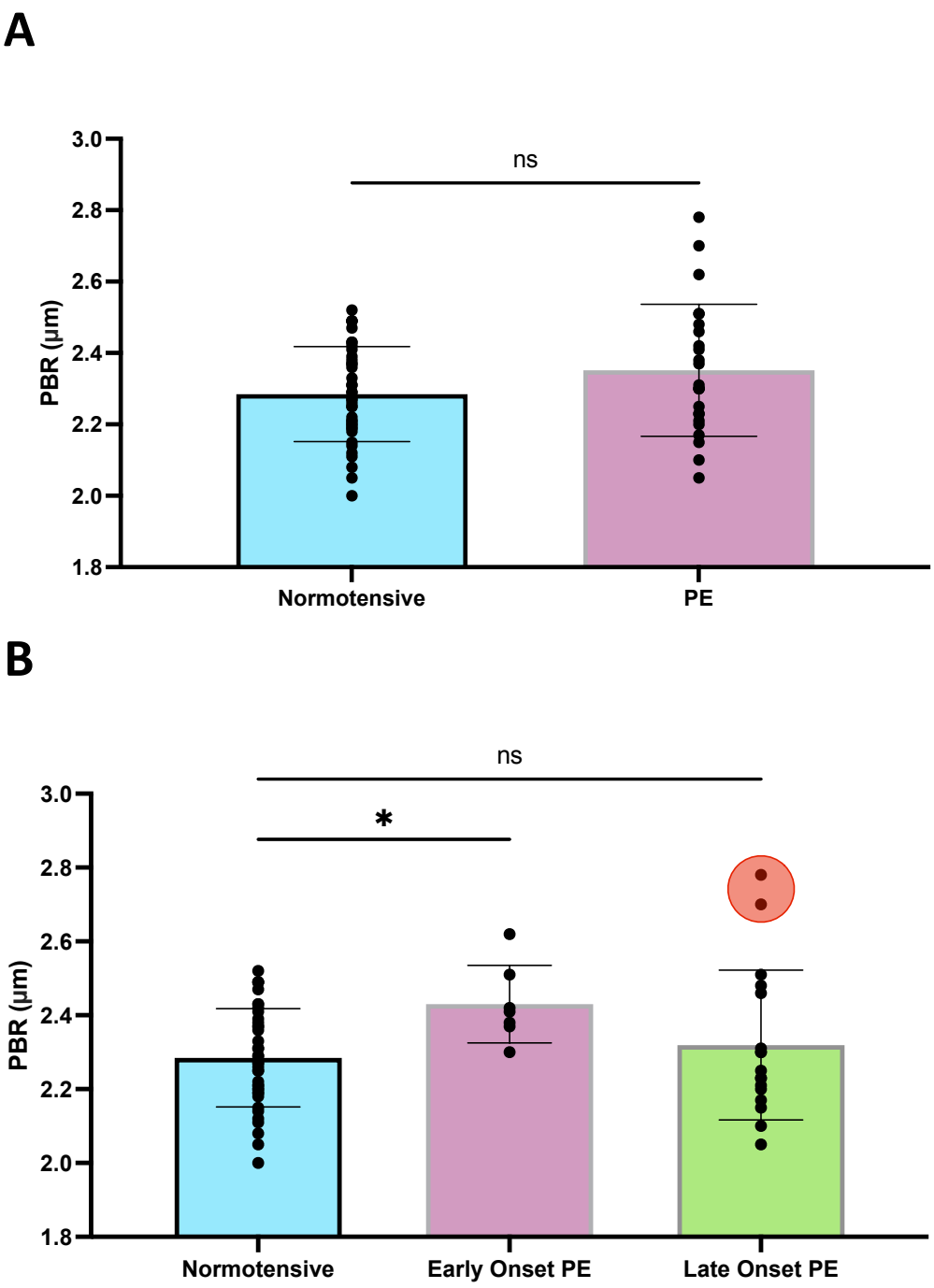

Figure 19 – PBR (5-25 µm) in Normotensive and Pre-eclamptic Pregnancy

There was no difference in the mean PBR values between normotensive controls and participants with pre-eclampsia, p = 0.10 (**A**). When pre-eclampsia was considered by gestation of onset, a significant increase in PBR is observed in women with early-onset disease, adjusted p value 0.046, but not in late-onset disease, adjusted p value 0.68. (**B**) The two highest PBR readings in the late-onset group (highlighted by red circle in **B**), were both preterm at 34+3 weeks, and would have been included in the early-onset subgroup had their presentation occurred 3 days earlier.

Vessel Size, µm	Proportion of total vessels (%)	PBR (± SD), µm			P Value
		Normotensive (n=40)	Early-Onset PE (n=7)	Late-Onset PE (n=17)	
5	0.4	0.83 (0.07)	0.89 (0.13)	0.84 (0.08)	0.20
6	3.1	0.91 (0.06)	0.93 (0.08)	0.92 (0.04)	0.91
7	9.0	1.02(0.07)	**1.10 (0.07) ***	1.07 (0.09)	**0.01**
8	11.7	1.26 (0.09)	**1.37 (0.09) ****	1.30 (0.09)	**0.006**
9	12.4	1.54 (0.12)	**1.68 (0.11) ***	1.58 (0.14)	**0.03**
10	10.6	1.84 (0.15)	1.90 (1.5)	1.86 (0.16)	0.58
11	9.1	2.09 (0.17)	2.07 (0.19)	2.06 (0.16)	0.81
12	7.8	2.28 (0.16)	2.26 (0.25)	2.31 (0.19)	0.85
13	6.1	2.41 (0.20)	2.51 (0.23)	2.46 (0.28)	0.47
14	5.7	2.55 (0.18)	**2.82 (0.30) ***	2.68 (0.29)	**0.009**
15	5.0	2.73 (0.22)	2.93 (0.18)	2.79 (0.24)	0.09
16	4.2	2.87 (0.21)	3.02 (0.28)	2.87 (0.29)	0.34
17	3.5	2.90 (0.26)	**3.24 (0.19) ***	2.90 (0.32)	**0.01**
18	2.6	2.95 (0.28)	3.07 (0.35)	2.99 (0.36)	0.60
19	2.4	2.97 (0.30)	3.15 (0.37)	3.03 (0.45)	0.47
20	1.9	2.92 (0.29)	3.21 (0.38)	2.95 (0.41)	0.13
21	1.6	2.85 (0.33)	3.08 (0.13)	**3.10 (0.41) ***	**0.02**
22	1.2	2.87 (0.45)	3.16 (0.31)	2.76 (0.45)	0.13
23	0.8	2.75 (0.51)	2.76 (0.31)	2.86 (0.41)	0.72
24	0.7	2.69 (0.52)	3.07 (0.29)	2.80 (0.64)	0.21
25	0.4	2.74 (0.74)	2.87 (0.51)	3.05 (0.64)	0.28

Table 6 – Perfused Boundary Region by Vessel Size

The PBR for each vessel size in pre-eclamptic pregnancy is compared to normotensive controls. An increased PBR is demonstrated in early-onset pre-eclampsia in vessels 7, 8, 9, 14 and 17 µm in diameter. PBR is increased in vessels 21 µm in diameter in late-onset disease. The relative contribution to the total number of vessels sampled is expressed as a percentage. Vessels of 9 µm occur most frequently, with vessels ≤ 6 and ≥ 15 each accounting for less than 5% of the total vessels. One-way ANOVA with post hoc Dunnett's multiple comparisons. P values are displayed as * = ≤ 0.05; ** = ≤ 0.01; and *** = ≤ 0.001

The mean frequency of each vessel size and its relative proportion to the total number of vessels for all the cases sampled (n=64), is presented in the histograms in Figure 20. Smaller vessels occur much more frequently than larger vessels in this population. The most commonly occurring vessel size was 9 µm, accounting for 12.4% of all vessels sampled. Vessels of 6 µm or less and 15 µm and greater each contributed less than 5% of the total number of vessels sampled.

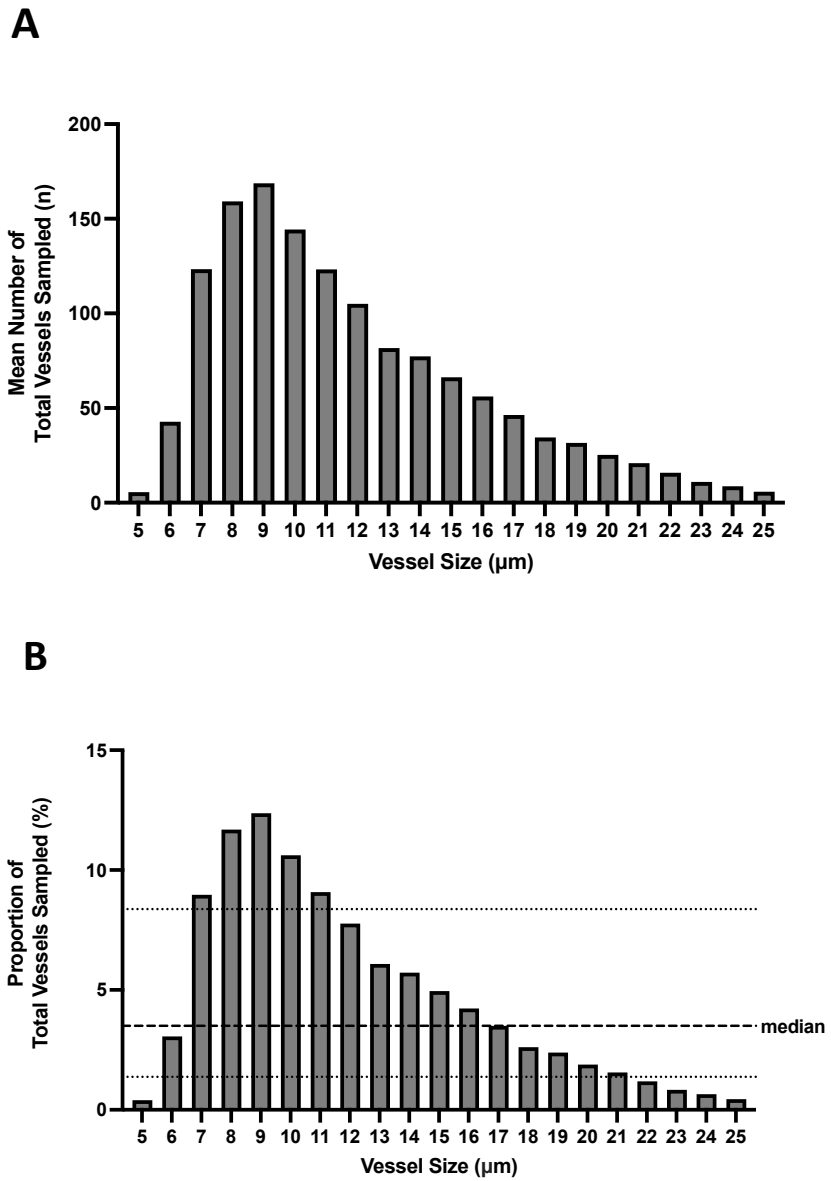

Figure 20 – Frequency of Vessel Size

Histogram demonstrating the mean frequency of each vessel diameter in all 64 participants (**A**). The distribution is skewed towards smaller vessels occurring more frequently. The same data is presented as a proportion of the total measurements (%) in **B**, with the median and interquartile ranges demonstrated.

3.5 Capillary Density and RBC Filling Percentage

GlycoCheck™ automatically calculates measurements of the RBC filling percentage and microvascular density. As described in section 2.3.1, GlycoCheck™ identifies and marks individual vascular segments at 10 µm intervals. Density is therefore calculated by multiplying the number of valid vascular segments by a factor of 10 and is expressed in mm^2. The RBC filling percentage is calculated as the number of vascular segments which have RBCs present in them during all 40 frames of the recording and is a marker of perfusion [220].

In vessels 5-25 µm there was no difference in microvascular density in either early- or late-onset pre-eclampsia when compared to normotensive controls; 17.8/mm^2 (SD ±14.8), 18.5/mm^2 (SD ± 13.9) and 18.7/mm^2 (SD ± 15.2) respectively, p = 0.98.

There was a trend towards a reduction in the RBC filling percentage in early-onset pre-eclampsia compared to normotensive controls, but this did not reach statistical significance, p = 0.17,Figure 21. There was a strong negative correlation between PBR and RBC filling, r = 0.79, p <0.001., suggesting that increased glycocalyx shedding is associated with decreased microvascular perfusion, Figure 22.

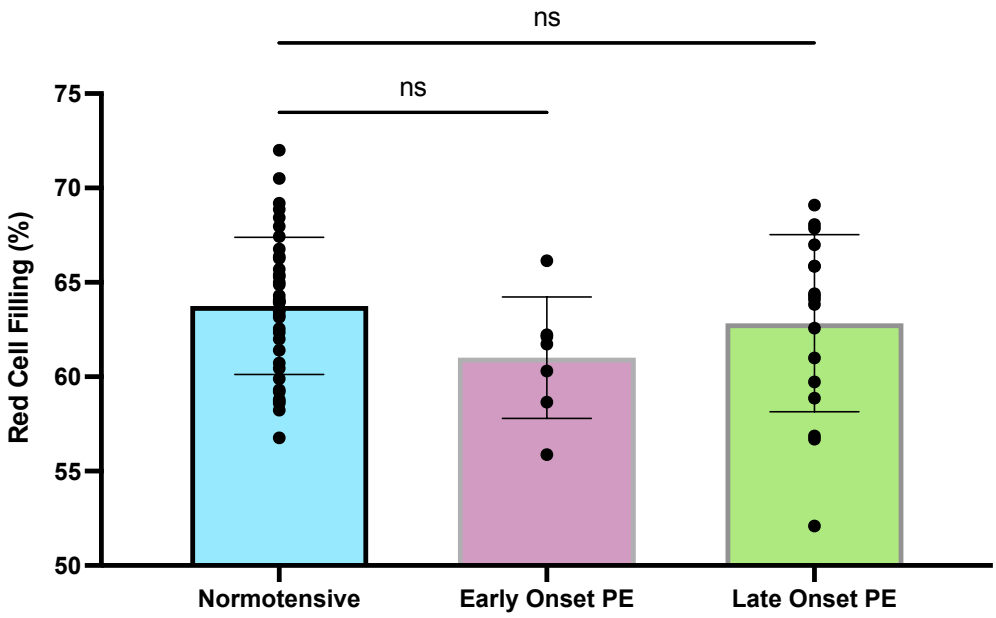

Figure 21 – RBC Filling

There was a trend towards a reduction in the percentage of red blood cells filling each vascular segment in all 40 frames of the recording in early-onset pre-eclampsia (61.0% ± 3.2), compared to normotensive controls (63.8% ± 3.6), adjusted p value = 0.17.

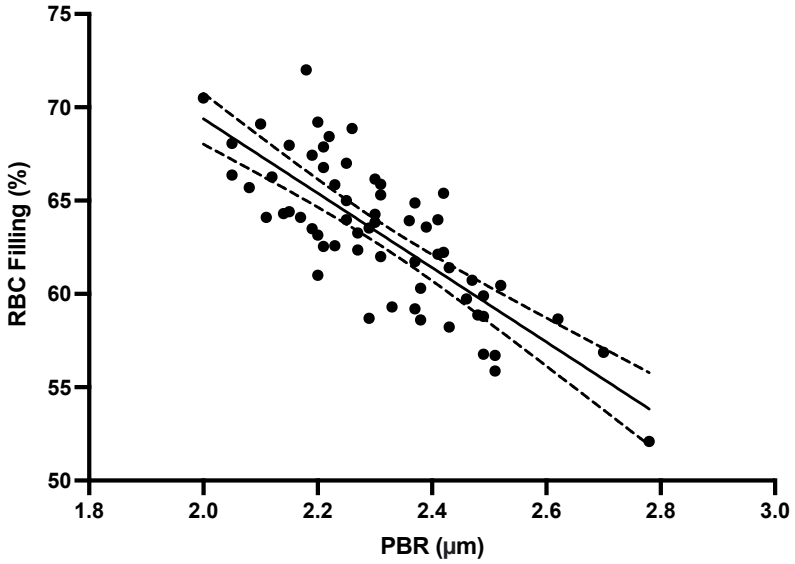

Figure 22 – RBC Filling vs PBR
There was a strong negative correlation between PBR (5-25 µm) and the percentage RBC filling, r = 0.79, p <0.001, demonstrating an association between glycocalyx shedding and decreased microvascular perfusion. Pearson correlation coefficient, with line of best fit produced through simple linear regression, with 95% confidence bands.

3.6 Other GlycoCheck™ Outputs

GlycoCheck™ calculates a score of overall health of the microvasculature. It is calculated through a combination of the capillary blood volume, red cell velocity and PBR and is termed the microvascular health score (MVHS) [260].

There was no difference in the MVHS between participants with either early- or late-onset pre-eclampsia compared to normotensive controls, p = 0.89.

3.7 Comparing PBR to Other Clinical Markers

The PBR value in 5-25 µm sized vessels was compared to other clinical markers and outcome data.

There was no association between PBR and blood pressure; MAP, r = 0.09. p = 0.46, or gestation at the time of testing, r = -0.08, p = 0.49. Similarly, there was no association with the severity of derangement of biochemical markers of end-organ dysfunction in pre-eclampsia, including ALT (r = -0.06 , p = 0.76), creatinine (r = 0.05 , p= 0.79), platelets (r = 0.08, p = 0.58) and urinary PCR (r = 0.20, p = 0.34).

There was a moderate negative correlation between the PBR and the recorded haemoglobin of the participant, r = -0.40 (95% CI -0.62 to -0.13), p = 0.005. This perhaps suggests an association between anaemia and increased glycocalyx shedding, or evidence that anaemia acts as a confounding factor within the GlycoCheck™ software, Figure 23.

A moderate negative correlation was demonstrated between PBR and the birth weight of the infant, r = -0.41 (95% CI -0.61 to -0.18), p = <0.001, although this association was weak when compared to the birth centile, r = -0.35 (95% CI -0.56 to -0.11), p = 0.004,Figure 23.

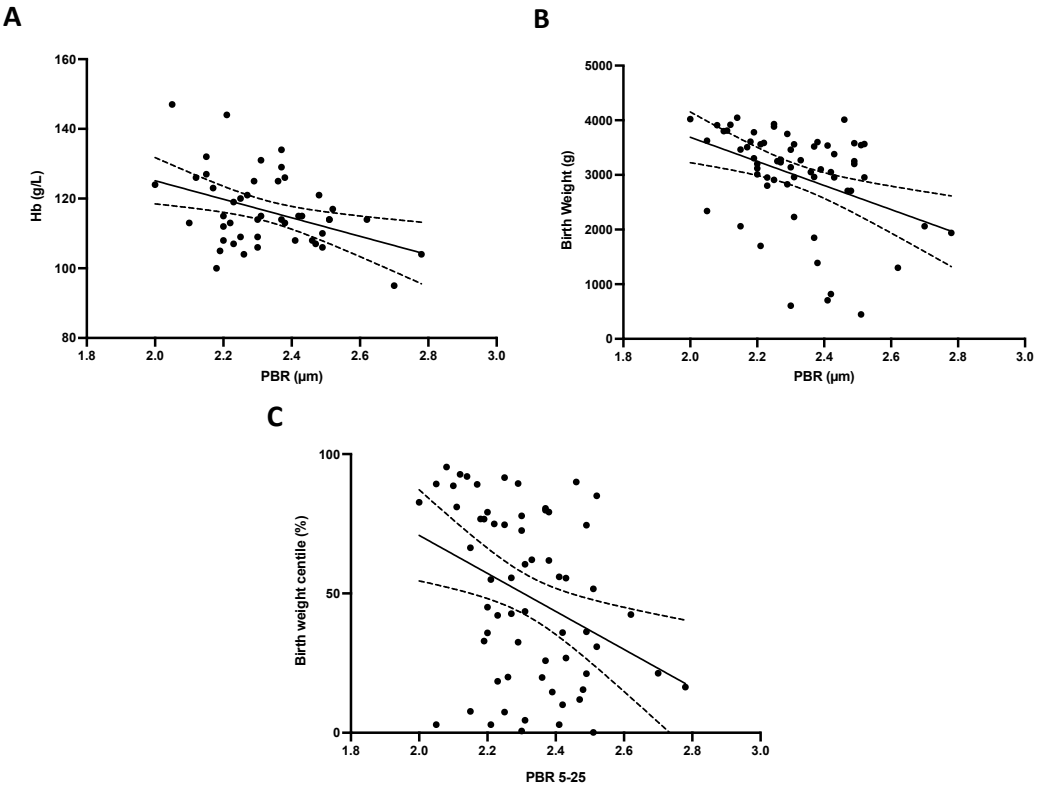

Figure 23 – PBR vs Hb, Birth Weight and Birth Centile

There was a moderate negative correlation between PBR and Hb, r = -0.40, p = 0.005, **A**. This may suggest a relationship between anaemia and glycocalyx shedding, or possibly a confounding variable in the GlycoCheck™ software. A similar moderate correlation was observed between PBR and the birth weight of the infant, r = -0.41, p = <0.001, **B**. This may suggest increased glycocalyx shedding is associated with a reduction in birth weight. This association was weak when birth centile was considered, r = -0.35, p = 0.004, **C**.
Pearson correlation coefficient for parametric, and Spearman's rank correlation coefficient for non-parametric data. Line of best fit produced through simple linear regression, with 95% confidence bands.

The association between both birthweight and birth centile with PBR was further studied in just the normotensive control group (n = 40), in case the previously described correlation was affected by the association between pre-eclampsia and fetal growth restriction. In normotensive controls there was a moderate negative correlation between both birth weight and PBR, r = -0.54 (95% CI -0.73 to -0.27), p = <0.001, and birth centile and PBR, r = 0.49 (95% CI -0.70 to -0.20), p = 0.002, Figure 24

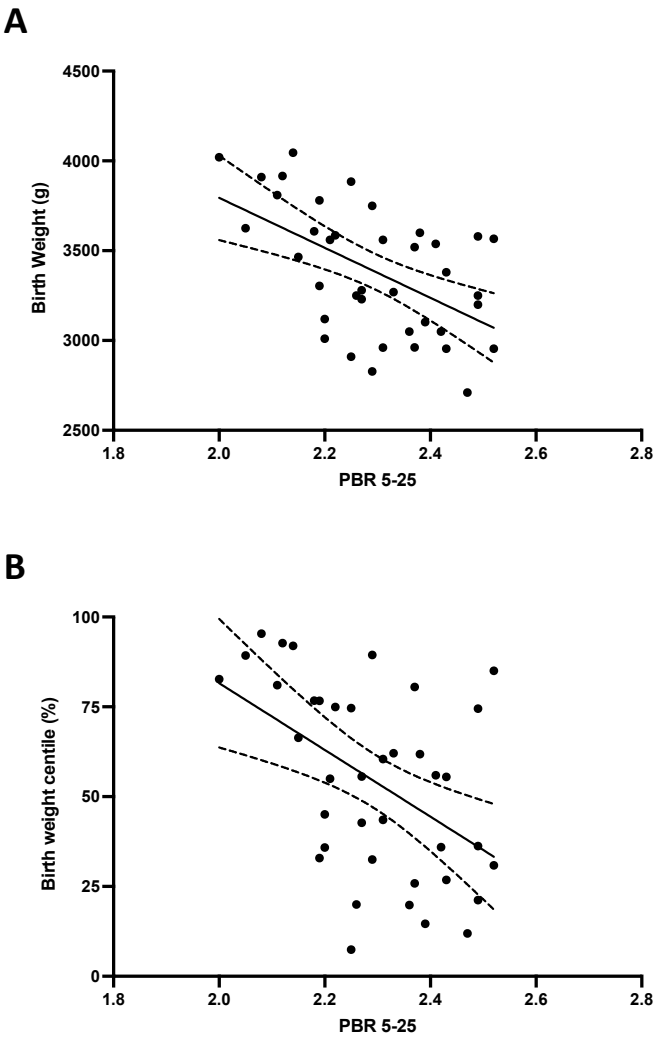

Figure 24 – PBR vs Birth Weight and Birth Centile in Normotensive Controls

There was a moderate negative correlation between birthweight and PBR, r = -0.54, p = <0.001, **A** and birth centile and PBR, r = 0.49, p = 0.002, **B**.
Pearson correlation coefficient. Line of best fit produced through simple linear regression, with 95% confidence bands.

3.8 Discussion

3.8.1 Usability and Reliability

The GlycoCheck™ device was found to be a highly usable device, with good acceptance by patients and researchers. After training, the process of image acquisition was quick and could be performed at different locations within the hospital setting.

Ensuring the reliability and reproducibility of results was important before proceeding with a wider study. I have demonstrated poor test-retest reliability, which was independent of vessel size and user experience. Similar poor intra-rater reliability has been demonstrated in number of studies [187, 257]. Rovas et al. attributes this to spatial heterogenicity within the sublingual microvasculature and suggests using the mean of two consecutive measures to correct for this [229]. Several authors have demonstrated improved reliability by combing multiple readings, with Eickhoff et al. suggesting a minimum of 3 consecutive measures [257].

It is worth noting, that GlycoCheck™ reports that it already accounts for microvasculature heterogeneity by including over 3,000 individual vascular segments in each recording [220]. Using the mean of multiple readings to improve device reliability, may also raise questions about the statistical validity.

Inter-observer reliability has also been addressed in several studies with a wide range of results reported. Rovas et al. in the 'GlycoNurse' study compared GlycoCheck™ measurements between doctors and nurses and found an excellent inter-observer reliability, ICC 0.88 for PBR [229]. Valerio et al and Eickhoff et al. found much lower values in the poor range at 0.33 and 0.30 respectively, which compare more closely to my findings [257, 258]. Some of the discrepancy could be due to differences in the application of the ICC statistic, with not all authors declaring which ICC test was used. This makes direct comparison more difficult.

Reassuringly, I have demonstrated no difference in the mean PBR values in a set of patients obtained by two operators. The Bland Altman plot demonstrates a good limit of agreement, with no bias. Despite the discrepancy in ICC, my Bland Altman plot is very similar to the result presented by Rovas et al, with a near identical SD [229]. It is possible that the small numbers included in my reliability study have affected the ICC statistic.

Chicchetti suggests a minimum of 30 participants and at least 3 users for an inter-rater reliability analysis [249].

It is important to note that the observed limits of agreement described in this, and other published work, fall very close to the observed differences observed between control and disease groups. For example, the 1.96 SD observed in the difference in PBR between observers in this study was between 0.48 and -0.58 µm. The observed difference between the control and early-onset pre-eclampsia group was only 0.14 µm. This would suggest caution needs to be used in interpreting individual values, and the role of GlycoCheck™ is likely limited to larger population studies, and not as a point of care diagnostic tool.

The association between PBR and Hb observed in my work is interesting. This finding was also present in a study of renal dialysis patients by Dr Hui Liew (unpublished). Erythrocytes have their own glycocalyx layer which is of a similar composition and negative charge as the endothelial glycocalyx. The zeta potential can be used to calculate the charge on the surface of red blood cells, and therefore can be considered a proxy measure of this layer [261]. The zeta potential has not been shown to be affected by anaemia [262].

Image acquisition with GlycoCheckTM, however, uses LEDs with the emission wavelength that corresponds to haemoglobin to detect the movement of erythrocytes [219]. It is perhaps more likely therefore, that the observed negative association between PBR and Hb, is a confounding factor in the way PBR is calculated by GlycoCheck™, and this should be accounted for when comparing groups.

3.8.2 Changes in PBR in Pre-eclampsia

Even with a relatively small sample size, this work has demonstrated that there is an increase in the PBR of women with early-onset pre-eclampsia. These findings compare favourably with data from Weissgerber et al, who in a larger study (n = 116) demonstrated a similar change in PBR [187]. If the Bristol and Weissgerber data sets are combined, the difference in PBR is even more compelling, 2.41 (SD ±0.21) vs 2.56 (SD ± 0.20) in normotensive pregnancy compared to early-onset pre-eclampsia, p = 0.009.

Although not statistically significant, my data also demonstrates the same trend in RBC filling percentage observed in the Weissgerber paper. This would support increased microvascular permeability in the early-onset pre-eclampsia group.

When considering PBR by individual vessel size, it was clear that the largest differences between the normotensive and early-onset pre-eclampsia groups occurred in the smaller vessels, specifically vessels between 7 – 9 µm. Smaller vessels also occurred much more frequently in the sublingual microvasculature, with the most common vessel size being 9 µm.

When calculating the PBR value in the 5-25 µm range, equal weight is proportioned to each vessel size class, despite the relative rarity of many larger vessels. This has the potential to skew results.

A pregnancy specific vessel range was suggested by Weissgerber et al. using 10 -16 µm vessels [187]. My data would also suggest a pregnancy specific range may be of benefit in excluding less frequently occurring vessels. One method of defining this range would be to use the median vessel frequency, or the upper quartile vessel frequency as can be demonstrated in Figure 20. This would produce ranges of 7 – 16 µm, or 7-11 µm respectively.

There are also sound physiological reasons for only including smaller vessels sizes when calculating PBR. Aside from their relative frequency, there is evidence that many key pathological processes observed in endothelial disease take place in smaller vessels [263]. Many would consider 'true' capillaries to be less than 10 µm in diameter. PBR changes that are specific to smaller capillaries have been demonstrated in other work, including sepsis [254].

The association between the gestation specific birth weight centile and PBR was expected and thought likely to be confounded by the strong association with fetal growth restriction and early-onset pre-eclampsia. What is more surprising, is that this moderate negative association persists in the normotensive control group. This would suggest a relationship between glycocalyx shedding and small birth weight infants and would be an interesting focus point for future study.

3.8.3 LIMITATIONS

The small sample size is clearly a limiting factor to this study, with only 5 participants included in the early-onset pre-eclampsia group. A post-hoc power calculation suggests a sample size of 31 in each group would be sufficient to detect a difference of 0.33 µm.

I have also not been able to correct for known confounders of GlycoCheck™, with caffeine intake in the preceding 6 hours the most recognised example [257]. The opportunistic nature of recruitment and small sample numbers did not allow for control of these variables.

3.9 CONCLUSION

The GlycoCheck™ device has good usability in the clinical setting and was accepted by patients.

Inter and intra-observer reliability for the device is an issue, but can be improved by obtaining repeated measures, 3 repeats is suggested. The variability between operators and the relatively small changes in PBR between control and disease groups means this device is unlikely to ever have a useful role in individual patient prognostication or diagnosis. It does, however, have important potential as a useful research tool in larger patient cohorts, especially to understand how the glycocalyx changes over time.

Early-onset pre-eclampsia is associated with glycocalyx shedding at the sublingual microvasculature, as evidenced by an increased PBR when compared to normotensive controls. There was no difference between control and late-onset disease.

4. Imaging The Placental Glycocalyx - Transmission Electron Microscopy

4.1 Introduction and Specific Aims

Historically the placental glycocalyx has been demonstrated by TEM by immersion or perfusion fixation in the presence of a cationic dye [193, 196, 198]. The success of such experiments is variable, largely depending on the methodology used. To my knowledge, no study has attempted to quantify the glycocalyx in normotensive or pre-eclamptic pregnancy glycocalyx using this method.

The benefit of TEM as a technique for visualising the glycocalyx is clear; the reported glycocalyx depth is often in the range of nanometres rather than micrometres and thus beyond the resolution of most light microscopy techniques.

In this chapter I will present methodologies for imaging the placental glycocalyx using TEM, describing the process of optimisation and standardisation of the technique. I will compare the relative benefit of different fixation methods and cationic dyes. Finally, I will present pilot data demonstrating the findings of the placental glycocalyx in normotensive and pre-eclamptic pregnancy.

4.2 Can the Placental Glycocalyx Be Imaged Following Immersion Chemical Fixation?

4.2.1 Syncytiotrophoblast Glycocalyx

Immersion fixation of placental tissue in the presence of a cation was able to demonstrate the syncytiotrophoblast glycocalyx as an electron dense layer at the microvillous brush border. The layer extended from the phospholipid bilayer into the intervillous space.

The three different combinations of cationic probe tested across the same placenta were all able to demonstrate the glycocalyx, but the measured depth was greatest with Alcian

blue and L-lysine, 76.8 nm (SEM ± 2.9), compared to ruthenium red and L-lysine, 68.1 nm (SEM ± 2.2), and lanthanum, dysprosium and L-lysine, 58.5 nm (SEM ± 4.3), p <0.001, Figure 25 (B-D).

L-lysine was used in combination with the cationic probes, as previous published work has demonstrated superior preservation of the glycocalyx through stabilisation of carbohydrate moieties [213]. When tissue was fixed in the presence of L-lysine, without another cationic dye, some glycocalyx preservation was demonstrated, but this was patchy,

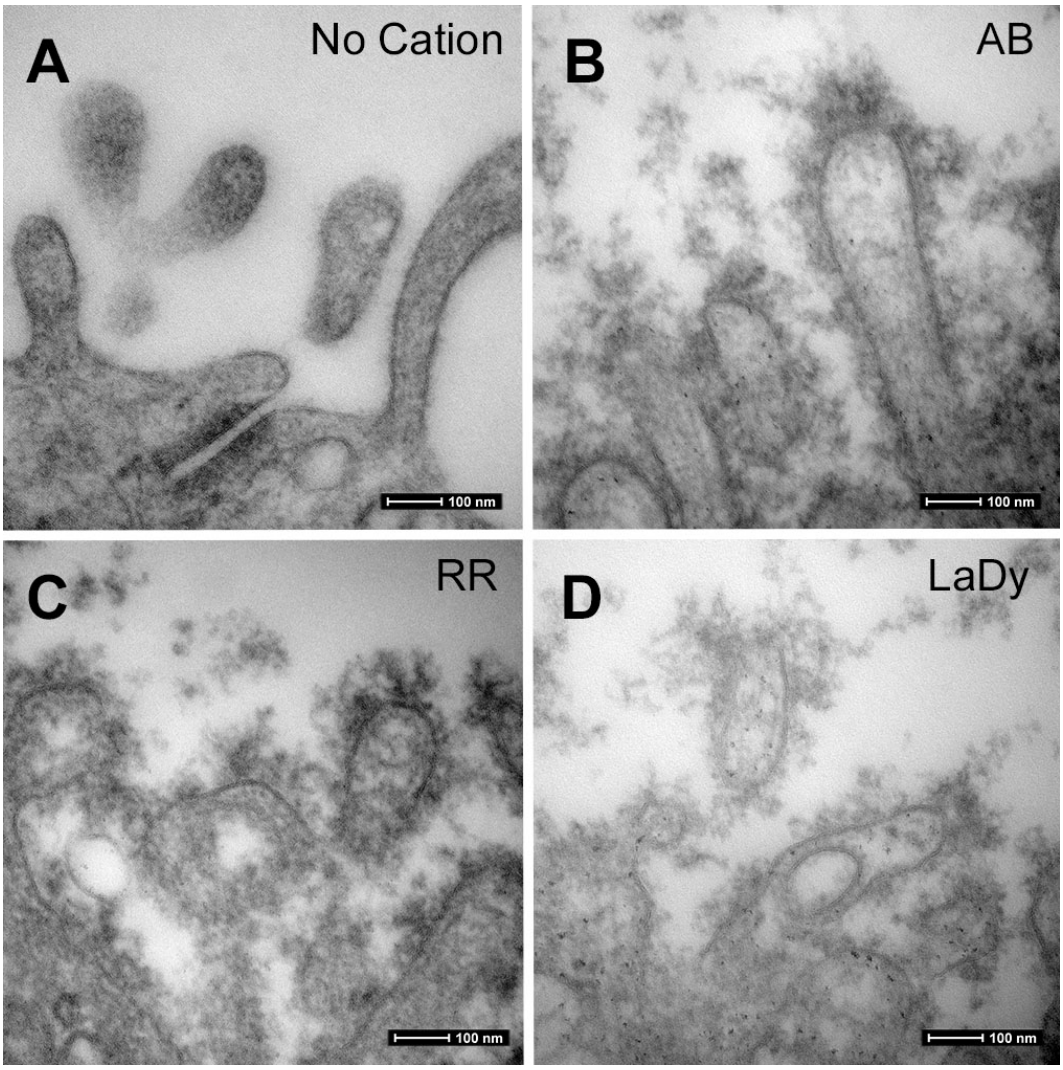

Figure 25 – Syncytiotrophoblast Glycocalyx by Immersion Fixation
Placental tissue was fixed by immersion in 2.5% glutaraldehyde and 0.1 M cacodylate buffer with either no cation (A), 0.1% Alcian blue and 75 mM L-lysine (B), 0.1% ruthenium red and 75 mM L-lysine (C) or 0.3% lanthanum, 0.3% dysprosium and 75 mM L-lysine (D). In the absence of a cationic probe the glycocalyx was not preserved. Glycocalyx was demonstrated with all of the cationic probes, but the depth was greatest with Alcian blue, 76.8nm (SEM ± 2.9). AB = Alcian blue; RR = ruthenium red; LaDy = lanthanum and dysprosium.

and the quality of glycocalyx preservation was generally poor. When tissue was fixed without either L-lysine or a cationic probe, no glycocalyx was observed, Figure 25 (A).

The combination of lanthanum, dysprosium, and L-lysine with glutaraldehyde in cacodylate buffer tended to form a gelatinous mixture which could adversely affect the specimen. This was particularly evident with longer fixation times and occurred regardless of temperature. This was therefore not considered in future experiments.

Both ruthenium red and Alcian blue would sometimes precipitate in the fixative, leading to poor quality fixation and glycocalyx staining. This was especially true for fixative that had been left for an extended period. In the case of Alcian blue, precipitation seemed to be batch specific, even in products bought from the same manufacturer.

An experiment was devised testing several different batches of Alcian blue that were available in the laboratory, at the working concentration of 0.1% Alcian blue with 75 mM L-lysine. After 24 hours they were visually assessed with a batch from Santa Cruz Biotechnology showing no evidence of precipitation. The same batch of Alcian blue was used in all subsequent experiments to ensure reliability in the fixation technique.

Given the superior glycocalyx preservation in the pilot work, Alcian blue with L-lysine was selected as the cationic probe of choice used in subsequent experiments. A working concentration of 0.1% Alcian blue, with 75 mM L-lysine, in 2.5% glutaraldehyde and 0.1 M cacodylate buffer was used, and always prepared fresh for each placental fixation.

4.2.2 Placental Endothelial Cell Glycocalyx

Immersion chemical fixation of placental tissue was not able to demonstrate the glycocalyx of the placental capillary endothelium. The capillary lumen appeared to contain plasma proteins and cellular debris, which may include shed glycocalyx components Figure 26.

4.3 Does Perfusion Fixation Improve Imaging of the Endothelial Cell Glycocalyx?

Perfusion fixation was able to demonstrate the glycocalyx at the luminal surface of the placental endothelium. It appeared as a continuous, electron dense layer, extending from the phospholipid bilayer into the vessel lumen. Glycocalyx could also be observed at the

tight junctions of two endothelial cells. The mean endothelial cell glycocalyx depth of three placentae from normotensive pregnancies was 55.3 nm (SEM ± 9.1).

Although sampling of the perfused placenta was from areas with the macroscopic appearance of successful perfusion (blue discolouration and change in texture after glutaraldehyde exposure), microscopic examination demonstrated quite a patchy result. Many vessels still contained frequent RBCs, suggesting they had not been flushed through by the fixative. Glycocalyx staining in these vessels was poor. The absence of RBCs in capillaries was used as a surrogate for successful perfusion, and only these vessels were considered for analysis and quantification of the glycocalyx depth.

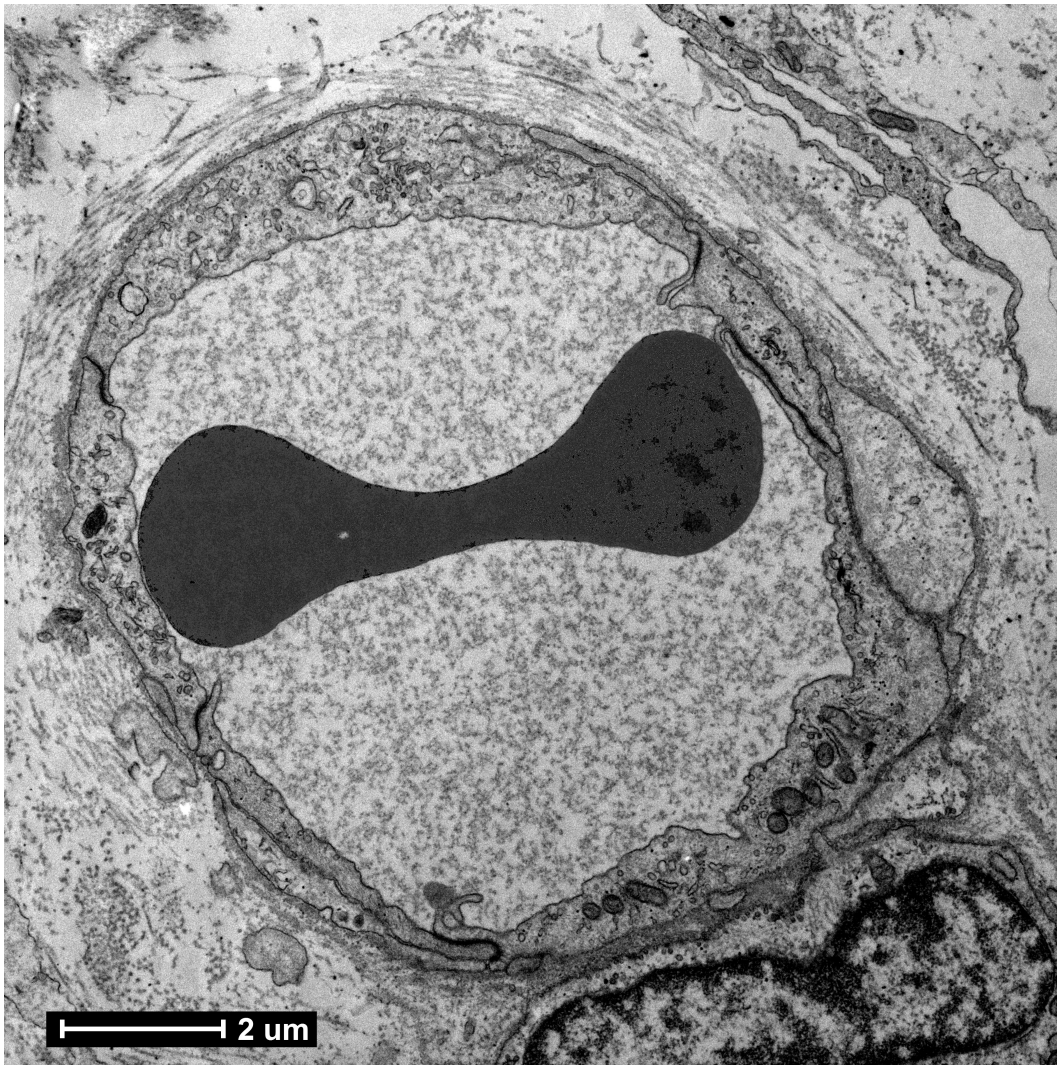

Figure 26 – Placental Capillary by Immersion Fixation
The placental endothelial glycocalyx could not be demonstrated by immersion fixation. The vessel lumen (with a RBC in cross section) contained plasma proteins and loose cellular debris, which may include shed glycocalyx components.

Perfusion of the placental vessels was technically challenging, perhaps hindered by suboptimal equipment and inexperience with the technique. Although the procedure became more refined with practice, it still would have required a significant amount of improvement to be used in a wider study. The procedure took a long time and required a significant amount of preparatory work that could only be completed on the day of the experiment, given the previous findings of precipitation of Alcian blue in fixatives that were not made fresh. Perfusion was resource intensive (and therefore expensive) as up to 500 ml of fixative was required for each experiment.

I was not able to demonstrate the syncytial glycocalyx through perfusion. In other perfusion systems a secondary circulation representing the maternal perfused blood into the intervillous space is created and has been successfully used to model the transfer of therapeutic drugs across the placenta. This was beyond the capability of the equipment available for this experiment, and given the other issues described with the model it was not prudent to spend time attempting to optimise this.

4.4 Can the Glycocalyx be Removed by Enzyme Stripping?

Placental perfusion of hyaluronidase in mammalian Ringer's solution, resulted in complete removal of the endothelial glycocalyx compared to placentae perfused with mammalian Ringer's solution without hyaluronidase; n = 2, Figure 27 (E and F).

The removal of the electron dense luminal layer by an enzyme specific to hyaluronan, supports the assumption that the identity of this layer must be the endothelial glycocalyx. It was, however, noted that hyaluronidase also affected the general tissue quality, with enzyme perfused tissues showing damage to the basement membrane and general ultrastructure (evident when comparing Figure 27 A with E).

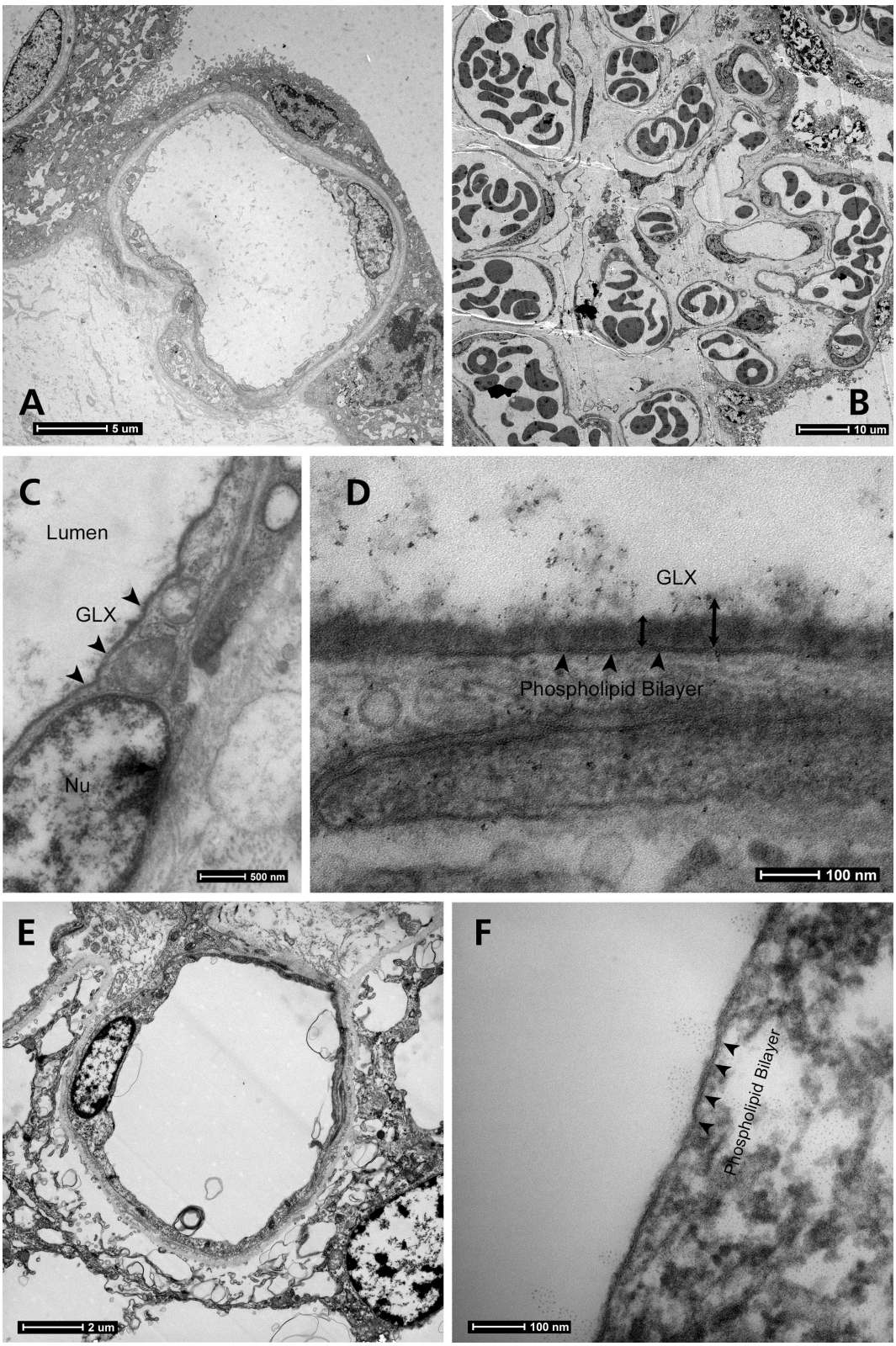

Figure 27 – Placental Perfusion Fixation

Adequate placental perfusion was determined by the absence of blood cells in the capillary (**A**), compared to areas of poor perfusion (**B**). When perfusion was adequate the endothelial glycocalyx was demonstrated at the luminal surface (**C**). At higher magnification the layer could be quantified, present in (**D**) over a tight junction of two endothelial cells, with a mean depth of 55.3 nm (SEM ± 9.1). The endothelial glycocalyx could be stripped by perfusion with hyaluronidase (**F**), but it was noted that the surrounding tissue integrity was also affected (**E**).

4.5 Does High Pressure Rapid Freeze Fixation Improve Imaging of the Placental Glycocalyx?

High-pressure rapid freeze fixation and subsequent freeze substitution with lanthanum and dysprosium did not demonstrate the glycocalyx at either the syncytiotrophoblast or placental capillary endothelium. General tissue fixation with this technique was acceptable and other elements of the placental ultrastructure were evident, suggesting the failure of the technique was specific to either glycocalyx preservation or effective glycocalyx staining Figure 28. The capillary lumen appeared to contain similar cellular debris and plasma proteins as observed in immersion chemical fixed tissue.

In summary immersion fixation demonstrates glycocalyx at the syncytiotrophoblast, perfusion fixation at the capillary endothelium and high pressure rapid freeze fixation did not demonstrate glycocalyx at either surface (figure 29).

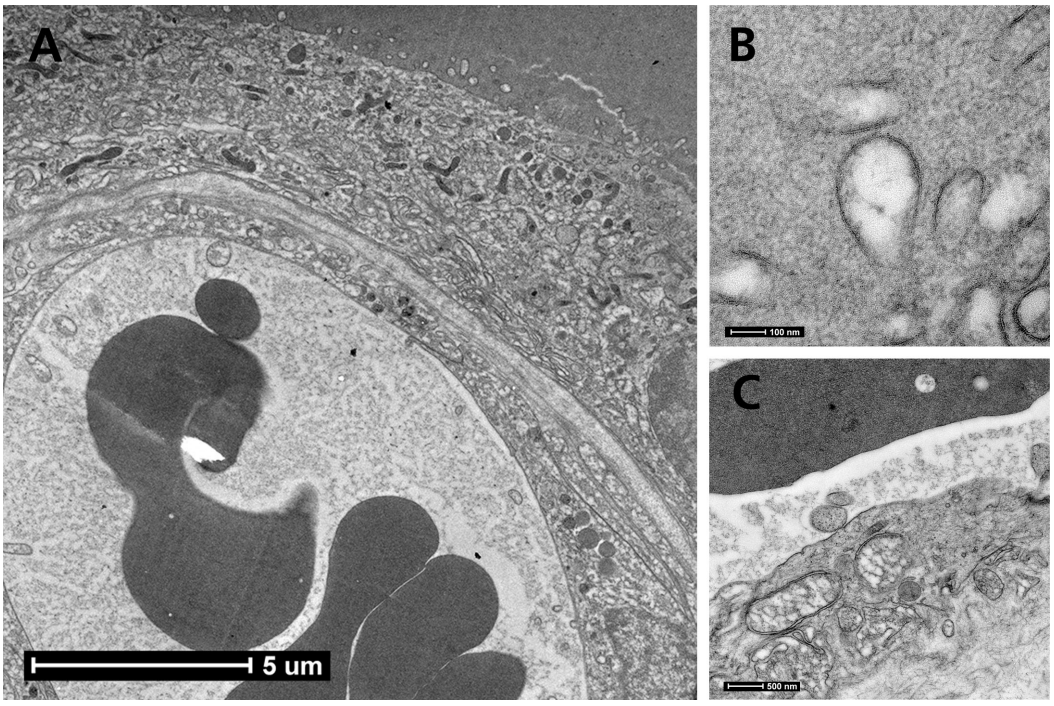

Figure 28 – High Pressure Rapid Freeze Fixation
The glycocalyx could not be demonstrated by high-pressure rapid freeze fixation (**A**), despite good preservation of the ultrastructure at the syncytiotrophoblast (**B**) and capillary endothelium (**C**) with preservation of the phospholipid bilayer at both structures.

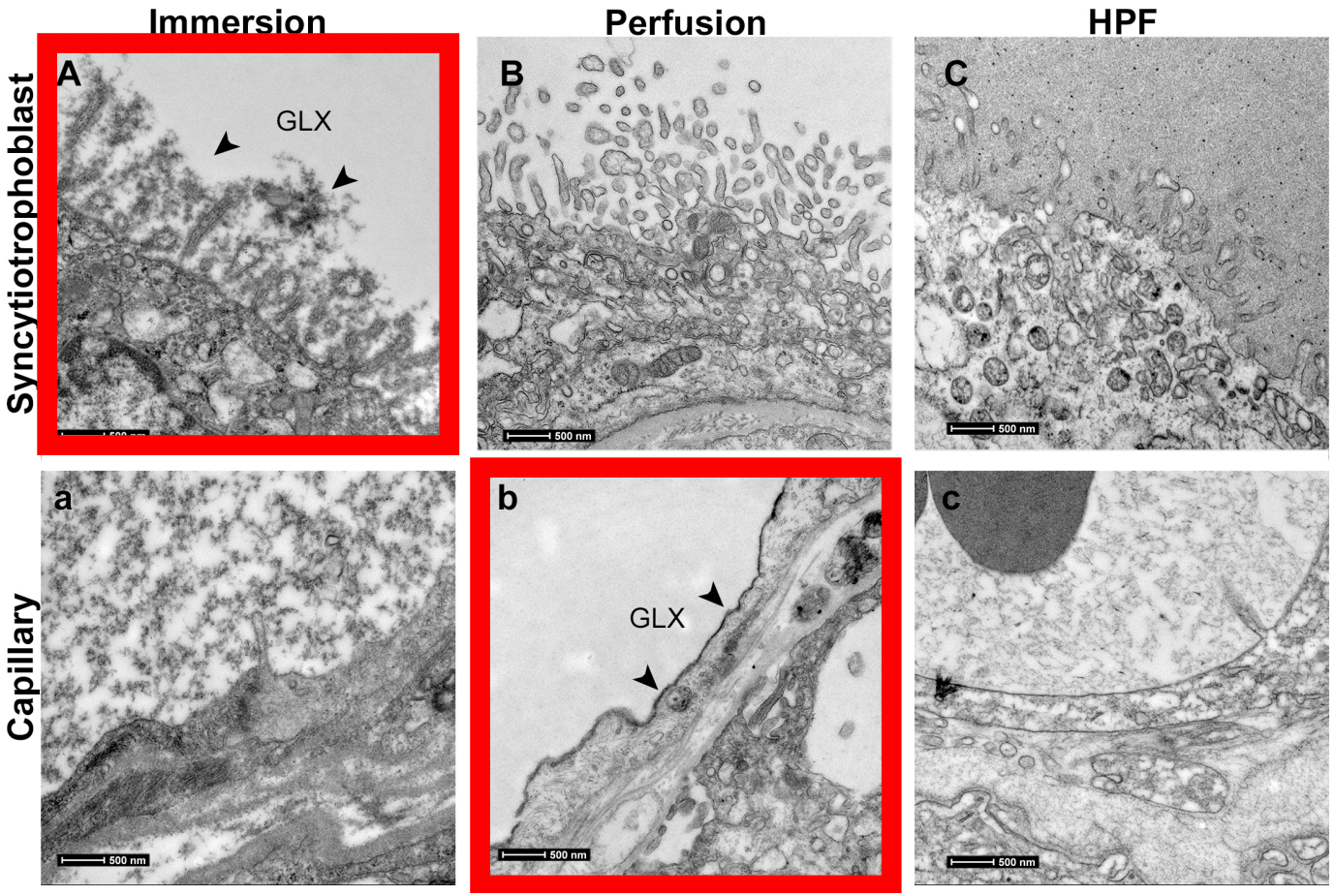

Figure 29 – Comparison of Fixation Methods for Visualising the Placental Glycocalyx
Immersion fixation was able to demonstrate the syncytiotrophoblast (A),but not the capillary glycocalyx (a) Placental perfusion fixation demonstrated the capillary (b) but not the syncytiotrophoblast glycocalyx (B). High pressure rapid freeze fixation did not demonstrate either the syncytiotrophoblast (C) or capillary (c) glycocalyx. HPF = high pressure freeze fixation; GLX = glycocalyx

4.6 How Stable is the Placental Glycocalyx Following Delivery?

In developing a reliable methodology for the large study, it was important to determine the stability of the glycocalyx in the placenta following delivery.

Five placentae delivered by caesarean section from normotensive controls were left at room temperature and sampled at different time points. The experiment was designed in a way that frequent biopsies were taken in the first hour at 0, 10, 20, 30 and 60 minutes as it was predicted that the glycocalyx would rapidly degrade. A further time point at 1440 mins (24 hours) was added to assess if placentae at this time point would be useful. After delivery in our unit, all placentae are routinely stored for this period prior to disposal, so the option of opportunistic recruitment after delivery was an appealing prospect.

The depth of the syncytial glycocalyx appeared stable at 10 minutes but then gradually declined. At 24 hours the difference in glycocalyx depth was statistically significant, 34.5 nm (SEM ± 9.8) vs 13 nm (SEM ± 4.2), adjusted p = 0.02. Glycocalyx coverage followed a similar trend, but this was not significant, p = 0.11, Figure 30.

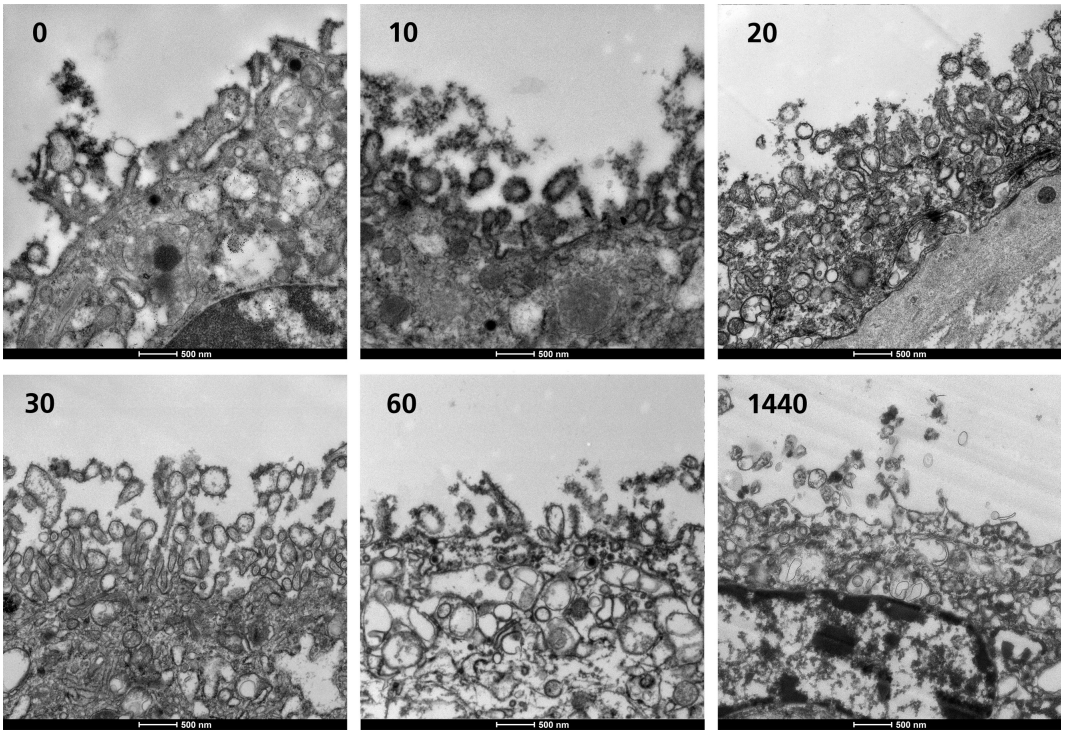

Figure 30 – Loss of the Syncytial Glycocalyx Over Time

When the placenta is left at room temperature, after around 10 minutes there is a progressive loss of both depth and coverage of the syncytiotrophoblast glycocalyx. These representative images provide a visual demonstration of the loss over time. Image numbers refer to the length time in minutes from delivery to sampling / immersion fixation.

On further analysis of the results, one value at the 0 minutes time point was a clear visual and statistical outlier (highlighted in red circle in Figure 31 A and B). This value was inconsistent with glycocalyx staining in other control placentae, and its exclusion from analysis appeared justified.

When this value was excluded from analysis there was a statistically significant reduction in the depth of the glycocalyx was demonstrated at 30 ($p = 0.02$), 60 ($p = 0.03$) and 1440 minutes ($p = <0.001$). Coverage was also significantly reduced but only at 1440 minutes ($p = 0.01$).

From the results of these experiments, it was decided that all placental sampling should occur within 10 minutes of the delivery of the placenta.

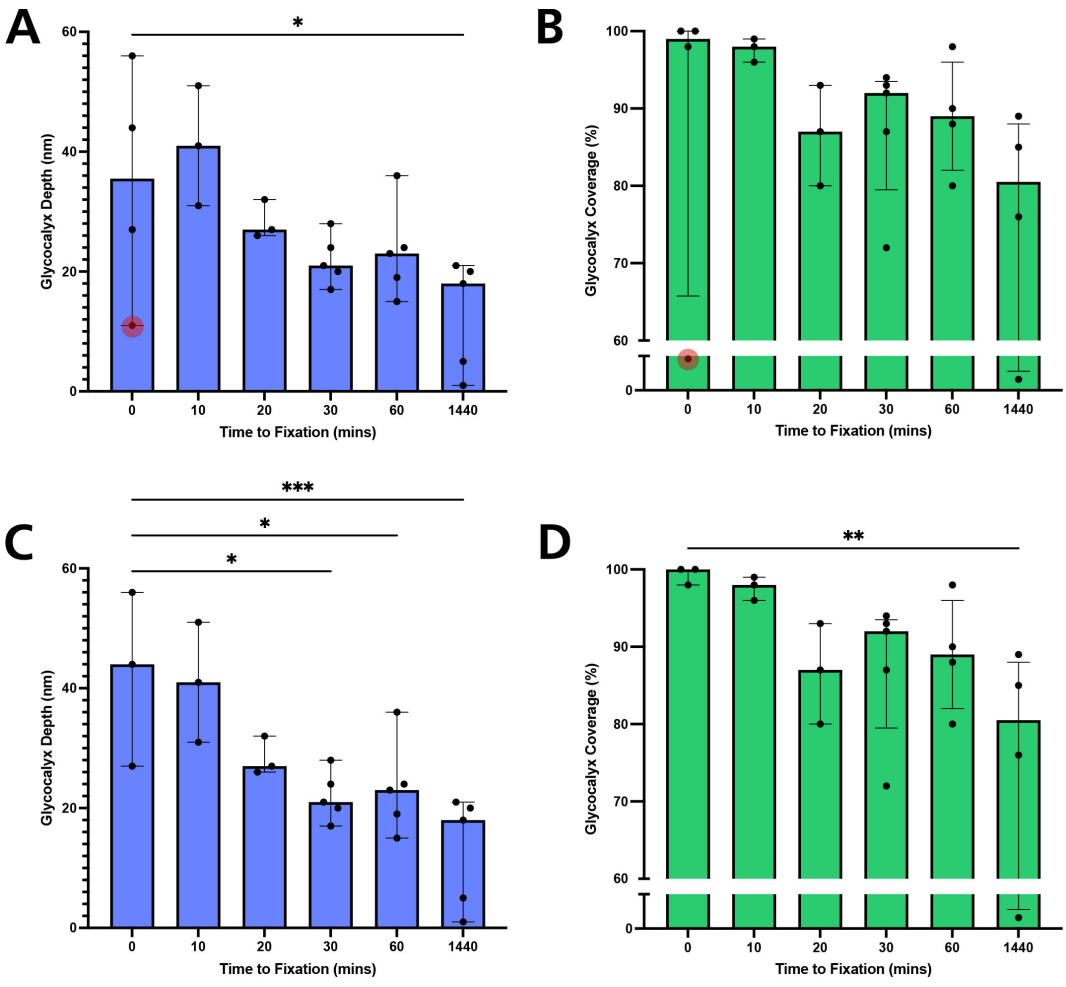

Figure 31 – Graphs Demonstrating Loss of the Syncytial Glycocalyx Over Time
The depth of the syncytiotrophoblast was significantly reduced by 24 hours (**A**). Coverage was not statistically different, but a trend towards a loss of coverage can be seen (**B**). When an outlier was removed (red circles), a significant reduction in depth is observed at 30, 60 and 1440 minutes (**C**). A significant reduction in coverage is observed at 1440 minutes (**D**)

4.7 Patient Characteristics

Twenty-seven participants were enrolled and had immersion chemical fixation of placental tissue, collected in a standardised way in accordance with the study protocol. Following the previously described experiments, sampling occurred within 10 minutes of delivery and fixation was for 24 hours in 2.5% glutaraldehyde in 0.1 M cacodylate buffer with 0.1% Alcian blue and 75 mM L-lysine. These methods are described in detail in section 2.4 and 2.5.

Of the 27 participants, 12 were normotensive controls, and 15 had pre-eclampsia. The pre-eclampsia group were further divided into 4 with early-onset pre-eclampsia and 11 with late-onset pre-eclampsia.

Demographic and outcome data was recorded for all participants. There was no difference in the age, smoking status, and ethnicity between the groups. The booking systolic blood pressure ($p = 0.03$), booking weight ($p = 0.03$) and BMI ($p = 0.01$), however, were significantly increased in the late-onset pre-eclampsia group compared to normotensive controls. These characteristics are all recognised risk factors for the development of pre-eclampsia.

The majority of women with pre-eclampsia were primiparous; 100% in the early-onset group, and 82% in the late-onset group. Conversely most participants in the control group were parous, with only 8% of women in their first pregnancy ($p = <0.001$). This statistic demonstrates a clear sampling bias in the way in which participants were recruited to the control group, with a large proportion recruited from elective caesarean sections lists. The most common indication for elective caesarean, was a previous caesarean, explaining the large number of women in the control group who had previous pregnancies.

This sampling bias is further evident when comparing mode of delivery. No women in the control group had a vaginal birth, whereas 45% of women achieved vaginal birth in the late-onset pre-eclampsia group ($p = 0.02$).

It was not possible to gestation match control and pre-eclampsia placentas, by the requirement of the placenta to be delivered to perform sampling. The majority of normotensive control subjects delivered at term; median gestation 39 week and 3 days

(IQR 38+2-39+4), vs 29 weeks and 1 day (IQR 26+5 - 29+6) in the early-onset group and 38 weeks and 1 day (IQR 35+0 - 39+4) in the late-onset group, p = 0.005.

Systolic, diastolic, and mean arterial blood pressure (MAP) were significantly higher in both the early- and late-onset pre-eclampsia groups compared to normotensive controls, p = <0.001. All pre-eclampsia participants were medicated with at least one anti-hypertensive.

Both pre-eclampsia subgroups had significant proteinuria, quantified by median urinary PCR of 481 mg/mmol (IQR 141-841) and 185 mg/mmol (SD 88-223) in the early- and late-onset groups respectively. Normotensive controls did not routinely have urinary PCR quantified, but all had a negative result for protein on urine dipstick analysis.

There was no difference in the sex of the infant. The median birthweight of the early-onset group was significantly smaller compared to normotensive controls, reflective of the earlier gestation at delivery, p = <0.001. Infants born to mothers with early-onset pre-eclampsia group were also significantly smaller by gestation specific birth centile, highlighting the known association with FGR in the subgroup (p = 0.04).

The participant characteristics are further displayed in Table 7.

	Normotensive (n=12)	Early-Onset PE (n=4)	Late-Onset PE (n=11)	P Value
Booking Demographics				
Age, years, median (IQR)	33 (25-36)	26 (19-34)	33 (24-34)	0.42
Primiparous, n (%)	1 (8)	4 (100)	9 (82)	**<0.001**
Weight, kg	67.8 (± 17.8)	63.5 (± 17.8)	86.5 (± 17)*	**0.03**
BMI, kg/m^2	24.1 (± 5.5)	23.5 (± 7.1)	32.5 (± 8.1)*	**0.01**
Booking Systolic BP, mmHg	107 (± 11)	110 (± 8)	119 (± 8)*	**0.03**
Booking Diastolic BP, mmHg	60 (± 7)	65 (± 5)	68 (± 9)	0.06
Smoker, n (%) yes	1 (8)	0 (0)	0 (0)	0.55
Ethnicity, n (%) White	12 (100)	3 (75)	10 (91)	0.25
On Admission to Labour Ward				
Systolic BP, mmHg	118 (± 11)	152 (± 11)***	146 (± 15)***	**<0.001**
Diastolic BP, mmHg	67 (± 12)	87 (± 11)***	85 (± 11)***	**<0.001**
MAP, mmHg	84 (± 11)	112 (± 7)***	106 (± 12)***	**<0.001**
Urine PCR, mg/mmol, median (IQR)	Not performed	481(141-841)	145 (88-223)	0.21
Hb, g/L	117 (± 10)	118 (± 8)	116 (± 11)	0.89
Antihypertensives, n (%), yes	0 (0)	4 (100)	11 (100)	**<0.001**
Delivery Outcomes				
Gestation, weeks+days, median (IQR)	39+3 (38+2 - 39+4)	29+1 ** (26+5 - 29+6)	38+1 (35+0 - 39+4)	**0.005**
Delivery, n (%) vaginal	0 (0)	0 (0)	5 (45)	**0.02**
Sex, n (%), male	6 (50)	2 (50)	5 (45)	0.91
Birth weight, kg, median (IQR)	3.42 (3.17-3.66)	0.97 (0.54-1.26)**	3.14 (1.94-3.55)	**0.005**
Birth Centile, %, median (IQR)	67.3 (45.3-90.8)	13.4 (1.5-37.2) *	51.7 (16.4-89.2)	**0.04**

Table 7 – Participant Demographics and Outcome Data

Results are displayed as mean (±SD) unless stated. Normally distributed continuous variables were compared by one-way ANOVA, with post hoc Dunnett's comparing individual groups to control. Non-parametric data was assessed by Kruskal-Wallis test, with post hoc Dunn's multiple comparisons. Categorical data was assessed by χ^2 test. BP is blood pressure, IQR is interquartile range, MAP is mean arterial pressure, NA is not applicable, and PE is pre-eclampsia. P values are displayed as * = ≤ 0.05; ** = ≤ 0.01; and *** = ≤ 0.001

4.8 Syncytiotrophoblast Glycocalyx by TEM in Pre-eclamptic and Normotensive Pregnancy

There was no difference in the glycocalyx depth at the syncytiotrophoblast when comparing placentae from women with pre-eclampsia to normotensive controls, mean depth 43 nm (SD ± 20) vs 36 nm (SD ± 28), p = 0.45, Figure 32A. When early- and late-onset pre-eclampsia were considered separately there was a trend towards a reduction in the glycocalyx depth in the early-onset group, mean depth 22 nm (SD ± 11), adjusted p = 0.24, but not in the late-onset group, 41 nm (SD ± 31), adjusted p = 0.97, Figure 32B.

There was a trend towards reduced glycocalyx coverage when women with pre-eclampsia were compared to normotensive controls, but this did not reach statistical significance, p = 0.11, Figure 33A. When early- and late onset groups were compared separately, this trend appeared more pronounced in the early-onset group, but again did not reach statistical significance, adjusted p = 0.15, Figure 33B.

On closer examination of the data there were several data points which visually appeared to be outliers. A statistical test combining robust regression and outlier removal (ROUT method) [264], with Q set at 1% was applied to the data. This identified two statistical outliers in the data, which confirmed the visual outliers and are highlighted in red in Figure 32A and B. The test could only be applied to depth data, as the coverage data did not follow a normal or log normal distribution.

When outliers were removed, there was a significant difference between the mean glycocalyx depths between the normotensive and pre-eclamptic groups (p = 0.02), Figure 32C. When the pre-eclampsia sub-groups were considered, the trend towards a reduction in glycocalyx depth in the early-onset group was clearer, although this did not reach statistical significance, adjusted p = 0.07, Figure 32D.

4.9 Comparing Syncytiotrophoblast Glycocalyx Depth to Other Clinical Markers

Syncytiotrophoblast glycocalyx depth demonstrated a moderate negative correlation with the systolic blood pressure on admission to labour ward, r = -0.43, p = 0.04, and MAP, r = -0.43, p = 0.03. This would be consistent with placental glycocalyx shedding in pre-eclampsia, as the participants with pre-eclampsia had a significantly higher blood pressure compared to normotensive controls, Figure 34.

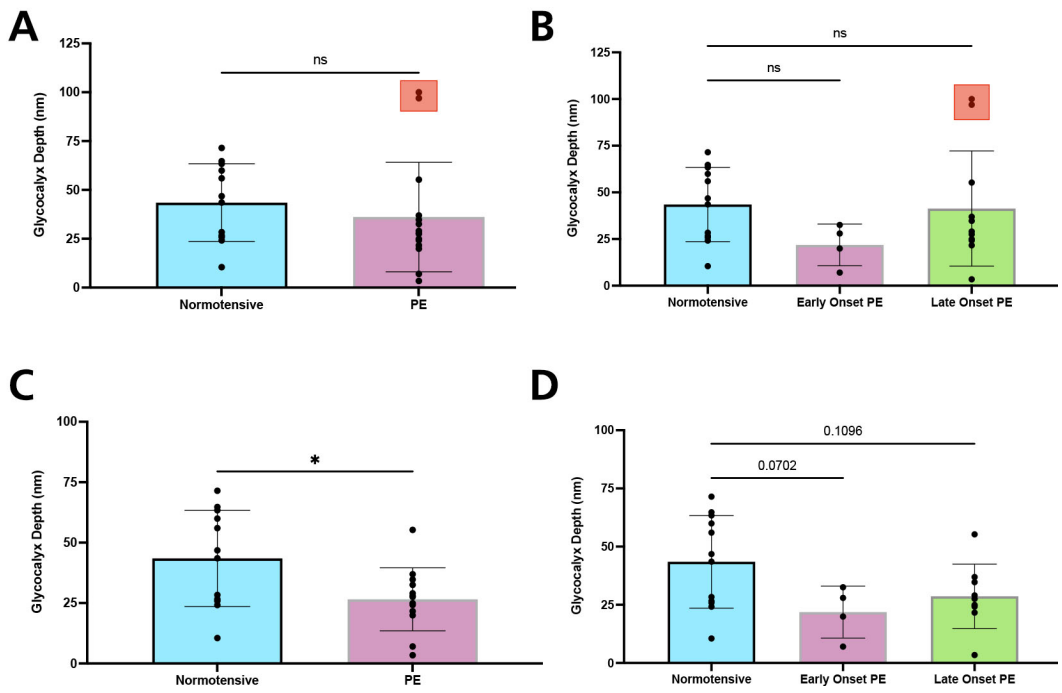

Figure 32 – Glycocalyx Depth in Pre-eclamptic and Normotensive Placenta
There was no difference in the glycocalyx depth at the syncytiotrophoblast in placentae from women with pre-eclampsia compared to normotensive controls (**A**). When early- and late-onset pre-eclampsia were considered, there was a trend towards a reduction in glycocalyx depth in early-onset pre-eclampsia but not in late-onset disease, but this was not statistically significant (**B**). Two results were visual and statistical outliers, highlighted in red in **A** and **B**. When these values were excluded, there a significant reduction in depth was observed in the pre-eclamptic group, compared to normotensive control, p 0.02 (**C**). The trend towards a reduction in the early-onset group was also more pronounced but did not reach statistical significance, p = 0.07 (**D**).

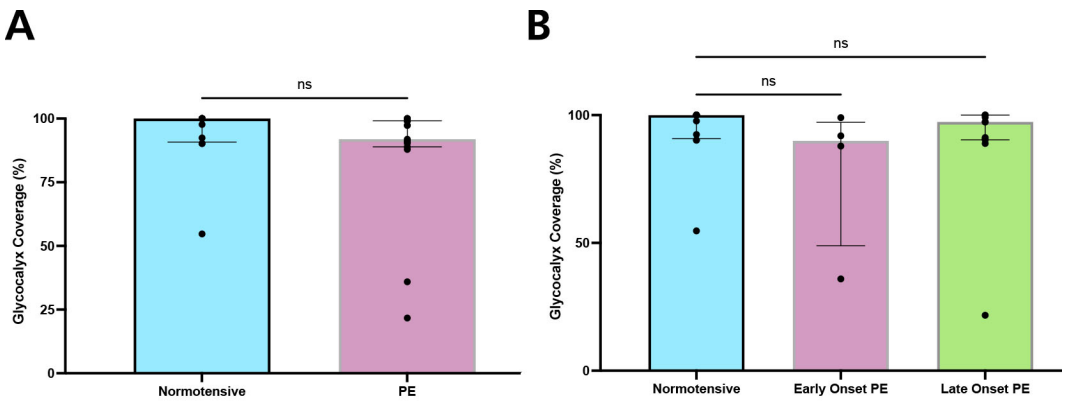

Figure 33 – Glycocalyx Coverage in Pre-eclamptic and Normotensive Placenta
There was a trend towards reduced glycocalyx coverage at the syncytiotrophoblast in pre-eclampsia compared to normotensive pregnancy, but this was not significant, p = 0.11 (**A**), which appeared more pronounced in the early-onset group, but still did not reach statistical significance, p = 0.15 (**B**).

When glycocalyx depth was compared to systolic blood pressure in just the pre-eclamptic group, there was no correlation present, r = 0.00, p = >0.999. This would add further evidence that the association between blood pressure and glycocalyx depth is due to the presence or absence of pre-eclampsia and not a direct relationship between placental glycocalyx shedding and blood pressure. This can be seen visually in Figure 34, with the two separate clusters of PE and normotensive patients driving the association.

Fourteen women who had placental sampling for TEM, also had a GlycoCheck™ measurements. There was no significant correlation between syncytiotrophoblast depth and PBR in the 5-25 µm vessels.

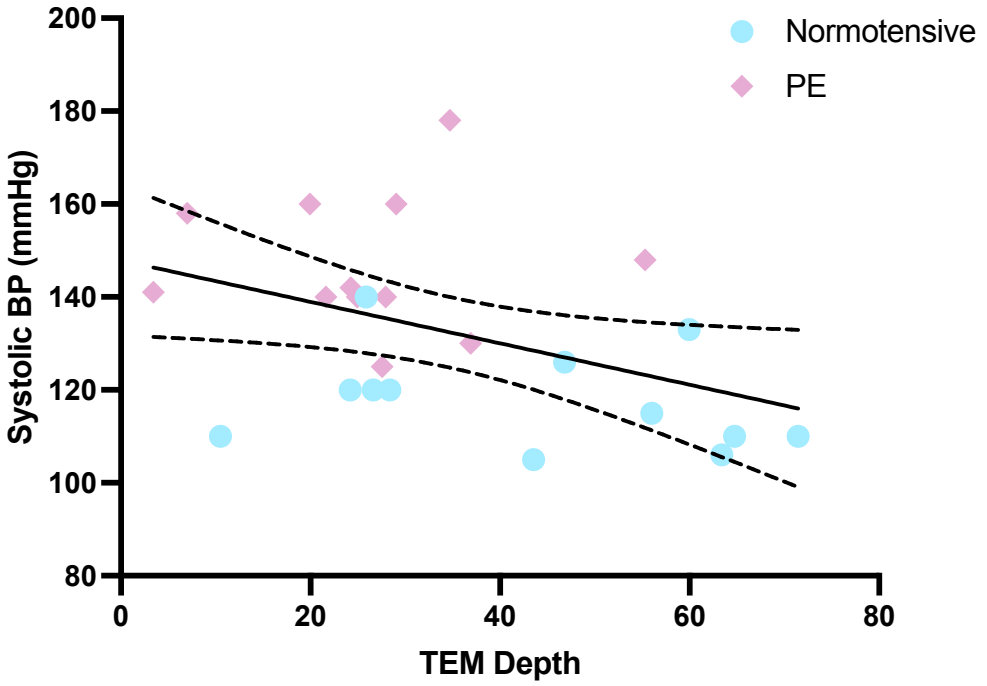

Figure 34 – Syncytiotrophoblast Glycocalyx Depth vs Systolic Blood Pressure
There was a moderate association between systolic blood pressure on admission to the labour ward and the placental glycocalyx depth at the syncytiotrophoblast, r = 0.43, p 0.04. On closer inspection you can see this relationship is caused by the relatively higher blood pressure in the pre-eclampsia group (pink diamonds), vs the lower blood pressure of the normotensive controls (blue circles). This would suggest the observed association is due to the presence and absence of pre-eclampsia rather than a direct relationship between systolic blood pressure and glycocalyx shedding. When the pre-eclamptic and control groups are considered individually, there is no association between blood pressure and glycocalyx depth.

4.10 Does Labour and Mode of Delivery Affect the Measurement of Glycocalyx Depth?

As previously described, there was a recruitment bias towards women in the normotensive control group delivering by caesarean section, compared to women with pre-eclampsia, where a significant number of women delivered vaginally; 0% vs 33% respectively.

It was postulated that vaginal delivery of the placenta may be detrimental to the glycocalyx due to an increased length of the 3rd stage or labour and the physiological process of delivering the placenta.

All placentae from both vaginal and caesarean births were delivered and biopsied within 10 minutes of the birth of the infant. In the pre-eclampsia group, 33% (n=5) of participants achieved a vaginal birth. There was no difference in the glycocalyx depth, compared to pre-eclamptic women who had a caesarean birth, p = 0.55, Figure35A.

When comparing participants with pre-eclampsia who had laboured (vaginal birth and intrapartum emergency caesarean birth) compared to those who had not laboured (pre-labour caesarean birth), there was a trend towards a reduction in the depth of the glycocalyx in the pre-labour group, p = 0.06, Figure35B. This result is heavily influenced by one participant that may represent an influencing observation.

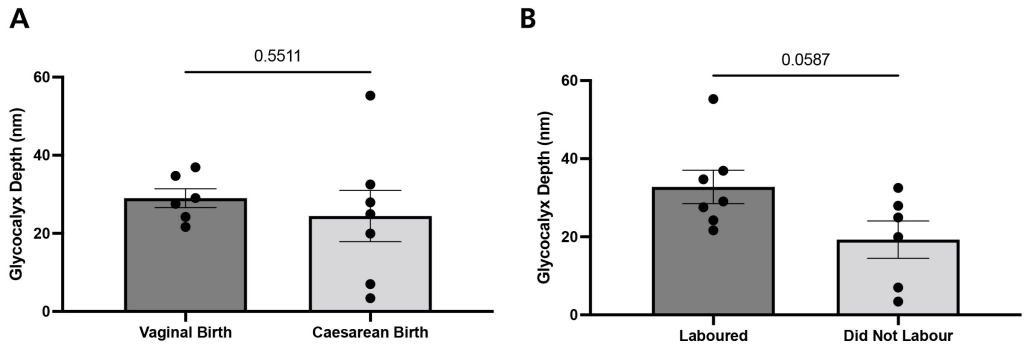

Figure 35 – The Effect of Mode of Delivery and Labour on the Placental Glycocalyx
In the pre-eclampsia group 33% of women delivered vaginally. Mode of delivery had no effect on the depth by the syncytiotrophoblast glycocalyx, p = 0.55, (**A**). There was a trend towards a reduction in glycocalyx depth in the group who did not labour, contrary to the hypothesis that labour may be detrimental to the glycocalyx (**B**). This, however, was not significant, p = 0.06, and was largely influenced by one result that may represent an outlier.

4.11 Discussion

4.11.1 Comparing Methodologies

In comparing different cationic probes, Alcian Blue provided the most reliable fixation of the glycocalyx with the greatest depth, there were however, significant limitations. All the probes performed better when made fresh and all were liable to precipitate, particularly in preparations that were left for more than 24 hours.

This had important implications in designing the methodology for the larger study, as fresh fixative had to be prepared for each placental sampling. This limited the ability to delegate the role of placental collection and ultimately affected the number of patients I was able to recruit for the study.

In comparing fixation techniques, immersion fixation reliably demonstrated the glycocalyx of the syncytiotrophoblast, but not the capillary endothelium. This has been previously shown by Martin et al. [198]. Immersion fixation of other tissue specimens has generally not been successful [214], so this finding is likely because of the unique anatomy of the placenta. When fixing placental tissue by immersion, the fixative will immediately access the intervillous space, this allows for direct access to the syncytiotrophoblast glycocalyx located at the brush border. In comparison, the placental capillary endothelial glycocalyx, like other tissues, is separated by several microns of tissue accounting for a longer diffusion and fixation time. Plasma present in the vessels may also impede access of the cation to the glycocalyx surface [265].

Placental perfusion was able to demonstrate the capillary endothelial glycocalyx. This has previously been shown by Leach et al. [193]. Generally, delivery of fixative by perfusion is far more recognised as a technique for visualisation of the glycocalyx and is frequently used in animal models. It has the benefit of flushing and removing plasma proteins and erythrocytes and allowing direct access to the endothelial surface for rapid fixation [153, 214]. The hyaluronidase stripping experiment provided useful data in confirming the identity of the electron dense layer as the glycocalyx.

In this study only a small number of perfusions were attempted as it was clear this was not going to be a useful methodology for the wider study. The procedure was intensive in preparation, labour, and materials. Equally, many of the placentae from women with pre-

eclampsia would be required to be sent for routine histological examination and thus not available for perfusion. Refinement of the procedure may have allowed dual visualisation of the endothelial and syncytiotrophoblast glycocalyx simultaneously but was not prioritised.

It is regretful that the high-pressure rapid freeze fixation methodology was not successful. Others have previously demonstrated the technique to be far superior in other tissue and cell types, demonstrating glycocalyx depths and structures many times greater than those observed with similar chemically fixed tissues [215]. The expense, specialist equipment and expertise required meant that it was not viable to pursue this technique. Further attempts with variation in the cation and freeze-substitution settings would have been a suitable next step had resources allowed.

4.11.2 Stability of the Glycocalyx

The time trial experiment has provided evidence to suggest the instability of the syncytiotrophoblast glycocalyx *ex-vivo*. In this work I demonstrated a significant reduction in the depth of the glycocalyx after 30 minutes from delivery of the placenta, but a trend towards reduction after 10 minutes. Although the glycocalyx is often reported as unstable *ex vivo*, this is the first time I am aware that this has been demonstrated over time.

This was incredibly important finding for the wider study design and all subsequent placental collections were within 10 minutes of delivery.

4.11.3 The Syncytiotrophoblast Glycocalyx in Pre-eclampsia

This study was not able to demonstrate a significant difference in the glycocalyx depth at the syncytiotrophoblast between normotensive and pre-eclamptic placentae. When potential outliers were removed, a trend towards a reduction in the early-onset group, which almost reached significance was present, replicating the pattern observed in the GlycoCheck™ study.

Caution is obviously needed in trying to make interpretations from such small data sets, similarly the removal of outliers may not be justified for similar reasons. Interestingly although the same pattern towards a reduction of glycocalyx depth was observed in the GlycoCheck™ study, the two groups did not correlate.

This study was severely limited by the small numbers enrolled, n = 4, in the early-onset group. A post hoc power calculation suggests 11 in each group would be sufficient to detect a difference of 0.58 µm.

The recorded depth of the glycocalyx in this work was comparable to other studies who have used TEM to quantify the glycocalyx but is likely not reflective of the true depth of the glycocalyx in normal physiology [151, 215, 266]. *In vivo* the glycocalyx forms a hydrated mesh, which other imaging modalities (confocal and SDF) would suggest is several microns thick [267]. The harsh dehydration and processing required for imaging with TEM is clearly detrimental to this fragile structure, and either removes or compresses key components. Making assessments of depth in this scenario may not be robust.

EM tissue processing and imaging is an incredibly time consuming, costly, and labour-intensive process. Its use in a large population study is very unlikely to be financially viable.

4.12 Conclusions

The placenta has a significant glycocalyx present at the syncytiotrophoblast and capillary endothelium, which can be demonstrated using TEM.

Immersion fixation in the presence of a cation (Alcian Blue) demonstrated the syncytial but not the endothelial glycocalyx. Placental perfusion was able to demonstrate the endothelial glycocalyx, but the expense and time required to achieve this restricted its use in a wider study.

In small cohort of women with pre-eclampsia, a trend towards glycocalyx loss in early-onset disease was observed but was not statistically significant. A larger study population is required to determine if syncytial glycocalyx shedding is a feature of pre-eclampsia.

5. Imaging the Placental Glycocalyx – Lectin Histochemistry

5.1 Introduction

Lectin histochemistry has been used as a light microscopy alternative to TEM in the study of the glycocalyx. Lectins are plant derived glycan binding proteins that have a high affinity to specific carbohydrate residues, including those of the glycocalyx.

The technique has several potential benefits compared to TEM, primarily in the fact that is much less cost and labour intensive, and large volumes of samples can be processed simultaneously. Tissue can be fixed and processed more conventionally and without many of the solvents and dangerous reagents required for TEM tissue processing.

In this chapter I will demonstrate the binding affinity of lectins to different parts of the placental glycocalyx and test a novel adaptation of a technique to quantify the placental glycocalyx at the syncytiotrophoblast and capillary endothelium. I will apply this technique to a cohort of patients with pre-eclampsia and normotensive controls to determine differences in the glycocalyx depth. The methodology will also be applied to an independent cohort of samples to further validate the technique.

5.2 Can the Placental Glycocalyx Be Imaged With Lectin Histochemistry?

Placental tissue from a normotensive control participant, delivered by elective caesarean section was sampled within 10 minutes of delivery, fixed with 4% PFA and processed as per the methodology described in section 2.5.4.

Sequential sections were cut from the same processed wax block as described in section 1.8, and a panel of 6 different lectins were used to determine the staining pattern, and specificity for the glycocalyx at both the syncytiotrophoblast and endothelial cell.

5.2.1 Syncytiotrophoblast Glycocalyx

Wheat germ agglutinin (WGA), *Lycopersicon esculentum* (LEL), and Concanavalin A (ConA) all demonstrated staining at the microvillus brush border of the syncytiotrophoblast, in the region of the glycocalyx, Figure 36.

WGA and LEL, both which have binding affinity for GlcNAc (one of the subunits that make HA and an integral part of many glycoproteins [268]), demonstrated similar staining patterns. Neither were specific for the brush border. WGA demonstrated staining of the syncytial basement membrane, cytotrophoblasts, stroma, endothelial cell, and RBCs but with much less intensity. LEL had a stronger granular staining of the syncytiotrophoblast, which made differentiation of the brush border and the cell more difficult. It had limited staining at the of the stroma, and none at the endothelial cell.

ConA binds to mannose residues, which are an important part of the *N*-glycan chains associated with many glycoproteins. In addition to staining at the brush border, there was significant stromal and endothelial cell staining, Figure 36.

When each lectin was compared to general membrane staining with R18, WGA visually appeared to demonstrate the 'thickest' glycocalyx, evidenced by the more intense lectin staining outside of the R18 staining in the intervillous space. When the glycocalyx was quantified using the peak-to-peak method described in section 2.12, it was LEL that demonstrated the thickest glycocalyx with a mean peak-to-peak measurement of 406 nm (SD ±106), compared to WGA 251 nm (SD ±88), and ConA -77 nm (SD ± 140). As previously described, LEL also demonstrated significant intracellular staining of the syncytiotrophoblast, and there was concern this could have affected the peak-to-peak measurement.

On balance, it was decided that WGA demonstrated the most reliable and specific binding of the brush border glycocalyx, and this was used for the larger comparative study.

5.2.2 Endothelial Cell Glycocalyx

Ulex europaeus I (UEA I) binds with alpha-1-fucose (αFuc), another component part of the *O*-glycosylation of many glycoproteins [268, 269]. It was highly specific for the luminal surface of the endothelial cell and did not stain other placental tissue, Figure 36. UEA-I

does, however, demonstrate blood type specific staining for H type 2 antigen, which is specific for blood group O [270].

Three-dimensional rendering of a z-stacked section clearly demonstrates that this is most likely glycocalyx staining, as the lectin is shown to be luminal to the R18 membrane stain, Figure 37.

Maackia amurensis II (MAL II) is specific for α2-3 linked sialic acids. Sialic acids often cap *N*-glycans and *O*-glycans of many glycoproteins and are common in the glyococalyx. MAL II demonstrated staining at the endothelial surface, but also to a lesser degree the stroma and trophoblast basement membrane, Figure 36. MAL II also binds RBCs, but in a non-type specific way [271].

As previously described WGA also demonstrated some staining at the endothelial cell, but this was comparatively less compared to both UEA-I and MAL-II.

The glycocalyx at the endothelial cell was quantified using the peak-to-peak method. With MAL-II the mean peak-to-peak value was 193 nm (SD ±92), compared to UEA I, 327nm (SD ±130). Due to the greater depth measurement and the specificity to the endothelial cell, UEA I was selected for estimation of the glycocalyx depth in the larger studies.

5.2.3 Differences in the Syncytial and Endothelial Glycocalyx

Differences in the staining pattern and affinity for certain lectins at both the syncytial and endothelial glycocalyx provide clear evidence that the glycosylation and composition of the glycocalyx is different at each surface. This may suggest differences in their relative function.

The binding of WGA and LEL to the syncytial brush border suggests strong expression of GlcNAc, within the glycocalyx at this location. By comparison, there was much less expression of GlcNAc at the endothelium, instead favouring expression of sialic acids. The relative expression and glycosylation of the placenta glycocalyx will be considered in greater detail later.

5.3 Correlative Microscopy to Demonstrate Lectin Staining of the Glycocalyx

Peak-to-peak analysis and quantification is an indirect measure of the depth of the glycocalyx. It uses the relative peak separation of a lectin and membrane stain to represent the depth. The true depth of the glycocalyx is very difficult to resolve with light microscopy, as the size of the glycocalyx is at the limit of the maximum resolution of light microscopy.

As previously described, lectin staining was not specific to the brush border and the endothelial glycocalyx, with intracellular staining of syncytiotrophoblasts, basement membrane, cytotrophoblasts and stoma depending on the lectin. The visual appearance of lectin present outside of the R18 staining in the intervillous space at the syncytiotrophoblast, and luminal to the R18 staining at the endothelium, was strong evidence to support staining of the glycocalyx but could not be considered conclusive.

A correlative electron and light microscopy technique was used by using Quantum Dot labelled lectins, which are photoluminescent and allow imaging by confocal microscopy and electrodense to allow for subsequent TEM of the same tissue.

Tissue was prepared and imaged in accordance with the methods described in section 2.13. Confocal microscopy demonstrated the familiar staining pattern of both WGA and UEA-1 as described in the previous section. DAPI was not used on these section as it shares a similar excitation as QDs.

Tissue was subsequently processed for TEM. The quality of the tissue was seriously degraded by the necessary processing steps required for the initial fixation and subsequent processing for TEM, as can be seen in the low powered images. Despite the tissue degradation, WGA-QDs can be clearly seen at the intervillous space of the brush border and UEA I-QDs could be identified at the luminal surface of endothelial cells, confirming glycocalyx staining, Figure 38.

As suspected, lectin staining was not specific for the glycocalyx, as lectin-QDs can also be seen present in other placental structures. The glycocalyx itself is not evident on the TEM images, as the tissues were not fixed with a cation.

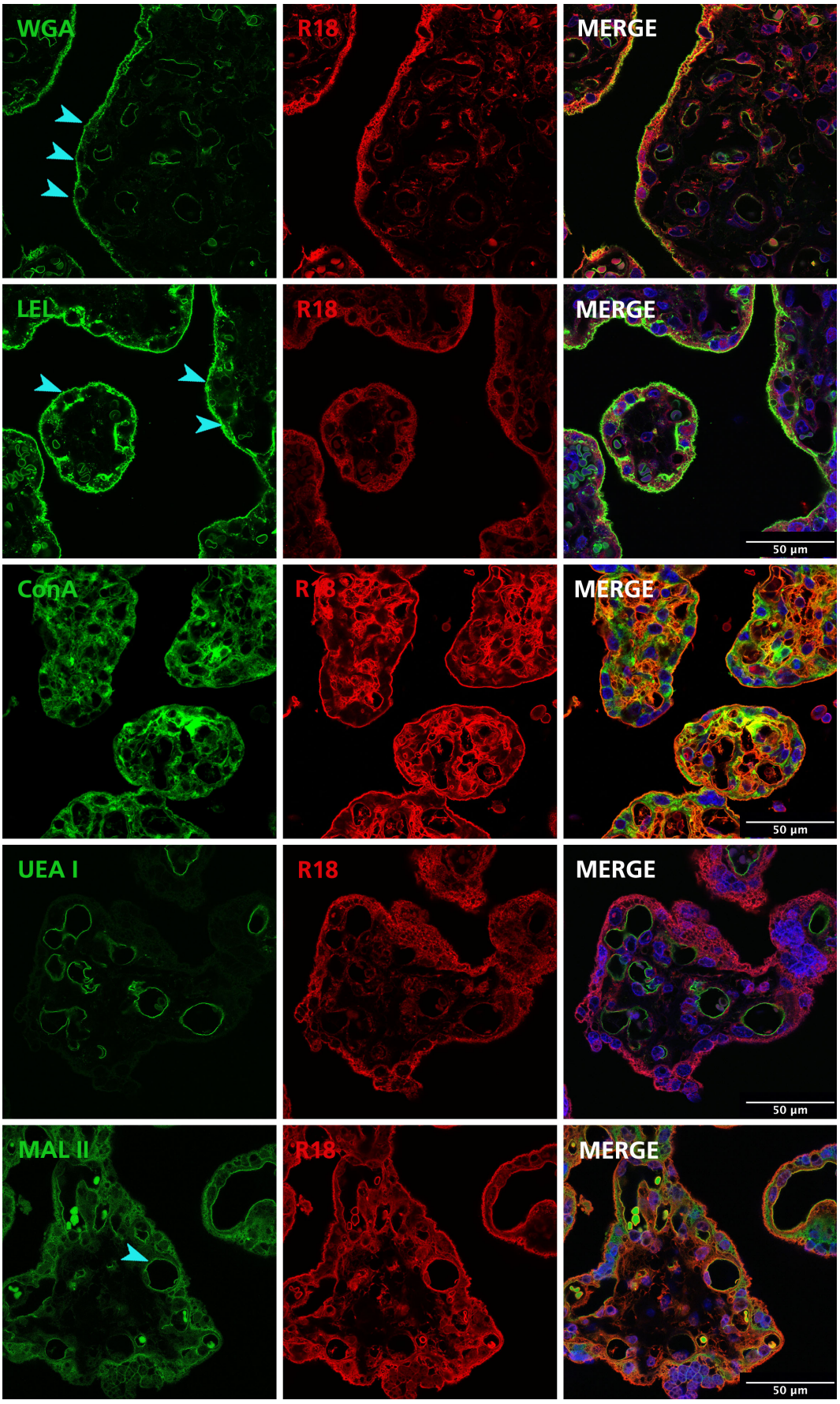
WGA
R18
MERGE
LEL
R18
MERGE
50 µm
ConA
R18
MERGE
50 µm
UEA I
R18
MERGE
50 µm
MAL II
R18
MERGE
50 µm

Figure 36 – Lectin Panel in a Term Normotensive Placenta (PREVIOUS PAGE)
WGA and LEL both demonstrated strong staining at the syncytiotrophoblast brush border (arrows), with evidence of staining into the intervillous space, outside of the R18 red membrane stain. LEL demonstrated granular staining of the syncytiotrophoblast cytoplasm, which was thought more likely to interfere when trying to quantify the brush border glycocalyx. ConA stained the brush border glycocalyx but demonstrated significant staining at several placental structures. UEA I was highly specific for the endothelial surface, with evidence of luminal staining by green lectin evident luminal to the red R18 membrane stain. MAL-II also demonstrated endothelial staining (arrow), but also the stroma and basement membrane to a lesser degree.

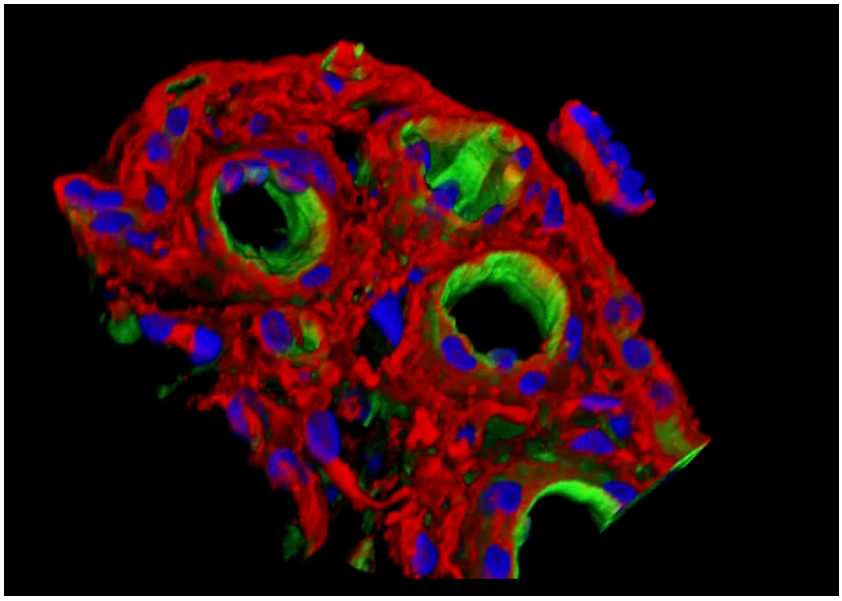

Figure 37 – Three-Dimensional Model of the Placental Endothelial Glycocalyx
Lectin histochemistry demonstrating the luminal staining of UEA I. An z-stack was created by sequential imaging at 0.2 µm intervals. 3D rendering created with Leica Application Suite X (Leica Microsystems, Wetzlar, Germany). The presence of UEA I luminally to the R18 staining, strongly suggests glycocalyx rather than intracellular staining.

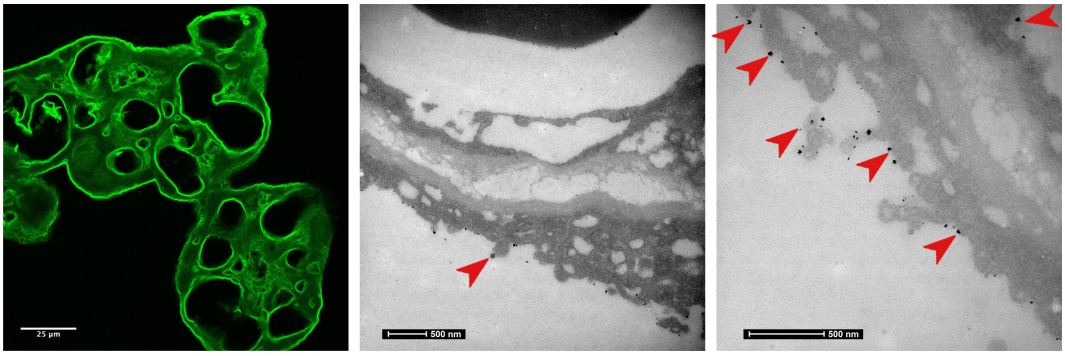

Figure 38 – Correlative Confocal and TEM with Q-Dot WGA
Placental tissue from a normotensive control participant is fixed in PFA. Glycocalyx is stained with WGA- Q-dot and imaged with confocal microscopy. WGA is intensely stained at the brush border and to a lesser degree the endothelium. Tissue was subsequently processed for TEM. Q-dots could be clearly seen at the surface of the brush border and the luminal surface of the endothelium (arrows), confirming the location of the WGA staining at the ultrastructural level.

5.4 Is Lectin Histochemistry Reproducible?

It was noted that there was a large degree of variation in the absolute peak-to-peak values obtained from lectin staining performed at different times. This was despite using the same reagents, to the same protocol and imaging with the same microscope using saved settings.

WGA staining of the syncytiotrophoblast was compared across experiments completed on 4 different days. Lectin staining followed the protocol as described in section 2.8. For experiment on day A and D a biotinylated WGA lectin was used, for experiments B and C a fluorescein pre-conjugated WGA lectin was used (Vector Laboratories, Burlingame, USA, Fl-1021-10). Some experiments contained duplicates (i.e., slides which had previously been stained on other days) to assess reproducibility. Each individual experiment contained control and pre-eclampsia specimens.

There was a large difference in the mean peak-to-peak value of the combined specimens processed on each day; A = 134 nm (SD ±52), B = 27 nm (SD ±41), C = -136 nm (SD ±59), D = 313 nm (SD ±57). It was noticeable that the pre-conjugated lectin produced significantly smaller (or negative) peak-to-peak values, Figure 39.

On the surface this is a worrying observation, suggesting that experiments performed at different times are not comparable. On closer inspection, however, although the means are very different, the spread around the mean is very similar in each experiment; the standard deviation ranges between 41 – 59 nm in the 4 trials.

This perhaps suggests that the observed difference in the means is more likely to due to an experimental variation, either at the staining or imaging stage, rather than true heterogeneity between specimens.

One method of correcting for this would be to normalise the data from each experiment. For this to be successful, a large enough sample, that is representative of the true distribution of the population sample would be needed. To avoid confusion, for the main comparison all samples were processed within one batch and imaged on the same occasion. The biotinylated rather than pre-conjugated WGA lectin was selected.

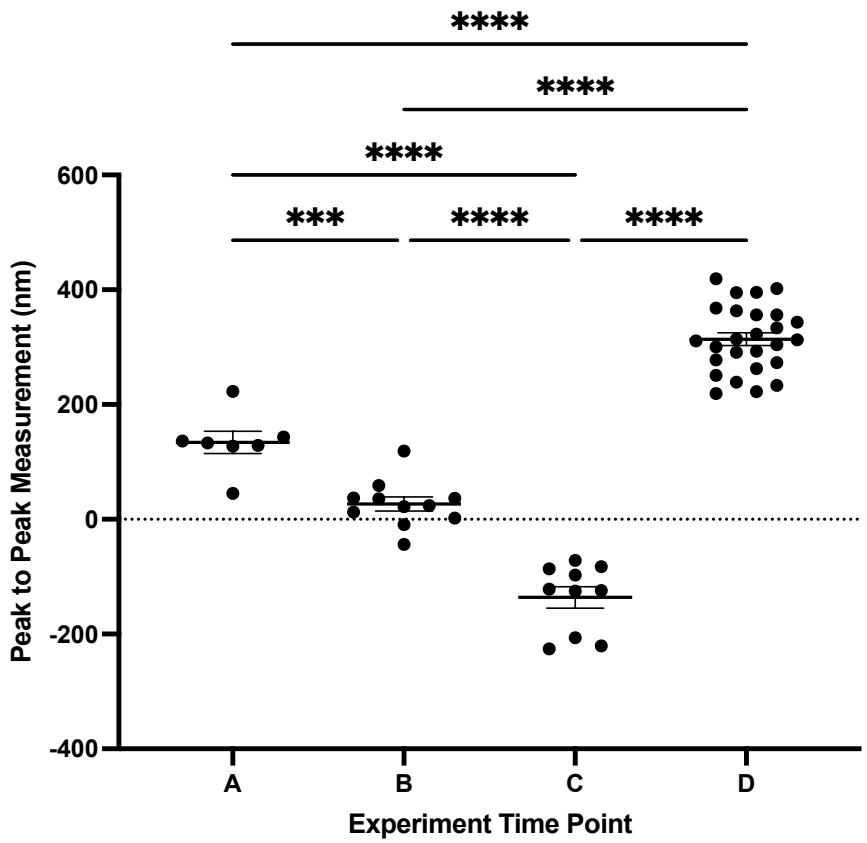

Figure 39 – Syncytiotrophoblast Lectin Staining by Day
Syncytiotrophoblast glycocalyx staining with WGA was performed on 4 different occasions, A-D. On each occasion there was some duplicate specimens from previous trials. Experiment A and D used biotinylated WGA, whereas B and C used a WGA pre-conjugated to FITC. The combined mean for each trial was significantly different, however the spread around the mean (SD) was very similar. This may suggest an experimental error that could be corrected for, rather than true heterogeneity between samples.

5.5 Reliability of Automated Glycocalyx Quantification

Development of an automated process to quantify the peak-to-peak measurement of the placental glycocalyx was very important to make the process fast and reliable. Taking manual measurements of the peak-to-peak value is a time consuming and cumbersome process and potentially biased.

In manual measurements the user selects areas of the vessel to sample. Although sampling points were chosen with only the R18 channel visible, the user would often manipulate the transection of the line to ensure a 'clean' peak. The process was also limited to a relatively small number of measurements (10 was typical) and therefore not necessarily representative of the glycocalyx as a whole.

The process was automated with the creation of two macros, one for each of the capillary endothelium and syncytiotrophoblast glycocalyx. The design and function of the macros has been described in detail in section 2.12. An excel spreadsheet embedded with a further macro would 'clean' the data by the application of a Gaussian correction and a further correction depending on the signal amplitude. This process was able to produce a large volume of data very quickly, with the glycocalyx measurement typically being made from over 50 peak-to-peak measurements per image or vessel.

A comparison between manual and automated measurements was compared in five placentae to assess reproducibility at both the syncytiotrophoblast and endothelial glycocalyx. In all five placenta there was no statistical difference between the mean glycocalyx depth measurement recorded by manual measurement compared to automated measurement. The standard deviation and standard error of the mean, however, was smaller when using the automated approach, giving greater confidence in the value. A two-way mixed model ICC with average measures, demonstrated an excellent intraclass correlation coefficient of 0.83 (95% CI 0.60-.93).

With the capillary macro there is still a degree of user input required, in the selection of vessels and the placement of the cursor in the vessel centre. An inter-rater reliability assessment between two operators, demonstrated excellent reliability, ICC 0.95 (95% CI 0.80-0.99).

These findings were supportive that the macro analysis of the placental glycocalyx was reliable, reproducible, and even advantageous in producing a mean value with a smaller SD and SEM. The automated macro was used for all subsequent glycocalyx peak-to-peak measurements.

5.6 Patient Characteristics

Twenty-six participants were enrolled and had placental tissue processed for light microscopy in accordance with the study protocol. Twelve participants were normotensive controls, and 17 had pre-eclampsia. The pre-eclampsia group were further divided into five with early-onset pre-eclampsia and 12 with late-onset pre-eclampsia. Most of the participants in this study were also included in the TEM experiments and therefore the patient characteristics between are almost identical to those previously described in section 4.6, and are updated in Table 8.

	Normotensive (n=9)	Early-Onset PE (n=5)	Late-Onset PE (n=12)	P Value
Booking Demographics				
Age, years, median (IQR)	33 (25-36)	26 (21-32)	32 (24-34)	0.36
Primiparous, n (%)	1 (11)	4 (80)	10 (83)	**0.002**
Weight, kg	63.9 (± 12.6)	63.4 (± 15.4)	84.7 (± 17)*	**0.08**
BMI, kg/m^2	22.9 (± 3.8)	24.0 (± 6.2)	31.8 (± 8.2)*	**0.01**
Booking Systolic BP, mmHg	107 (± 11)	110 (± 7)	119 (± 8)*	**0.02**
Booking Diastolic BP, mmHg	60 (± 8)	67 (± 6)	68 (± 8)	0.09
Smoker, n (%) yes	0 (0)	0 (0)	0 (0)	NA
Ethnicity, n (%) White	9 (100)	4 (80)	11 (92)	0.40
On Admission to Labour Ward				
Systolic BP, mmHg	116 (± 10)	145 (± 18)**	144 (± 15)***	**<0.001**
Diastolic BP, mmHg	67 (± 12)	85 (± 16)*	85 (± 11)**	**0.01**
MAP, mmHg	84 (± 10)	105 (± 16)*	105 (± 12)**	**0.001**
Urine PCR, mg/mmol, median (IQR)	Not performed	322 (62-774)	129 (101-222)	NA
Hb, g/L	120 (± 10)	117 (± 7)	115 (± 11)	0.55
Antihypertensives, n (%), yes	0 (0)	5 (100)	11 (92)	**<0.001**
Delivery Outcomes				
Gestation, weeks+days, median (IQR)	39+3 (38+4 - 39+4)	28+4 ** (27+1 - 29+6)	38+5 (35+4 - 40+2)	**0.002**
Delivery, n (%) vaginal	0 (0)	0 (0)	6 (50)	**0.01**
Sex, n (%), male	4 (44)	2 (40)	6 (50)	0.92
Birth weight, kg, median (IQR)	3.38 (3.17-3.52)	0.82 (0.62-1.22)**	3.30 (2.16-3.54)	**0.002**
Birth Centile, %	64.4 (± 19.9)	15.9 (± 16.8)*	52.4 (± 34.4)	**0.01**

Table 8 – Participant Demographics and Outcome Data

Results are displayed as mean (±SD) unless stated. Normally distributed continuous variables were compared by one-way ANOVA, with post hoc Dunnett's comparing individual groups to control. Non-parametric data was assessed by Kruskal-Wallis test, with post hoc Dunn's multiple comparisons. Categorical data was assessed by χ^2 test. BP is blood pressure, IQR is interquartile range, MAP is mean arterial pressure, NA is not applicable, and PE is pre-eclampsia. P values are displayed as * = ≤ 0.05; ** = ≤ 0.01; and *** = ≤ 0.001

5.7 Lectin Histochemistry to Quantify the Placental Glycocalyx in Pre-eclampsia

5.7.1 Syncytiotrophoblast Glycocalyx

Lectin histochemistry with WGA was used to quantify the placental syncytiotrophoblast glycocalyx in pre-eclampsia and normotensive controls. The peak-to-peak value and coverage were automatically calculated using a macro as described in section 2.12.

There was no difference in the glycocalyx peak-to-peak value when comparing normotensive and pre-eclamptic pregnancy; 316 nm (SD ±57) vs 312 nm (SD ±59), p = 0.88. When early- and late-onset pre-eclampsia were considered separately, there was a trend towards a reduction in the peak-to-peak value compared to normotensive controls, but this did not reach statistical significance; 276.8 (SD ±50), adjusted p = 0.37. There was no difference in the late-onset pre-eclampsia group, Figure 40.

Similarly, there was no difference in the syncytiotrophoblast glycocalyx coverage when normotensive controls were compared to participants with pre-eclampsia, 57% (SD ±9) vs 61% (SD ±11), p = 0.43. When the pre-eclampsia sub-groups were considered, there was a trend towards an increase in glycocalyx coverage in the early-onset group, although again this did not reach statistical significance, 66% (SD ±8), adjusted p = 0.27.

When the glycocalyx peak-to-peak measurement was compared to coverage, there was a moderate negative correlation, r = -0.46, p = 0.02. This would suggest that glycocalyx coverage increases with glycocalyx shedding, Figure 41.

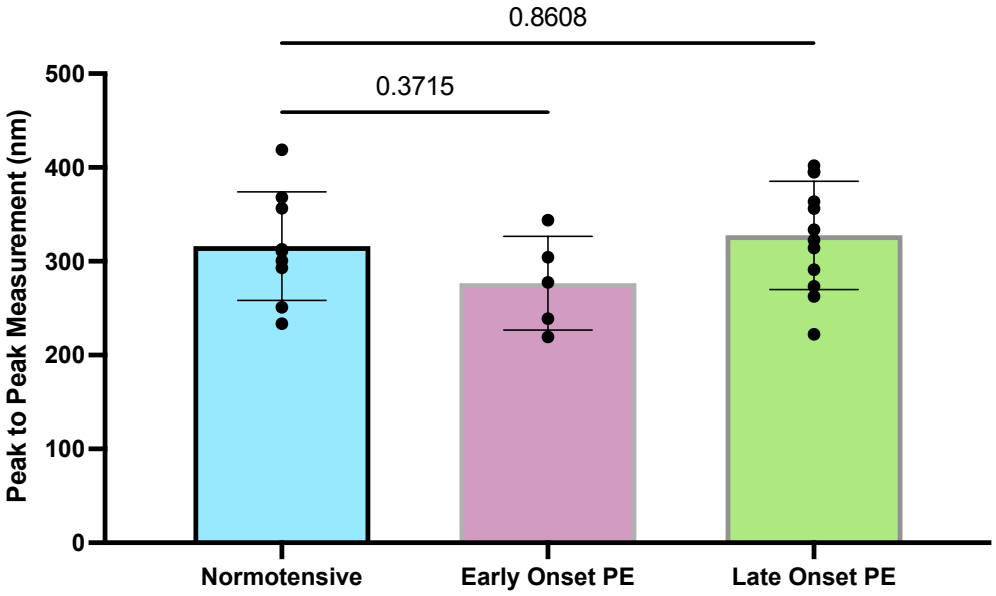

Figure 40 – Glycocalyx Peak-to-Peak Measurement at the Syncytiotrophoblast (WGA)
Although not statistically significant, there was a trend towards a reduction in syncytiotrophoblast glycocalyx depth in early-onset pre-eclampsia. This pattern was previously seen in data obtained from the maternal sublingual glycocalyx with GlycoCheck™

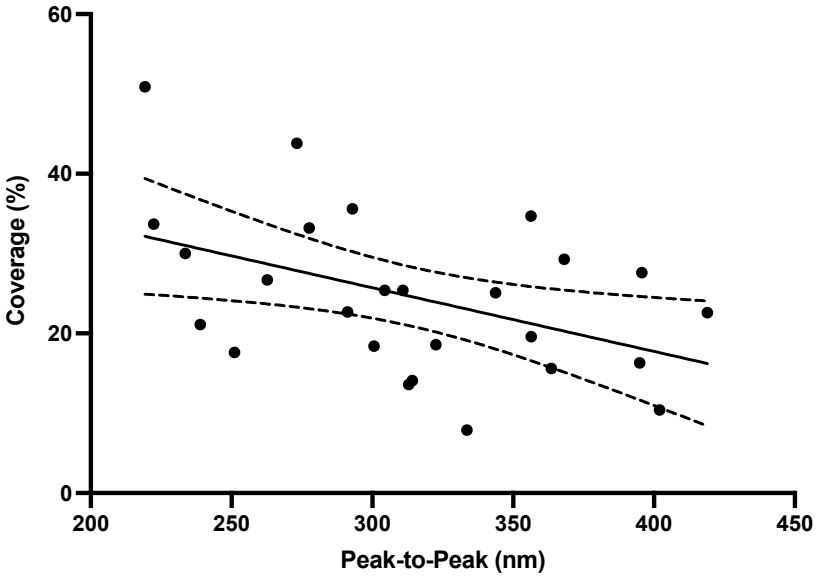

Figure 41 – Glycocalyx Peak-to-Peak vs Coverage at the Syncytiotrophoblast (WGA)
A moderate negative correlation was present between the observed peak-to-peak value and the glycocalyx coverage percentage, r = -0.46, p = 0.02. This suggests that coverage increases in response to loss of glycocalyx depth.

5.7.2 Placental Endothelial Glycocalyx

The endothelial glycocalyx was assessed by lectin histochemistry with UEA I. The peak-to-peak and glycocalyx coverage percentage was automatically calculated using a macro.

There was no difference in the mean peak-to-peak measurement when comparing placentae from normotensive controls and participants with pre-eclampsia, 254 nm (SD ±62) vs 238 nm (SD ±91), p = 0.66. When early- and late-onset pre-eclampsia were considered separately, there was also difference compared to normotensive controls, p = 0.91, Figure 42.

There was also no difference in the glycocalyx coverage percentage when normotensive controls were compared against pre-eclampsia, p = 0.15, or when the pre-eclampsia subgroups were considered separately, p = 0.18.

When glycocalyx coverage was compared to the peak-to-peak value, there was no association, r = 0.23, p = 0.28.

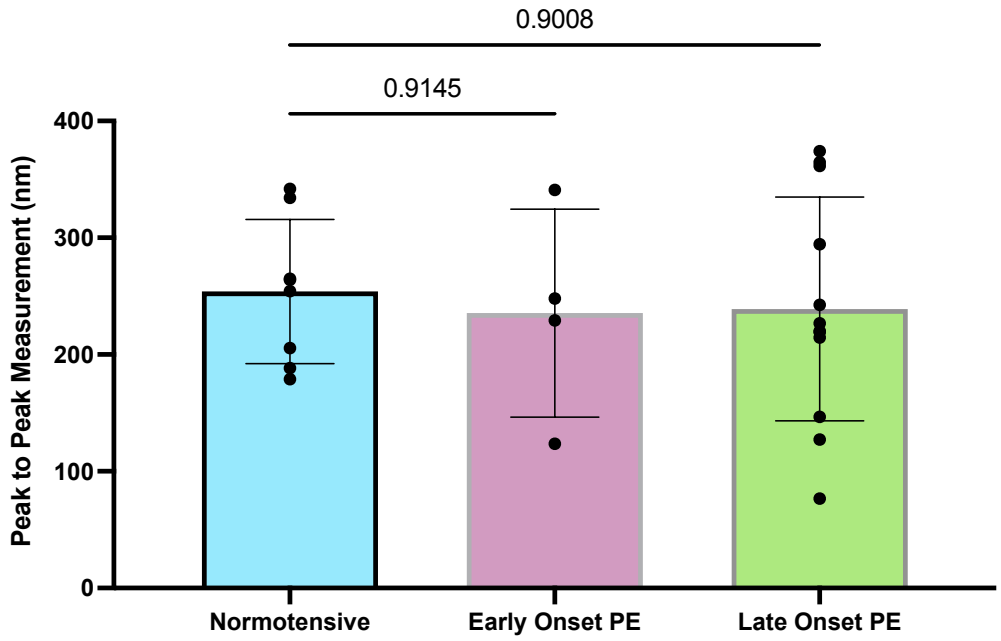

Figure 42 – Glycocalyx Peak-to-Peak Measurement at the Endothelium (UEA I)
There was no difference between the peak-to-peak measurement at the placental capillary endothelium when comparing normotensive and pre-eclamptic pregnancy, p = 0.91.

5.7.3 Syncytiotrophoblast vs Endothelial Glycocalyx

WGA staining of the syncytiotrophoblast and UEA I staining at the endothelium was compared. No associations were observed in either the peak-to-peak value, r = -0.19, p = 0.35, or glycocalyx coverage percentage, r = 0.15, p =0.49.

5.8 Comparing Lectin Histochemistry to Other Clinical Markers

The syncytiotrophoblast and endothelial glycocalyx peak-to-peak measurements were compared against a range of clinical markers, including blood pressure, biochemical and haematological markers, and birth outcomes. No associations were present.

5.9 Comparing Lectin Histochemistry to TEM and GlycoCheck™

5.9.1 Lectin Histochemistry vs TEM

Twenty-three participants had syncytiotrophoblast glycocalyx measured by both TEM and lectin histochemistry using WGA. Eight patients were normotensive controls, four had early-onset pre-eclampsia, and 11 had late-onset pre-eclampsia.

When the mean glycocalyx depth measure by TEM was compared to the peak-to-peak measurement, there was no correlation, r = 0.03, p = 0.87. Similarly, when glycocalyx coverage calculated by TEM was compared with glycocalyx coverage by lectin histochemistry there was no association, r = 0.20, p = 0.37.

5.9.2 Lectin Histochemistry vs GlycoCheck™

Seventeen patients had placental sampling with quantification of the syncytiotrophoblast glycocalyx by lectin histochemistry with WGA, and calculation of the sublingual PBR with GlycoCheck™. This included four normotensive controls, four early-onset pre-eclampsia and 10 with late-onset pre-eclampsia.

There was a moderate negative correlation between the syncytiotrophoblast peak-to-peak value and the PBR in 5-25 µm vessels, r = 0.59, p = 0.01, Figure43A. This would suggest that loss of the glycocalyx at the placenta is associated with loss of the glycocalyx in the maternal sublingual capillaries. This lends to the suggestion that the trend observed towards a reduction in the glycocalyx peak-to-peak value observed with WGA in early-onset pre-eclampsia, is perhaps a true reflection, that may reach statistical significance with a larger cohort.

A moderate positive correlation was observed was also observed between the peak-to-peak value and the RBC filling percentage, r = 0.59, p = 0.01, Figure 43B. This again suggests an association between glycocalyx shedding at the placenta and increased microvascular permeability.

When glycocalyx coverage at the syncytiotrophoblast was considered, a strong positive association was observed, r = 0.72, p = 0.001, with a similar moderate negative correlation with RBC filling, r = 0.60, p = 0.01, Figure 43C and D. This fits with the previously described negative correlation between the peak-to-peak measurement and coverage and suggests an association with increased coverage with increased glycocalyx shedding and microvascular permeability.

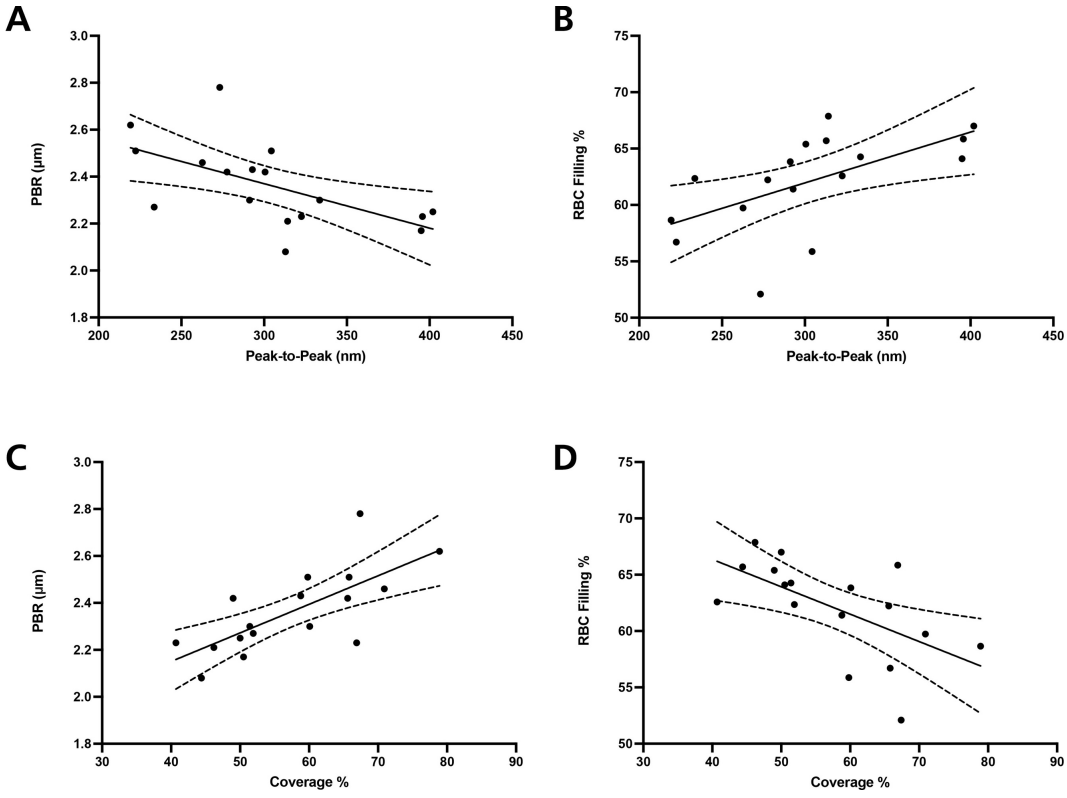

Figure 43 – WGA Lectin Histochemistry vs GlycoCheck™

There was a moderate negative correlation between the peak-to-peak glycocalyx depth at the syncytiotrophoblast and the PBR in 5-25 µm vessels, r = 0.59, p = 0.01 (**A**), and a moderate positive correlation between the peak-to-peak value and the RBC filling percentage, r = 0.59, p = 0.01 (**B**). This suggests an association between glycocalyx shedding at the placenta and increased glycocalyx shedding and microvascular permeability in the maternal sublingual capillaries. The inverse relationship between PBR (**C**) and RBC filling (**D**) was observed when comparing the syncytiotrophoblast glycocalyx coverage.

When UEA I staining of the endothelial glycocalyx was compared against PBR, no associations were demonstrated.

5.10 Lectin Histochemistry in an Independent Cohort

To further validate the technique of lectin histochemistry and increase the sample size for the comparison study, an application was made to the University of Nottingham for access to a placental biobank.

Specimens were collected and processed to paraffin blocks in a very similar way to the protocol developed in the local study. The primary difference was the fixation period which was in formalin and for up to two weeks, compared to the Bristol samples which were fixed for 24 hours in 4% PFA.

Sections were received from 36 placentae, which included 24 normotensive controls and 12 from women with pre-eclampsia. The pre-eclampsia group was further divided into six with early-onset disease and six with late-onset disease.

Glycocalyx staining with WGA and UEA I was performed for identification and measurement of the syncytiotrophoblast and endothelial glycocalyx respectively, in accordance with the protocol previously described. For the prevention of experimental bias which had previously been demonstrated with day-to-day variation, all specimens were processed and imaged in one batch.

5.10.1 Syncytiotrophoblast Glycocalyx

WGA staining of the syncytial glycocalyx demonstrated no difference in the mean peak-to-peak value between normotensive controls and placentae from women with pre-eclampsia, 219 nm (SD ±60) vs 223 nm (SD ±70), $p = 0.88$. When pre-eclampsia subgroups were considered separately, there was no difference compared to normotensive controls, $p = 0.91$, Figure 44A.

When glycocalyx coverage was studied, there was no difference between normotensive controls and placentae from women with pre-eclampsia, $p = 0.90$, or when pre-eclampsia subgroups were considered, $p = 0.07$.

When the glycocalyx peak-to-peak value was compared to the coverage placenta, no association was observed, r = -0.06, p = 0.73, contrary to the findings with the Bristol data.

5.10.2 Endothelial Cell Glycocalyx

The staining of the placental endothelial glycocalyx with UEA I demonstrated a trend towards a reduction in the glycocalyx in women with pre-eclampsia compared to normotensive controls, p = 0.07. When the pre-eclampsia sub-groups were considered

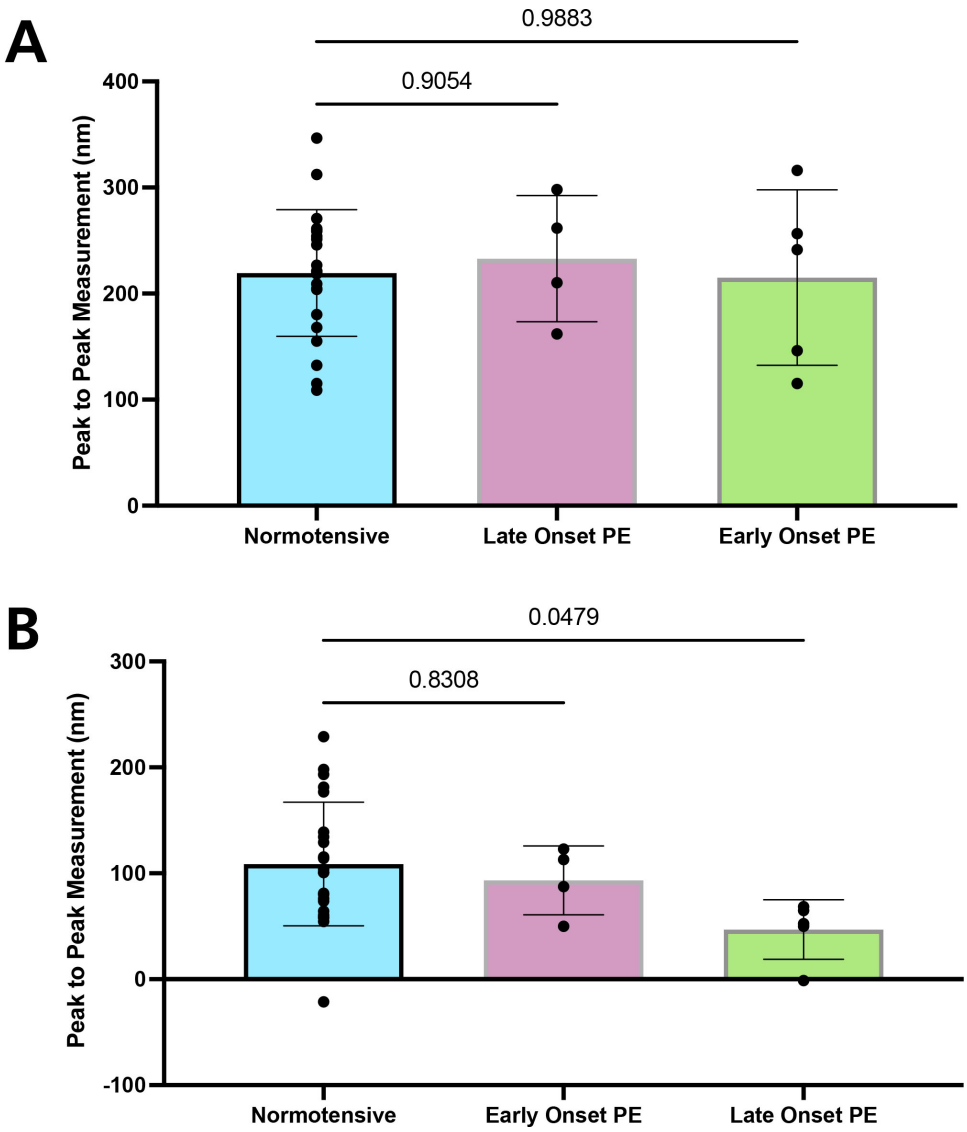

Figure 44 – Glycocalyx Peak-to-Peak Measurement in the Nottingham Cohort
The Nottingham cohort demonstrates no difference in the peak-to-peak glycocalyx measurement at the syncytiotrophoblast (WGA) when comparing pre-eclampsia to normotensive controls, p = 0.91, (**A**), or at the placental endothelial glycocalyx, p = 0.07 (**B**)

separately, it was clear the trend was driven by the late-onset group, p = 0.08, with adjusted p after post hoc Dunnett's multiple comparisons test 0.05, Figure 44B.

When glycocalyx coverage was considered, there was no difference between normotensive controls and pre-eclampsia and its subgroups. There was no association between glycocalyx coverage and the peak-to-peak value.

5.10.3 Comparing the Nottingham and Bristol Data

Due to the experimental variation described in section 5.4, it is difficult to combine the Bristol and Nottingham data sets.

When the raw WGA peak-to-peak values were considered, the mean of the combined Bristol data was significantly higher than the mean of the Nottingham data set, 313nm vs 220 nm, p = <0.001, Figure 45B. This may reflect a true difference in the Bristol and Nottingham populations, or in the way the tissues were fixed and processed, however, given the previously demonstrated experimental variation with lectin histochemistry this may also be a factor.

When the raw values were combined there was a significant increase in the glycocalyx peak-to-peak value at the syncytiotrophoblast in late-onset pre-eclampsia, compared to normotensive controls, adjusted p = 0.03, Figure 45A.

To account for the potential for experimental bias in the lectin histochemistry , the mean of the Nottingham and Bristol data was normalised to the column mean. This makes the big assumption that the sample populations are reflective of the true population means and that there is no genuine difference in the Bristol and Nottingham populations.

When the combined normalised data was compared in this way, there was no difference in the mean peak-to-peak value at the syncytiotrophoblast in normotensive controls or either pre-eclampsia sub-group, p = 0.35, Figure 45C. The same was true for the glycocalyx at the endothelium with UEA I staining, and glycocalyx coverage at both surfaces.

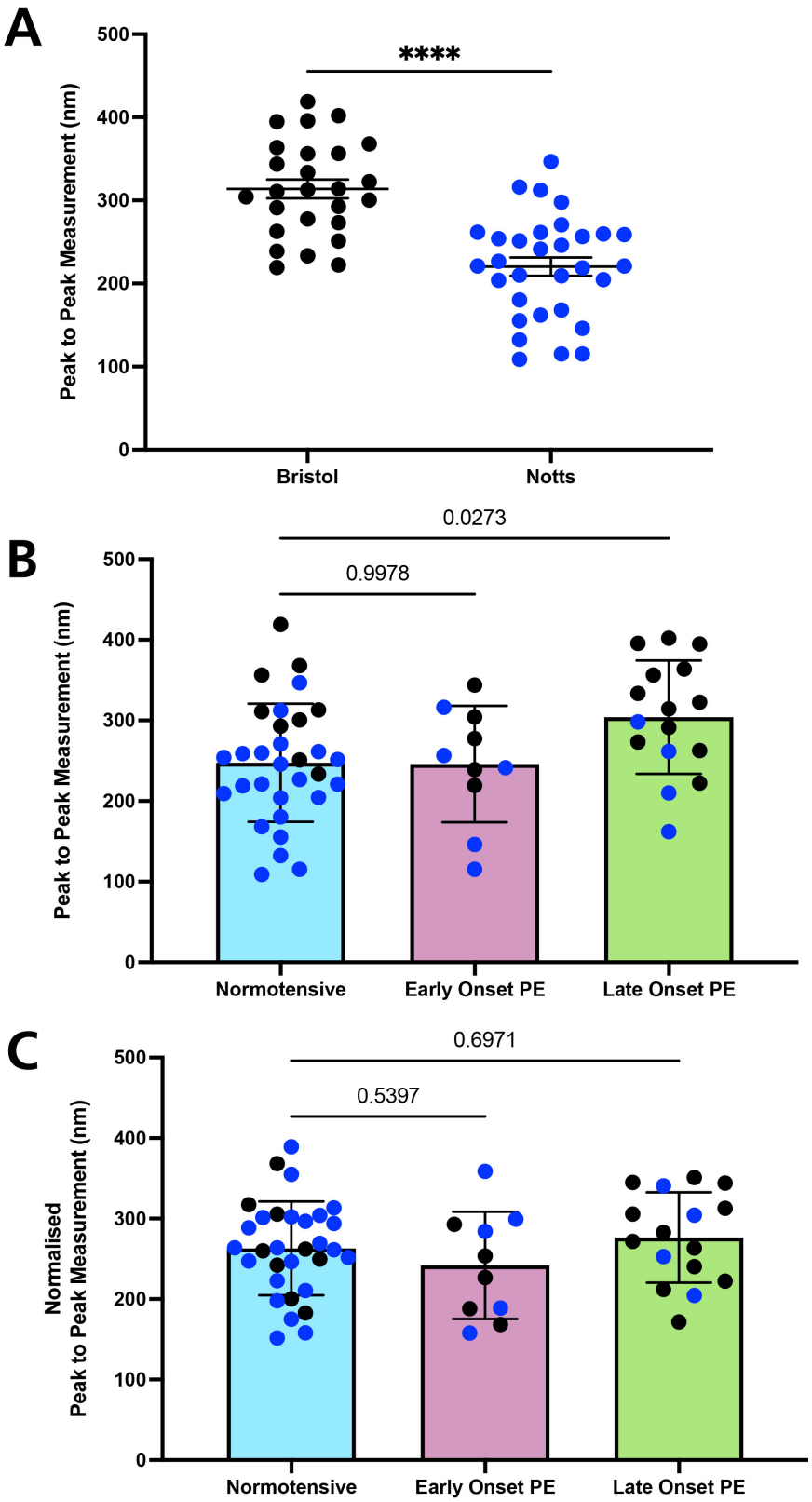

Figure 45 – Combining the Bristol and Nottingham Data - WGA

When the combined means of the Bristol and Nottingham data sets are compared, the syncytiotrophoblast peak-to-peak value is significantly bigger in the Bristol cohort, p = <0.001 (**A**). If the raw data sets are combined a significant increase in the peak-to-peak value is seen in the late-onset pre-eclampsia group, p = 0.03 (**B**). Assuming the sample means should be equal, each dataset can be normalised. When the data is normalised, there is no difference in the peak-to-peak measurement between the groups, p = 0.35 (**C**).

5.11 Discussion

5.11.1 Comparing Lectin Staining

This research has highlighted a different staining pattern at the syncytiotrophoblast and capillary endothelial cell glycocalyx. This may suggest a different composition of these two structures, or at least a difference in the expression of sugar residues.

These findings compare favourably with other published works which have demonstrated strong expression of the GlcNAc at the brush border (LEL and WGA staining), with a more granular pattern within the cytoplasm of the syncytiotrophoblast that may reflect intracellular transport of glycocalyx components [241, 242].

The capillary endothelium expressed fucose and sialic acid residues, evident by its UEA-1, MAL-II and WGA staining. UEA-I is a common lectin used for the human endothelial glycocalyx and has been observed in several tissues [272, 273].

Heterogeneity in the composition of the glycocalyx between the two sites of the placenta is perhaps not surprising; several authors have reported dynamic changes in the glycocalyx in response to different functional demands required of it [274, 275]. It is likely that a similar situation exists in the placenta.

Although lectins are highly specific for their target carbohydrate residues, one of their key limitations is that these residues occur frequently as part of many glycocalyx components and are not specific to particular GAGs. The role of lectin histochemistry is therefore limited to detecting changes in the structure and in the distribution of sugar residues, but not in determining the specific composition of the glycocalyx [153].

5.11.2 Evaluating Peak-to-Peak

The concept of using the peak-to-peak measurement as a proxy for glycocalyx depth was first reported by Betteridge et al. They tested several methodologies of quantifying glycocalyx depth and found this method compared most reliably with TEM in matched tissue [217].

In this study I have shown how the principles of peak-to-peak can be applied to the placenta, with specific adaptations described for measuring the syncytial and endothelial

glycocalyx. Through a process of robust analysis, I have demonstrated an automated technique of achieving this with a high degree or reliability and reproducibility.

This technique has been validated in other models assessing the endothelial glycocalyx and has been shown to be able to demonstrate changes in the glycocalyx depth [276, 277].

One potential criticism in applying this technique to the syncytiotrophoblast is that this method is not able to account for the presence of the microvillous brush border which is not present at the endothelial cell. The microvilli are known to alter in size with gestation, peaking in the first trimester, and to be arranged in an irregular honeycomb pattern [85]. It is possible that the peak-to-peak values could be affected by heterogeneity of this layer and may account for the relatively larger glycocalyx observed at the syncytiotrophoblast compared to the capillary (316 vs 254 nm).

5.11.3 Glycocalyx Depth in Pre-eclampsia

This study has demonstrated a trend towards a reduction in glycocalyx depth at the syncytiotrophoblast of women with early-onset pre-eclampsia, however this did not reach statistical significance. There was no difference in the placental endothelial cell glycocalyx.

As with the EM data, caution must be employed when trying to make interpretation of small data sets. A post hoc power calculation suggests group sizes of 27 would be required to detect a difference in the placental glycocalyx.

The moderate correlations that have been demonstrated between the lectin data and GlycoCheck™, do add weight to the theory that the placental glycocalyx may also be affected in pre-eclampsia. An increased PBR and therefore shedding at the maternal endothelial glycocalyx, was associated with a similar decline in syncytiotrophoblast glycocalyx depth. This suggests the syncytial glycocalyx may mirror changes in the maternal microvasculature.

The same trends observed in the Bristol data were not present in the Nottingham cohort, and when the data sets were normalised and combined, the previously observed trend towards a reduction in syncytial glycocalyx depth in early onset pre-eclampsia was no longer evident.

This may be an accurate reflection of the syncytial glycocalyx, or at least our ability to measure it using confocal microscopy, but certain considerations should be made prior to accepting the null hypothesis.

The major difference in the study protocols between the Bristol and Nottingham cohorts was the fixation methodology. In our study fixation was in PFA for a short time, whereas in the Nottingham cohort fixation was with formaldehyde and for extended periods. Formaldehyde and extended fixation periods have been shown to alter the binding of specific lectins and cause damage to certain sugar moieties [278].

5.12 Conclusion

Lectin histochemistry demonstrates a significant glycocalyx at the syncytiotrophoblast and capillary endothelium, but the glycosylation pattern of each structure is different.

I have validated and automated the peak-to-peak method in quantifying the depth of the glycocalyx at both the syncytiotrophoblast and capillary endothelium and applied this to samples from two prospective cohorts.

In the Bristol cohort, a trend was observed towards a reduction in the depth of the syncytiotrophoblast glycocalyx in placentae from women with early-onset pre-eclampsia, but this was not statistically significant. There was a moderate negative correlation between the sublingual PBR determined by GlycoCheck^{TM} and the depth of the syncytial glycocalyx. This would suggest that the changes in the maternal sublingual microvasculature are perhaps mirrored at the syncytiotrophoblast.

When an independent cohort of placentae were examined, no differences could be determined between pre-eclamptic and normotensive pregnancies.

6. DISCUSSION

6.1 METHODOLOGY FOR THE QUANTIFICATION OF THE GLYCOCALYX

6.1.1 GLYCOCALYX – LINKING THE TWO-STAGE HYPOTHESIS

The revised two-stage model of pre-eclampsia presented by Staff in 2019 gives our best understanding of how a disease of the placenta (syncytial stress), can lead to activation of the maternal endothelium and result in the many varied manifestations of pre-eclampsia [103].

When considering this model, the glycocalyx becomes an attractive research target. Present at both the placental syncytiotrophoblast and the maternal endothelium, the glycocalyx represents the first barrier of the maternal-fetal interface and represents an important link between the placental disease of stage-one, and the endothelial dysfunction of stage-two.

Our increasing recognition of the glycocalyx as a bioactive layer with roles in vascular permeability and immune modulation has applied focus in trying to determine the health of this layer in diseases like pre-eclampsia [168]. Studying the differences in the glycocalyx between the placenta and maternal endothelium may be key to unlocking the link between the two stages of the pre-eclampsia model and may represent a novel therapeutic target.

This work has highlighted the well-recognised difficulties in trying to quantify the glycocalyx. It is a highly dynamic structure in a constant state of synthesis and shear mediated shedding *in-vivo.* The combination of its small size and vulnerability to conventional methods of tissue fixation make it especially challenging to study [153].

In this thesis I have presented three different imaging modalities, that I have adapted and developed to provide a reliable methodology for the quantification of the glycocalyx at the maternal endothelium and placenta in both health and disease.

I applied these methodologies to a small population of women with pre-eclampsia and normotensive pregnant controls, validating the techniques for use in a larger study and providing important pilot data to direct further research.

6.1.2 Maternal Endothelial Glycocalyx

Imaging the maternal sublingual microvasculature with GlycoCheck™ has demonstrated clear evidence that glycocalyx shedding is a feature of early-onset, but not late-onset pre-eclampsia. Similar results have recently been published in a larger trial [187].

Endothelial activation and vascular inflammation are well recognised features of pre-eclampsia [11, 279]. Women who have pre-eclampsia with severe features have been demonstrated to have higher levels of circulating pro-inflammatory cytokines consistent with endothelial cell activation and dysfunction [280]. Pre-eclampsia with severe features is more common in women who have early-onset disease, compared to late-onset disease where the process of delivery may moderate the outcome [42]. Further phenotypic and mechanistic differences between early- and late-onset disease are likely but still poorly understood [42, 50].

The location of the glycocalyx at the interface of the maternal endothelial cell suggests an important role in the normal functioning of the cell. This is now supported by a growing body of evidence suggesting glycocalyx dysfunction is present in many conditions characterised by endothelial dysfunction. Inflammatory cytokines have been demonstrated to have a deleterious effect to the glycocalyx leading to increased leukocyte adhesion [173-175].

Aside from SDF imaging, most data supporting a role for glycocalyx dysfunction come from the measurement of shed glycocalyx components that can be detected in blood and urine samples. As previously described interpretation of this data is difficult as results have often been conflicting. Syndecan-1, a major structural proteoglycan of the glycocalyx, has been shown to be both increased [206], decreased [204, 205, 207] or unaffected in pregnancies with pre-eclampsia [187]. Variations in patient populations, pre-eclampsia phenotypes and in the assay used to measure may affect this.

There is an urgent need for the development of new assays to determine glycocalyx function *in vivo.* Currently GlycoCheck™ is the most recognised and has definite

advantages in its ease of use and automated processes for data analysis. Its poor inter and intra observer reliability, however, will restrict its use to larger comparative studies, rather than individual patient analysis and prognostication.

Establishing the mechanisms that lead to glycocalyx shedding in pre-eclampsia is an important future research direction of translational potential. Understanding how and why the glycocalyx is shed, may conceivably lead to new therapeutic targets to help restore the glycocalyx and moderate the endothelial dysfunction. For example, inducing $VEGF_{165}b$ upregulation in a diabetic mouse model, prevented functional and histological features of diabetic nephropathy, normalised glomerular permeability, and restored the glomerular glycocalyx [146].

Disruption and remodelling of the glycocalyx is not unique to pre-eclampsia and has been demonstrated in several other endothelial diseases [181-187]. A central consideration of the two-stage hypothesis is that the endothelial response in stage-two, takes place in the context of the background maternal endothelial condition and risk-factors [103]. Imaging the glycocalyx during pregnancy represents a 'snapshot' in time, but it is clear, that changes in the endothelial glycocalyx are also occurring both pre- and post-pregnancy. Given the increasing evidence that pre-eclampsia represents a significant risk factor for the development of cardiovascular disease in future life, longitudinal data on the role the glycocalyx might play in this is an a further research consideration [113].

6.1.3 The Placental Glycocalyx

This work has provided strong evidence for the presence of a significant glycocalyx at the syncytiotrophoblast of the human placenta. Quantification of this layer is more difficult but two methodologies using immersion fixed placental tissue have been presented using TEM and confocal microscopy.

Application of these methodologies to a small pilot study have demonstrated feasibility. Although not statistically significant, a trend was observed towards a reduction in glycocalyx depth at the syncytiotrophoblast in pre-eclampsia. When measured with confocal microscopy, these findings demonstrated a moderate correlation with the GlycoCheck^{TM} data, suggesting the placental glycocalyx may mirror the maternal endothelial glycocalyx.

The trend towards a reduction in glycocalyx depth in early-onset pre-eclampsia was not replicated in an independent cohort, although the procedure for tissue fixation differed.

It is unclear if the glycocalyx in the delivered placenta is truly representative of the placenta *in-vivo*. The fragility of the glycocalyx has been presented in this work, demonstrating a significant reduction in glycocalyx depth within 20 minutes of delivery. It is unclear how the process of parturition and delivery of the placenta may affect the placental glycocalyx. Certainly, MMPs which are known to cause shedding at the glycocalyx have been shown to an important role in parturition [281].

Other methodologies have been used to determine the composition of the placental glycocalyx. Expression of known glycocalyx components such as syndecans-1 and glypican-1 have been demonstrated to be reduced in pre-eclampsia [200, 201]. Lectins have also been used to determine the relative expression of different carbohydrate residues, suggesting an altered glycome in pre-eclampsia [282].

6.2 Concluding Remarks

The endothelial and placental glycocalyx represents an exciting research direction in the search for the pathogenesis of pre-eclampsia. As the direct interface of the maternal and fetal circulations it may represent the link between syncytial stress and maternal endothelial dysfunction.

This research has demonstrated 3 methodologies for imaging the glycocalyx and applied them to a small pilot study.

Shedding of the endothelial glycocalyx, represented by an increase in PBR, has been shown at the maternal sublingual microvasculature in women with early- but not late- onset pre-eclampsia. Imaging of the syncytial glycocalyx using TEM and confocal microscopy with lectin histochemistry has demonstrated a similar trend towards a reduction in depth at the syncytial glycocalyx, but this did not reach statistical significance.

Further mechanistic work is needed to determine how syncytial stress leads to glycocalyx shedding.

REFERENCES

1. Farrington, B., J. Chadwick, and W. Mann. *The medical works of Hippocrates*. 1950.
2. Chesley, L.C., A Short History of Eclampsia. Obstetrics & Gynecology, 1974. **43**(4).
3. Birkwood, K. *Annotating Hippocrates: who was reading the Coan prenotions?* March 2021]; Available from: https://history.rcplondon.ac.uk/blog/annotating-hippocrates-who-was-reading-coan-prenotions.
4. Johns, R., *Observations on puerperal convulsions.* Dublin Journal of Medical Science (1836-1845), 1843. **24**(1): p. 101-115.
5. National Guideline, A., *National Institute for Health and Care Excellence: Clinical Guidelines*, in *Hypertension in pregnancy: diagnosis and management*. 2019, National Institute for Health and Care Excellence (UK): London.
6. *National Institute for Health and Care Excellence: Clinical Guidelines*, in *Antenatal care for uncomplicated pregnancies*. 2019, National Institute for Health and Care Excellence (UK): London.
7. Lever, J.C.W., *Cases of Puerperal Convulsions, with Remarks*. 1843: Palmer & Clayton.
8. Ballantyne, J.W., *Sphygmographic Tracings in Puerperal Eclampsia.* Trans Edinb Obstet Soc, 1885. **10**: p. 56-70.
9. Gillon, T.E., et al., *Hypertensive disorders of pregnancy: a systematic review of international clinical practice guidelines.* PLoS One, 2014. **9**(12): p. e113715.
10. Zhang, J., M.A. Klebanoff, and J.M. Roberts, *Prediction of adverse outcomes by common definitions of hypertension in pregnancy.* Obstet Gynecol, 2001. **97**(2): p. 261-7.
11. Roberts, J.M., et al., *Preeclampsia: an endothelial cell disorder.* Am J Obstet Gynecol, 1989. **161**(5): p. 1200-4.
12. Brown, M.A., et al., *The hypertensive disorders of pregnancy: ISSHP classification, diagnosis & management recommendations for international practice.* Pregnancy Hypertension, 2018. **13**: p. 291-310.
13. Rana, S., et al., *Preeclampsia: Pathophysiology, Challenges, and Perspectives.* Circ Res, 2019. **124**(7): p. 1094-1112.
14. Redman, C.W.G., A.C. Staff, and J.M. Roberts, *Syncytiotrophoblast stress in preeclampsia: the convergence point for multiple pathways.* American Journal of Obstetrics and Gynecology, 2021.
15. Myatt, L. and J.M. Roberts, *Preeclampsia: Syndrome or Disease?* Curr Hypertens Rep, 2015. **17**(11): p. 83.
16. Say, L., et al., *Global causes of maternal death: a WHO systematic analysis.* Lancet Glob Health, 2014. **2**(6): p. e323-33.
17. *Trends in maternal mortality 2000 to 2017 : Estimates by WHO, UNICEF, UNFPA, World Bank Group and the United Nations Population Division* 2019, Geneva: World Health Organization.
18. Tommy's. *Pre-eclampsia statistics*. [cited 2021; Available from: https://www.tommys.org/pregnancy-information/pregnancy-complications/pre-eclampsia.
19. Shennan, A.H., M. Green, and L.C. Chappell, *Maternal deaths in the UK: pre-eclampsia deaths are avoidable.* Lancet, 2017. **389**(10069): p. 582-584.
20. *NHS Conditions: Pre-eclampsia*. [cited 2021 29/03/2021]; Available from: https://www.nhs.uk/conditions/pre-eclampsia/.

21. Lawn, J.E., et al., *Stillbirths: rates, risk factors, and acceleration towards 2030.* Lancet, 2016. **387**(10018): p. 587-603.
22. van Esch, J.J.A., et al., *Early-onset preeclampsia is associated with perinatal mortality and severe neonatal morbidity.* The Journal of Maternal-Fetal & Neonatal Medicine, 2017. **30**(23): p. 2789-2794.
23. Stevens, W., et al., *Short-term costs of preeclampsia to the United States health care system.* Am J Obstet Gynecol, 2017. **217**(3): p. 237-248.e16.
24. Redman, C.W., G.P. Sacks, and I.L. Sargent, *Preeclampsia: an excessive maternal inflammatory response to pregnancy.* Am J Obstet Gynecol, 1999. **180**(2 Pt 1): p. 499-506.
25. *Gestational Hypertension and Preeclampsia: ACOG Practice Bulletin, Number 222.* Obstet Gynecol, 2020. **135**(6): p. e237-e260.
26. Homer, C.S., et al., *Non-proteinuric pre-eclampsia: a novel risk indicator in women with gestational hypertension.* J Hypertens, 2008. **26**(2): p. 295-302.
27. Palei, A.C., et al., *Pathophysiology of hypertension in pre-eclampsia: a lesson in integrative physiology.* Acta physiologica (Oxford, England), 2013. **208**(3): p. 224-233.
28. Stillman, I.E. and S.A. Karumanchi, *The glomerular injury of preeclampsia.* J Am Soc Nephrol, 2007. **18**(8): p. 2281-4.
29. Prakash, J. and V.C. Ganiger, *Acute Kidney Injury in Pregnancy-specific Disorders.* Indian journal of nephrology, 2017. **27**(4): p. 258-270.
30. Benedetti, T.J., R. Kates, and V. Williams, *Hemodynamic observations in severe preeclampsia complicated by pulmonary edema.* Am J Obstet Gynecol, 1985. **152**(3): p. 330-4.
31. Thornton, C.E., et al., *Acute pulmonary oedema as a complication of hypertension during pregnancy.* Hypertens Pregnancy, 2011. **30**(2): p. 169-79.
32. Zeeman, G.G., *Neurologic complications of pre-eclampsia.* Semin Perinatol, 2009. **33**(3): p. 166-72.
33. Mikolasevic, I., et al., *Liver Disease During Pregnancy: A Challenging Clinical Issue.* Medical science monitor : international medical journal of experimental and clinical research, 2018. **24**: p. 4080-4090.
34. Perry, K.G., Jr. and J.N. Martin, Jr., *Abnormal hemostasis and coagulopathy in preeclampsia and eclampsia.* Clin Obstet Gynecol, 1992. **35**(2): p. 338-50.
35. Wadsack, C., G. Desoye, and U. Hiden, *The feto-placental endothelium in pregnancy pathologies.* Wien Med Wochenschr, 2012. **162**(9-10): p. 220-4.
36. Roberts, J.M. and C. Escudero, *The placenta in preeclampsia.* Pregnancy hypertension, 2012. **2**(2): p. 72-83.
37. Magee, L.A., et al., *The CHIPS Randomized Controlled Trial (Control of Hypertension in Pregnancy Study): Is Severe Hypertension Just an Elevated Blood Pressure?* Hypertension (Dallas, Tex. : 1979), 2016. **68**(5): p. 1153-1159.
38. Payne, B., et al., *PIERS proteinuria: relationship with adverse maternal and perinatal outcome.* J Obstet Gynaecol Can, 2011. **33**(6): p. 588-597.
39. Chan, P., et al., *Proteinuria in pre-eclampsia: how much matters?* BJOG, 2005. **112**(3): p. 280-5.
40. Barton, J.R. and B.M. Sibai, *Diagnosis and management of hemolysis, elevated liver enzymes, and low platelets syndrome.* Clin Perinatol, 2004. **31**(4): p. 807-33, vii.
41. Abildgaard, U. and K. Heimdal, *Pathogenesis of the syndrome of hemolysis, elevated liver enzymes, and low platelet count (HELLP): a review.* Eur J Obstet Gynecol Reprod Biol, 2013. **166**(2): p. 117-23.

42. Staff, A.C. and C.W.G. Redman, *The Differences Between Early- and Late-Onset Pre-eclampsia*, in *Preeclampsia: Basic, Genomic, and Clinical*, S. Saito, Editor. 2018, Springer Singapore: Singapore. p. 157-172.
43. Tranquilli, A.L., et al., *The definition of severe and early-onset preeclampsia. Statements from the International Society for the Study of Hypertension in Pregnancy (ISSHP).* Pregnancy Hypertension: An International Journal of Women's Cardiovascular Health, 2013. **3**(1): p. 44-47.
44. Roberts, C.L., et al., *Population-based trends in pregnancy hypertension and pre-eclampsia: an international comparative study.* BMJ Open, 2011. **1**(1): p. e000101.
45. Murphy, D.J. and G.M. Stirrat, *Mortality and morbidity associated with early-onset preeclampsia.* Hypertens Pregnancy, 2000. **19**(2): p. 221-31.
46. Verlohren, S., et al., *Uterine artery Doppler, birth weight and timing of onset of pre-eclampsia: providing insights into the dual etiology of late-onset pre-eclampsia.* Ultrasound Obstet Gynecol, 2014. **44**(3): p. 293-8.
47. Mifsud, W. and N.J. Sebire, *Placental pathology in early-onset and late-onset fetal growth restriction.* Fetal Diagn Ther, 2014. **36**(2): p. 117-28.
48. Xiong, X., et al., *Impact of preeclampsia and gestational hypertension on birth weight by gestational age.* Am J Epidemiol, 2002. **155**(3): p. 203-9.
49. Douglas, K.A. and C.W. Redman, *Eclampsia in the United Kingdom.* BMJ, 1994. **309**(6966): p. 1395-400.
50. Raymond, D. and E. Peterson, *A critical review of early-onset and late-onset preeclampsia.* Obstet Gynecol Surv, 2011. **66**(8): p. 497-506.
51. Yoder, S.R., L.L. Thornburg, and J.D. Bisognano, *Hypertension in pregnancy and women of childbearing age.* Am J Med, 2009. **122**(10): p. 890-5.
52. Barton, J.R., et al., *Mild gestational hypertension remote from term: progression and outcome.* Am J Obstet Gynecol, 2001. **184**(5): p. 979-83.
53. Saudan, P., et al., *Does gestational hypertension become pre-eclampsia?* BMJ, 1998. **105**(11): p. 1177-84.
54. Bramham, K., et al., *Chronic hypertension and pregnancy outcomes: systematic review and meta-analysis.* Bmj, 2014. **348**: p. g2301.
55. Morton, A., et al., *Changes in proteinuria and diagnosing preeclampsia in CKD pregnancy.* Pregnancy Hypertens, 2020. **20**: p. 92-95.
56. Soto-Wright, V., et al., *The changing clinical presentation of complete molar pregnancy.* Obstet Gynecol, 1995. **86**(5): p. 775-9.
57. Sibai, B.M., *Diagnosis, controversies, and management of the syndrome of hemolysis, elevated liver enzymes, and low platelet count.* Obstet Gynecol, 2004. **103**(5 Pt 1): p. 981-91.
58. Bartsch, E., et al., *Clinical risk factors for pre-eclampsia determined in early pregnancy: systematic review and meta-analysis of large cohort studies.* BMJ, 2016. **353**: p. i1753.
59. Gebremedhin, A.T., et al., *Interpregnancy interval and hypertensive disorders of pregnancy: A population-based cohort study.* Paediatr Perinat Epidemiol, 2020.
60. Duckitt, K. and D. Harrington, *Risk factors for pre-eclampsia at antenatal booking: systematic review of controlled studies.* BMJ, 2005. **330**(7491): p. 565.
61. Young, J., *The AEtiology of Eclampsia and Albuminuria and their Relation to Accidental Haemorrhage: (An Anatomical and Experimental Investigation.).* Proc R Soc Med, 1914. **7**(Obstet Gynaecol Sect): p. 307-48.
62. Huppertz, B., *The anatomy of the normal placenta.* J Clin Pathol, 2008. **61**(12): p. 1296-302.

63. Sadovsky, Y. and T. Jansson, *Chapter 39 - Placenta and Placental Transport Function*, in *Knobil and Neill's Physiology of Reproduction (Fourth Edition)*, T.M. Plant and A.J. Zeleznik, Editors. 2015, Academic Press: San Diego. p. 1741-1782.
64. Cartwright, J.E., et al., *Remodelling at the maternal-fetal interface: relevance to human pregnancy disorders.* Reproduction, 2010. **140**(6): p. 803-13.
65. Sato, Y., H. Fujiwara, and I. Konishi, *Mechanism of maternal vascular remodeling during human pregnancy.* Reproductive medicine and biology, 2011. **11**(1): p. 27-36.
66. Jackson, M.R., T.M. Mayhew, and P.A. Boyd, *Quantitative description of the elaboration and maturation of villi from 10 weeks of gestation to term.* Placenta, 1992. **13**(4): p. 357-70.
67. Whitley, G.S. and J.E. Cartwright, *Cellular and molecular regulation of spiral artery remodelling: lessons from the cardiovascular field.* Placenta, 2010. **31**(6): p. 465-74.
68. Pijnenborg, R., L. Vercruysse, and M. Hanssens, *The uterine spiral arteries in human pregnancy: facts and controversies.* Placenta, 2006. **27**(9-10): p. 939-58.
69. Craven, C.M., T. Morgan, and K. Ward, *Decidual spiral artery remodelling begins before cellular interaction with cytotrophoblasts.* Placenta, 1998. **19**(4): p. 241-52.
70. Smith, S.D., et al., *Evidence for immune cell involvement in decidual spiral arteriole remodeling in early human pregnancy.* Am J Pathol, 2009. **174**(5): p. 1959-71.
71. Kaufmann, P., S. Black, and B. Huppertz, *Endovascular trophoblast invasion: implications for the pathogenesis of intrauterine growth retardation and preeclampsia.* Biol Reprod, 2003. **69**(1): p. 1-7.
72. Burton, G.J., E. Jauniaux, and A.L. Watson, *Maternal arterial connections to the placental intervillous space during the first trimester of human pregnancy: the Boyd collection revisited.* Am J Obstet Gynecol, 1999. **181**(3): p. 718-24.
73. Genbacev, O., et al., *Regulation of human placental development by oxygen tension.* Science, 1997. **277**(5332): p. 1669-72.
74. Caniggia, I., et al., *Oxygen and placental development during the first trimester: implications for the pathophysiology of pre-eclampsia.* Placenta, 2000. **21 Suppl A**: p. S25-30.
75. Chen, Q., et al., *Interaction of Jar choriocarcinoma cells with endothelial cell monolayers.* Placenta, 2005. **26**(8-9): p. 617-25.
76. Harris, L.K., et al., *Invasive trophoblasts stimulate vascular smooth muscle cell apoptosis by a fas ligand-dependent mechanism.* Am J Pathol, 2006. **169**(5): p. 1863-74.
77. Harris, L.K. and J.D. Aplin, *Vascular remodeling and extracellular matrix breakdown in the uterine spiral arteries during pregnancy.* Reprod Sci, 2007. **14**(8 Suppl): p. 28-34.
78. Khong, T.Y., I.H. Sawyer, and A.R. Heryet, *An immunohistologic study of endothelialization of uteroplacental vessels in human pregnancy--evidence that endothelium is focally disrupted by trophoblast in preeclampsia.* Am J Obstet Gynecol, 1992. **167**(3): p. 751-6.
79. Burton, G.J., E. Jauniaux, and D.S. Charnock-Jones, *The influence of the intrauterine environment on human placental development.* Int J Dev Biol, 2010. **54**(2-3): p. 303-12.
80. Rodesch, F., et al., *Oxygen measurements in endometrial and trophoblastic tissues during early pregnancy.* Obstet Gynecol, 1992. **80**(2): p. 283-5.
81. Coppens, M., et al., *Longitudinal evaluation of uteroplacental and umbilical blood flow changes in normal early pregnancy.* Ultrasound Obstet Gynecol, 1996. **7**(2): p. 114-21.

82. Basta, M. and B.J. Lipsett, *Anatomy, Abdomen and Pelvis, Umbilical Cord*, in *StatPearls*. 2022, StatPearls Publishing Copyright © 2022, StatPearls Publishing LLC.: Treasure Island (FL)
83. Kaufmann, P., *Basic morphology of the fetal and maternal circuits in the human placenta.* Contrib Gynecol Obstet, 1985. **13**: p. 5-17.
84. Wang, Y. and S. Zhao, in *Vascular Biology of the Placenta*. 2010: San Rafael (CA).
85. Jones, C.J.P. and H. Fox, *Ultrastructure of the normal human placenta.* Electron Microscopy Reviews, 1991. **4**(1): p. 129-178.
86. Robertson, W.B., I. Brosens, and H.G. Dixon, *The pathological response of the vessels of the placental bed to hypertensive pregnancy.* J Pathol Bacteriol, 1967. **93**(2): p. 581-92.
87. Redman, C.W., *Current topic: pre-eclampsia and the placenta.* Placenta, 1991. **12**(4): p. 301-8.
88. Red-Horse, K., et al., *Trophoblast differentiation during embryo implantation and formation of the maternal-fetal interface.* J Clin Invest, 2004. **114**(6): p. 744-54.
89. Staff, A.C., et al., *Failure of physiological transformation and spiral artery atherosis: their roles in preeclampsia.* Am J Obstet Gynecol, 2022. **226**(2s): p. S895-s906.
90. Burton, G.J., et al., *Rheological and physiological consequences of conversion of the maternal spiral arteries for uteroplacental blood flow during human pregnancy.* Placenta, 2009. **30**(6): p. 473-82.
91. Redman, C.W., I.L. Sargent, and A.C. Staff, *IFPA Senior Award Lecture: making sense of pre-eclampsia - two placental causes of preeclampsia?* Placenta, 2014. **35 Suppl**: p. S20-5.
92. Falco, M.L., et al., *Placental histopathology associated with pre-eclampsia: systematic review and meta-analysis.* Ultrasound Obstet Gynecol, 2017. **50**(3): p. 295-301.
93. Sheppard, B.L. and J. Bonnar, *The ultrastructure of the arterial supply of the human placenta in pregnancy complicated by fetal growth retardation.* BJOG, 1976. **83**(12): p. 948-59.
94. Kajdy, A., et al., *Molecular Pathways of Cellular Senescence and Placental Aging in Late Fetal Growth Restriction and Stillbirth.* Int J Mol Sci, 2021. **22**(8).
95. Sultana, Z., et al., *Is there a role for placental senescence in the genesis of obstetric complications and fetal growth restriction?* Am J Obstet Gynecol, 2018. **218**(2s): p. S762-s773.
96. von Zglinicki, T., R. Pilger, and N. Sitte, *Accumulation of single-strand breaks is the major cause of telomere shortening in human fibroblasts.* Free Radic Biol Med, 2000. **28**(1): p. 64-74.
97. Sultana, Z., et al., *Oxidative stress, placental ageing-related pathologies and adverse pregnancy outcomes.* Am J Reprod Immunol, 2017. **77**(5).
98. Burton, G.J. and H.W. Yung, *Endoplasmic reticulum stress in the pathogenesis of early-onset pre-eclampsia.* Pregnancy Hypertens, 2011. **1**(1-2): p. 72-8.
99. Burton, G.J., H.W. Yung, and A.J. Murray, *Mitochondrial - Endoplasmic reticulum interactions in the trophoblast: Stress and senescence.* Placenta, 2017. **52**: p. 146-155.
100. Loukeris, K., R. Sela, and R.N. Baergen, *Syncytial knots as a reflection of placental maturity: reference values for 20 to 40 weeks' gestational age.* Pediatr Dev Pathol, 2010. **13**(4): p. 305-9.
101. Heazell, A.E., et al., *Formation of syncytial knots is increased by hyperoxia, hypoxia and reactive oxygen species.* Placenta, 2007. **28 Suppl A**: p. S33-40.
102. Wright, D., et al., *A competing risks model in early screening for preeclampsia.* Fetal Diagn Ther, 2012. **32**(3): p. 171-8.

103. Staff, A.C., *The two-stage placental model of preeclampsia: An update.* J Reprod Immunol, 2019. **134-135**: p. 1-10.
104. Serov, A.S., et al., *Optimal villi density for maximal oxygen uptake in the human placenta.* J Theor Biol, 2015. **364**: p. 383-96.
105. Dahlstrøm, B., et al., *Placenta weight in pre-eclampsia.* Acta Obstet Gynecol Scand, 2008. **87**(6): p. 608-11.
106. Bdolah, Y., et al., *Twin pregnancy and the risk of preeclampsia: bigger placenta or relative ischemia?* Am J Obstet Gynecol, 2008. **198**(4): p. 428.e1-6.
107. Avagliano, L., et al., *Abnormal spiral artery remodelling in the decidual segment during pregnancy: from histology to clinical correlation.* J Clin Pathol, 2011. **64**(12): p. 1064-8.
108. Bianchi, C., et al., *The role of obesity and gestational diabetes on placental size and fetal oxygenation.* Placenta, 2021. **103**: p. 59-63.
109. Lopez-Jaramillo, P., et al., *Obesity and Preeclampsia: Common Pathophysiological Mechanisms.* Frontiers in physiology, 2018. **9**: p. 1838-1838.
110. Kalafat, E. and B. Thilaganathan, *Cardiovascular origins of preeclampsia.* Curr Opin Obstet Gynecol, 2017.
111. Melchiorre, K., V. Giorgione, and B. Thilaganathan, *The placenta and preeclampsia: villain or victim?* Am J Obstet Gynecol, 2022. **226**(2s): p. S954-s962.
112. Melchiorre, K., et al., *Mid-gestational maternal cardiovascular profile in preterm and term pre-eclampsia: a prospective study.* BJOG, 2013. **120**(4): p. 496-504.
113. Melchiorre, K., et al., *Hypertensive Disorders of Pregnancy and Future Cardiovascular Health.* Frontiers in cardiovascular medicine, 2020. **7**: p. 59-59.
114. Friedman, S.A., et al., *Biochemical corroboration of endothelial involvement in severe preeclampsia.* Am J Obstet Gynecol, 1995. **172**(1 Pt 1): p. 202-3.
115. Hsu, C.D., et al., *Elevated circulating thrombomodulin in severe preeclampsia.* Am J Obstet Gynecol, 1993. **169**(1): p. 148-9.
116. Maynard, S.E., et al., *Excess placental soluble fms-like tyrosine kinase 1 (sFlt1) may contribute to endothelial dysfunction, hypertension, and proteinuria in preeclampsia.* Journal of Clinical Investigation, 2003. **111**(5): p. 649-658.
117. Ferrara, N., H.P. Gerber, and J. LeCouter, *The biology of VEGF and its receptors.* Nat Med, 2003. **9**(6): p. 669-76.
118. Li, X. and U. Eriksson, *Novel VEGF family members: VEGF-B, VEGF-C and VEGF-D.* Int J Biochem Cell Biol, 2001. **33**(4): p. 421-6.
119. de Vries, C., et al., *The fms-like tyrosine kinase, a receptor for vascular endothelial growth factor.* Science, 1992. **255**(5047): p. 989-91.
120. Terman, B.I., et al., *Identification of the KDR tyrosine kinase as a receptor for vascular endothelial cell growth factor.* Biochem Biophys Res Commun, 1992. **187**(3): p. 1579-86.
121. Park, J.E., et al., *Placenta growth factor. Potentiation of vascular endothelial growth factor bioactivity, in vitro and in vivo, and high affinity binding to Flt-1 but not to Flk-1/KDR.* J Biol Chem, 1994. **269**(41): p. 25646-54.
122. Olsson, A.K., et al., *VEGF receptor signalling - in control of vascular function.* Nat Rev Mol Cell Biol, 2006. **7**(5): p. 359-71.
123. Ferrara, N., *Vascular Endothelial Growth Factor: Basic Biology and Clinical Applications.* Vol. 1. 2009. 11-21.
124. Hiratsuka, S., et al., *MMP9 induction by vascular endothelial growth factor receptor-1 is involved in lung-specific metastasis.* Cancer Cell, 2002. **2**(4): p. 289-300.

125. Kendall, R.L. and K.A. Thomas, *Inhibition of vascular endothelial cell growth factor activity by an endogenously encoded soluble receptor.* Proc Natl Acad Sci U S A, 1993. **90**(22): p. 10705-9.
126. Kendall, R.L., G. Wang, and K.A. Thomas, *Identification of a natural soluble form of the vascular endothelial growth factor receptor, FLT-1, and its heterodimerization with KDR.* Biochem Biophys Res Commun, 1996. **226**(2): p. 324-8.
127. Pandey, A.K., et al., *Mechanisms of VEGF (Vascular Endothelial Growth Factor) Inhibitor-Associated Hypertension and Vascular Disease.* Hypertension, 2018. **71**(2): p. e1-e8.
128. Papapetropoulos, A., et al., *Nitric oxide production contributes to the angiogenic properties of vascular endothelial growth factor in human endothelial cells.* J Clin Invest, 1997. **100**(12): p. 3131-9.
129. Wheeler-Jones, C., et al., *Vascular endothelial growth factor stimulates prostacyclin production and activation of cytosolic phospholipase A2 in endothelial cells via p42/p44 mitogen-activated protein kinase.* FEBS Lett, 1997. **420**(1): p. 28-32.
130. Charnock-Jones, D.S. and G.J. Burton, *Placental vascular morphogenesis.* Baillieres Best Pract Res Clin Obstet Gynaecol, 2000. **14**(6): p. 953-68.
131. Levine, R.J., et al., *Circulating angiogenic factors and the risk of preeclampsia.* N Engl J Med, 2004. **350**(7): p. 672-83.
132. Chen, J. and R.A. Khalil, *Chapter Four - Matrix Metalloproteinases in Normal Pregnancy and Preeclampsia*, in *Progress in Molecular Biology and Translational Science*, R.A. Khalil, Editor. 2017, Academic Press. p. 87-165.
133. Chaiworapongsa, T., et al., *Plasma soluble vascular endothelial growth factor receptor-1 concentration is elevated prior to the clinical diagnosis of pre-eclampsia.* J Matern Fetal Neonatal Med, 2005. **17**(1): p. 3-18.
134. Lecarpentier, E., et al., *Total Versus Free Placental Growth Factor Levels in the Pathogenesis of Preeclampsia.* Hypertension, 2020. **76**(3): p. 875-883.
135. Nagamatsu, T., et al., *Cytotrophoblasts up-regulate soluble fms-like tyrosine kinase-1 expression under reduced oxygen: an implication for the placental vascular development and the pathophysiology of preeclampsia.* Endocrinology, 2004. **145**(11): p. 4838-45.
136. Sela, S., et al., *A novel human-specific soluble vascular endothelial growth factor receptor 1: cell-type-specific splicing and implications to vascular endothelial growth factor homeostasis and preeclampsia.* Circ Res, 2008. **102**(12): p. 1566-74.
137. Duhig, K.E., et al., *Placental growth factor testing to assess women with suspected pre-eclampsia: a multicentre, pragmatic, stepped-wedge cluster-randomised controlled trial.* Lancet, 2019. **393**(10183): p. 1807-1818.
138. Wikström, A.K., et al., *Placental growth factor and soluble FMS-like tyrosine kinase-1 in early-onset and late-onset preeclampsia.* Obstet Gynecol, 2007. **109**(6): p. 1368-74.
139. St-Jacques, S., et al., *Localization of endoglin, a transforming growth factor-beta binding protein, and of CD44 and integrins in placenta during the first trimester of pregnancy.* Biol Reprod, 1994. **51**(3): p. 405-13.
140. Venkatesha, S., et al., *Soluble endoglin contributes to the pathogenesis of preeclampsia.* Nat Med, 2006. **12**(6): p. 642-9.
141. Rana, S., S.D. Burke, and S.A. Karumanchi, *Imbalances in circulating angiogenic factors in the pathophysiology of preeclampsia and related disorders.* Am J Obstet Gynecol, 2022. **226**(2s): p. S1019-s1034.
142. Esser, S., et al., *Vascular endothelial growth factor induces endothelial fenestrations in vitro.* The Journal of cell biology, 1998. **140**(4): p. 947-959.

143. Hermann, M., A. Flammer, and T.F. Lüscher, *Nitric oxide in hypertension.* J Clin Hypertens (Greenwich), 2006. **8**(12 Suppl 4): p. 17-29.
144. Karumanchi, S.A., et al., *Preeclampsia: A renal perspective.* Kidney International, 2005. **67**(6): p. 2101-2113.
145. Li, Z., et al., *Recombinant vascular endothelial growth factor 121 attenuates hypertension and improves kidney damage in a rat model of preeclampsia.* Hypertension, 2007. **50**(4): p. 686-92.
146. Oltean, S., et al., *Vascular Endothelial Growth Factor-A165b Is Protective and Restores Endothelial Glycocalyx in Diabetic Nephropathy.* J Am Soc Nephrol, 2015. **26**(8): p. 1889-904.
147. Stevens, M., et al., *VEGF-A(165)b protects against proteinuria in a mouse model with progressive depletion of all endogenous VEGF-A splice isoforms from the kidney.* The Journal of Physiology, 2017. **595**(19): p. 6281-6298.
148. Onions, K.L., et al., *VEGFC Reduces Glomerular Albumin Permeability and Protects Against Alterations in VEGF Receptor Expression in Diabetic Nephropathy.* Diabetes, 2019. **68**(1): p. 172-187.
149. Butler, M.J., et al., *The Pathological Relevance of Increased Endothelial Glycocalyx Permeability.* Am J Pathol, 2020. **190**(4): p. 742-751.
150. BENNETT, H.S., *MORPHOLOGICAL ASPECTS OF EXTRACELLULAR POLYSACCHARIDES.* Journal of Histochemistry & Cytochemistry, 1963. **11**(1): p. 14-23.
151. Luft, J.H., *Fine structures of capillary and endocapillary layer as revealed by ruthenium red.* Fed Proc, 1966. **25**(6): p. 1773-83.
152. Curry, F.E., *Layer upon layer: the functional consequences of disrupting the glycocalyx-endothelial barrier in vivo and in vitro.* Cardiovascular research, 2017. **113**(6): p. 559-561.
153. Dane, M.J., et al., *A microscopic view on the renal endothelial glycocalyx.* Am J Physiol Renal Physiol, 2015. **308**(9): p. F956-66.
154. Jackson, R.L., S.J. Busch, and A.D. Cardin, *Glycosaminoglycans: molecular properties, protein interactions, and role in physiological processes.* Physiol Rev, 1991. **71**(2): p. 481-539.
155. Weinbaum, S., J.M. Tarbell, and E.R. Damiano, *The structure and function of the endothelial glycocalyx layer.* Annu Rev Biomed Eng, 2007. **9**: p. 121-67.
156. Carey, D.J., *Syndecans: multifunctional cell-surface co-receptors.* The Biochemical journal, 1997. **327 (Pt 1)**(Pt 1): p. 1-16.
157. Afratis, N.A., et al., *Syndecans - key regulators of cell signaling and biological functions.* Febs j, 2017. **284**(1): p. 27-41.
158. Jokimaa, V., et al., *Expression of syndecan-1 in human placenta and decidua.* Placenta, 1998. **19**(2-3): p. 157-63.
159. Fransson, L.A., et al., *Novel aspects of glypican glycobiology.* Cell Mol Life Sci, 2004. **61**(9): p. 1016-24.
160. van Deurs, B., et al., *Caveolae: anchored, multifunctional platforms in the lipid ocean.* Trends Cell Biol, 2003. **13**(2): p. 92-100.
161. Oohira, A., T.N. Wight, and P. Bornstein, *Sulfated proteoglycans synthesized by vascular endothelial cells in culture.* J Biol Chem, 1983. **258**(3): p. 2014-21.
162. Shriver, Z., et al., *Heparin and heparan sulfate: analyzing structure and microheterogeneity.* Handbook of experimental pharmacology, 2012(207): p. 159-176.
163. Huffman, F.G., *URONIC ACIDS*, in *Encyclopedia of Food Sciences and Nutrition (Second Edition)*, B. Caballero, Editor. 2003, Academic Press: Oxford. p. 5890-5896.

164. Mo, W., et al., *The influence of hyaluronic acid on vascular endothelial cell proliferation and the relationship with ezrin/merlin expression.* Acta Biochimica et Biophysica Sinica, 2011. **43**(12): p. 930-939.
165. Tammi, M.I., A.J. Day, and E.A. Turley, *Hyaluronan and homeostasis: a balancing act.* J Biol Chem, 2002. **277**(7): p. 4581-4.
166. Toole, B.P., *Hyaluronan: from extracellular glue to pericellular cue.* Nat Rev Cancer, 2004. **4**(7): p. 528-39.
167. Turley, E.A., P.W. Noble, and L.Y. Bourguignon, *Signaling properties of hyaluronan receptors.* J Biol Chem, 2002. **277**(7): p. 4589-92.
168. Reitsma, S., et al., *The endothelial glycocalyx: composition, functions, and visualization.* Pflugers Archiv, 2007. **454**(3): p. 345-359.
169. Curry, F.E. and R.H. Adamson, *Endothelial glycocalyx: permeability barrier and mechanosensor.* Ann Biomed Eng, 2012. **40**(4): p. 828-39.
170. van Haaren, P.M., et al., *Localization of the permeability barrier to solutes in isolated arteries by confocal microscopy.* Am J Physiol Heart Circ Physiol, 2003. **285**(6): p. H2848-56.
171. Vink, H. and B.R. Duling, *Capillary endothelial surface layer selectively reduces plasma solute distribution volume.* Am J Physiol Heart Circ Physiol, 2000. **278**(1): p. H285-9.
172. Vink, H. and B.R. Duling, *Identification of distinct luminal domains for macromolecules, erythrocytes, and leukocytes within mammalian capillaries.* Circ Res, 1996. **79**(3): p. 581-9.
173. Imhof, B.A. and D. Dunon, *Leukocyte Migration and Adhesion*, in *Advances in Immunology*, F.J. Dixon, Editor. 1995, Academic Press. p. 345-416.
174. Schmidt, E.P., et al., *The pulmonary endothelial glycocalyx regulates neutrophil adhesion and lung injury during experimental sepsis.* Nat Med, 2012. **18**(8): p. 1217-23.
175. Vink, H., A.A. Constantinescu, and J.A. Spaan, *Oxidized lipoproteins degrade the endothelial surface layer : implications for platelet-endothelial cell adhesion.* Circulation, 2000. **101**(13): p. 1500-2.
176. Yilmaz, O., et al., *The role of endothelial glycocalyx in health and disease.* Clinical Kidney Journal, 2019. **12**(5): p. 611-619.
177. Fernandes, D.C., et al., *Chapter 7 - Hemodynamic Forces in the Endothelium: From Mechanotransduction to Implications on Development of Atherosclerosis*, in *Endothelium and Cardiovascular Diseases*, P.L. Da Luz, et al., Editors. 2018, Academic Press. p. 85-95.
178. Florian, J.A., et al., *Heparan sulfate proteoglycan is a mechanosensor on endothelial cells.* Circ Res, 2003. **93**(10): p. e136-42.
179. Yen, W., et al., *Endothelial surface glycocalyx can regulate flow-induced nitric oxide production in microvessels in vivo.* PLoS One, 2015. **10**(1): p. e0117133.
180. Mulivor, A.W. and H.H. Lipowsky, *Inflammation- and ischemia-induced shedding of venular glycocalyx.* Am J Physiol Heart Circ Physiol, 2004. **286**(5): p. H1672-80.
181. Lopez-Quintero, S.V., et al., *High glucose attenuates shear-induced changes in endothelial hydraulic conductivity by degrading the glycocalyx.* PloS one, 2013. **8**(11): p. e78954-e78954.
182. Ostrowski, S.R., et al., *Sympathoadrenal activation and endothelial damage in patients with varying degrees of acute infectious disease: an observational study.* J Crit Care, 2015. **30**(1): p. 90-6.
183. Hayashida, K., W.C. Parks, and P.W. Park, *Syndecan-1 shedding facilitates the resolution of neutrophilic inflammation by removing sequestered CXC chemokines.* Blood, 2009. **114**(14): p. 3033-43.

184. Cancel, L.M., et al., *Endothelial glycocalyx, apoptosis and inflammation in an atherosclerotic mouse model.* Atherosclerosis, 2016. **252**: p. 136-146.
185. Martens, R.J., et al., *Sublingual microvascular glycocalyx dimensions in lacunar stroke patients.* Cerebrovasc Dis, 2013. **35**(5): p. 451-4.
186. Kumase, F., et al., *Glycocalyx degradation in retinal and choroidal capillary endothelium in rats with diabetes and hypertension.* Acta Med Okayama, 2010. **64**(5): p. 277-83.
187. Weissgerber, T.L., et al., *Early Onset Preeclampsia Is Associated With Glycocalyx Degradation and Reduced Microvascular Perfusion.* J Am Heart Assoc, 2019. **8**(4): p. e010647.
188. Eustes, A.S., et al., *Heparanase expression and activity are increased in platelets during clinical sepsis.* J Thromb Haemost, 2021. **19**(5): p. 1319-1330.
189. Gil, N., et al., *Heparanase is essential for the development of diabetic nephropathy in mice.* Diabetes, 2012. **61**(1): p. 208-16.
190. Dogné, S., et al., *Hyaluronidase 1 Deficiency Preserves Endothelial Function and Glycocalyx Integrity in Early Streptozotocin-Induced Diabetes.* Diabetes, 2016. **65**(9): p. 2742-53.
191. Ramnath, R., et al., *Matrix metalloproteinase 9-mediated shedding of syndecan 4 in response to tumor necrosis factor α: a contributor to endothelial cell glycocalyx dysfunction.* Faseb j, 2014. **28**(11): p. 4686-99.
192. Endo, K., et al., *Cleavage of syndecan-1 by membrane type matrix metalloproteinase-1 stimulates cell migration.* J Biol Chem, 2003. **278**(42): p. 40764-70.
193. Leach, L. and J.A. Firth, *Fine structure of the paracellular junctions of terminal villous capillaries in the perfused human placenta.* Cell Tissue Res, 1992. **268**(3): p. 447-52.
194. Eaton, B.M., L. Leach, and J.A. Firth, *Permeability of the fetal villous microvasculature in the isolated perfused term human placenta.* J Physiol, 1993. **463**: p. 141-55.
195. Crescimanno, C., et al., *Expression pattern alterations of syndecans and glypican-1 in normal and pathological trophoblast.* J Pathol, 1999. **189**(4): p. 600-8.
196. Hofmann-Kiefer, K.F., et al., *Placental syncytiotrophoblast maintains a specific type of glycocalyx at the fetomaternal border: the glycocalyx at the fetomaternal interface in healthy women and patients with HELLP syndrome.* Reprod Sci, 2013. **20**(10): p. 1237-45.
197. Marzioni, D., et al., *Hyaluronate and CD44 expression patterns in the human placenta throughout pregnancy.* Eur J Histochem, 2001. **45**(2): p. 131-40.
198. Martin, B.J., S.S. Spicer, and N.M. Smythe, *Cytochemical studies of the maternal surface of the syncytiotrophoblast of human early and term placenta.* Anat Rec, 1974. **178**(4): p. 769-85.
199. Gunatillake, T.C., A.; Said, J.M., *The Role of the Placental Glycosaminoglycans in the Prevention of Pre-Eclampsia.* J Glycobiol, 2013. **2**: p. 105.
200. Jokimaa, V.I., et al., *Placental expression of syndecan 1 is diminished in preeclampsia.* Am J Obstet Gynecol, 2000. **183**(6): p. 1495-8.
201. Chui, A., et al., *The expression of placental proteoglycans in pre-eclampsia.* Gynecol Obstet Invest, 2012. **73**(4): p. 277-84.
202. Dempsey, L.A., et al., *Heparanase expression in invasive trophoblasts and acute vascular damage.* Glycobiology, 2000. **10**(5): p. 467-75.
203. Rohde, L.H., et al., *Complementary expression of HIP, a cell-surface heparan sulfate binding protein, and perlecan at the human fetal-maternal interface.* Biol Reprod, 1998. **58**(4): p. 1075-83.

204. Gandley, R.E., et al., *Low Soluble Syndecan-1 Precedes Preeclampsia.* PLoS One, 2016. **11**(6): p. e0157608.
205. Kuessel, L., et al., *Dynamics of soluble syndecan-1 in maternal serum during and after pregnancies complicated by preeclampsia: a nested case control study.* Clin Chem Lab Med, 2019. **58**(1): p. 50-58.
206. Hofmann-Kiefer, K.F., et al., *Increased serum concentrations of circulating glycocalyx components in HELLP syndrome compared to healthy pregnancy: an observational study.* Reprod Sci, 2013. **20**(3): p. 318-25.
207. Kornacki, J., P. Wirstlein, and E. Wender-Ozegowska, *Levels of syndecan-1 and hyaluronan in early- and late-onset preeclampsia.* Pregnancy Hypertens, 2019. **18**: p. 108-111.
208. Romero, R., *Giants in Obstetrics and Gynecology Series: a profile of Christopher Redman, MB, BChir, MRCP, FRCP.* American journal of obstetrics and gynecology, 2019. **220**(5): p. 420-427.e1.
209. Megens, R.T., et al., *Two-photon microscopy of vital murine elastic and muscular arteries. Combined structural and functional imaging with subcellular resolution.* J Vasc Res, 2007. **44**(2): p. 87-98.
210. van den Berg, B.M., H. Vink, and J.A. Spaan, *The endothelial glycocalyx protects against myocardial edema.* Circ Res, 2003. **92**(6): p. 592-4.
211. Arkill, K.P., et al., *3D reconstruction of the glycocalyx structure in mammalian capillaries using electron tomography.* Microcirculation (New York, N.Y. : 1994), 2012. **19**(4): p. 343-351.
212. Clough, G., *The steady-state transport of cationized ferritin by endothelial cell vesicles.* J Physiol, 1982. **328**: p. 389-401.
213. Fassel, T.A., et al., *Superior preservation of the staphylococcal glycocalyx with aldehyde-ruthenium red and select lysine salts using extended fixation times.* Microsc Res Tech, 1998. **41**(4): p. 291-7.
214. Chevalier, L., et al., *Electron microscopy approach for the visualization of the epithelial and endothelial glycocalyx.* Morphologie, 2017. **101**(333): p. 55-63.
215. Ebong, E.E., et al., *Imaging the Endothelial Glycocalyx In Vitro by Rapid Freezing/Freeze Substitution Transmission Electron Microscopy.* Arteriosclerosis, thrombosis, and vascular biology, 2011. **31**(8): p. 1908-1915.
216. Hempel, C., et al., *The need to freeze-Dehydration during specimen preparation for electron microscopy collapses the endothelial glycocalyx regardless of fixation method.* Microcirculation, 2020. **27**(7): p. e12643.
217. Betteridge, K.B., et al., *Sialic acids regulate microvessel permeability, revealed by novel in vivo studies of endothelial glycocalyx structure and function.* J Physiol, 2017. **595**(15): p. 5015-5035.
218. Kataoka, H., et al., *Fluorescent imaging of endothelial glycocalyx layer with wheat germ agglutinin using intravital microscopy.* Microsc Res Tech, 2016. **79**(1): p. 31-7.
219. Treu, C.M., et al., *Sidestream dark field imaging: the evolution of real-time visualization of cutaneous microcirculation and its potential application in dermatology.* Arch Dermatol Res, 2011. **303**(2): p. 69-78.
220. Lee, D.H., et al., *Deeper penetration of erythrocytes into the endothelial glycocalyx is associated with impaired microvascular perfusion.* PLoS One, 2014. **9**(5): p. e96477.
221. Brands, J., et al., *Noninvasive sublingual microvascular imaging reveals sex-specific reduction in glycocalyx barrier properties in patients with coronary artery disease.* Physiol Rep, 2020. **8**(2): p. e14351.

222. Miranda, C.H., et al., *Evaluation of the endothelial glycocalyx damage in patients with acute coronary syndrome.* Atherosclerosis, 2016. **247**: p. 184-8.
223. Padberg, J.S., et al., *Damage of the endothelial glycocalyx in chronic kidney disease.* Atherosclerosis, 2014. **234**(2): p. 335-43.
224. Anand, D., et al., *Evolution of serum hyaluronan and syndecan levels in prognosis of sepsis patients.* Clin Biochem, 2016. **49**(10-11): p. 768-76.
225. Zuspan, F.P. and M.C. Ward, Treatment of Eclampsia. South Med J, 1964. **57**: p. 954-9.
226. Digital, N. *NHS Maternity Statistics, England 2019-20*. 2020 [cited 2021; Available from: https://digital.nhs.uk/data-and-information/publications/statistical/nhs-maternity-statistics/2019-20.
227. BD Diagnostics Preanalytical Systems. *Product Catalogue*. 2021 [cited 2021; Available from: http://www.bd.com/resource.aspx?idx=30770.
228. Cray, C., et al., *Effects of Storage Temperature and Time on Clinical Biochemical Parameters from Rat Serum.* Journal of the American Association for Laboratory Animal Science : JAALAS, 2009. **48**(2): p. 202-204.
229. Rovas, A., et al., *Bedside analysis of the sublingual microvascular glycocalyx in the emergency room and intensive care unit - the GlycoNurse study.* Scandinavian journal of trauma, resuscitation and emergency medicine, 2018. **26**(1): p. 16-16.
230. *Guidelines for Glycocalyx Assessment*. [cited 2021; Available from: https://glycocheck.com/microvascular-health-score-measurement/.
231. Lipowsky, H.H. and A. Lescanic, *Inhibition of inflammation induced shedding of the endothelial glycocalyx with low molecular weight heparin.* Microvascular research, 2017. **112**: p. 72-78.
232. Begley, C.M., et al., *Active versus expectant management for women in the third stage of labour.* Cochrane Database Syst Rev, 2019. **2**(2): p. Cd007412.
233. Burton, G.J., et al., *Optimising sample collection for placental research.* Placenta, 2014. **35**(1): p. 9-22.
234. Park, C., Kim, H., Rhyu, I., Uhm, C., *How to get well-preserved samples for Transmission Electron Microscopy.* Applied Microscopy, 2016. **46(4)**: p. 188-192.
235. Graham, L. and J.M. Orenstein, *Processing tissue and cells for transmission electron microscopy in diagnostic pathology and research.* Nature Protocols, 2007. **2**(10): p. 2439-2450.
236. Desideri, S., et al., *A novel assay provides sensitive measurement of physiologically relevant changes in albumin permeability in isolated human and rodent glomeruli.* Kidney Int, 2018. **93**(5): p. 1086-1097.
237. Leskova, W., et al., *Effect of diabetes and hyaluronidase on the retinal endothelial glycocalyx in mice.* Experimental eye research, 2019. **179**: p. 125-131.
238. Zeng, Y., et al., *The structural stability of the endothelial glycocalyx after enzymatic removal of glycosaminoglycans.* PLoS One, 2012. **7**(8): p. e43168.
239. Mascorro, J.A., *Propylene Oxide: To Use or Not to Use in Biological Tissue Processing.* Microscopy Today, 2004. **12**(1): p. 45-45.
240. Heyer-Chauhan, N., et al., *Placental syndecan-1 and sulphated glycosaminoglycans are decreased in preeclampsia.* J Perinat Med, 2014. **42**(3): p. 329-38.
241. Marini, M., et al., *Distribution of sugar residues in human placentas from pregnancies complicated by hypertensive disorders.* Acta Histochem, 2011. **113**(8): p. 815-25.
242. Tatsuzuki, A., et al., *Characterization of the sugar chain expression of normal term human placental villi using lectin histochemistry combined with immunohistochemistry.* Arch Histol Cytol, 2009. **72**(1): p. 35-49.

243. Williams, D.B., Carter, C.B., *The Transmission Electron Microscope. In: Transmission Electron Microscopy*. 2009, Springer: Boston, MA.
244. *Confocal Microscopy Tutorial - Part 1 Principles of Confocal Microscopy*. 2004 June 2021; Available from: http://www.hi.helsinki.fi/amu/AMU%20Cf_tut/Cf_tut_part1-3.htm.
245. *Confocal Microscopy Tutorial - Part 3 Operation, Optimization of Leica SP2 LSCM*. 2004 June 2021]; Available from: http://www.hi.helsinki.fi/amu/AMU%20Cf_tut/Opt_ScanRes.htm.
246. Schindelin, J., et al., *Fiji: an open-source platform for biological-image analysis.* Nat Methods, 2012. **9**(7): p. 676-82.
247. Cotta, M.A., *Quantum Dots and Their Applications: What Lies Ahead?* ACS Applied Nano Materials, 2020. **3**(6): p. 4920-4924.
248. Schober, P., C. Boer, and L.A. Schwarte, *Correlation Coefficients: Appropriate Use and Interpretation.* Anesthesia & Analgesia, 2018. **126**(5): p. 1763-1768.
249. Cicchetti, D.V., *Guidelines, criteria, and rules of thumb for evaluating normed and standardized assessment instruments in psychology.* Psychological assessment, 1994. **6**(4): p. 284.
250. Faul, F., et al., *G*Power 3: a flexible statistical power analysis program for the social, behavioral, and biomedical sciences.* Behav Res Methods, 2007. **39**(2): p. 175-91.
251. Faul, F., et al., *Statistical power analyses using G*Power 3.1: tests for correlation and regression analyses.* Behav Res Methods, 2009. **41**(4): p. 1149-60.
252. Wadowski, P.P., et al., *Microvascular rarefaction in patients with cerebrovascular events.* Microvasc Res, 2022. **140**: p. 104300.
253. Ikonomidis, I., et al., *Impaired Endothelial Glycocalyx Predicts Adverse Outcome in Subjects Without Overt Cardiovascular Disease: a 6-Year Follow-up Study.* Journal of Cardiovascular Translational Research, 2021.
254. Belousoviene, E., et al., *Links between Endothelial Glycocalyx Changes and Microcirculatory Parameters in Septic Patients.* Life (Basel), 2021. **11**(8).
255. Rovas, A., et al., *Microvascular dysfunction in COVID-19: the MYSTIC study.* Angiogenesis, 2021. **24**(1): p. 145-157.
256. Lambadiari, V., et al., *Effects of Different Antidiabetic Medications on Endothelial Glycocalyx, Myocardial Function, and Vascular Function in Type 2 Diabetic Patients: One Year Follow-Up Study.* J Clin Med, 2019. **8**(7).
257. Eickhoff, M.K., et al., *Assessment of the sublingual microcirculation with the GlycoCheck system: Reproducibility and examination conditions.* PLoS One, 2020. **15**(12): p. e0243737.
258. Valerio, L., et al., *Reproducibility of sublingual microcirculation parameters obtained from sidestream darkfield imaging.* PloS one, 2019. **14**(3): p. e0213175-e0213175.
259. Bol, M.E., et al., *Variability of Microcirculatory Measurements in Critically Ill Patients.* Shock, 2020. **54**(1): p. 9-14.
260. GlycoCheck. *The Only Video Microscope and Software System That Analyzes and Objectively Reports a Single Overall Microvascular Health Score*. 2019 [cited 2019; Available from: http://glycocheck.com.
261. Karemore, M.N. and J.G. Avari, *Zeta potential as a novel diagnostic tool for preeclampsia.* Pregnancy Hypertension, 2018. **13**: p. 187-197.
262. Bull, B.S. and J.D. Brailsford, *The Zeta Sedimentation Ratio.* Blood, 1972. **40**(4): p. 550-559.

263. Rovas, A., et al., *Association of sublingual microcirculation parameters and endothelial glycocalyx dimensions in resuscitated sepsis.* Crit Care, 2019. **23**(1): p. 260.
264. Motulsky, H.J. and R.E. Brown, *Detecting outliers when fitting data with nonlinear regression - a new method based on robust nonlinear regression and the false discovery rate.* BMC Bioinformatics, 2006. **7**: p. 123.
265. Baldwin, A.L. and C.P. Winlove, *Effects of perfusate composition on binding of ruthenium red and gold colloid to glycocalyx of rabbit aortic endothelium.* J Histochem Cytochem, 1984. **32**(3): p. 259-66.
266. Chappell, D., et al., *The glycocalyx of the human umbilical vein endothelial cell: an impressive structure ex vivo but not in culture.* Circ Res, 2009. **104**(11): p. 1313-7.
267. Thi, M.M., et al., *The role of the glycocalyx in reorganization of the actin cytoskeleton under fluid shear stress: a "bumper-car" model.* Proc Natl Acad Sci U S A, 2004. **101**(47): p. 16483-8.
268. Reily, C., et al., *Glycosylation in health and disease.* Nat Rev Nephrol, 2019. **15**(6): p. 346-366.
269. Hormia, M., V.P. Lehto, and I. Virtanen, *Identification of UEA I-binding surface glycoproteins of cultured human endothelial cells.* Cell Biol Int Rep, 1983. **7**(6): p. 467-75.
270. Matsui, T., et al., *Comparative study of blood group-recognizing lectins toward ABO blood group antigens on neoglycoproteins, glycoproteins and complex-type oligosaccharides.* Biochim Biophys Acta, 2001. **1525**(1-2): p. 50-7.
271. Laboratories, V. *Lectins and Glycobiology*. 2017 [cited 2022; Available from: https://vectorlabs.com/media/docs/brochures/LectinBrochure_2017.F.v3.web.pdf.
272. Meyer, W., S. Godynicki, and A. Tsukise, *Lectin histochemistry of the endothelium of blood vessels in the mammalian integument, with remarks on the endothelial glycocalyx and blood vessel system nomenclature.* Ann Anat, 2008. **190**(3): p. 264-76.
273. Roussel, F. and J. Dalion, *Lectins as markers of endothelial cells: comparative study between human and animal cells.* Lab Anim, 1988. **22**(2): p. 135-40.
274. Brouland, J.P., et al., *Macro and microheterogeneity in normal endothelial cells: differential composition of luminal glycocalyx and functional implications.* Endothelium, 1999. **6**(3): p. 251-62.
275. Curry, F.R., *Microvascular solute and water transport.* Microcirculation, 2005. **12**(1): p. 17-31.
276. Ramnath, R.D., et al., *Blocking matrix metalloproteinase-mediated syndecan-4 shedding restores the endothelial glycocalyx and glomerular filtration barrier function in early diabetic kidney disease.* Kidney International, 2020. **97**(5): p. 951-965.
277. Butler, M.J., et al., *Aldosterone induces albuminuria via matrix metalloproteinase-dependent damage of the endothelial glycocalyx.* Kidney Int, 2019. **95**(1): p. 94-107.
278. Lee, M.C. and I. Damjanov, *Lectin histochemistry of human placenta.* Differentiation, 1984. **28**(2): p. 123-8.
279. O'Brien, M., D. Baczyk, and J.C. Kingdom, *Endothelial Dysfunction in Severe Preeclampsia is Mediated by Soluble Factors, Rather than Extracellular Vesicles.* Sci Rep, 2017. **7**(1): p. 5887.
280. Szarka, A., et al., *Circulating cytokines, chemokines and adhesion molecules in normal pregnancy and preeclampsia determined by multiplex suspension array.* BMC Immunol, 2010. **11**: p. 59.

281. Vadillo-Ortega, F. and G. Estrada-Gutiérrez, *Role of matrix metalloproteinases in preterm labour.* BJOG, 2005. **112 Suppl 1**: p. 19-22.
282. Sukhikh, G.T., et al., *Differences of glycocalyx composition in the structural elements of placenta in preeclampsia.* Placenta, 2016. **43**: p. 69-76.

APPENDIX 1 – PUBLICATIONS

The Pathological Relevance of Increased Endothelial Glycocalyx Permeability

Matthew J. Butler, Colin J. Down, Rebecca R. Foster, and Simon C. Satchell

The American Journal of Pathology
Vol. 190, No. 4, April 2020, Pages 742-751

https://doi.org/10.1016/j.ajpath.2019.11.015

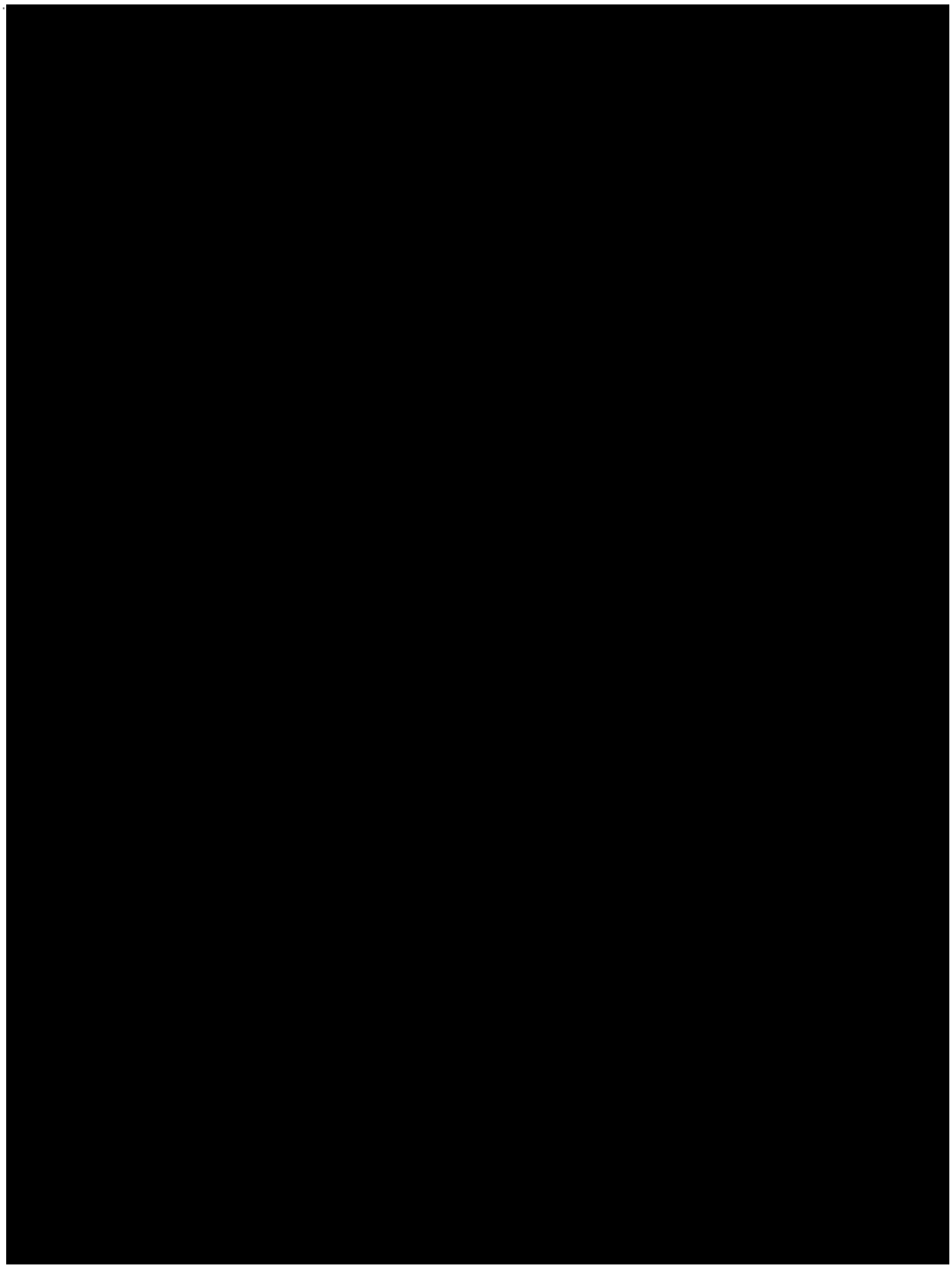

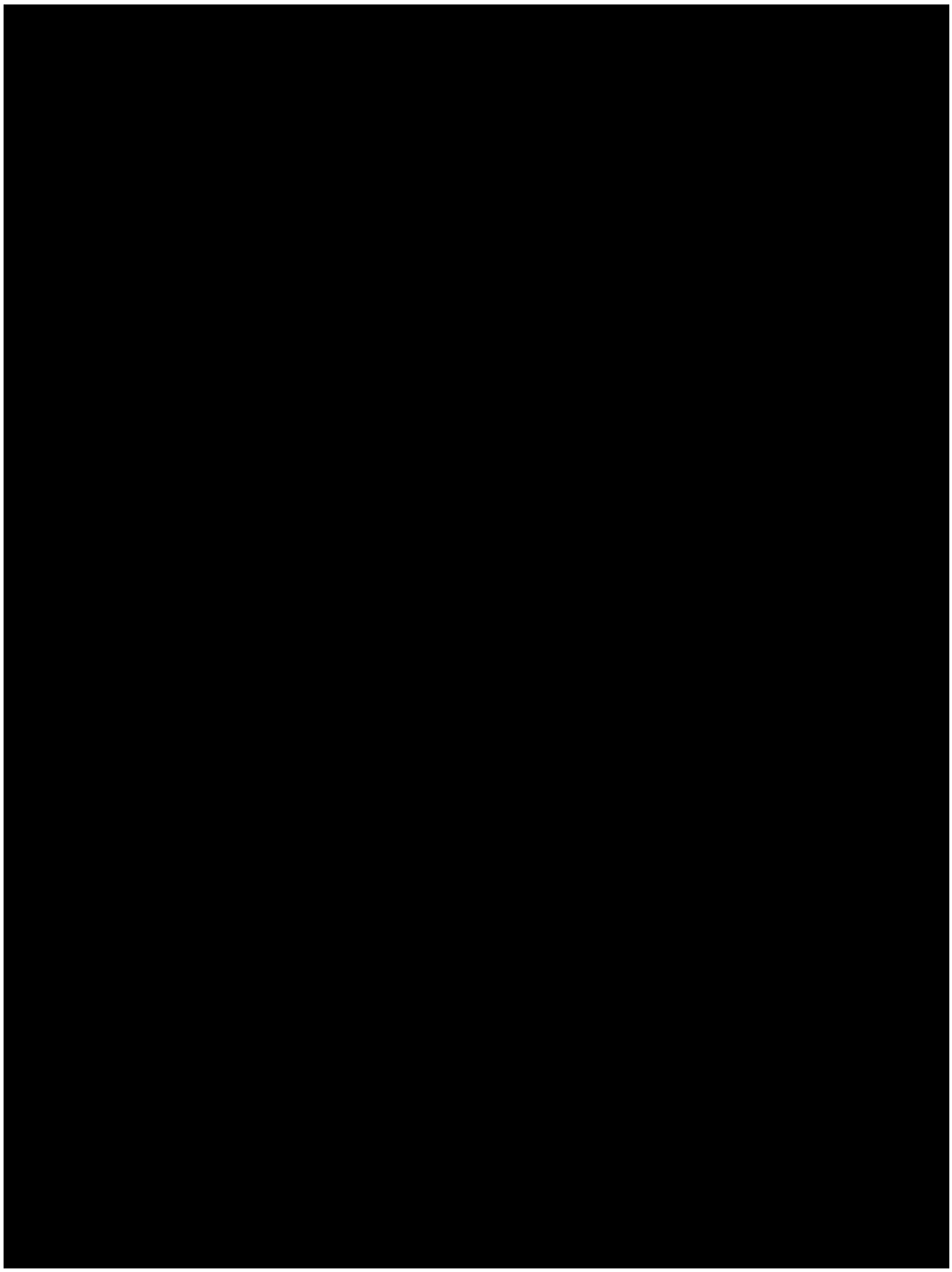

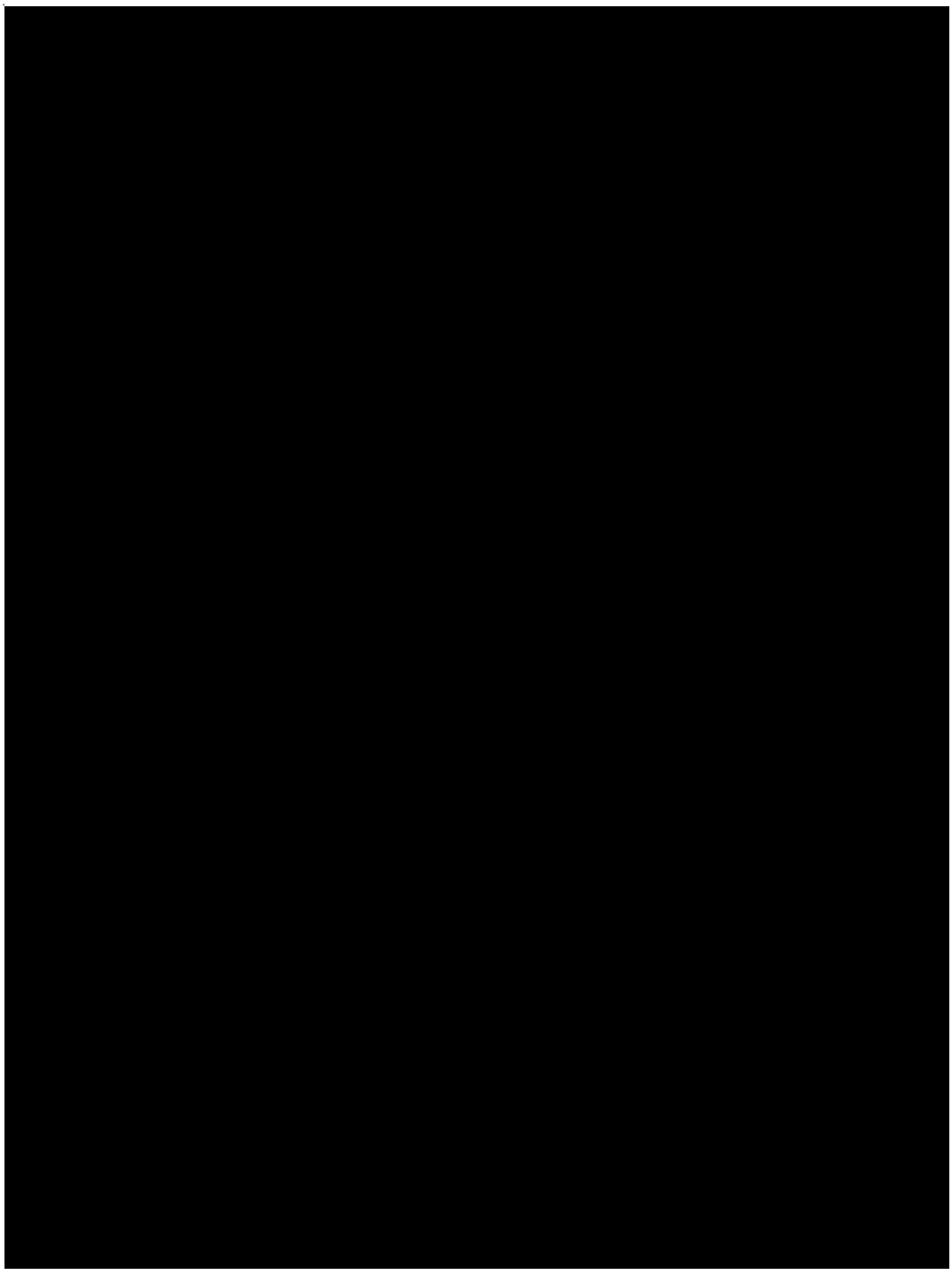

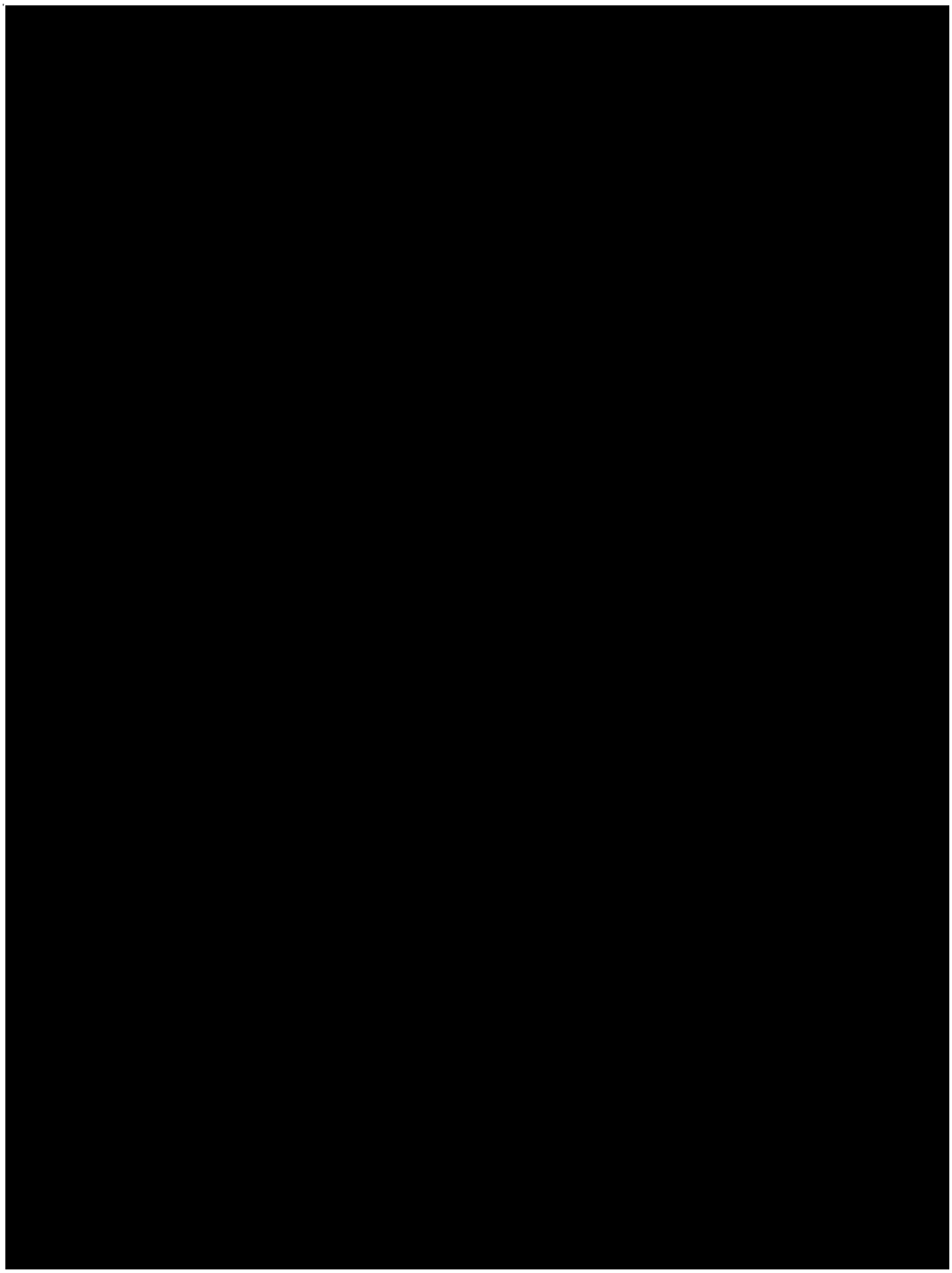

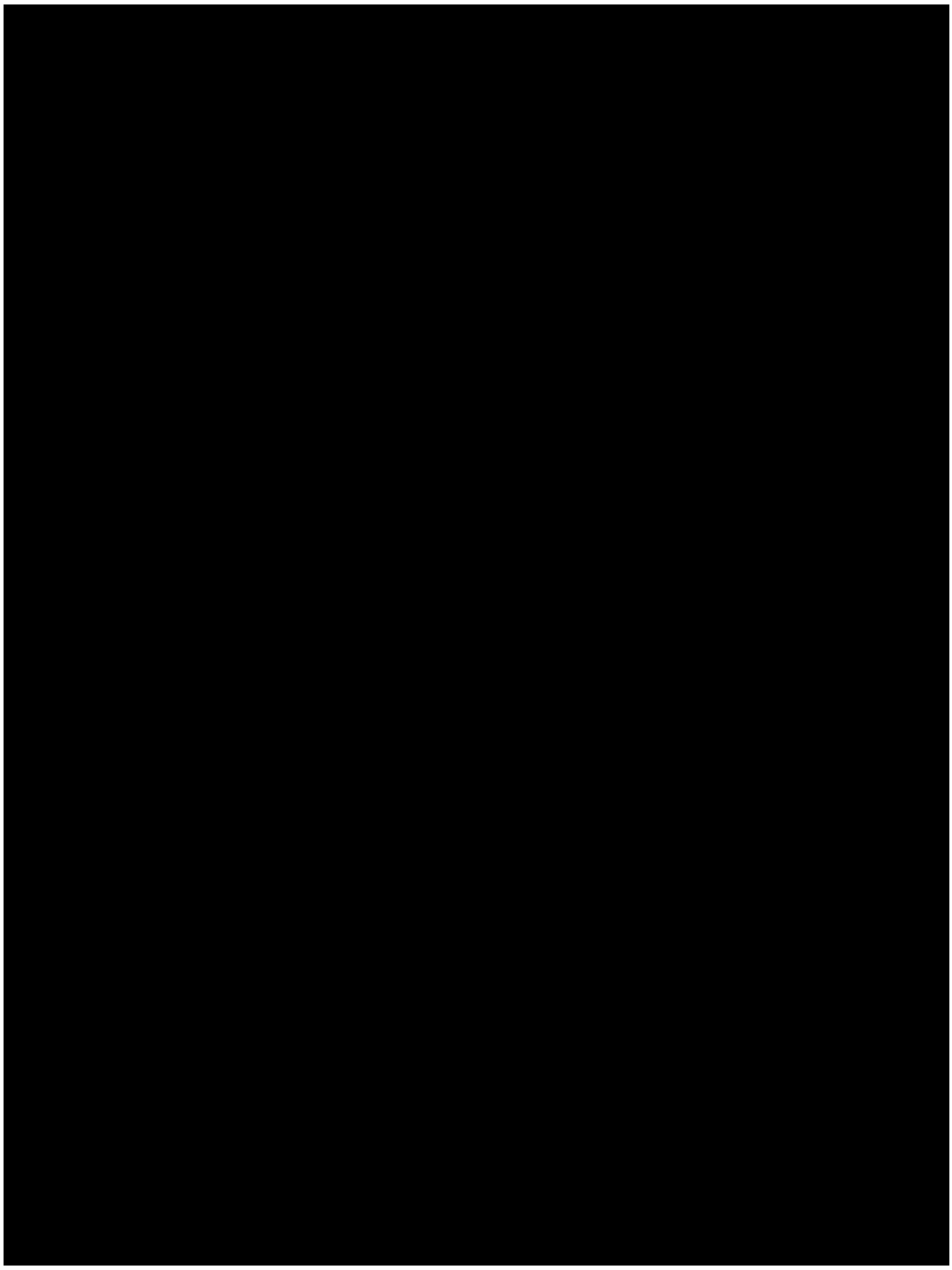

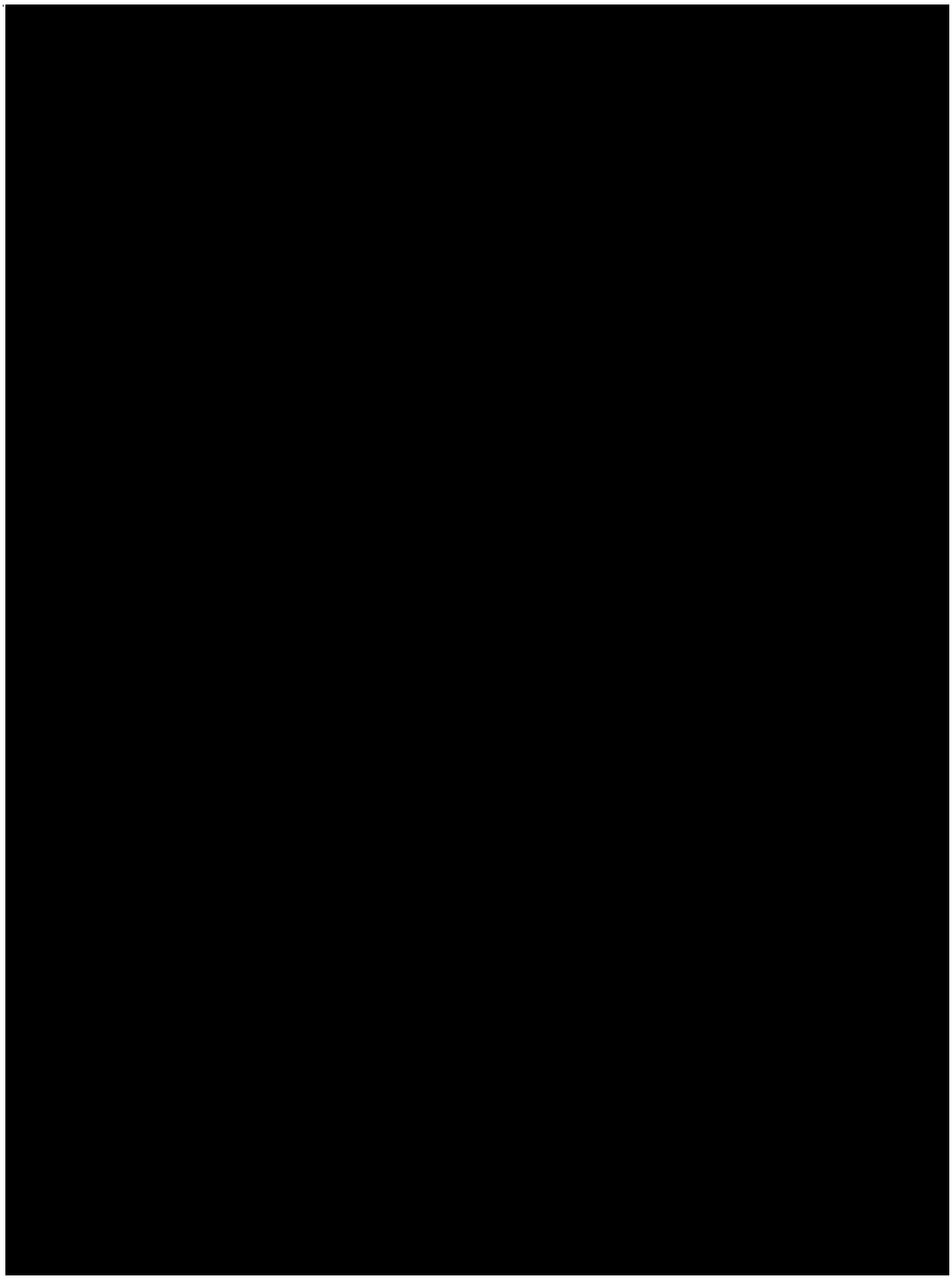

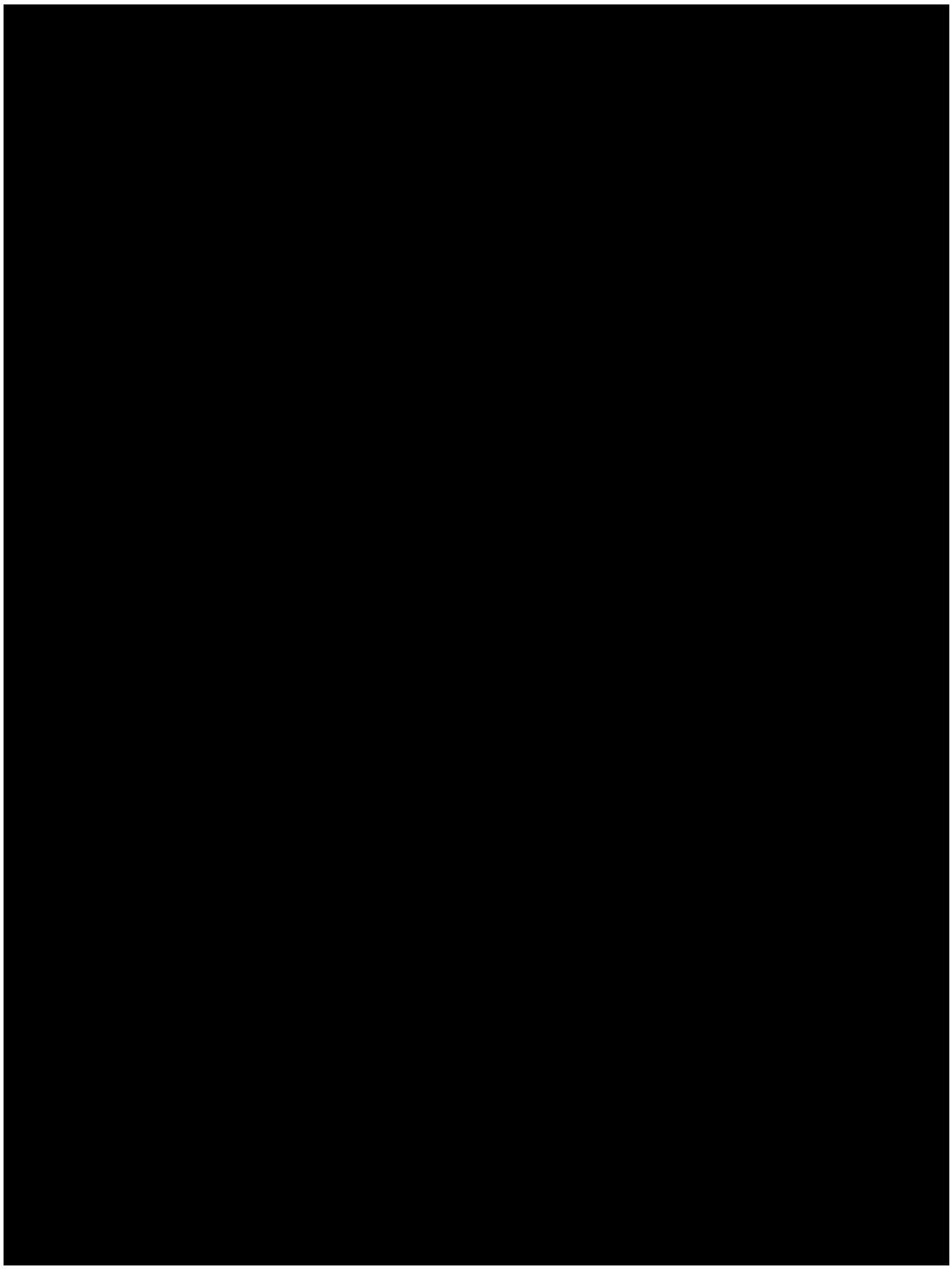

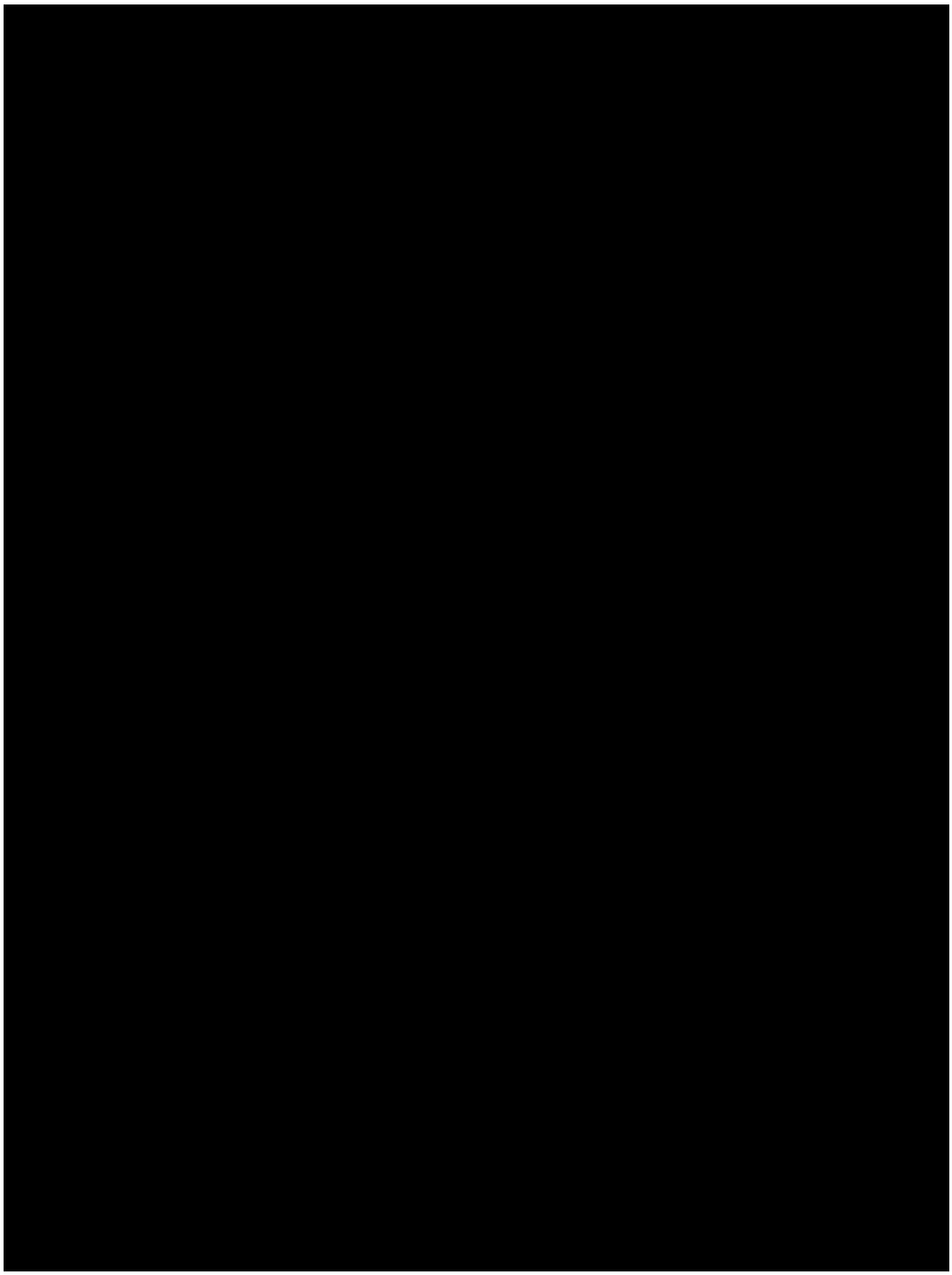

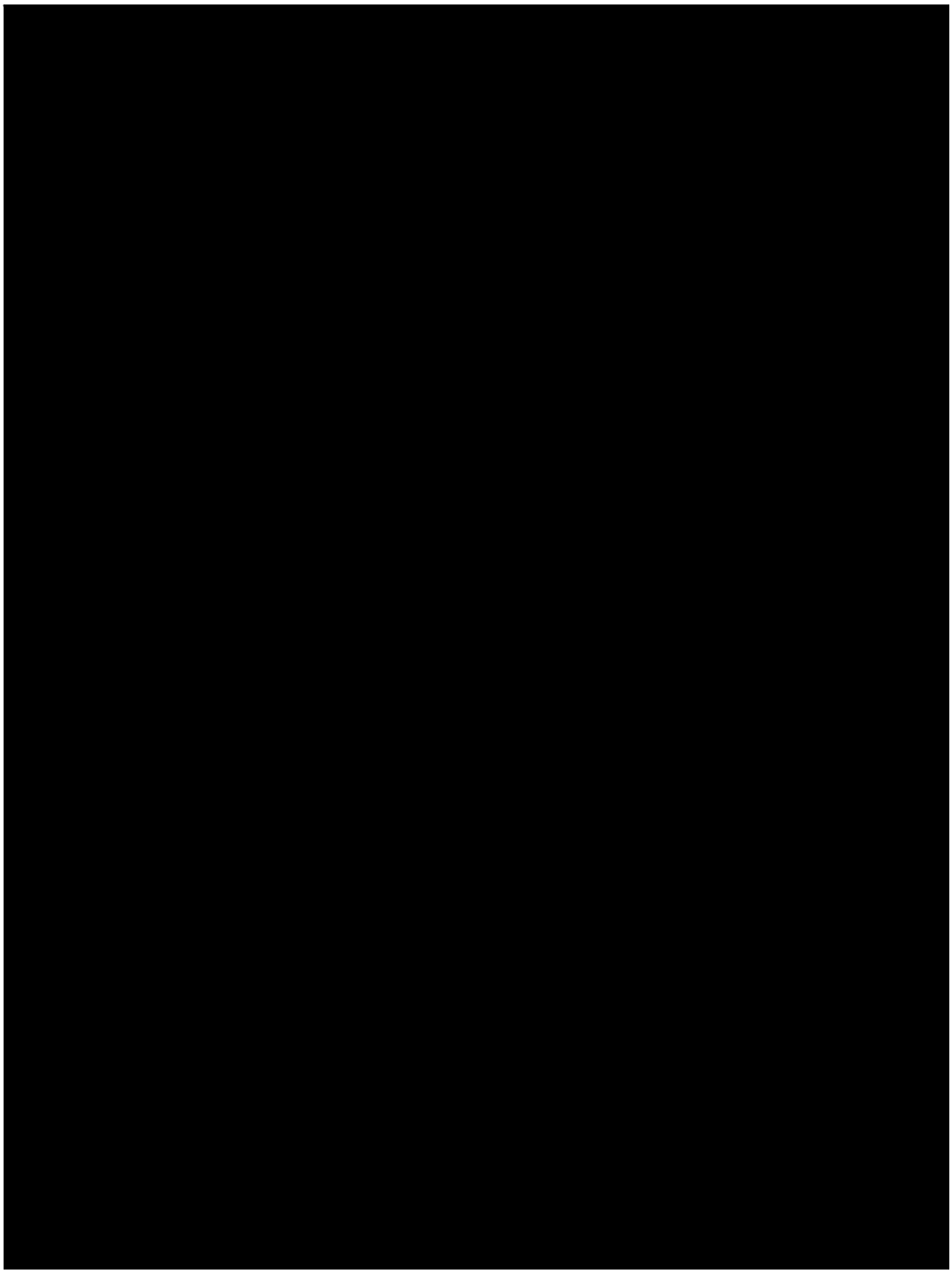

APPENDIX 2 – PUBLICATIONS

Imaging the placental glycocalyx with transmission electron microscopy

Anna C.M. Fabre-Gray, Colin J. Down, Christopher R. Neal, Rebecca R. Foster, Simon C. Satchell, Victoria L. Bills

Placenta
Volume 74, 15 December 2018, Pages 59-61

https://doi.org/10.1016/j.placenta.2018.12.004

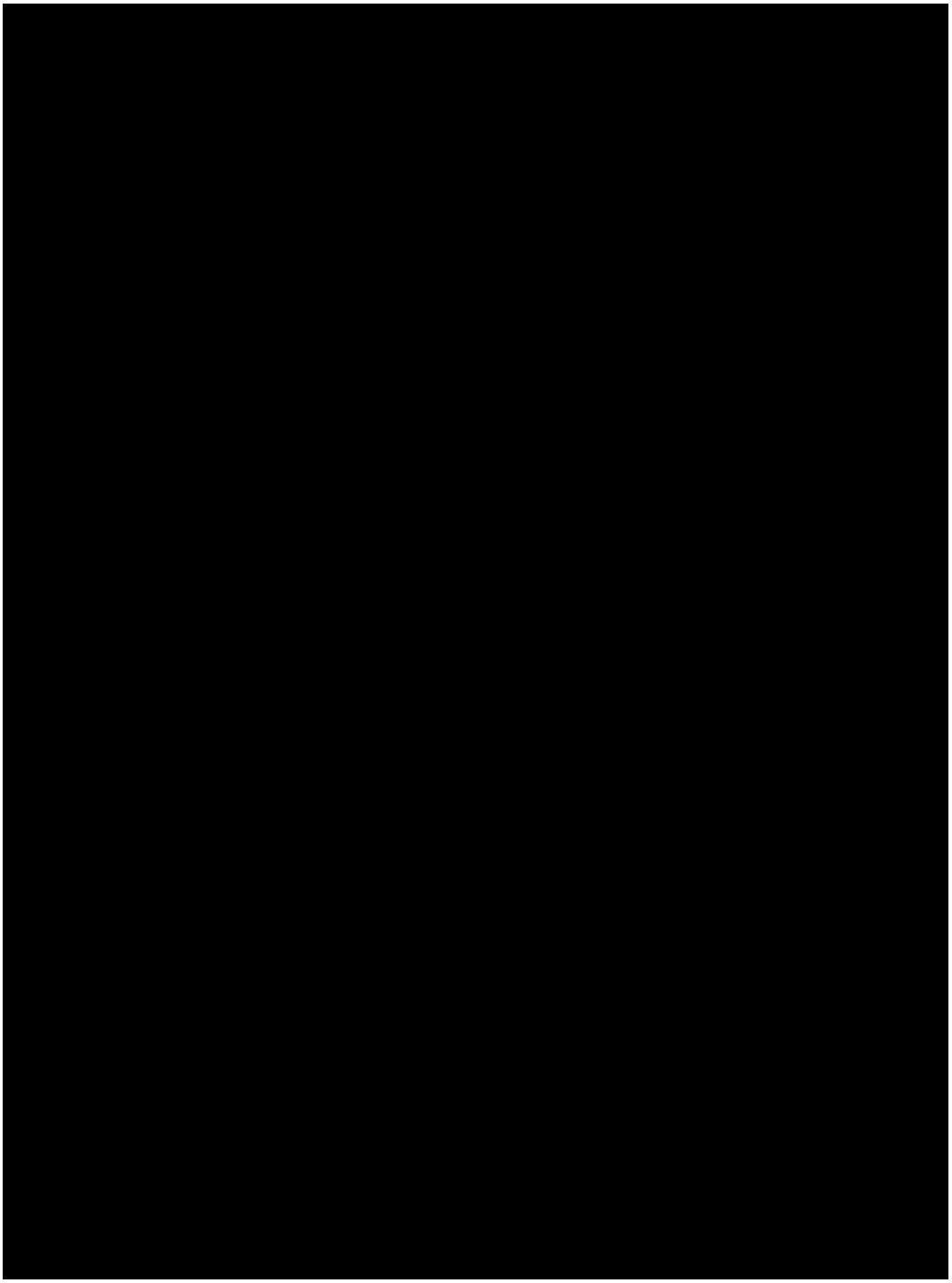

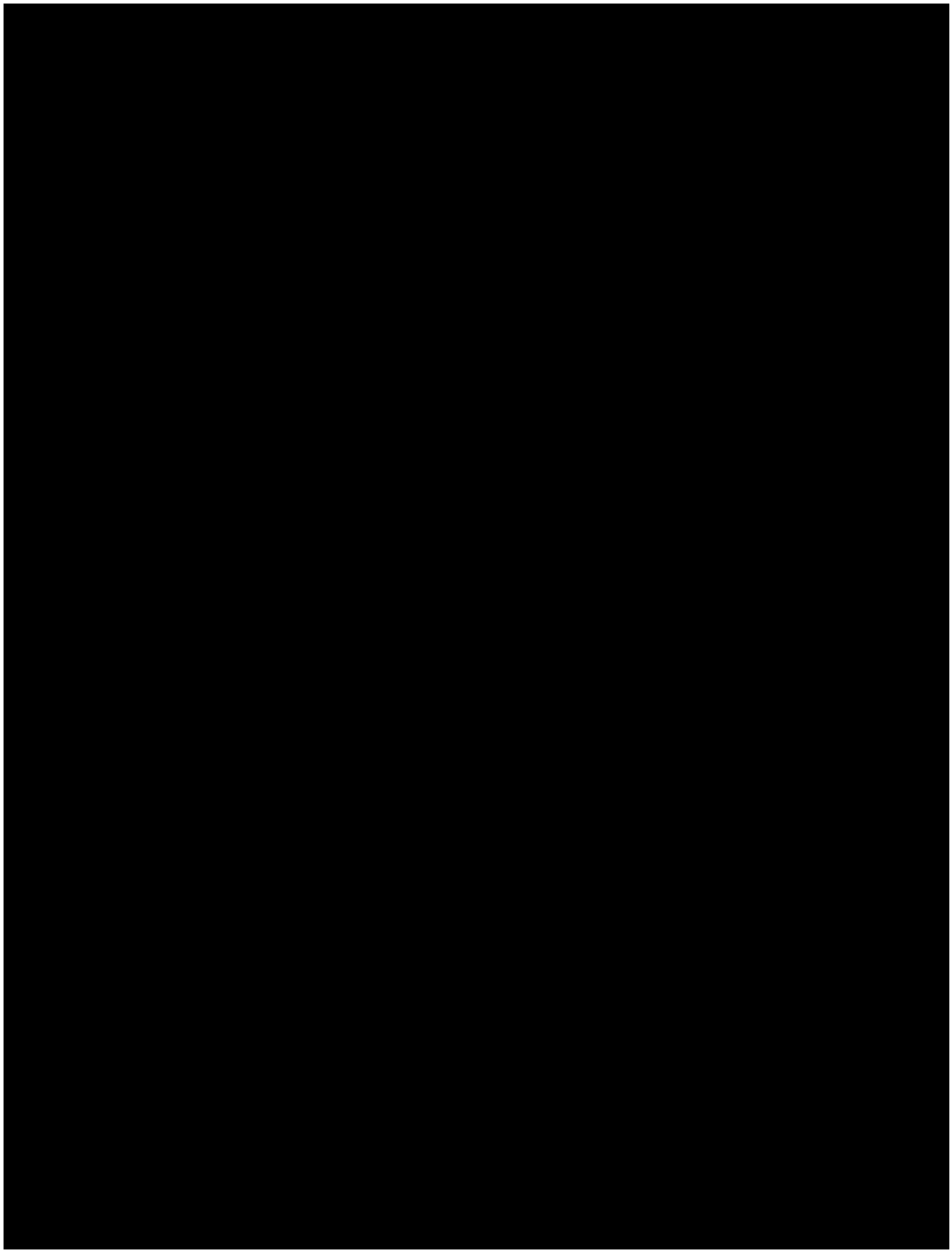

APPENDIX 3 – PARTICIPANT INFORMATION SHEET

Participant Information Sheet
February 2019 – Version 8

University of BRISTOL

Dr Colin Down
Researcher
Level D, Research Office
St Michael's Hospital, Southwell St
Bristol, BS2 8EG

T: **0117 3425622**
Email: colin.down@uhbristol.nhs.uk

INVESTIGATING BLOOD VESSEL LEAKINESS IN PREGNANCY

VASCULAR PERMEABILITY IN PRE-ECLAMPSIA AND DIABETES

Invitation
You are being invited to take part in a research study. Before you decide to take part, it is important for you to understand why the research is being done and what it will involve. Please take time to read the following information and discuss it with others if you wish. You can ask the research team any questions you might have before deciding whether or not you wish to take part.

Purpose of this study
All blood vessels in the body are lined by a cell layer called endothelium; in turn this is covered in another layer called glycocalyx. There is lots of evidence to say that the glycocalyx is important for the way blood vessels work.

Pre-eclampsia is a condition which develops in pregnancy and can cause high blood pressure and protein in the urine. Very rarely it can also cause life-threatening complications in both mothers and their babies. Gestational diabetes is another pregnancy condition causing high blood sugars in pregnancy, which can also have complications for mothers and their babies. Although we can monitor and treat women with these conditions, there is no cure other than delivery of the baby.

In both pre-eclampsia and gestational diabetes blood vessels become leakier. We think that this may be because the glycocalyx is damaged, although this has never been studied before. This research will help show what happens in these conditions and may help develop a way to diagnose, treat or prevent them in the future.

Why have I been chosen?
Thankfully the majority of women will not develop pre-eclampsia or diabetes in their pregnancies, and will form part of our healthy control group, making a vital contribution to the study. Similarly, a group of non-pregnant healthy women will also allow for comparison of glycocalyx levels outside of pregnancy. Other women will have been selected because you have been diagnosed with either pre-eclampsia or diabetes.

Do I have to take part?
It is entirely up to you to decide if you want to take part in the study or not. If you change your mind after enrolling in the study, you can stop participating at any time without providing a reason. This will not affect your normal pregnancy care.

What will happen to me if I take part?
During your pregnancy you still have the normal care offered to all pregnant women and you will see you midwife or doctor at regular intervals. If you choose to take part in the study, you will also be invited to meet a member of the research team on up to 4 occasions about a month apart until you have your baby. Usually there will be at the same time as your routine appointments, but some may involve coming to hospital for an extra visit.

The visits will usually last no longer that 30 minutes and may involve the following:

1) A measurement of your blood pressure
2) A blood test (about 2 ½ teaspoons is required)
3) Collection of a sample of urine
4) A measurement of the blood vessels under your tongue. This involves a small camera being placed under the tongue of up to two minutes. It is similar to having your temperature taken and is completely painless.

After you deliver your baby, we also request a small $1cm^3$ sample of your placenta. Your placenta is normally disposed of by hospital staff unless you wish to take it home. If you were to deliver your baby by caesarean section the surgeon may also take a small 0.5 cm^3 sample of your womb muscle for the study. This will add no more than 1 minute to the operating time and poses no additional risk.

All samples will be processed and stored securely. With your permission these samples may also be used in future research studies that have appropriate ethical approval.

What are the disadvantages and risks of taking part?
The visits may take up to 30 minutes of your time, although we try to organise this when you are already at the hospital. Unfortunately, we are unable to fund travel expenses.

What are the benefits of taking part?
There are no personal benefits to you in taking part, however, we hope the results will let us understand more about why some women get pre-eclampsia and gestational diabetes, benefiting pregnant women in the future.

What if new information becomes available?
Sometimes during a study new information on the topic of investigation is published by someone else. If this happens, we will discuss whether you want to continue with the study.

What if something goes wrong?
The study will be registered with the University of Bristol Insurance Scheme. If you are unhappy about your treatment during this study and wish to complain, the National Health Service's complaints protocol will be available to you.

Will my taking part be kept confidential?
Yes. Data will be stored confidentially with only members of the research team and regulatory authorities allowed access. With your consent, we will let your GP know that you are taking part.

What will happen to the results of the research study?
The results will not be available immediately, it may take several years to analyse and draw conclusions. We intend to publish the results of the study in professional medical journals, please let the research team know if you would like to receive a copy of any publications.

Who is funding and organising the study?
The David Telling Charitable Trust and The Capella Foundation have awarded the University of Bristol and the research team with the funding for this study.

Who has reviewed this study?
South West - Central Bristol Research Ethics Committee has reviewed this study and has granted it ethical approval.

Thank you for reading this information sheet.
Feel free to ask any questions before deciding whether to participate. If you would like to know more about pre-eclampsia or gestational diabetes please ask a member of the research team.

APPENDIX 4 – CONSENT FORM

Dr Colin Down
Researcher
Level D, Research Office
St Michael's Hospital, Southwell St
Bristol, BS2 8EG

T: 0117**3425622**
Email: colin.down@uhbristol.nhs.uk

Study Identification Number:
Patient T Number:

CONSENT FORM

Title of Project: Vascular Permeability in Pre-eclampsia and Diabetes

Name of Researchers: Dr Colin Down, Dr Charles Heffer, Dr Victoria Bills,

Please initial box

1. I confirm that I have read and understand the participant information sheet dated **February 2019 (version 8)** and have had the opportunity to ask questions. ☐

2. I understand that my participation is voluntary and that I am free to withdraw at any time, without providing a reason. My medical care or legal rights are unaffected. ☐

3. I understand that relevant sections of my medical notes may be looked at by responsible individuals from the research team and regulatory authorities. I give permission for these individuals to have access to my records. ☐

4. I agree to that samples of my tissue, blood and urine may be used as described in the participant information sheet. If I decide to stop taking part in the study, I can request that samples already collected are destroyed. I understand any experimental results already obtained would be kept. ☐

5. I agree that my data and samples of tissue, blood and urine can be securely stored and used for future studies that have received ethical approval. ☐

6. I agree for you to contact my GP to advise them of my participation in this study. ☐

7. I agree to take part in the study as described in the participant information sheet ☐

_____	_____	_____
Name of participant	Date	Signature
_____	_____	_____
Name of person taking consent	Date	Signature

APPENDIX 5 – CASE REPORT FORM

University of BRISTOL

University Hospitals Bristol NHS Foundation Trust

PARTICIPANT ID: _____

HOSPITAL NUMBER: _____

VASCULAR PERMEABILITY IN PRE-ECLAMPSIA & DIABETES

CASE REPORT FORM

SECTION A: Confirmation of Eligibility

The following criteria MUST be answered YES for participant inclusion	**Yes**	**No**
Viable pregnancy ≥ 12 weeks' gestation	☐	☐
Singleton pregnancy	☐	☐
Age ≥ 18 years	☐	☐

At least ONE of the following criteria MUST be answered YES for inclusion		
Diagnosis of pre-eclampsia = A + B or C A) New onset hypertension after 20 weeks' gestation. Systolic BP ≥140 or diastolic ≥90 on two occasions 4 hours apart OR systolic BP ≥160 or diastolic BP ≥ 110 on one occasion. B) Significant proteinuria. PCR ≥ 30 mg/mmol or ≥ 300mg / 24 hours. C) Evidence of end-organ involvement (in the absence of another cause). i) Platelets < 100,000 µ/L ii) ALT/AST twice upper limit of normal iii) Serum creatinine > 97 µmol/L or > double baseline iv) Utero-placental dysfunction (IUGR, abnormal dopplers, stillbirth) **Diagnosis of superimposed pre-eclampsia** B and/or C presenting after 20 weeks' gestation in a patient with pre-existing hypertension	☐	☐
Diagnosis of Gestational Diabetes Mellitus = A or B A) Fasting glucose ≥ 5.6 mmol/L B) 2-hour glucose ≥ 7.8 mmol/L **Pre-existing Diabetes Mellitus** Pre-existing diagnosis of type 1 or type 2 diabetes mellitus controlled with diet, oral medication or insulin	☐	☐
Control Pregnancy without pre-eclampsia, superimposed pre-eclampsia or diabetes.	☐	☐

Participant's Eligibility - Investigator Sign-Off:	
Is the participant eligible to take part in the study?	☐ Yes ☐ No
Investigator's Signature: _____ **Date:** __ __ / __ __ / __ __ __ __ (DD / MM / YYYY) **Investigator's Name:** _____	Record on subject screening and recruitment record

University of BRISTOL

NHS University Hospitals Bristol NHS Foundation Trust

SECTION B: Demographics and Booking History

Complete for all participants at enrolment (history from medical record)

Date form completed: __ __ / __ __ / __ __ __ __
(DD / MM / YYYY)

Informed Consent			
Date participant signed written consent form:	__ __ / __ __ / __ __ __ __ (DD / MM / YYYY)	Date copy of consent form to patient and GP.	__ __ / __ __ / __ __ __ __ (DD / MM / YYYY)
Name of person taking informed consent: _____			

Date of Birth:	__ __ / __ __ / __ __ __ __ (DD / MM / YYYY)	Date of booking visit	__ __ / __ __ / __ __ __ __ (DD / MM / YYYY)
Confirmed EDD (by USS)	__ __ / __ __ / __ __ __ __ (DD / MM / YYYY)		

Booking Examination	
Booking Blood Pressure ___ ___ ___ / ___ ___ ___ mmHg	
Booking Weight: ___ ___ ___ . ___ kg	Height: ___ . ___ ___ m BMI: ___ ___ . ___ kg/m^2
Booking dipstick Proteinuria (≥1+):	☐ No ☐ Yes
If yes, PCR sent?	☐ No ☐ Yes PCR result ___ ___ ___ mg/mmol

Has the Participant Ever Smoked? ☐ **No** ☐ **Yes,** Complete Below	
☐ Current Smoker	Participant's average daily use: ___ ___ / day
☐ Former smoker	Smoking ceased within 12 months prior to conception? ☐ No ☐ Yes

University of BRISTOL

University Hospitals Bristol NHS Foundation Trust

PARTICIPANT ID: _____

HOSPITAL NUMBER: _____

Date form completed: __ __ / __ __ / __ __ __ __
(DD / MM / YYYY)

Previous Pregnancy		☐ **No** ☐ **Yes,** Complete below			
Non-registerable births (miscarriage or termination of pregnancy <24 weeks)					
Date (DD/MM/YYYY)	Gestation (weeks + days)	Pregnancy complications			
___/____/____					
___/____/____					
___/____/____					
Registerable Births (live births of any gestation or stillbirths ≥ 24 weeks gestation)					
Date (DD/MM/YYYY)	Gestation at delivery (weeks + days)	Mode of delivery (SVD / Forceps / ventouse / LSCS)	Birth weight (kg)	Sex	Pregnancy complications (including previous PET and GDM)
___/____/____					
___/____/____					
___/____/____					
___/____/____					
___/____/____					
Continue on separate sheet if required					

University of BRISTOL

NHS University Hospitals Bristol NHS Foundation Trust

Date form completed: __ / __ / ____

Hypertension Risk Factors at Booking					
Minor risk factors (2 required)			**Major risk factors (1 required)**		
Primiparity	☐ No	☐ Yes	Hypertension in previous pregnancy	☐ No	☐ Yes
Age ≥ 40	☐ No	☐ Yes	Chronic kidney disease	☐ No	☐ Yes
Pregnancy interval > 10 years	☐ No	☐ Yes	Autoimmune disease (APLS / SLE)	☐ No	☐ Yes
BMI ≥ 35	☐ No	☐ Yes	Type 1 or 2 diabetes	☐ No	☐ Yes
Family History of pre-eclampsia	☐ No	☐ Yes	Chronic hypertension	☐ No	☐ Yes
Multiple pregnancy	☐ No	☐ Yes			

Antenatal Aspirin Offered?	☐ No	☐ Yes

Pregnancy risk factors		
Pregnancy risk factors highlighted by midwife? (e.g. significant medical history, SGA pathway etc.)	☐ No	☐ Yes
If yes, please list:		
Referred for Consultant led care?	☐ No	☐ Yes

Ethnicity							
White	White British	☐	White Irish	☐	White Other	☐	
Mixed race	White & Black Caribbean	☐	White & Black African	☐	White & Asian	☐	Other mixed background ☐
Asian or Asian British	Indian	☐	Bangladeshi	☐	Pakistani	☐	Other Asian background ☐
Black or Black British	Caribbean	☐	African	☐	Black Other	☐	
Chinese or other	Chinese	☐	Other ☐ (please specify)				

University of BRISTOL

NHS University Hospitals Bristol NHS Foundation Trust

PARTICIPANT ID: _____

HOSPITAL NUMBER: _____

SECTION C: Study visit
Complete at enrolment

Date form completed: __ __ / __ __ / __ __ __ __
(DD / MM / YYYY)

Gestation ___ ___ weeks ___ days		Blood Pressure ___ ___ ___ / ___ ___ ___ mmHg
Current antihypertensive therapy?	☐ No ☐ Yes	☐ Labetalol ☐ Methyldopa ☐ Nifedipine ☐ Other _____
Current diabetic therapy?	☐ No ☐ Yes	☐ Metformin ☐ Insulin ☐ Other _____
Current LMWH Heparin (Clexane) If yes, timing of last dose	☐ No ☐ Yes	__ __ / __ __ / __ __ __ __ (DD/MM/YYY) ___ ___ : ___ ___ (HH:MM)
Any other current medication?	☐ No ☐ Yes	

GlycoCheck			
Readings taken after 5-minute period of rest. When recording the camera should be slowly moved to a neighbouring position of the sublingual mucosa and remain there for 5 seconds, aiming for around 10 different positions. Minimum 3 repeats.			
Time since last ate ___ ___ : ___ ___ HH : MM		Time since last drank ___ ___ : ___ ___ HH : MM	
Caffeine in last 6 hours	☐ No ☐ Yes		
GlycoCheck Reading 1 (PBR 5 – 25)	___ . ___ ___ µm	Reading taken by	_____
GlycoCheck Reading 2 (PBR 5 – 25)	___ . ___ ___ µm	Reading taken by	_____
GlycoCheck Reading 3 (PBR 5 – 25)	___ . ___ ___ µm	Reading taken by	_____
Test comments?			

University of BRISTOL

NHS University Hospitals Bristol NHS Foundation Trust

Date form completed: __ __ / __ __ / __ __ __ __
(DD / MM / YYYY)

Haematology / Biochemistry		
Has the patient had any haematology or biochemistry tests performed in the last **2 weeks** as part of their medical care? If yes, please complete **most recent** result below		☐ No ☐ Yes
Haemoglobin (Hb)	___ ___ ___ g/L	__ __ / __ __ / __ __ __ __ (DD/MM/YYYY)
Platelets (plts)	___ ___ ___ x10^9/L	__ __ / __ __ / __ __ __ __ (DD/MM/YYYY)
Creatinine (Cr)	___ ___ ___ µmol/L	__ __ / __ __ / __ __ __ __ (DD/MM/YYYY)
Alanine Aminotransferase (ALT)	___ ___ ___ IU/L	__ __ / __ __ / __ __ __ __ (DD/MM/YYYY)
Glycosylated Haemoglobin (HbA1c)	___ ___ . ___ mmol/mol	__ __ / __ __ / __ __ __ __ (DD/MM/YYYY)
Urine Protein/Creatinine Ratio	___ ___ ___ mg/mmol	__ __ / __ __ / __ __ __ __ (DD/MM/YYYY)

Study Samples			
Date of sample collection __ __ / __ __ / __ __ __ __ (DD/MM/YYYY)			
Venepuncture (x2 EDTA & x2 Red)?	☐ No ☐ Yes	Clean catch urine sample in clear specimen container?	☐ No ☐ Yes
Centrifuge whole blood at 3000 rpm for 10 minutes within 1 hour of collection. Separated plasma / serum and urine is divided into 500 µL and frozen at -20°C for maximum 1 month before transfer to -80°C			
Record participation in hand-held notes and leave note or sticker on front of partogram: **"CONSENTED TO SPADE STUDY, CALL COLIN WHEN PRESENTS IN LABOUR (DAY OR NIGHT)"**			

University of BRISTOL

University Hospitals Bristol NHS Foundation Trust

PARTICIPANT ID: _____

HOSPITAL NUMBER: _____

SECTION D: Delivery Outcomes

Date form completed: __ __ / __ __ / __ __ __ __
(DD / MM / YYYY)

Pre-Labour				
Were antenatal steroids administered?	☐ No ☐ Yes			
If yes, when?	Dose 1	__ __ / __ __ / __ __ __ __ (DD/MM/YYY) __ __ : __ __ (HH:MM)	Dose 2	__ __ / __ __ / __ __ __ __ (DD/MM/YYY) __ __ : __ __ (HH:MM)
Prolonged Rupture of membranes (> 24 hours)?	☐ No ☐ Yes			

Blood Pressure		
Admission BP ___ ___ ___ / ___ ___ ___ mmHg	Highest Blood Pressure in labour ___ ___ ___ / ___ ___ ___ mmHg	
Antihypertensive therapy at time of admission to labour ward or in labour?	☐ No ☐ Yes	☐ Labetalol ☐ Methyldopa ☐ Nifedipine ☐ Other _____
Intravenous antihypertensives used?	☐ No ☐ Yes	☐ Labetalol ☐ Hydralazine ☐ Other _____
$MgSO_4$ used for pre-eclampsia?	☐ No ☐ Yes	
Evidence of severe pre-eclampsia*	☐ No ☐ Yes	

*** Definition of severe pre-eclampsia (ACOG 2013)**

- **Blood Pressure:** Systolic blood pressure ≥ 160 mmHg or diastolic ≥ 100 mmHg
- **Thrombocytopaenia:** Platelets < 100 x 10^9 L
- **Liver:** ALT twice normal range or persistent right upper quadrant pain unresponsive to analgesia in the absence of an alternative diagnosis
- **Renal:** Serum creatinine > 97 µmol/L or > double baseline Cr
- **Lung:** Pulmonary oedema
- **CNS:** cerebral or visual disturbance including eclampsia

University of BRISTOL

NHS University Hospitals Bristol NHS Foundation Trust

Date form completed: __ __ / __ __ / __ __ __ __
(DD / MM / YYYY)

Glycaemic control in labour		
Diabetic therapy at time of admission to labour ward?	☐ No ☐ Yes	☐ Metformin ☐ Insulin ☐ Insulin Sliding Scale ☐ Other _____

Infection		
Evidence of infection / sepsis prior to delivery? Antibiotics used?	☐ No ☐ Yes	☐ Cefuroxime ☐ Metronidazole ☐ Teicoplanin ☐ Gentamicin ☐ Other _____

LWMH		
Antenatal LMWH? If yes, timing of last dose	☐ No ☐ Yes	__ __ / __ __ / __ __ __ __ (DD/MM/YYY) __ __ : __ __ (HH:MM)

Other medication received in 6 hours prior to placenta delivery (see drug chart +/- anaesthetic chart)					
Analgesia		Omeprazole	☐	**Preterm Labour**	
Paracetamol	☐	Ondansetron	☐	Magnesium Sulphate	☐
Dihydrocodeine	☐	Metoclopramide	☐	Atosiban	☐
Oromorph	☐	Cyclizine	☐	**GBS prophylaxis**	
Entonox	☐	**Uterotonics**		Benzylpenicillin	☐
Readymix (epidural)	☐	Oxytocin	☐	Vancomycin	☐
Anti-emetics and Gastroprotection		Syntometrine	☐	Amoxicillin	☐
Ranitidine	☐	Carbetocin	☐	Cefuroxime	☐
Other (please specify)					

University of BRISTOL

NHS University Hospitals Bristol NHS Foundation Trust

PARTICIPANT ID: _____

HOSPITAL NUMBER: _____

Date form completed: __ __ / __ __ / __ __ __ __
(DD / MM / YYYY)

Delivery Outcome				
Date of Delivery	__ __ / __ __ / __ __ __ __ (DD/MM/YYY)	Time of Delivery	__ __ : __ __ (HH:MM)	
Placenta Delivery Time	__ __ : __ __ (HH:MM)			
Onset of labour	☐ Spontaneous ☐ Induction ☐ Did not labour			
Indication if induction				
Mode of Delivery	☐ Spontaneous vaginal ☐ Assisted vaginal ☐ Pre-labour emergency caesarean ☐ Intrapartum emergency caesarean ☐ Elective caesarean			
Indication if operative birth				
Birth Weight __ __ __ __ g		Apgars 1 min __ __ 5 min __ __ 10 min __ __		
Umbilical Cord Gases Performed		☐ No ☐ Yes		
Result:	Arterial pH __. __ __ __	Arterial BE __ . __	Venous pH __ . __ __ __	Venous BE __ . __
Admission to NICU?		☐ No ☐ Yes		

University of BRISTOL

NHS University Hospitals Bristol NHS Foundation Trust

Date form completed: __ __ / __ __ / __ __ __ __
(DD / MM / YYYY)

Haematology / Biochemistry		
Has the patient had any haematology or biochemistry tests performed prior to delivery? If yes, please record the most recent (do not duplicate if same as previous)		☐ No ☐ Yes ☐ As previous
Haemoglobin (Hb)	___ ___ ___ g/L	__ __ / __ __ / __ __ __ __ (DD/MM/YYY)
Platelets (plts)	___ ___ ___ x10^9/L	__ __ / __ __ / __ __ __ __ (DD/MM/YYY)
Creatinine (Cr)	___ ___ ___ µmol/L	__ __ / __ __ / __ __ __ __ (DD/MM/YYY)
Alanine Aminotransferase (ALT)	___ ___ ___ IU/L	__ __ / __ __ / __ __ __ __ (DD/MM/YYY)
Urine Protein/Creatinine Ratio	___ ___ ___ mg/mmol	__ __ / __ __ / __ __ __ __ (DD/MM/YYY)

Placental Sampling
Electron Microscopy: Prepare 2 ml 0.2M CaC, and 2 ml 5% GA in 0.1% Alcian Blue (0.004g). 1 x 1 cm placental biopsy. Immersion fixation. Store at 4°C overnight (up to maximum 36 hours) and then wash 3 x 10 mins in 0.1M CaC. Remain in 0.1M CaC until processing. Lectins: Prepare 1 ml 0.4M PO_4 buffer (pH 7.20), 1ml 16% PFA, 2 ml distilled H_2O x 2. 1 x 1 cm placental biopsy. 1 x 1 cm cord biopsy. Immersion fixation. Store at 4°C overnight (up to maximum 36 hours) and then wash 3 x 10 mins in 0.1M PO_4 buffer. Leave in 70% ETOH until histology processing.
Time from placenta delivery to fixation ___ ___ : ___ ___ (HH:MM)

APPENDIX 6 – MACRO CODE CAPILLARY

```
mainWin = getTitle();

// Get position of marker
Roi.getCoordinates(xpoints, ypoints);
xCent = xpoints[0];
yCent = ypoints[0];

// Show dialog
Dialog.create("Settings");
Dialog.addNumber("Start radius (px)", 0);
Dialog.addNumber("End (px)",30);
Dialog.addNumber("Starting angle (degs)",0);
Dialog.addNumber("Ending angle (degs)",360);
Dialog.addNumber("Number of radial measurements",200);
Dialog.show();

startRadPx = Dialog.getNumber();
endRadPx = Dialog.getNumber();
thStart = Dialog.getNumber();
thEnd = Dialog.getNumber();
nMeas = Dialog.getNumber();

// Extract channels of interest
selectWindow(mainWin);
run("Make Substack...", "channels=2");
ch2 = getTitle();
selectWindow(mainWin);
run("Make Substack...", "channels=3");
ch3 = getTitle();

// Taking radial intensity measurements
takeMeas(ch2,thStart,thEnd,nMeas,xCent,yCent,startRadPx,endRadPx,"CH2");
takeMeas(ch3,thStart,thEnd,nMeas,xCent,yCent,startRadPx,endRadPx,"CH3");

measurePeakDifference("[CH2] Peak pos (px)","[CH3] Peak pos (px)","Peak separation (px)");
measurePeakDifference("[CH2] Fit b","[CH3] Fit b","Fit separation (px)");

run("Summarize");

function takeMeas(imageName, thStart, thEnd, nMeas, xCent, yCent, startRadius, endRadius, label) {
    thStep = (thEnd-thStart)/nMeas;
    for (i=0; i<nMeas; i++) {
        selectWindow(imageName);
        th = (thStart + i*thStep)*PI/180;

        // Selecting the line
        makeLine(xCent+startRadius*cos(th), yCent + startRadius*sin(th), xCent+endRadius*cos(th), yCent + endRadius*sin(th));
        setLineWidth(1);

        // Recording the intensity profile and adding it to a results table
        profile = getProfile();

        // Getting x-coordinates
        x = newArray(lengthOf(profile));
        for (j=0;j<lengthOf(x);j++) x[j] = j;

        setResult("Angle (degs)", i, th*180/PI);

        // Iterate over each profile, getting the raw peak position
        peakPos = getPeakPosition(x,profile);
        setResult("["+label+"] Peak pos (px)", i, peakPos[0]);

        // Fitting a Gaussian to each profile
        Fit.doFit("Gaussian (no offset)", x, profile);
        Fit.plot();
        close();

        // Iterate over each profile fit, getting the peak position
        setResult("["+label+"] Fit a (amplitude)", i, Fit.p(0));
        setResult("["+label+"] Fit b", i, Fit.p(1));
        setResult("["+label+"] Fit c (width)", i, Fit.p(2));

    }
}

function getPeakPosition(xx,yy) {
    xMax = 0;
    yMax = 0;
    for (i=0;i<lengthOf(xx);i++) {
        if (yy[i] > yMax) {
            xMax = xx[i];
            yMax = yy[i];
        }
    }

    return newArray(xMax,yMax);

}

function measurePeakDifference(labelIn1, labelIn2, labelOut) {
    for (i=0;i<nResults();i++) {
        peak1 = getResult(labelIn1, i);
        peak2 = getResult(labelIn2, i);

        difference = peak2-peak1;

        setResult(labelOut, i, difference);

    }
}
```

APPENDIX 7 – MACRO CODE SYNCYTIOTROPHOBLAST

```
// Variables
minHoleSize = 300000;
fitW = 20;
roiW = 50;
everyNth = 10;
showPlots = true;
showSelections = true;

// Preparing ImageJ
mainWin = getTitle();
setOption("BlackBackground", false);
setBatchMode("hide");
close("Results");

// Get different images
run("Make Substack...", "channels=1");
rename("BlueWin");
run("Duplicate...", " ");
run("Enhance Contrast", "saturated=0.35");
run("Enhance Contrast", "saturated=0.35");
run("Enhance Contrast", "saturated=0.35");
run("Apply LUT");
rename("BlueNormWin");
selectWindow(mainWin);
run("Make Substack...", "channels=2");
rename("GreenWin");
run("Duplicate...", " ");
run("Enhance Contrast", "saturated=0.35");
run("Enhance Contrast", "saturated=0.35");
run("Enhance Contrast", "saturated=0.35");
run("Apply LUT");
rename("GreenNormWin");
selectWindow(mainWin);
run("Make Substack...", "channels=3");
rename("RedWin");
run("Duplicate...", " ");
run("Enhance Contrast", "saturated=0.35");
run("Enhance Contrast", "saturated=0.35");
run("Enhance Contrast", "saturated=0.35");
run("Apply LUT");
rename("RedNormWin");

getDimensions(width, height, channels, slices, frames);
maxW = maxOf(fitW,roiW);

// Image pre-processing
imageCalculator("Add create", "BlueNormWin","GreenNormWin");
rename("CombiWin");
imageCalculator("Add", "CombiWin","RedNormWin");
run("Median...", "radius=20");
run("Auto Threshold", "method=Percentile white");
run("Erode");
run("Analyze Particles...", "size="+minHoleSize+"-Infinity pixel show=Masks include");
rename("BinaryWin");
run("Invert LUT");
run("Duplicate...", " ");
rename("EdgeWin");
run("Outline");
run("Skeletonize");

greenProfile = newArray(roiW*2+1);
redProfile = newArray(roiW*2+1);

var xArr = 0;
var yArr = 0;

// Iterating over all pixels, looking for edge pixels (except the outer ring)
nMeas = 0;
count = -1;
for (x=maxW;x<width-maxW;x++) {
    for (y=maxW;y<height-maxW;y++) {
        selectWindow("EdgeWin");
        if (getPixel(x, y) == 0) {
            count = count + 1;

            if (count % everyNth == 0) {
                // Get local line centred on point
                count = countLocalPoints(x,y,fitW);

                // Getting arrays of local points
                xArr = newArray(count);
                yArr = newArray(count);
                getLocalPoints(x,y,fitW);

                // Fitting a line to the points
                Fit.doFit("Straight Line", xArr, yArr);

                Array.getStatistics(xArr, min, max, mean, stdDev);
                if (min == max) theta = PI/2;
                else theta = atan(Fit.p(1));
```

```
91
92                  // Creating a line with this gradient
93                  x1 = x-roiW*cos(theta);
94                  x2 = x+roiW*cos(theta);
95                  y1 = y-roiW*sin(theta);
96                  y2 = y+roiW*sin(theta);
97
98                  // Check if coordinates need to be flipped
99                  if (testInversion("BinaryWin",x1,y1,x2,y2)) {
100                     x3 = x1;
101                     y3 = y1;
102                     x1 = x2;
103                     y1 = y2;
104                     x2 = x3;
105                     y2 = y3;
106                 }
107
108                 greenProfile = addProfile("GreenWin",x1,y1,x2,y2,greenProfile);
109                 redProfile = addProfile("RedWin",x1,y1,x2,y2,redProfile);
110                 if (showSelections) showProfile(mainWin,x1,y1,x2,y2);
111
112                 nMeas = nMeas + 1;
113
114             }
115         }
116     }
117 }
118
119 finalGreenPro = getAverageProfile(greenProfile,nMeas);
120 finalRedPro = getAverageProfile(redProfile,nMeas);
121
122 // Getting x-coordinates
123 x = newArray(lengthOf(finalGreenPro));
124 for (i=0;i<lengthOf(x);i++) x[i] = i;
125
126 // Fitting a Gaussian to green profile
127 Fit.doFit("Gaussian", x, finalGreenPro);
128 Fit.plot();
129 Plot.getValues(xx, greenFit);
130 if (!showPlots) close();
131
132 greenPeakPos = getPeakPosition(xx,greenFit);
133 print("Green channel peak at "+greenPeakPos[0]+" px");
134 print("Green channel peak height "+greenPeakPos[1]);
135 print("Green channel fit a (amplitude) = "+Fit.p(0));
136 print("Green channel fit b = "+Fit.p(1));
137 print("Green channel fit c (x-position) = "+Fit.p(2));
138 print("Green channel fit d (width) = "+Fit.p(3));
139
140 // Adding a blank line to the output
141 print(" ");
142
143 Fit.doFit("Gaussian", x, finalRedPro);
144 Fit.plot();
145 Plot.getValues(xx, redFit);
146 if (!showPlots) close();
147 redPeakPos = getPeakPosition(xx,redFit);
148 print("Red channel peak at "+redPeakPos[0]+" px");
149 print("Red channel peak height "+redPeakPos[1]);
150 print("Red channel fit a (amplitude) = "+Fit.p(0));
151 print("Red channel fit b = "+Fit.p(1));
152 print("Red channel fit c (x-position) = "+Fit.p(2));
153 print("Red channel fit d (width) = "+Fit.p(3));
154
155 // Showing the distance between peaks
156 print(" ");
157 ppDist = redPeakPos[0] - greenPeakPos[0];
158 print("Distance between Gaussian peaks (px) = "+ppDist);
159
160 // Closing unwanted windows
161 selectWindow("BlueWin");
162 close();
163 selectWindow("BlueNormWin");
164 close();
165 selectWindow("GreenNormWin");
166 close();
167 selectWindow("RedNormWin");
168 close();
169 selectWindow("CombiWin");
170 close();
171 selectWindow("BinaryWin");
172 close();
173 selectWindow("GreenWin");
```

```
close();
selectWindow("RedWin");
close();

setBatchMode("exit and display");

function countLocalPoints(x,y,fitW) {
    count = 0;
    for (xx=x-fitW;xx<x+fitW;xx++) {
        for (yy=y-fitW;yy<y+fitW;yy++) {
            if (getPixel(xx,yy) == 0) count = count + 1;
        }
    }
    return count;
}

function getLocalPoints(x,y,fitW) {
    count = 0;
    for (xx=x-fitW;xx<x+fitW;xx++) {
        for (yy=y-fitW;yy<y+fitW;yy++) {
            if (getPixel(xx,yy) == 0) {
                xArr[count] = xx;
                yArr[count] = yy;
                count = count + 1;
            }
        }
    }
}

function testInversion(winName,x1,y1,x2,y2) {
    // Measure from the inside out, so if the first point is white, flip the array
    selectWindow("BinaryWin");
    makeLine(x1,y1,x2,y2);
    run("Rotate...", "angle=90");
    testProfile = getProfile();

    // Returns true if inversion is required
    return (testProfile[0] == 255);

}

function addProfile(winName,x1,y1,x2,y2,profile) {
    // Recording the intensity profile
    selectWindow(winName);
    makeLine(x1,y1,x2,y2);
    run("Rotate...", "angle=90");
    newProfile = getProfile();

    // Adding new results to profile
    for (j=0;j<lengthOf(profile);j++) profile[j] = profile[j]+newProfile[j];

    return profile;

}

function showProfile(winName,x1,y1,x2,y2) {
    // Recording the intensity profile
    selectWindow(winName);
    makeLine(x1,y1,x2,y2);
    run("Rotate...", "angle=90");
    run("Add Selection...");

}

function getAverageProfile(profile,nMeas) {
    // Creating an empty array to hold the average profile
    nRows = lengthOf(profile);
    avProfile = newArray(nRows);

    for (row=0; row<nRows; row++) avProfile[row] =  profile[row]/nMeas;

    return avProfile;

}

function getPeakPosition(xx,yy) {
    xMax = 0;
    yMax = 0;
    for (i=0;i<lengthOf(xx);i++) {
        if (yy[i] > yMax) {
            xMax = xx[i];
            yMax = yy[i];
        }
    }

    return newArray(xMax,yMax);

}
```